The effects of body composition and body configuration on impact dynamics during lateral falls: insights from *in-vivo*, *in-vitro*, and *in-silico* approaches

by

Iris Claire Levine

A thesis
presented to the University of Waterloo
in fulfillment of the
thesis requirement for the degree of
Doctor of Philosophy
in
Kinesiology

Waterloo, Ontario, Canada, 2017

Examining Committee Membership

The following served on the Examining Committee for this thesis. The decision of the Examining Committee is by majority vote.

External Examiner	Yunhua Luo, Ph.D. Associate Professor University of Manitoba
Supervisor(s)	Andrew Laing, Ph.D. Associate Professor, Kinesiology
Internal Members	Jack Callaghan, Ph.D. Professor, Kinesiology, Mechanical and Mechatronics Engineering
	Lora Giangregorio, Ph.D. Associate Professor, Kinesiology
Internal-external Member	John McPhee, Ph.D. Professor, Systems Design Engineering

Author's Declaration

This thesis consists of material all of which I authored or co-authored: see Statement of Contributions included in the thesis. This is a true copy of the thesis, including any required final revisions, as accepted by my examiners.

I understand that my thesis may be made electronically available to the public.

Statement of Contributions

I would like to acknowledge the following collaborators for their contributions to the work presented in this thesis:

Study 1,
- Janice Skafel, medical imaging
- Shivam Bhan and Daniel Martel, assistance with data collection

Study 2,
- Steven Pretty, assistance with data collection

Study 3,
- John McPhee and Joydeep Banerjee, assistance with model development

Study 4,
- Steven Pretty and Daniel Martel, assistance with data collection

Study 5,
- Steven Pretty, assistance with data collection

Abstract

Fall-related injuries are the current leading accidental cause of emergency room and hospital visits, hospitalizations, and injury-related deaths in Ontario. Hip fractures in particular are associated with poor functional and survival outcomes, and high medical and rehabilitation costs. While nearly a third of older adults fall in Canada each year, only 2% of falls result in a hip fracture, and only 10-37% of falls result in any injury requiring medical attention. The Factor of Risk model (i.e. applied loads/fracture tolerance) has been proposed as a conceptual model to explain this discrepancy, however, current approaches used to screen for hip fracture risk focus primarily on bone strength (i.e. only fracture tolerance) and population-level clinical risk factors for which the mechanistic link to fracture risk is unclear. Individual faller and falling characteristics have been proposed to influence the application and distribution of loads during a fall which could add predictive value to the Factor of Risk approach. However, the magnitude and interaction of these factors has not been quantified.

Therefore, the focus of this thesis was to examine the influence and interaction of individual anthropometry and falling configuration on impact dynamics during simulated falls, and development of a computational model to predict the magnitude and distribution of loads in the pelvis during a fall. The overarching theme was supported through five studies, with objectives to i) define the relationship between elements of body size (e.g. height) and composition (e.g. percent fat mass, trochanteric soft tissue thickness) and impact dynamic outcomes (i.e. peak vertical force, pressure, contact area and deflection) during a simplified simulated fall protocol; ii) determine the relationship between individual characteristics and model parameters for one- and three-dimensional contact models with elastic and viscoelastic components; iii) assess model performance (namely, Mass Spring, Voigt, Hertz, Hunt-Crossley and Volumetric) for the prediction of applied loads during simulated falls; iv) determine how trochanteric soft tissue influences deflection of skeletal structures during a controlled impact; and iv) examine how the relationships between body size and composition are affected when more complex fall simulation protocols are implemented. Studies 1 and 5 employed *in vivo* fall simulation protocols, Studies 2-3 were performed *in silico* based on parameters and outcomes drawn from *in vivo* fall simulations, with comparisons based on both peak and time-varying force outcomes, and in Study 4 an *in vitro* drop tower protocol was used to apply loads directly to the greater trochanter.

In Study 1, pelvis impact dynamics were strongly related to individual characteristics, providing support for the development of a subject-specific hip fracture model. Peak force was strongly linearly related to mass, while peak pressure, contact area, and deflection were more strongly related to the quantity of adipose tissue overlying the hip. In Study 2, elastic parameters for the Voigt and Hertz models were not linked to any individual characteristic, while the Mass-Spring, Hunt-Crossley and Volumetric elastic parameters were related to body fat, sex and trochanteric soft tissue thickness, respectively. Damping parameters for the Voigt model differed between males and females; for the Hunt-Crossley and Volumetric models varied based on pelvis width. In Study 3, model performance was strongest for the Hunt-Crossley model compared to all other models tested, and improved for three- vs one-dimensional models and models including dampers compared to elastic-only models. In Study 4, when cadaveric greater trochanters were laterally impacted using a drop tower protocol, greater and more consistent deflection was found at the anterior superior iliac spine than the greater trochanter, and low, but substantial, deflection occurred medially at the lateral apex of the pelvic ring and medial border of the ilium. Deflections distributed between structures were different during conditions where trochanteric soft tissues were present vs. conditions where soft tissues were removed. In Study 5, while impact characteristics continued to link closely with individual faller characteristics, they were more strongly linked to fall simulation method. Though vertical impact velocity was similar between protocols, shear forces and pressure were greater when participants initiated a simulated fall from a squat position compared to initiation from a kneeling position or a passive "pelvis release" fall simulation.

In sum, the results of these studies provide evidence of the importance of faller characteristics, particularly trochanteric soft tissue thickness, and falling configuration, in predicting the magnitude and distribution of loads during a fall impacting the hip. Additionally, the modeling components point towards the ease of developing and implementing an individualized and mechanistic method of predicting fracture risk in older adults. The results of these studies help to illuminate why some fallers in some configurations experience different risk of injury than would be predicted based on clinical risk factors. These results can be used to improve screening of individuals who might be at greater risk of injury due to poor absorption or distribution of energy by the trochanteric soft tissues. Further, these results may be used to identify which type of hip protector may be appropriate based on individual anthropometry. Finally, risky falling configurations have been identified and can be linked to falling patterns within epidemiological and balance literature—these can be used to develop exercise- and environment-based interventions. Future work should focus on determining how faller strategy influences falling configuration and impact dynamics. Additionally, further model expansion and validation is required to improve the external validity of the models proposed and tested within this thesis, particularly with regards to non-vertical impact dynamics and load distribution within the femur and pelvis.

Acknowledgements

While at times completing my doctorate has felt like a solitary challenge, there are many people who were instrumental to the achievement.

First, those who supported my basic needs. Anne and Ian for keeping a roof over my head and reminding me that the only way out is to finish. The mob for caring for me when I was sick, showing me the more important parts of life and blanketing me with love. Karen, Tom and the rest of the SWK family for inviting me in, making sure I was taken care of, and teaching me to value and hone my creativity. Hughanna and Man-Yee for giving me a quiet place to rest and a full belly.

Second, those who challenged me. Alex for providing foresight, hindsight and pointing out when I was nearsighted and had tunnel vision. Natalie and Mark for keeping my head on straight. Bart, work for it:

H	ρ	θ
0	1.25	0
1	0.15	-3.16
2	0.26	-0.40
3	0.33	0.97
4	0.01	0
5	0.01	0

Third, to my family. Thank you for understanding why this was important to me, for missing me, and for letting me know that I could still move back home even if I flunked. Knowing I make you proud is the reason I pause to think about my accomplishments. I would not be who I am without the encouragement and independence you've given me.

Finally, to those who I literally could not have accomplished this without. Joseph Choi, Mike Boos, Yves Gonthier and Masoud Nasiri Sarvi: you can count me amongst the few who have read your thesis cover to cover. Joydeep for giving me a head start with the model. Cheryl, Craig, Denise, Jeff, Jenny, Jeremy, Marg, Rebecca, Ruth, Tamara, Tracy: thank you for your continued support. My labmates, from beginning to end: I could not imagine a better team to have by my side. Tyler, if I'm the lab mom, I don't know what that makes you, but you've been a great co-parent. Pari, Dan and Alyssa, thank you for all of your help through the long hours of data collection. Steve, you have been a fantastic right-hand man, and I have been honored to share my work with you and see you grow (if not mature . . .). Dr. Duckster for mentoring me with open wings and helping me deal with my bugs. The dozens of people who fell for me, donors and their families, thank you. Dr. Callaghan for pushing me towards technical excellence throughout my time at Waterloo. Dr. Giangregorio, for helping me to understand the context. Dr. Luo, for pushing the pace and working along the same path, even before you were part of the committee. Dr. McPhee for your never-ending curiosity with the project and helping me find the tools I needed. Last but never least, Andrew for your continued mentorship, encouragement and the hours you've spent helping me work through challenges. From the day I showed up at your office as an orphaned graduate student you have given me endless opportunities to grow professionally, academically and personally, and I cannot thank you enough.

Thank you.

Table of Contents

Examining Committee Membership ii

Author's Declaration iii

Statement of Contributions iv

Abstract v

Acknowledgements viii

Table of Contents ix

List of Figures xiv

List of Tables xvi

Chapter 1 Global Introduction 1

1.1 Fall-Related Injuries in Older Adults 1

1.2 Community and Personal Cost 1

1.3 Overview of Current Explanatory Factors 2

1.3.1 Bone Mineral Density and Bone Quality 2

1.3.2 Impacting Segment Stiffness 3

1.3.3 Falling and Impact Configuration 5

1.3.4 Models of fracture risk estimation 5

1.4 Thesis Rationale 6

1.4.1 STUDY 1: Force Attenuation and Distribution during Impacts to the Hip are Affected Differentially by Elements of Body Size and Composition 6

1.4.2 STUDY 2: Parameter Identification for a Multibody Approach to Predicting Impact Characteristics During Lateral Impacts to the Hip 7

1.4.3 STUDY 3: Comparison of the Accuracy of Hip Impact Contact Models 7

1.4.4 STUDY 4: In Vitro Determination of the Anatomical Sources of Pelvic Stiffness Components 8

1.4.5 STUDY 5: The Relationship Between Experimental Fall Simulation Paradigm, Individual Body Composition and Impact Characteristics 8

Chapter 2 Literature Review: Mechanical approaches for determination of fracture risk 10

2.1 Body Composition and Aging 10

2.2 Review of relevant anatomy and typical fracture mechanisms 11

2.3 Hayes' Factor of Risk and the Nevitt and Cummings Hypothesis 14
2.4 Fracture tolerance perspective 16
2.4.1 Mechanical Tolerance 16
2.4.2 Assessment of fracture tolerance 17
2.4.3 Limitations of fracture tolerance assessment and treatment 19
2.5 Applied Load Perspective: Importance of Fall Mechanics 20
2.5.1 Preceding Circumstances and Causes of Falls 21
2.5.2 Impact Characteristics 24
2.5.3 Protective Responses and Mechanisms 29
2.6 Methods of Assessing Loading and Load Distribution During Falls 37
2.6.1 Analysis of falls in real-life scenarios 37
2.6.2 *In Vivo* fall simulation 38
2.6.3 *In Vitro* and mechanical impact simulation 41
2.6.4 Modeling approaches 43
2.7 Literature summary and specific questions to be addressed 56
Chapter 3 , Study 1: Force Attenuation and Distribution during Impacts to the Hip are Affected Differentially by Elements of Body Size and Composition 58
3.1 Introduction 58
3.2 Methods 60
3.2.1 Participants 60
3.2.2 Body Composition Assessment 61
3.2.3 Instrumentation and experimental impact protocol 64
3.2.4 Image treatment, signal conditioning and data reduction 66
3.2.5 Statistical Analysis 68
3.3 Results 69
3.4 Discussion 77
Chapter 4 , Study 2: Parameter Identification for a Multibody Approach to Predicting Impact Characteristics During Lateral Impacts to the Hip 82
4.1 Introduction 82
4.2 Methods 83
4.2.1 Experimental Protocol 84

4.2.2 Signal Processing..86

4.2.3 Statistical analysis 90

4.3 Results 91

4.4 Discussion 96

Chapter 5 , Study 3: Comparison of the Accuracy of Hip Impact Contact Models 101

5.1 Introduction 101

5.2 Methods 104

5.2.1 Experimental protocol 105

5.2.2 Signal Processing...105

5.2.3 Characterization of impact dynamics and definition of model parameters 106

5.2.4 Model simulation..108

5.2.5 Model evaluation..108

5.2.6 Statistical Analysis 110

5.3 Results 111

5.4 Discussion 115

Chapter 6 , Study 4: *In Vitro* Determination of the Anatomical Sources of Pelvic Stiffness Components..121

6.1 Introduction 121

6.2 Methods 123

6.2.1 Dissection process and specimen preparation 123

6.2.2 Instrumentation..126

6.2.3 Experimental protocol 127

6.2.4 Signal Conditioning and Data Reduction 127

6.3 Results 129

6.3.1 Specimen fracture patterns 133

6.4 Discussion 138

Chapter 7 , Study 5: The Relationship Between Experimental Fall Simulation Protocol, Individual Body Composition and Impact Characteristics 146

7.1 Introduction 146

7.2 Methods 148

7.2.1 Experimental Protocol 149

7.2.2 Signal Processing and Data Reduction 150
7.2.3 Statistical Analysis 151
7.3 Results 152
7.4 Discussion 156
Chapter 8 Thesis Synthesis and Conclusions 163
8.1 How do individual body size or body composition characteristics relate to impact dynamics during a lateral fall? 163
8.2 Can we incorporate individual characteristics in a mechanistic hip impact model? 165
8.3 What happens when we simulate the impact phase of the fall using different fall simulation protocols? 167
8.4 From a clinical perspective, what are the most critical research findings? 168
8.5 Summary of Contributions 170
Global Summary: The Take-Home Statement 170
Bibliography 171
Appendix 1 Do Obese Long-Term Care Residents Fall Differently than Underweight Residents? .. 188
A1.1 Introduction 188
A1.2 Methods 188
A1.3 Results 188
A1.4 Discussion and Implications for this Thesis 195
Appendix 2 Peak pressure and contact profile during sideways falls on the hip: links with individual characteristics and falling configuration 197
A2.1 Introduction 197
A2.2 Methods 199
A2.2.1 Experimental Protocol 200
A2.2.2 Signal Processing 202
A2.2.3 Data Analysis 203
A2.3 Results 203
A2.4 Discussion 211
Appendix 3 Comparison of regressed vs individual parameters 214
Appendix 4 Extended statistical analysis of model parameters 218

Appendix 5 Paradigms for simulating falls to the hip: differences in impact configuration, loading and reliability 227
A5.1 Introduction 227
A5.2 Methods 228
A5.2.1 Experimental Protocol 228
A5.2.2 Signal Processing 230
A5.2.3 Statistical Analysis 231
A5.3 Results 231
A5.4 Discussion 235

List of Figures

Figure 2.1 Critical Anatomical Components of the Proximal Femur 11

Figure 2.2 Types of Proximal Femur Fractures 12

Figure 2.3 Major Components of the Pelvis 14

Figure 2.4 Cummings and Nevitt Hypothesis of The Causes of Hip Fractures 15

Figure 2.5 Simplified schematic of stiffness components during a lateral hip impact 36

Figure 2.6 Behavior of the pelvis during impact 43

Figure 2.7 Model Schematics for the Mass-Spring, Voigt, Maxwell, Standard Linear Solid, Hertzian, Hunt-Crossley and Volumetric Contact Models 45

Figure 2.8 Vibration Analysis Method of Estimating Effective Pelvic Stiffness 46

Figure 2.9 Force-deflection Stiffness Estimation Methods 48

Figure 2.10 Schematic of the Basic Hertzian Contact Model 51

Figure 2.11 Schematic of the Volumetric Contact Model 54

Figure 3.1 Ultrasound image of soft tissue overlying the greater trochanter 62

Figure 3.2 Full body DXA image and analysis results within the Hologic software 63

Figure 3.3 Support sling for the pelvis release protocol 65

Figure 3.4 Critical timepoints used to define impact initiation, time of peak force and trial endpoint 67

Figure 3.5 Participant characteristics correlated with F_{max} 73

Figure 3.6 Scatterplots of D_{peak} vs. participant characteristics including 74

Figure 3.7 Scatterplots of CA_{peak} vs. participant characteristics including 75

Figure 3.8 Scatterplots of P_{peak} vs. participant characteristics including 76

Figure 4.1 Initial position of the participant during the pelvis release protocol 84

Figure 4.2 Least-squares curve fits for estimation of MS and HZ stiffness components 87

Figure 4.3 Characterization of velocity-independent stiffness and velocity-dependent damping components 89

Figure 4.4 Demonstration of curve fit to experimental data for MS, HZ, VG, HC and VO 90

Figure 4.5 Groupwise differences and strongest correlations for k_{MS} and k_{HZ} 93

Figure 4.6 Groupwise differences and strongest correlations for $k_{VG,}$ k_{HC} and k_{VO} 93

Figure 4.7 Groupwise differences and strongest correlations for b_{VG}, a_{HC} and a_{VO} 94

Figure 5.1Model Schematics and normal force formulae for the MS, VG, HZ, HC and VO 102
Figure 5.2 Initial position of the participant during the pelvis release protocol 105
Figure 5.3 Experimentally-determined loading response corridors 106
Figure 5.4 Demonstration of final curve fit to experimental data for MS, HZ, VG, HC and VO 107
Figure 5.5 Demonstration of time-varying model performance within the 2 SD (95% CI) corridors 109
Figure 5.6 Model absolute and directional performance for peak criteria 114
Figure 5.7 Distribution of contact stress for models 117
Figure 5.8 Nonlinearity in the force and deflection data during the initial impact phase 120
Figure 6.1 Orientation of the pelvis for the testing protocol 125
Figure 6.2 Pelvis drop tower 126
Figure 6.3 Demonstration of the method of calculating landmark deflection 128
Figure 6.4 Critical timepoints 129
Figure 6.5 Peak force, force attenuation and duration of loading 131
Figure 6.6 Deflection at time of peak force 132
Figure 6.7 Time delay between force initiation (T1) and deflection initiation 133
Figure 6.8 High-speed video stills and dissection of PMHS 14089 135
Figure 6.9 High-speed video stills and dissection of PMHS 14090 136
Figure 6.10 High-speed video stills and dissection of PMHS 14091 137
Figure 6.11 Demonstration of the biphasic loading behavior 142
Figure 7.1 Initial position and motion path of the Pelvis (a), Kneeling (b), and Squat Release (c). .. 149
Figure 7.2 Interaction effect of STT group and fall simulation protocol on F_{shear} 154
Figure 7.3 Main effect of fall simulation protocol on $F_{vertical}$ 154
Figure 7.4 Main effects of TSTT group and fall simulation protocol on *CA* 155
Figure 7.5 Main effect of fall simulation protocol on P_{peak} 155
Figure 7.6 Backwards rotation during the Squat Release Protocol 156
Figure 7.7 Box and whisker plot demonstrating the separation of the outlying trial means 159
Figure 7.8 Demonstration of time-varying loading response during a Pelvis (a), Kneeling (b) and Squat Release (c) 161
Figure 8.1 Relationship between individual characteristics and impact dynamics 163
Figure 8.2 Graphical display of relationship between TSTT and peak pressure 164

List of Tables

Table 2.1 Comparison of Currently Employed *In Vivo* Simulated Fall Techniques........................... 40

Table 3.1 Recruited Participant Characteristics 60

Table 3.2 Independent-Dependent variable sets for hypothesis tests.. 69

Table 3.3 Dependent-Global Independent-Local Independent Variable Sets..................................... 69

Table 3.4 Impact characteristics... 70

Table 3.5 Participant characteristics correlated with F_{max} 71

Table 3.6 Correlations with D_{peak}, CA_{peak} and P_{peak} 72

Table 3.7 Comparison of Local vs. Global Body Composition Variable Relationships with Outcome Variables 77

Table 4.1: Mean (SD) participant anthropometric characteristics for participants with complete data 84

Table 4.2 Model normal force formulae 87

Table 4.3 Cost functions for viscoelastic models 88

Table 4.4 Summary of ANOVA results for Hypothesis 1 92

Table 4.5 Bivariate correlation results for model parameters with body size and composition elements 95

Table 4.6 Final model parameters and regression equations for determining model parameters based on individual characteristics 96

Table 5.1: Mean (SD) participant anthropometric characteristics. STT represents trochanteric soft tissue thickness. BMI represents body mass index 104

Table 5.2 Model parameters 107

Table 5.3 Model normal force formulae 108

Table 5.4: Model evaluation criteria 109

Table 5.5 Summary of ANOVA results.. 112

Table 5.6 Pairwise comparisons between models for significant model error differences................ 113

Table 5.7 Improvement over MS, in percentage points 115

Table 6.1 Post-mortem human donor characteristics 123

Table 6.2 Component Deflection 131

Table 7.1: Mean (SD) participant anthropometric characteristics. 148

Table 7.2 Summary of main effects, interactions, and significant pairwise comparisons 153

Chapter 1 Global Introduction

1.1 Fall-Related Injuries in Older Adults

Fall-related injuries are the current leading accidental cause of emergency room and hospital visits, hospitalizations, and injury-related deaths in Ontario (OIDR 2012). Over 200,000 falls on level ground resulting in trips to hospitals were reported between 2007 and 2009, and more than 60,000 injuries to the hip and thigh, as a result of a fall, required emergency medical attention. In 2011, unintentional falls caused more major injury hospitalizations and in-hospital deaths than motor vehicle collisions (CIHI 2013). According to widely cited epidemiological data, underweight females suffer greater rates of hip fracture compared to normal BMI and obese fallers (Grisso, Kelsey et al. 1991; Compston, Watts et al. 2011; Tanaka, Kuroda et al. 2013), with increased bone mineral density (Hayes, Myers et al. 1996) and soft tissue thickness (Bouxsein, Szulc et al. 2007) cited as potential explanatory factors. However, more recent evidence also identifies overweight fallers as a high-risk group for fragility and fall-related fracture (Fjeldstad, Fjeldstad et al. 2008; Winter 2009; Armstrong, Cairns et al. 2012; Nielson, Srikanth et al. 2012). Unfortunately, individuals with high BMI appear to derive less mechanical protection from intervening materials such as hip protectors (Choi, Hoffer et al. 2010) or compliant floors (Bhan, Levine et al. 2013) than underweight fallers. This new pool of epidemiological literature allows us to expand biomechanical research to newly-identified at-risk groups, and introduces greater variability of potential explanatory variables to explore the mechanisms of fall-related injuries.

1.2 Community and Personal Cost

Fall-related injuries are accompanied by high personal and community financial impact, The latest economic data cites a yearly burden for Ontario of $2.1 billion dollars, and $6.2 billion dollars Canada wide (SMARTRISK 2009). Average per-patient costs for falls in the United States range from $849 for minor treatment not requiring hospitalization to $19,672 for hospitalized injuries and $22,187 for fatal injuries (WISQARS 2005). Falls also account for 47% of injuries resulting in partial disability, and 50% of injuries resulting in total permanent disability (SMARTRISK 2009), with estimated average work loss costs from $3,200 for minor injuries to $35,628 for injuries requiring hospitalization (WISQARS 2005).

Hip fractures are associated with particularly poor functional and survival outcomes, with only 63% of long-term care patients surviving one year post-fracture (Neuman, Silber et al. 2014), with men experiencing lower survivability rates than women. Less than 30% of independently-mobile older adults are able to move independently 180 days post-fracture, while more than 30% of the same group has died (Neuman, Silber et al. 2014).Outcomes for fractures in those already requiring supervision or assistance for locomotion are worse, with only one in five patients resuming similar levels of independence post-fracture (Neuman, Silber et al. 2014). In survivors, one year post-fracture deficits in Activities of Daily Living (ADL) ability are greatest for activities requiring balance, and lower limb strength and power, such as stair climbing, bathing, dressing, and performing chair and bed transfers (Alarcón, González-Montalvo et al. 2011). Hip fractures represent a category of injuries with high cost, but risk of such incidents can be reduced through greater understanding of the factors involved.

1.3 Overview of Current Explanatory Factors

Several factors influence the likelihood of fracture. Mechanically, the risk of fracture can be estimated via the factor-of-risk method: a ratio of the load applied to the expected service load of the impacted bone (Hayes, Myers et al. 1996). Bone mineral density and bone quality have been heavily investigated (Cheng, Lowet et al. 1998; Bouxsein, Coan et al. 1999; Crabtree, Lunt et al. 2000; Pulkkinen, Jämsä et al. 2008) in regards to their contributions to fracture load, and have been the perspective selected for the development of many pharmacological (Crabtree, Kroger et al. 2002) interventions. The magnitude of loads applied to the proximal femur can be modified through several avenues. Two that will be explored in this thesis are energy absorption via pelvic stiffness, and modification of potential energy via falling configuration.

1.3.1 Bone Mineral Density and Bone Quality

While there are many clinical risk factors linked to fracture risk, bone mineral density (BMD) and bone quality (BQ) have been a strong focus of fracture prevention. The World Health Organization's Fracture Risk Assessment Tool (FRAX; Kanis, Hans et al. 2011) is a clinical tool, which utilizes BMD, or a BMI-based estimate of BMD. However, direct identification (Lewiecki, Compston et al. 2011) and treatment (Lewiecki, Compston et al. 2011; McCloskey, Vasikaran et al. 2011) of poor

BMD is dependent on access to diagnostic equipment, such as Dual X-Ray Absorptiometry (DXA) scanners, as well as prescription of such imaging by healthcare professionals. In one study of patients presenting with incident fragility fractures, risk factors for not receiving diagnostic BMD analysis prior to the incident fracture include good health (three or fewer comorbid conditions), young age and male gender (Riggs and Melton 1995). In another, only 24% of 1162 women with osteoporosis-related distal radius fractures had received a BMD assessment or osteoporosis interventions such as pharmacological treatment or implementation of a nutritional or physical activity plan (Blecher, Wasrbrout et al. 2013). While BMD analysis may present the best current method of fracture prediction, its implementation is limited amongst those at risk for fall-relate fractures.

Despite generally positive relationships between bone mineral density and body mass (Reid 2002) there are indications that high body mass is not definitively associated with high BMD (Travison, Araujo et al. 2008), and that the rate of weight gain is not linked with an appropriate increase in bone mass (Stone, Seeley et al. 2003). Lifestyle factors such as lack of exercise and decreased activity level (Armstrong, Spencer et al. 2011), poor nutrition and nutrient absorption due to diet (Di Monaco, Vallero et al. 2011) or surgical bariatric intervention (Schneider, Börner et al. 1993), and metabolic disorders such as diabetes (Tanaka, Kuroda et al. 2013) are all potential causes of poor bone quality (both trabecular and cortical) and bone strength in overweight and obese individuals.

Finally, imaging-based fracture prediction is typically based on BMD and does not normally include structural properties like femoral neck geometry which have been identified as important for predicting where (anatomically) and if a fracture will occur (Cody, Gross et al. 1999; Pulkkinen, Eckstein et al. 2006; Pulkkinen, Jämsä et al. 2008; NCGC 2012). Therefore, solely basing prediction of hip fracture risk on BMD or surrogate measures limits the number of patients who will be identified as at a high risk of hip fracture or in need of intervention to reduce the likelihood of fall-related injuries.

1.3.2 Impacting Segment Stiffness

A modifier of loads applied to an impacting body segment is the stiffness of the tissues within the impacting region, as well as any overlying personal or environmental protective equipment such as wearable hip protectors or compliant flooring. In its simplest form, the mechanical effectiveness of compliant tissues can be described by a mass-spring model (discussed and illustrated in greater depth in Section 2.6.4), in which stiffness is modified by the amount of compression or displacement of the tissues within the structure, and the material properties of those tissues.

Several hypotheses regarding hip fracture outcomes have been attributed to the protective energy absorption capacity of soft tissue. However, using a pelvis release methodology, we have found that the increases in soft tissue thickness associated with participants with high BMI were not great enough to overcome increases in effective mass (Levine 2011; Levine, Bhan et al. 2013), delivering greater absolute peak forces to the proximal femur than in participants with low BMI. While high BMI is associated with greater energy absorption (Bhan, Levine et al. 2013), there is some evidence that effective pelvic stiffness, as currently modeled, does not differ between participants with low- and high-BMI (Levine 2011; Levine, Bhan et al. 2013). Considering these discrepancies between hypothesized mechanisms and outcomes, two explanations become apparent. One possibility is that mechanisms of energy absorption may not protect against hip fracture as expected due to the complex nature of the biological tissues and structures of those tissues. A second explanation is that current experimental methods and models do not capture the mechanisms that are most important for estimating impact characteristics.

To highlight this, simplified mass-spring models best predict loads applied at the hip only within a narrow range of body composition (Levine 2011; Levine, Bhan et al. 2013). A vibration-based method of estimating pelvic stiffness results in poor estimation of peak impact force in participants outside of a 'normal' BMI range (<22.5 or >28 kg/m^2) (Levine, Bhan et al. 2013). It is hypothesized that this is due to the interfering vibration of multiple structures (e.g. the femur, pelvis, and soft tissues vibrating at different frequencies), which makes it challenging to determine which vibrational frequency is most critical to the prediction of peak force, or how to include all components appropriately. A linear force-deflection method performs slightly better, but also has drawbacks. The linear model is unable to capture a difference in pelvic stiffness between participants with low- and high-BMI, and does not capture the non-linear characteristics of the experimental impact data (Laing and Robinovitch 2010; Levine, Bhan et al. 2013). A non-linear stiffness component alone results in over-prediction of peak force (Laing and Robinovitch 2010). A piecewise model, including a non-linear region during initial impact, followed by a linear region, offers an improvement over either entirely linear or entirely non-linear models (Levine 2011). However, how these mathematical models relate to structural and material elements of the impacting biological components has not yet been explored. Therefore, currently used simple mass-spring models neither predict impact characteristics well enough, nor are they helpful in explaining the mechanics behind how loads are distributed and dissipated during a fall-related impact. Inclusion of factors such as tissue composition (adipose vs. muscle), contact area, soft tissue depth and pelvis circumference may explain anthropometry-related differences in energy absorption and pelvic stiffness, and corresponding absolute peak forces.

1.3.3 Falling and Impact Configuration

A third potential source for the BMI-fracture rate relationship is falling configuration. Postmenopausal women with high BMI suffer a greater rate of falls than normal and underweight women (Armstrong, Spencer et al. 2011; Hergenroeder, Wert et al. 2011), with ankle (Armstrong, Cairns et al. 2012) fractures more common in obese women, rib fractures more common in normal-BMI women (Compston, Watts et al. 2011), and hip, pelvis and wrist fractures more common in underweight women (Compston, Watts et al. 2011). Further, moderate and severely-obese older adults self-report greater fear of falling and poor mobility and perform more poorly on mobility tasks requiring rapid changes in direction (Figure-8 test, 4 meter gait speed, Get Up & Go test and chair stand test) and prolonged movement (six-minute walk test), as well as static and dynamic balance tests (including challenging narrow walk tests and obstacle avoidance tasks) (Hergenroeder, Wert et al. 2011). Poor center of mass control in the sarcopenic obese (Ochi, Tabara et al. 2010) points towards an effect of neurologically controllable (i.e. muscle) and uncontrollable (i.e. adipose) mass on balance control. The combination of poor balance and mobility, with epidemiological evidence of fracture location, points towards potential differences in falling configuration between fallers with differing body composition. Falling configuration likely has a critical effect on where, and in which segments, greatest moments and bone stresses are generated during falls, as well as how the total falling energy is distributed between segments.

1.3.4 Models of fracture risk estimation

Fracture risk in older adults is currently estimated via one of several models, including FRAX (Kanis, Hans et al. 2011), QFracture (Lewiecki, Compston et al. 2011), Garvan (van den Berghe, Geel et al. 2010) and CAROC (Lentle, Cheung et al. 2010). These models include risk factors which address fracture tolerance, and more indirectly, loads applied during a fall. The models are based on large-scale epidemiological data, and can be easily implemented in a clinical scenario with simple measurements (e.g. height, weight) and a questionnaire. However, the mechanistic links between some of the included risk factors and fracture risk are not clear. Additionally, several factors which affect load magnitude and distribution have not been included in these models. Better understanding of how factors such as body size, body composition and falling configuration influence impact mechanics may highlight their utility alongside current fracture risk prediction models.

1.4 Thesis Rationale

While a large body of research has focused on identifying clinical indicators of poor bone strength and development of fracture prediction models, there are gaps in the literature regarding the applied loads portion of the Factor of Risk equation. The assessment of the mechanistic contribution of individual characteristics and falling configuration to the applied loads component could provide a substantial improvement to fracture risk assessment at a population level. Stronger understanding of a mechanistic pathway could lead to the development and simulation of intervention approaches *a priori*, which is not possible with a typical *post hoc* epidemiological approach. This thesis will explore the interaction of impact configuration and individual anthropometrics (body size and composition) to influence magnitude and distribution of loads at the pelvis. The five studies will then be synthesized to arrive at recommendations for improvements in fall force prediction and injury prevention.

1.4.1 STUDY 1: Force Attenuation and Distribution during Impacts to the Hip are Affected Differentially by Elements of Body Size and Composition

While it is widely theorized that trochanteric soft tissues play a large role in attenuation of hip impact forces, it is unclear why this attenuation is ineffective at preventing hip fractures in some cases, and is more effective in some groups than others (e.g. more protective for females than males) (Bouxsein, Szulc et al., 2007; Nielson, Bouxsein et a., 2009). Additionally, increased body mass is associated with reduction of normalized impact force, but not frontal plane deflection-based estimates of system stiffness, suggesting that soft tissue acts along more dimensions to modify applied loads (Levine, Bhan et al., 2013). While more complex models have been posed, we must first determine 1) whether the behavior (i.e. change in geometry and viscoelasticity) of the pelvis during impact is appropriately represented by the assumptions and limitations of such models, and 2) which measurable elements of body composition can be simplified as model parameters. Therefore, the primary goal of this study is to explore relationships between contact area, pressure, deflection, and peak force during impact with respect to body composition. Nineteen university-aged females consented to participate in this study. Each underwent four lateral pelvis release trials with an impact velocity of 1 m/s, which involved the lateral aspect of the hip impacting a pressure plate mounted on a force plate. Body composition using two imaging techniques (i.e. ultrasound, DXA) and easily accessible surrogate techniques (e.g. waist circumference, skinfold measurements) was correlated with the impact characteristics to determine relationships between specific elements of body composition and impact characteristics. The results of this study were used to refine the variables explored in Study 2 and 5, and informed model development in Study 3.

1.4.2 STUDY 2: Parameter Identification for a Multibody Approach to Predicting Impact Characteristics During Lateral Impacts to the Hip

A major drawback to current methods of predicting osteoporotic fractures is that they are based on population-level statistics rather than a mechanistic solution to a mechanical problem (Luo 2016). This study draws on relationships between individual faller characteristics and impact dynamics (Robinovitch, Hayes et al. 1991; Robinovitch, McMahon et al. 1995; Robinovitch, Hayes et al. 1997; Laing and Robinovitch 2010; Levine 2011; Levine, Bhan et al. 2013) and builds on the relationships developed in Study 1 to characterize stiffness and damping characteristics for point- and distributed-contact models of impacts to the lateral hip. Thirty-one participants underwent a modified pelvis release protocol to characterize model characteristics based on force, deflection and contact area during 1 m/s impacts and quasi static loading of the pelvis. We then developed regression equations to predict model parameters based on individual parameters, which were implemented in Study 3.

1.4.3 STUDY 3: Comparison of the Accuracy of Hip Impact Contact Models

Impacts to the hip have been, until recently, modeled as a simple point-contact model, consisting of a mass and spring, or mass, spring and damper (Robinovitch, Hayes et al. 1991; Robinovitch, Hayes et al. 1997; Laing and Robinovitch 2010). However, as identified in Section 1.3.2, there are both theoretical, application, and biofidelity drawbacks to these simplified models. The results of the first three studies will be synthesized to develop a pool of potential variables which could be included in mathematical models in hip impacts. The objective of this study will be to develop, validate, and contrast several mechanical and statistical models of varying levels of complexity for the prediction of pelvis impact characteristics during sideways falls. We hypothesized that model performance would be positively influenced by inclusion of damping and geometry components. The limitations of this model, in its current implementation, were used to drive research questions for Studies 4 and 5.

1.4.4 STUDY 4: In Vitro Determination of the Anatomical Sources of Pelvic Stiffness Components

While it has been established that pelvic stiffness is a critical component of energy absorption during impacts to the hip (Lauritzen and Askegaard 1992; Bhan, Levine et al. 2013), and that differences in pelvic stiffness exist between sexes and BMI groups (Levine 2011; Levine, Bhan et al. 2013), sources of these differences have only been theorized. Potential sources include adipose tissue, muscle tissue, ligament laxity or damage, and movement of the femur within the hip joint. The sources of pelvic stiffness during impact scenarios were assessed using a cadaveric model through a series of *in vitro* impact simulations, with and without trochanteric soft tissues. The goal of this study was to characterize anatomical sources of frontal plane pelvic stiffness within the proximal femur and pelvis, as well as determine how these anatomical component deflections changed with the inclusion of a trochanteric adipose pad. We then linked these strains to injury outcomes and made recommendations for future development of this project.

1.4.5 STUDY 5: The Relationship Between Experimental Fall Simulation Paradigm, Individual Body Composition and Impact Characteristics

Few studies have explored how involuntary falls influence impact configurations, and more importantly, how impact configuration and body composition affect how loads are distributed. No study to date explores how general anthropometric factors (height, weight, body mass index) interact with falling configuration to influence distribution of loads at the hip, despite strongly divergent injury patterns between anthropometry-based groupings of fallers. Through a preliminary study examining real-life falling configuration in older adults in long term care, (Appendix 1), we have identified common falling configurations in older adults, as well as key differences between fallers in groups based on gender and BMI. Based on this research, laboratory-based experimental fall protocol was performed by 44 young adult participants. The overall goal of this study was to expand on the relationships between body composition and impact dynamics, established in Study 1, to determine how impact configuration and body composition interact to influence load magnitude and distribution during three simulated fall protocols. We hypothesized that the different fall simulation protocols would produce different impact dynamics protocols (vertical force, shear force, peak pressure and contact area), in addition to the influence of TSTT. We used the results of this study to drive a discussion how impact configuration influences injury risk, as well as how falling configuration might be incorporated into a multibody model to simulate falling.

Chapter 2 Literature Review: Mechanical approaches for determination of fracture risk

While the majority of hip fractures (90%) and pelvis fractures (83%) are the result of a fall from standing height rather than other causes such as automobile collisions or spontaneous fractures (Grisso, Kelsey et al. 1991; Cummings and Melton 2002; Guggenbuhl, Meadeb et al. 2005), only approximately 2% of falls from standing height actually result in a hip fracture (Hayes, Piazza et al. 1991). However, with 30,000 serious injuries to the hip or thigh requiring medical attention every year (OIDR 2012), falls resulting in hip fracture are not an uncommon problem in Canada. I believe a biomechanical approach considering both the loads applied to the hip, as well as the material and structural properties of the proximal femur and surrounding tissue, is key to providing better prediction and prevention of hip fractures. This chapter will review relevant literature to support the rationale for the studies that will be presented in Chapters 3-7.

2.1 Body Composition and Aging

Body composition has fairly recently come to light in the realm of fall-related injuries, with implications for cause and configuration of the fall (Madigan, Rosenblatt et al. 2014), outcome (Armstrong, Cairns et al. 2012), and impact mechanics. Therefore, both the literature review and the studies in this thesis will reflect the recognized differences between young and older adults with regards to BMI-based assessment of body composition and the effect of body size on the mechanics of fall-related injuries.

Recent analysis of body composition within adults (over the age of 20) indicates that over 30% of North Americans are obese (BMI >35), while more than 70% of men and 65% of women are either overweight or obese (BMI>30, (Flegal, Carroll et al. 2010)). For men, the prevalence of obesity (37.1%) or overweight and obesity (78.4%) is increased in those over the age of 65 compared to their younger counterparts, while for women prevalence of both conditions are more stable relative to younger groups (33.6% and 68.6%, respectively (Flegal, Carroll et al. 2010)). In contrast, the prevalence of underweight adults over the age of 60 is less than 5% (CDC 2012).

In a review of all-cause mortality in older adults, only 4 out of 26 authors used the standard established BMI ranges for to classification of participants as overweight (25– 29.9 kg/m^2) or obese

(≥30 kg/m^2), and definitions of "optimal BMI" ranged from <20 kg/m^2 to >28 kg/m^2 with nearly as many variations on the defining values as there were papers. The "optimal BMI" range skews slightly higher in older adults, relative to young adults, but is not necessarily related to quantity of fat or lean mass, or fat distribution, particularly when influenced by sarcopenia.

2.2 Review of relevant anatomy and typical fracture mechanisms

Fractures to the hip occur mainly in the proximal end of the femur (Figure 2.1), which is bound most proximally by the rounded half-sphere head of the femur (J). Extending distally from the head of the femur is a narrowed femoral neck (width NM, length HI). Major proximal muscular attachments for the proximal femur occur at the greater (G) and lesser (E) trochanters. The femoral shaft (width DB, length indicated by the vertical component of the neck-shaft angle) and femoral neck are both constructed with thickened areas of cortical bone (FE, CB). Fractures of the proximal femur can be

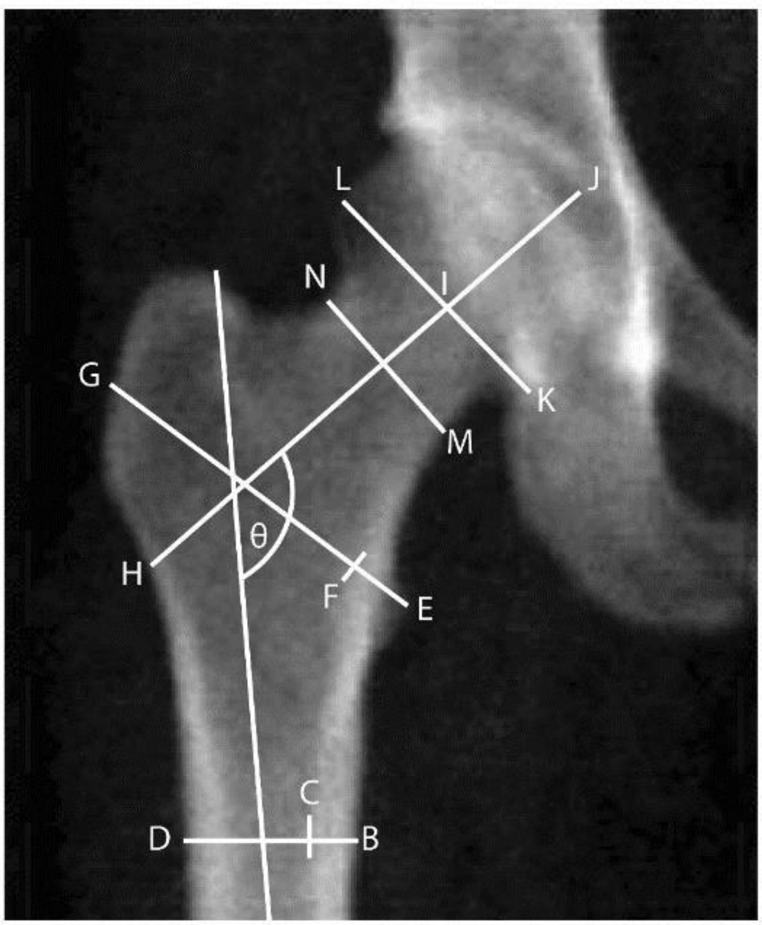

Figure 2.1 Critical Anatomical Components of the Proximal Femur

Skeletal components identified as potentially critical for the prediction of proximal femur fractures (Pulkkinen, Eckstein et al. 2006) include: femoral shaft width (DB); femoral neck width (NM); femoral head width (LK); femoral neck axis length A (HI), and B (HJ); intertrochanteric width (GE); inferior cortical thickness (CB); superior cortical thickness (FE); and neck-shaft angle (θ).

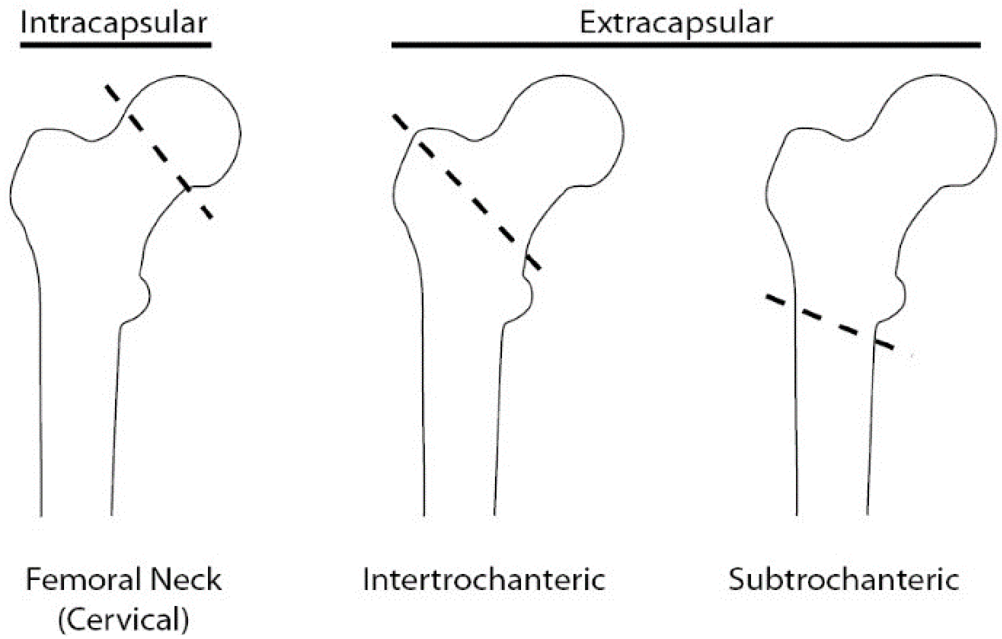

Figure 2.2 Types of Proximal Femur Fractures

Fractures of the proximal femur can be categorized as occurring at the femoral neck (cervical), between the greater and lesser trochanter (intertrochanteric), or distal to both trochanters (subtrochanteric) (Marks, Allegrante et al. 2003). Fracture location is dependent on individual geometry and bone quality, as well as loading factors, described in greater detail in the text.

categorized as occurring at the femoral neck (cervical), between the greater and lesser trochanter (intertrochanteric), or distal to both trochanters (subtrochanteric, Figure 2.2) (Marks, Allegrante et al. 2003). Women are more likely to suffer a cervical femur fracture than men ($p=0.002$) (Pulkkinen, Eckstein et al. 2006; Pulkkinen, Jämsä et al. 2008). Higher BMI ($p<0.05$), poorer mobility (both objectively testing and self-reported) are also risk factors for cervical fracture, while advanced age ($p<0.001$) is associated with trochanteric fracture (Jokinen, Pulkkinen et al. 2010). Femurs fracturing at lower applied loads are more likely to be characterized as cervical fractures, while intertrochanteric fractures are more common in femurs that are able to tolerate greater loads (Pulkkinen, Eckstein et al. 2006).

Experimental fracture testing of the proximal femur along with high speed video indicates that fractures to the proximal femur typically follow a two-stage yielding process. An initial crack due to compressive stress on the superior femoral neck (N in Figure 2.1) is followed by a second crack initiation at the inferior femoral neck (M in Figure 2.1) (de Bakker, Manske et al. 2009). Buckling at the superolateral cortical surface of the femoral neck has also been proposed as a mechanism (Mayhew, Thomas et al. 2005; de Bakker, Manske et al. 2009). However, experimental testing of the proximal femur requires strict methodology with regards to consistent positioning of the specimen and points of load application, and rate and magnitude of loading; the experimental conditions producing these failure patterns may not represent those that occur in real life, and to date no investigator has studied failure of the proximal femur in vivo during real falls.

Applied loads during a lateral fall are also distributed medially to the pelvis (Figure 2.2). The pelvis is composed of a semi-rigidly fixed ilium, ischium and pubis, which join at the acetabulum. The proximal femur forms the hip joint with the acetabulum. The pelvis is semi-rigidly (dependent on age, gender, injury and hormonal status) attached to the sacrum, the most distal vertebra of the spine. The sacrum, ilium, ischium and pubis form the pelvic ring, the location of the majority of fractures to the pelvis (Viano, Lau et al. 1989; Cavanaugh, Walilko et al. 1990; Etheridge, Beason et al. 2005) (Matsui, Kajzer et al. 2003). The inferior ramus of the ischium is a weight-bearing structure during sitting, while the acetabulum bears weight during standing. For clarity, the pelvic bones will be referred to as the “pelvis”, while the pelvis and femur *in situ* will be referred to as the “pelvis system”.

The pelvis and femur are surrounded by soft tissue, including layers of muscle, fascia, adipose, skin, and the trochanteric bursa. Collectively, the thickness of the soft tissues (i.e. all soft tissue layers) is dependent on sex (approximately 10 mm, or 30% lower in males, and hip posture (increasing relative to quiet stance in both extension and flexion directions, (Levine, Minty et al. 2015). The greater trochanter, the most prominent structure during impacts to the hip, serves as an insertion point for several muscles, and therefore is not directly overlaid in most positions by muscular tissue. Because of this, muscle activation has little effect on soft tissue thickness over the greater trochanter (e.g. Tensor fascia lata activation (Levine, Minty et al. 2015)), which contrasts with findings regarding muscle tissue overlying other anatomical structures (Hodges, Pengel et al. 2003;

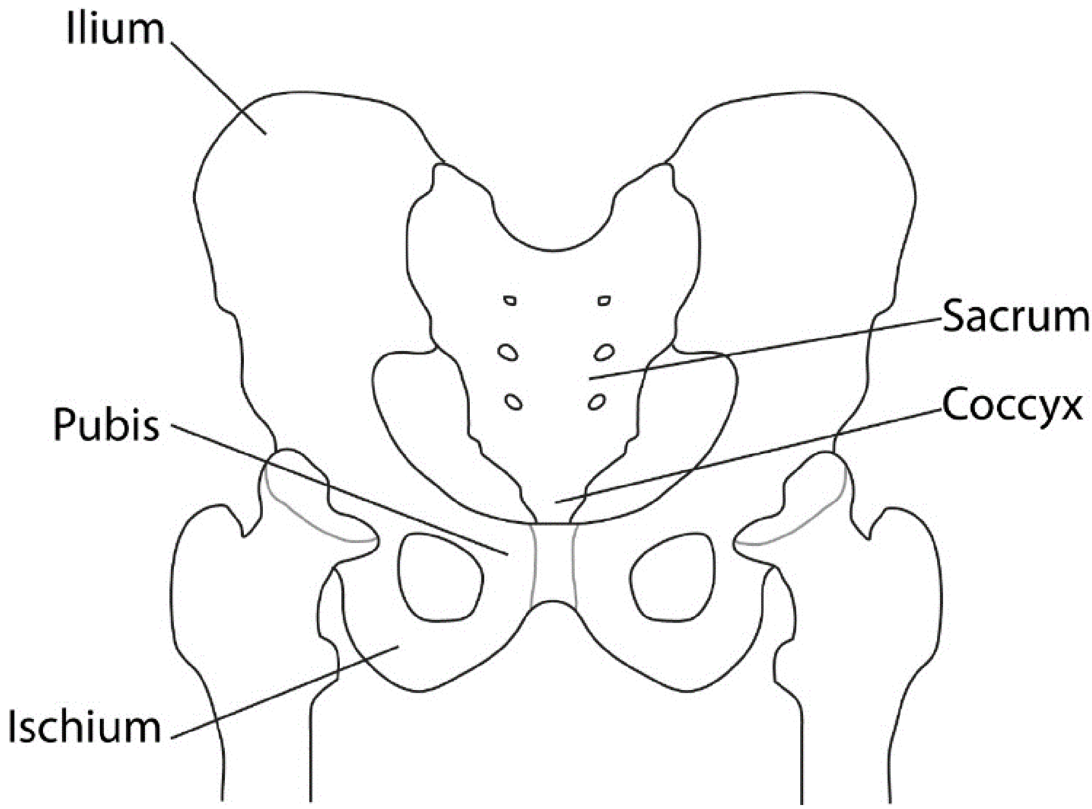

Figure 2.3 Major Components of the Pelvis

The pelvis is a ring-shaped structure composed of three fused structures, the ilium, ischium and pubis, which join to form the acetabulum. The medial aspect of the ilium is semi-rigidly attached to the sacrum, the most distal vertebra of the spine.

Makhsous, Lin et al. 2011). Trochanteric soft tissues are theorized to provide energy absorption during impact, which will be discussed in Section 2.5.3.2.

2.3 Hayes' Factor of Risk and the Nevitt and Cummings Hypothesis

The factor of risk (FoR) is a biomechanical tool used to predict likelihood of tissue damage, such as a fracture. FoR is a ratio of applied load to tissue tolerance (the force that can be sustained by the structure prior to damage). The applied load (and corresponding characteristics such as loading rate and direction) are influenced by activity, while the failure load is dependent on structural and material properties of the tissue in question. For example, climbing stairs has a FoR as high as 0.6 for the elderly, while lifting heavy loads or falling on the hip can have a FoR greater than 1.0

(Hayes, Piazza et al. 1991). FoR values greater than 1.0 indicate increased likelihood of damage to the structure.

The more complex Cummings and Nevitt Hypothesis (CNH, Figure 2.4) (1989) cites four biomechanical factors as contributing to the cause of hip fractures. These factors include, in order of temporal importance, a poor impact orientation, insufficient protective responses, insufficient "Local Shock Absorbers" (i.e. compliant soft tissue) and inadequate bone strength to resist fracture against the residual energy of the impact. Therefore, exposure to injurious impact

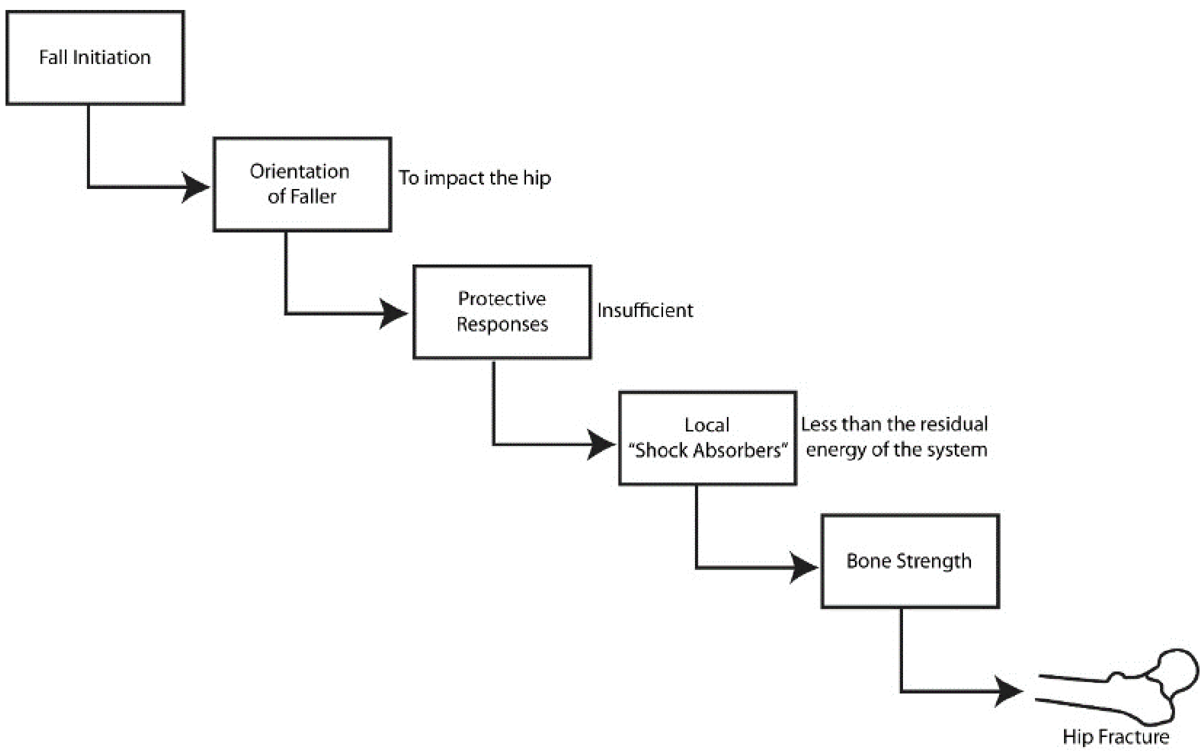

Figure 2.4 Cummings and Nevitt Hypothesis of The Causes of Hip Fractures

The Cummings and Nevitt Hypothesis introduces an order effect into the study of hip fractures, i.e., simply having poor bone strength or inadequate protective responses individually will not cause a fracture, but presented in a specific order, a fracture is likely. Further, if one of the initial conditions is met (e.g. orientation), a fracture can be prevented through the other components.

conditions are required rather than just poor bone quality or a lack of soft tissue for energy absorption.

While the FoR method offers simplicity, the CNH proposes four critical mechanical factors, as well as an importance of order between those factors. Neither method currently has immediate clinical utility, and only the QFracture prediction model includes both elements of the FoR, let alone all four factors of CNH (NCGC 2012). The FoR method is well accepted in biomechanical literature for several tissue types, while the CNH has been supported by research of actual falls in long-term care (Grisso, Kelsey et al. 1991; Yang, Schonnop et al. 2013) and serve as the basis for fall modeling efforts (Becker, Schwickert et al. 2012). This thesis will include elements of both the FoR (i.e. quantifying the numerator of the factor) and CNH (i.e. quantifying the orientation and local shock absorber components) methods of fracture prediction.

2.4 Fracture tolerance perspective

From the tissue tolerance perspective, the likelihood of survival of a tissue is dependent on both its material and structural properties, which are dependent on factors such as age, sex, and health status. Bone mineral density is the most commonly studied element within fracture tolerance, and is the only direct mechanical fracture tolerance element included in fracture prediction models such as FRAX and QFracture (Kanis, Hans et al. 2011; Lewiecki, Compston et al. 2011).

2.4.1 Mechanical Tolerance

The load sustainable by the proximal femur ranges from just shy of just over 900 N to greater than 10,000 N, depending on factors such as sex, body size, impact orientation, loading rate and bone quality (Cheng, Lowet et al. 1997; Lochmüller, Zeller et al. 1998; Lochmüller, Groll et al. 2002). Male femurs, during cadaveric testing of the proximal femur, can sustain an average of 1.5 kN (41%) more force than female femurs ($p<0.01$) (Cheng, Lowet et al. 1998; Lochmüller, Groll et al. 2002). Fracture tolerance is slightly (1 – 1.5 times) greater in a vertical loading direction (such as during standing) than a sideways loading direction (such as during a fall to the hip) (Lochmüller, Groll et al. 2002). Fracture tolerance is also rate dependent, with a 100 mm/s loading rate associated with a 20% increase in failure load and 100 % increase in stiffness within the proximal femur, relative to a 2 mm/s loading rate (Courtney, Wachtel et al. 1994). The compressive tolerance of the entire pelvis system ranges from 23-32.3% (Viano, Lau et al. 1989; Cavanaugh, Walilko et al. 1990; Etheridge, Beason et al. 2005) while the tolerance of the skeletal pelvis components alone is 8%. (Matsui, Kajzer et al. 2003) . In sum, femoral fracture tolerance is highly variable in magnitude, and dependent on material and structural properties, as well as how loads and strains are applied.

2.4.2 Assessment of fracture tolerance

Low bone mineral density is commonly associated with bone fractures, both in experimental testing, and in use as a clinical predictor of fracture risk. Under the type of loading applied during a fall to the hip, the failure load of the proximal femur is positively correlated with BMD, with r^2 values ranging from 0.64 to 0.88 for femoral neck BMD, r^2=0.72 for trochanteric BMD, and r^2=0.76 for total BMD (Cheng, Lowet et al. 1998; Pulkkinen, Jämsä et al. 2008). Cortical BMD within the femur is also positively, but weakly, associated with fracture strength (trochanteric, r^2=0.28; neck, r^2=0.07) (Cheng, Lowet et al. 1997). Of mechanically-relevant variables, clinical predictions of hip fracture risk have therefore focused on BMD as a patient-specific predictor of hip fracture risk.

However, use of radiation for imaging, expense and equipment access (and other factors, discussed in Section 2.4.3) are drawbacks of direct BMD assessment, so surrogate measures have been used to assess whether a patient is at high risk for osteoporosis. Femoral neck BMD is most strongly associated with sex (β=0.095, $p<0.001$), lean mass (β=0.083, $p<0.001$), and age (β=-0.052, $p<0.001$), and more weakly associated with fat mass (men, β=0.013, $p<0.001$, women, β=0.021, $p<0.001$) and total body height (β=-0.010, $p<0.001$) (Gjesdal, Halse et al. 2008). These associations may be appropriate for estimating groups of patients who fit into high-risk categories, such as frail, older females, but do little to predict fracture risk in the individual, or explain the mechanisms behind why some patients suffer from low bone density.

Total body mass, lean mass, fat mass and mass location all have different effects on bone strength. Kilogram for kilogram, lean mass has six times the effect on BMD than fat (Gjesdal, Halse et al. 2008). The correlation between total body weight and femoral BMD (r = 0.47, $p<0.001$) is slightly stronger than the relationship between BMI and BMD (r = 0.39, p=0.02) (Bouxsein, Szulc et al. 2007). Large quantities of adipose tissue are associated with high levels of parathyroid hormone and estrogen in both genders, both of which are associated with calcium metabolism outcomes which are detrimental to bone strength (Shapses and Sukumar 2012). The mass of non-weight-bearing body segments has a significant, but limited effect (e.g. for trunk fat mass, $p < 0.001$, but $r = 0.237$) on increase in BMD (Kuwahata, Kawamura et al. 2008). Dynamic loading of bone is associated with increases in bone strength rather than static loading, which is attributed to the viscoelastic properties of the tissue (Shapses and Sukumar 2012), which may explain the differential effect lean and fat mass on bone strength. However, estimates of BMD based on lean mass and bone mineral content (BMC) result in overestimates, suggesting an additional physiological mechanism associated with excess adipose and metabolic issues rather than a purely biomechanical relationship (Reid 2008). Therefore, the relationship between body size and BMD is not always stable, and therefore cannot be used to accurately predict bone strength in a patient.

Adding to this, relationships between body size and bone quality become even weaker when weight change is involved. In injury literature, a 5-10% decrease in body mass from the lifetime maximum doubles the risk of fracture (Langlois, Mussolino et al. 2001). Fleischer and colleagues (2008) reporting a strong correlation ($r = 0.90$, $p < 0.001$) between the amount of weight lost following surgery and the decrease in femoral neck BMD. However, extreme weight loss and weight loss surgery (such as gastric bypass) have also been associated with greater than expected decrease in BMD, potentially linked to poor nutritional status (Meyer, Tverdal et al. 1998; Carrasco, Ruz et al. 2009). A hypothesis regarding cyclic weight loss suggests that the slow process of bone metabolism is out of phase with weight change, resulting in time points during which a high weight but low BMD (or vice versa) is experienced. While general relationships exist between personal characteristics, such as body size, and BMD, the strength of these connections is too dependent on specific lifestyle and health factors to accurately predict bone quality for many patients.

Neither QCT or DXA imaging methods for the assessment of BMD perform alone as well as methods including geometric factors in the prediction of femur strength (Cody, Gross et al. 1999). Several skeletal geometry factors contribute to likelihood and location of fracture due to local differences in tissue tolerance. Hip axis length (Broy, Cauley et al. 2015), along with the angle between the femur neck and shaft, and femoral neck width (Pulkkinen, Eckstein et al. 2006; Pulkkinen, Jämsä et al. 2008; Pulkkinen, Saarakkala et al. 2013) have been identified as potentially important geometric factors for hip fracture prediction. Even in a simplified single-degree-of-freedom model of an impact to the hip, loads applied to the proximal femur are directed perpendicular to the femoral shaft, and at an angle (approximately 50°) to the femoral neck. This highlights the importance of the structure of the proximal femur in addition to bone quality. Further, how femoral geometry and impact dynamics interact to affect the moments, stresses and strains generated during an impact would provide a more holistic understanding of hip fracture mechanics. However, the importance of skeletal geometry is dependent on the direction, magnitude and distribution of loads applied to the hip—that is, the generation of stress within the femur is dependent on the loading at the skin-floor interface.

2.4.3 Limitations of fracture tolerance assessment and treatment

There are limitations in clinical assessment and treatment of poor bone quality. Access to BMD assessment is limited by location, physician prescription and cost. While BMD test access has improved, less than 20% of women in Ontario over the age of 70 undergo the test. (Jaglal, Weller et al. 2005). This low rate of diagnostic imaging is not necessarily applied to the appropriate patients either—fewer than 25% of a cohort of women with osteoporotic fractures had received BMD assessment or treatment prior to their fracture (Blecher, Wasrbrout et al. 2013). Risk factors for not receiving BMD assessment include good health (three or fewer comorbid conditions), young age and male gender (Riggs and Melton 1995), with women receiving a DXA scan ten to sixteen times more frequently than men (Jaglal, Weller et al. 2005). DXA imaging is also limited by the maximum table capacity of the device, as well as the image window, which limits its use in obese patients (Rothney, Brychta et al. 2009). Even when BMD assessment is prescribed, the method has better predictive capability over the short term (<5 years) than the long term, suggesting that repeated scans are required to maintain an accurate assessment of fracture risk (Stone, Seeley et al. 2003). Finally, only 37-40% of long term care residents with osteoporosis receive pharmaceutical treatment (including dietary supplements, such as Vitamin D or Calcium) (Colon-Emeric, Lyles et al. 2007; Giangregorio, Jantzi et al. 2009). In an extreme case, only 12% of patients who had already presented with a fragility fracture had been diagnosed with low BMD and begun treatment after six months (Bessette, Ste-Marie et al. 2008).

There are limitations to who is, and who can be, diagnosed with low BMD via current imaging and diagnostic techniques, and only some of those who should be treated for low fracture tolerance are. While several risk factors for osteoporotic fracture are captured by current models, the predictive capability may be improved by the addition of factors which influence the applied loads portion of the Factor of Risk equation. For example, an older adult with very low bone density or several bone-quality-related risk factors would typically be flagged by a fracture assessment screening; however, they may benefit from the force attenuation provided by trochanteric soft tissue, and have lower fracture risk than predicted by current models. Conversely, an older adult with only moderately low bone density and few risk factors may not be screened as high-risk for fracture; however, understanding how low trochanteric soft tissue thickness or falling configuration might increase the patients fall risk may help guide more appropriate interventions. Additionally, further interventions from the applied load perspective, such as introducing safety floors in high-fall-risk areas, may present solutions which reach a greater proportion of those at risk for hip fracture.

2.5 Applied Load Perspective: Importance of Fall Mechanics

Mechanical prediction of injury can be simplified to a ratio of the applied load to the expected service load of a biological structure (Hayes, Piazza et al. 1991). Even in healthy, young adults, (ages 15-49), the impact associated with a fall from standing height can be great enough to cause hip fracture(Kannus, Leiponen et al. 2006). However, the most commonly used methods of fracture prediction such as QFracture or FRAX take into account only fall history as a binary variable, or no element of fall mechanics at all (NCGC 2012). The World Health Organization suggests a correction of +30% risk for each fall within the last year (up to five falls), to correct for underestimation of fracture risk due to exclusion of fall history (Masud, Binkley et al. 2011). The Garvan Model employs both fall history (over the last 12 months) as well as low-trauma fracture history (after age 50); however, while the effect of including these factors results in significant improvement in fracture prediction accuracy, they are given limited weighting relative to other factors such as age and BMD, particularly in men (Nguyen, Frost et al. 2008). In the factor-of-risk model, the applied loads are equally as important as the strength of the bones impacted, but prediction of such loads is not a simple task.

The amount of energy available to be applied to an impacting segment is determined by simple mechanics; assuming constant gravity and stiffness, a pelvis with a larger mass will, in general, impact with greater force. Holding the mass of the pelvis constant, as would be the case when comparing fall scenarios within the same faller, energy is determined by the initial height of the pelvis. In a simplified freefall scenario, the initial height is directly related to velocity of the segment at impact by the relationship:

$$\boldsymbol{v} = \sqrt{\boldsymbol{2gh}} \qquad (2.1)$$

Therefore, the height from which a person falls is critical for the prediction of impact velocity and the resulting force. The simplest estimate of hip impact velocity during a fall is based on full body height (h) (Dufour, Roberts et al. 2012), where free-fall height is estimated at 0.5*h. This estimation method assumes that the pelvis is located at the center of the total body height, experiences a 90° rotation about the anterior-posterior axis, and undergoes a freefall with no control mechanisms or interference from other objects. For a female of 1.64m in height, this would result in an impact velocity of 4.01 m/s; for a male of 1.75m in height, this would result in a 4.14 m/s impact velocity. However, real-world falls rarely result in vertical hip impact velocities as high as would be expected based on this prediction. Factors such as starting condition (standing, sitting, lying down, or transitioning between states), neuromuscular control over loss of balance and descent, or voluntary and involuntary impacts by other body segments can all affect the impact velocity and kinetic energy associated with a fall. A more complicated model, the inverted pendulum, assumes the feet remain stationary, and act as a pivot point for the rest of the body to fall as a single pendulum unit. This model acknowledges the involvement of non-vertical movement and impact characteristics. However, real-life falls in older adults have pelvis impact velocities on average 46% lower than the simple freefall model, and 38% lower than the pendulum estimate (Choi, Wakeling et al. 2015). However, due to the limitations of capturing and analyzing data during accidental falls (Section 2.6.1), these models serve as an acceptable method of estimating the energy available during a worst-case scenario.

Despite these limitations, several studies have been conducted which examine falling scenarios.

2.5.1 Preceding Circumstances and Causes of Falls

Of circumstances surrounding falls in older adults, falls from standing height are not only frequent, but are also associated with a higher impact velocity than those from beds or chairs. Simply walking forward accounts for 24% of all falls in long-term care (Robinovitch, Feldman et al. 2013), while standing quietly, initiating walking, walking backwards, sideways or turning, or reaching while standing account for a further 49% of all falls in the older adult population. Transitioning between seated and standing positions is associated with a further 22% of falls (Robinovitch, Feldman et al. 2013) and falls from a seated position are associated with 5% of falls. The rates of falls in each of these categories is influenced by factors such as health status and activity level. A common example given is that older adults who spend less time in active standing or ambulating activities experience lower exposure to higher-velocity fall conditions. However, spending a greater time in active standing-height activities may better prepare an older adult to respond to balance perturbations than one who spends a large amount of time seated or in bed (Armstrong, Spencer et al. 2011). Falls from standing height, therefore, represent a diverse cause category in both exposure and mechanics.

Falls from standing height can be subdivided into several categories, which may increase the energy available during impact relative to a simple fall from standing height. Incorrect weight transfer is associated with the greatest number (41%) of falls in older adult long-term care residents (Robinovitch, Feldman et al. 2013), but does not carry the large non-vertical velocity components that tripping or stumbling (21%), slipping (3%) or a hit or bump (11%) might (Robinovitch, Feldman et al. 2013). Stumbling events carry more than twice the joint contact forces at the hip than level walking (Bergmann, Graichen et al. 2004), which are below the fracture threshold of the proximal femur (Taddei, Palmadori et al. 2014) but are also much greater forces and moments which must be controlled to prevent the center of mass from moving beyond controllable limits. Fall causes with backwards, sideways or straight-down initial motion (such as incorrect weight transfer or slip) are 10-15 times more likely to cause a hip fracture than fall causes with forward motion (such as tripping) (Hwang, Lee et al. 2011). Not only do these higher-velocity fall causes have the potential to cause greater amounts of energy available at impact, they may also precede a lack of control over the descent phase of the fall.

Exposure to different environmental conditions have a significant effect on likelihood of fall and injury risk. Women who land on a hard surface are more 2.8 times likely to suffer a fracture than those who fell on a softer surface (Nevitt and Cummings 1993). While falls in older adults occur fairly evenly between indoor (53.3%) and outdoor (46.7%) environments, personal characteristics in part govern where the fall will occur (Kelsey, Berry et al. 2010). Outdoor fallers tend to be younger, healthier active, and male, while indoor fallers tend to be older and more disabled, with more comorbid conditions and medications. This is reflected in differences in body mass index, with normal- or underweight (BMI <25) fallers incurring exclusively indoor (28.2%), outdoor (32.3%) and indoor and outdoor (39.3%) incidents fairly evenly, while obese fallers (BMI >30.0) experiencing indoor falls (53.6%) more than twice as often as outdoor falls (23.7%) or both indoor and outdoor falls (22.6%). Indoor and outdoor falls are associated with different environmental factors related to both fall causation (e.g. immovable sidewalk and curb trip hazards outside compared to more movable furniture trip hazards indoors) and impact surface (e.g. stiff concrete vs. compliant carpet) which will affect injury likelihood.

Body size also appears to have an effect on the type of event which causes a fall. Stumbling rates in community-dwelling obese older adults (32%) are more than twice that of normal-weight older adults (14%) (Fjeldstad, Fjeldstad et al. 2008; Madigan, Rosenblatt et al. 2014). Stumbling is defined in these papers as ‘a loss of balance that did not result in a fall to the ground or other lower level’ (Madigan, Rosenblatt et al. 2014), however, other authors (Robinovitch, Feldman et al. 2013; Yang, Schonnop et al. 2013) include stumbles as a potential fall cause. While overall rates of trips or slips does not differ between obese and normal-weight groups, rates of falls following these events (rather than recovered events) are higher in obese older adults than normal-weight older adults (Madigan, Rosenblatt et al. 2014) (Appendix 1). Obese older adults trip slightly more frequently when obstacle heights are between 2.4 and 4.2 centimeters (Garman, Franck et al. 2015). Therefore, not only fall cause, but recoverability, are important considerations when analyzing the events preceding a fall, and circumstances which are avoidable or recoverable by some older adults may not be by others.

The circumstances preceding falls become a critical link to predicting impact characteristics. Initial height and velocity of the center of mass influence how much energy is available prior to impact, and the primary direction of the load vector. For example, a faller who trips while walking will likely continue to have a large forward velocity during the fall. If this faller then lands in an (unlikely) perfectly lateral impact configuration, there will be a large normal force vector component due to the decrease in height, as well as a large shear component directed inferiorly through the femoral neck due to the forward motion. In contrast, an older adult who suffers a loss-of-consciousness might fall directly downwards from a standing position. This may change the landing configuration to a posterior orientation, which would expose other anatomical structures, such as the coccyx or lower spine, to injury rather than the proximal femur.

While these relationships have been explored to the extent described above, and in Appendix 1, it is more important to consider, in the context of this thesis, how preceding circumstances have been considered in experimental studies of fall-related injuries, and what effect they have on the external validity of these studies. In order to maintain rigid control over such experiments, as well as reduce the chance of injuring participants, most experimentation has focused on highly repeatable experimental protocols (described more thoroughly in Section 2.6.2) which are low in energy and limit non-vertical impact characteristics. Additionally, the vertical ground reaction force has been the primary outcome used to define whether or not an injury is likely to occur. The work presented in this thesis aims to incorporate non-vertical impact characteristics in order to improve understanding of the direction and point of application of impact loads during a fall incident.

2.5.2 Impact Characteristics

2.5.2.1 Impact Velocity, and Acceleration, and Loads

Observed real-world vertical hip impact velocities range from 1 to 4.0 m/s (Van den Kroonenberg, Hayes et al. 1995; Nankaku, Kanzaki et al. 2005; Feldman and Robinovitch 2007; Choi, Wakeling et al. 2015) . Despite the appearance of 1 m/s as a potentially innocuous impact velocity, impacts of this velocity are associated with impact forces exceeding the lower range fracture thresholds in older adults (Bouxsein, Coan et al. 1999; Levine, Bhan et al. 2013). Horizontal impact velocities average 1.16 (SD 1.42) m/s at the pelvis, less than half the horizontal velocity of impacts to the head (2.64 (1.12) m/s) (Choi, Wakeling et al. 2015). Anthropometric characteristics such as total body height and greater trochanter-lateral malleolus distance are strongly correlated (all $r > 0.70$) with impact forces for falls in lateral, posterior and posterolateral fall directions, likely due to their link with increased impact velocity (Nankaku, Kanzaki et al. 2005).

Accelerometer-based analysis of fall characteristics has been used to in both experimental and real-world settings to improve upon the challenges posed by optical methods. In the field of wearable sensors, for example, accelerometers can be used to determine whether body-worn accelerometers could be used to identify several types of falls (syncope, tripping, sitting on "air", slipping, lateral fall and rolling out of bed) and resulting impact configurations (Kangas, Vikman et al. 2009; Kangas, Vikman et al. 2012). When comparing real-life falls to simulated experimental falls, the former resulted in multiple impact signatures (e.g. a hand and a hip impacting separately, or a hip impacting, lifting slightly and impacting again) rather than a single, distinct impact. Three of the five real-life falls had impact velocities less than 1.5 m/s, which was lower than expected based on the experimental results, but similar resultant impact accelerations of 3-5 g at impact. Only the fall resulting in hip fracture had a high impact velocity (5.6 m/s) and a pre-impact acceleration signature detectably different from normal activity.

In experimental falls with young, healthy adults, impact velocities typically range from 2-3 m/s (Hsiao and Robinovitch 1997; Robinovitch, Inkster et al. 2003). Anterior perturbations (2.55±0.85) and lateral perturbations with anterior torso rotations (2.45±0.77) have lower impact velocities than lateral perturbations with posterior torso rotations (2.95±0.25) (Hsiao and Robinovitch 1997; Robinovitch, Inkster et al. 2003). Differences between experimental and real-life fall impact velocity may be attributed to initial starting position and activity. Typical fall experiments begin with the participant standing upright, and may be instructed which strategies (if any) to use to control their descent. Young, healthy participants may also anticipate little risk during a fall onto a padded surface, which may influence their descent control and impact characteristics. Therefore, while experiments in younger adults may provide insight into common patterns regarding impact velocity, they may not provide the best absolute estimates of such characteristics.

Generally corresponding with impact velocity, backwards falls have the greatest impact loads, ranging from 3,250N (Nankaku, Kanzaki et al. 2005) to 7500N (Sran and Robinovitch 2008). Directly lateral falls have lower peak loads (2,251 (442) N) (Nankaku, Kanzaki et al. 2005), which can be attributed to several sources. The contact of other body segments, such as the arm or shoulder, prior to the hip, can increase or decrease peak forces at the hip (discussed in Section 2.5.3), however, the posterior falling direction has been cited as a difficult configuration to brace against using the arms (Nankaku, Kanzaki et al. 2005). Contributions of the torso to effective mass during impact would be dependent on torso bracing and inclination angle. In a successful bracing attempt, the torso would be constrained by the distal contact (thigh) and proximal contact (upper limb), distributing the load between the impacting segments (Robinovitch, Hayes et al. 1997), however, magnitude of this effect is only ~15% in a "relaxed" state. In finite element simulation of impacts to the pelvis (with no torso), simply increasing the pelvis inclination angle between 0° (i.e. falling flat on the back) to 80° (nearly seated) increased peak resultant impact force less than 8 kN to nearly 17 kN, highlighting the importance of pelvis configuration during impact (Majumder, Roychowdhury et al. 2009). As well, estimated effective mass (based on total body mass and inclination angle) has a substantial link to both impact velocity (i.e. a control of system energy) and impact force (Sarvi, Luo et al. 2014). In an unsuccessful bracing attempt, the torso is unsupported by the upper body, directing the load associated with its mass distally towards the hip. Differing control strategies during descent can also have varying effects (also discussed in Section 2.5.3). Between these two anatomical directions, unbraced posterolateral falls are associated with a greater impact velocity (2.5 (0.35) m/s), but lower mean impact force (2497.7 (457.0) N) than directly posterior falls, indicating that there is an interaction between impact velocity and other components, such as compliant soft tissue or pelvis orientation, in the determination of peak force.

Within the literature examined, the vertical components of fall-related impacts have been the primary interest of previous explorations of fall-related injuries. However, given the non-vertical velocity and acceleration components preceding real-life impacts, such as initial forward velocity during walking, or rotation of the pelvis around a stationary foot position, it is clear that shear forces, rotational acceleration of the pelvis, and other components beyond a strictly vertical impact configuration may be important factors to consider when analyzing impacts. Some of these factors will be explored within Study 5.

2.5.2.2 Impact Configuration

Impact configuration is a critical component in assessing which body segments are exposed to potential injury. Directly forward falls typically increase risk for head, neck and arm injuries, but are protective against hip fractures (Groen, Weerdesteyn et al. 2008). Similarly, directly backwards falls also reduce the risk of hip fracture, but through a different mechanism. Even though backwards falls are associated with a greater amount of energy (due to greater impact velocity and effective mass) at impact, a posterior impact orientation places the hip under the protection of greater soft tissue absorption of energy (Groen, Weerdesteyn et al. 2008). A 20° anterior rotation of the pelvis during impact is associated with a 16% reduction in peak force compared to a lateral impact configuration, and a 24% reduction compared to a posteriorly-rotated impact configuration; in absolute numbers, this is a reduction of approximately 250 N (Choi, Hoffer et al. 2010). There is an interaction of complex anatomical structures which influence these loads, with positions where the proximal femur is least protected by skeletal or soft tissue components producing the riskiest scenarios.

How the load is directed through the proximal femur has a strong effect on fracture risk. The orientation of the femur in the posterolateral fall direction is associated with the greatest risk of fracture (Ford, Keaveny et al. 1996; Keyak, Skinner et al. 2006), while load points stressed during normal activity, such as walking, are able to sustain more than twice the load (Keyak, Skinner et al. 2001; Keyak, Skinner et al. 2006). The fracture thresholds of these two orientations are linearly related ($r=0.91$, $p<0.001$)—i.e. a weaker femur will fracture at a lower threshold, regardless of orientation. This highlights exercise-based intervention as a promising strategy for reducing fracture risk (Keyak 2000; Keyak, Skinner et al. 2001). During a fall, a change of 30° in loading direction, from anterolateral to posterolateral, is associated with a 24% decrease (from 4050 (900) N to 3060 (890) N) in fracture tolerance—a similar decrease in fracture tolerance to that associated with aging from 25 to 65 years (Pinilla, Boardman et al. 1996). A loading direction more perpendicular to the frontal plane of the proximal femur (associated with a posterolateral impact) is associated with approximately half the tolerance of a load directed parallel to, and through the femoral neck (Keyak 2001). These studies give insight into the sensitivity of the proximal femur to loading direction, and help explain why impact configurations might be associated with injury outcome and fracture location. However, the load inputs are based only on estimates of what the point and direction of application might be rather than data from actual impacts. Additionally, these studies only included isolated femurs, and not the femur *in situ* within the pelvis. It is unclear whether the pelvis, acting as a spring in series with the femur, would change loading direction, or how directional loading of the femur might change its orientation within the acetabulum (i.e. loading direction may be dynamic).

A few studies have instead focused on loading of entire pelvis system. Directly lateral impacts to a hip flexed to approximately 90° (such as in a sideways collision in an automobile) are more likely to result in fracture to the pelvic ring and acetabulum rather than the more lateral proximal femur (Beason, Dakin et al. 2003; Etheridge, Beason et al. 2005). With a similar degree of hip flexion and an impact to the distal femur (such as in a forwards collision in an automobile), hip dislocation and damage to the posterior acetabulum are common initial injuries (Sahin, Karakas et al. 2003), with associated avascular necrosis of the proximal femur resulting in secondary hip fractures after the initial event (Alonso, Volgas et al. 2000). While not all of these configurations are directly relatable to those resulting from a fall (differing in hip orientation angles, inclination angles and loading direction), they illustrate the importance of pelvis-femur configuration during an impact scenario.

Control of the muscles and joints surrounding the pelvis has the potential to affect the stiffness of the pelvis system, and corresponding dynamic outcomes. In a recent study, Choi and colleagues (Choi, Cripton et al. 2015) investigated the effect of knee boundary conditions (i.e. the femur not affixed to the impact surface, firmly affixed to the impact surface or linked to the impact surface via a spring) and simulated muscle activity (*gluteus maximus*, *gluteus medius* and *adductor magnus*) using a surrogate pelvis and inverted pendulum impact protocol. Simulated muscle activation had a significant effect ($p<0.0005$) on all outcome variables (shear stress, compressive stress, tensile stress and peak bending moment) except for peak force; specifically, increasing the force simulated by *gluteus maximus* and *gluteus medius* to 1200 N decreased peak compressive stress by 24% and shear stress by 56% relative to a 400 N contribution of those muscles. There was also a critical effect of knee boundary conditions, with the free knee condition (i.e. not affixed to the impact surface) and spring knee conditions reducing peak stress, force and bending moment in all directions ($p<0.005$). The free knee condition reduced peak compressive stress by 40%, peak tensile stress by 51%, peak shear stress by 45%, peak shear force by 45%, peak bending moment by 45%, and peak axial force by 25% compared to the firmly fixed knee condition. However, the total force reduction between the free and fixed knee conditions was only 5%, suggesting that the conditions have an effect of load redistribution rather than pure reduction. Under static conditions, activation of the muscles surrounding the pelvis results in altered pelvis stiffness ("stability"), particularly for females (Pool-Goudzwaard, van Dijke et al. 2004; Pel, Spoor et al. 2008). However, Gnat et al. (Gnat, Spoor et al. 2013) found that simulated tension of the abdominal muscles (*transversus abdominus*) did not result in increased stiffness of the pelvis—likely because under lateral loading of the pelvis, tension applied to the abdominal muscles by the skeletal structures is reduced.

Finally, the positioning of the torso is a critical element of impact configuration, which has a significant effect on the effective mass, or how much mass from the body is directed over the hip during an impact. In a two-link (leg and trunk segment) model, a vertical torso at impact is associated with more than double the effective mass of an impact with the torso held at 45° from vertical (52.5kg vs. 24.5 kg for a 95th percentile female) (Van den Kroonenberg, Hayes et al. 1995). A relaxed-muscle descent is associated with a 38% more vertical torso during impact than when muscle activation is used to control descent (van den Kroonenberg, Hayes et al. 1996).

2.5.3 Protective Responses and Mechanisms

Several techniques, both voluntary and involuntary are utilized by fallers to reduce or redistribute the energy of an impact.

2.5.3.1 Active Protective Responses

The effect of attempting to control the descent during a fall can have conflicting results. For example, an appropriate generation of power at the knee joint can reduce impact velocity experienced by the pelvis prior to impact. Theoretically, eccentric contraction of leg muscles during descent could provide up to 150 J of energy absorption during descent (Robinovitch, Chiu et al. 2000; Sandler and Robinovitch 2001). However, an overly stiff or lax response at the knee would have the opposite effect. Briefly, assuming the feet of the faller remain stationary (i.e. not a slip or stumble), an overly stiff control (i.e. too much eccentric contraction and power generation) of the hip and knee joints would be a poor response to a lateral or anterior-posterior balance perturbation, and cause the pelvis to fall similarly to an inverted pendulum, with high rotational acceleration. This type of fall, which includes large horizontal excursions of the COM, has been theorized to be a risky impact scenario due to the lack of energy absorption at the joints of the lower limb during descent (Robinovitch, Chiu et al. 2000). An overly lax control of the hip and knee joints (i.e. crumpling; too little eccentric contraction, too little power generation, or too slow a reaction) would handle the lateral and anterior-posterior perturbations more successfully, but result in with high linear acceleration. A fall scenario with a lower risk of injury to the hip could be produced by moderating both linear and rotational accelerations through generation of appropriate strength and power. In a comparison of posterior falls, when participants used a squat starting position, they were able to reduce their impact velocity by 18% and energy at impact by 43% compared to a pendulum-style fall; however, participants performed more poorly when a greater initial lean angles was used, the authors argued that the magnitude of reduction in velocity is dependent on what stage of descent the squat is achieved (Robinovitch, Brumer et al. 2004). A modeled analysis found that high levels of activation of muscles surrounding the ankles and hips, but little activation of those surrounding the knees, provided the “best-case” impacts (i.e. lowest energy at impact), with strength a critical factor (Sandler and Robinovitch 2001). However, generation of force at the knee just prior to impact resulted in a transfer of 90 J to horizontal kinetic energy rather than vertical. Therefore, control of descent is dependent not only on the magnitude of strength and power generated in multiple joints, but also how well the faller is able to generate an appropriate response and response timing without over- or under-reacting to the perturbation.

When assessed using electromyography (EMG), inexperienced fallers use greater, or less effective, muscle activation to employ protective techniques such as eccentric control of descent or bracing (Weerdesteyn, Groen et al. 2008). In a study of muscular activation during experimental falls in the lateral, posterolateral and posterior directions, only rectus femoris activation during lateral falls was strongly correlated ($r = 0.74$) with impact load, with impact velocity a major component of this decrease (Nankaku, Kanzaki et al. 2005). Bracing of the muscles surrounding the pelvis and trunk also have the potential to change the energy of the impact by increasing the stiffness of the impacting segments (in the sense of a mass-spring model, increasing the stiffness, k, of the system). In another study, a “tensed” fall (activating the muscles surrounding the hips) from kneeling height, peak forces at the hip were significantly greater (2.76 (0.83) * BW) than relaxed falls (2.69 (0.68) * BW) (Sabick, Hay et al. 1999). For a female of 65kg body mass, however, this only represents a decrease in peak force of 45 N (from 1760 to 1715N), which may be of limited clinical significance. This difference, however, may be more important for understanding the magnitude of effect different types of soft tissue (i.e. neurologically active muscle vs. depth of soft tissue) have on pelvic stiffness and peak forces during impacts to the hip. However, experimental results indicate that the effect of this is mixed or limited, at best, and dependent on other variables such as falling configuration (Robinovitch, Hayes et al. 1991; Robinovitch, Hayes et al. 1997; Choi, Cripton et al. 2015).

Bracing against impact using the upper extremity reduces hip impact forces through two mechanisms: decreasing the impact velocity of the pelvis and providing an alternative outlet for the kinetic energy of the fall. In young adults, impacts to the hands occurs just over 100 ms before impact to the pelvis (Hsiao and Robinovitch 1997). Bracing using the upper extremity is more common in young older adults, and decreases in effectiveness in older adults (Sran, Stotz et al. 2009) or in those with high BMI (Compston, Watts et al. 2011). Fallers with high-BMI also suffer a greater rate of elbow and proximal humerus fractures (Johansson, Kanis et al. 2014), which may be a result of less effective bracing, and a greater amount of energy applied to the upper arm rather than the hand and forearm. Low triceps strength (Nevitt and Cummings 1993) is associated with a greater risk of hip fracture ($p<0.05$), while a posterolateral fall direction is cited as a falling configuration in which fallers are unable to use the upper extremity to brace against (Nankaku, Kanzaki et al. 2005).

However, the use of arms to brace against impacts to the hip has conflicting results with regards to reduction of peak loads at the hip (Sabick, Hay et al. 1999; Groen, Weerdesteyn et al. 2008; Weerdesteyn, Groen et al. 2008). Martial-arts trained young-adult participants were able to reduce their mean impact velocity from 1.37 (0.12) m/s to 1.18 (0.12) m/s, and peak force from 4.14 (0.43) N/kg*g to 2.83 (0.51) N/kg*g (Groen, Weerdesteyn et al. 2008). However, the magnitude of the protective effect of this technique was reduced in inexperienced fallers following a 30-minute training period (Weerdesteyn, Groen et al. 2008), which poses a challenge for the introduction of the technique into exercise and fall-prevention programs for older adults. In a study of real falls in long-term care, bracing with the hands were associated with impact velocity of 2.19 (0.61) m/s compared to 2.41 (0.85) m/s, a more realistic 9.1% decrease in impact velocity rather than the 13.8% reduction found by Groen and colleagues. Further, a more upright torso position is associated with an increase in peak force and pelvic stiffness compared to an impact in which the sagittal planes of the torso and pelvis are parallel to the floor (Robinovitch, Hayes et al. 1997). While bracing against impact may reduce hip impact forces in some fallers, bracing successfully is a challenge for others, and may actually increase loads at the hip.

Involuntary impacts by other body segments also represents a significant source of variance in loads applied to the hip during a fall. Success of these fall-arrest or redistribution attempts varies based on both age and body composition. Impacts to the hip can be arrested by preceding impacts to the knee (Feldman and Robinovitch 2007), which greatly decreases the vertical impact velocity of the pelvis, as well as changes the rotational acceleration of the pelvis during a fall. Impacts to the knee are slightly more common in older adults with high BMI than those with normal or low BMI (Appendix 1). However, in a pelvis release paradigm, in which the participant impacts in a side-lying position, only 15% of the impact load was distributed to body segments other than the pelvis (Robinovitch, Hayes et al. 1997).

To summarize, there are several protective responses that can reduce the energy applied to the hip during a fall, either through reducing impact velocity or redistribution. However, several of these techniques may actually increase injury risk. Others require special skills or training that may make them unrealistic for older adults to employ during an emergency situation. Regardless, these may be valuable configurations to include in future experimental testing and modeling attempts.

2.5.3.2 Soft Tissue Energy Absorption

Soft tissue energy absorption has frequently been cited as a cause of different hip fracture rates between fallers of varying body composition (Robinovitch, Hayes et al. 1991; Robinovitch, McMahon et al. 1995; Beck, Petit et al. 2009). In an *in vitro* study of soft tissue energy absorption, a 1 mm increase of soft tissue thickness is associated with a 70 N decrease in impact force, and a 1.7 J increase in energy absorption during a simulated hip impact (Robinovitch, McMahon et al. 1995). In a case-control study of 49 cadaveric specimens, trochanteric soft tissue thickness was lower ($p=0.04$) and estimated peak force, adjusted for estimated soft tissue-related force attenuation, was higher in fracture cases ($p=0.07$) (Bouxsein, Szulc et al. 2007). In magnitude, a 1-SD decrease in soft tissue thickness was associated with 1.8-fold increase in hip fracture risk; even after adjusting for femoral BMD, a 1 SD decrease in soft tissue thickness is still associated with a 1.4-fold increase in fracture risk (Bouxsein, Szulc et al. 2007). Inclusion of a soft tissue component (estimated after Robinovitch, et al. 1995, described above in prediction of peak force (i.e. attenuated peak force) decreased risk by approximately 50%. Therefore, in controlled experimental studies, soft tissue has both a mechanical effect as well as provides a reduction in hip fracture risk.

However, in application, soft tissue thickness alone has not been as strong a predictor of fracture risk as BMD (Bouxsein, Szulc et al. 2007). Further, in actual fall-related injury cases, trochanteric soft tissue thickness cannot be used to differentiate between male fracture cases and controls (Nielson, Bouxsein et al. 2009). These limitations have sources in both imaging and application. During a DXA estimate of soft tissue depth (measured at convenience alongside BMD and femoral geometry assessment), the soft tissues are displaced laterally, resulting in an overestimate of depth (Maitland, Myers et al. 1993; Nielson, Bouxsein et al. 2009). Decreases in trochanteric soft tissue stiffness (2.9-fold) and damping (3.5-fold) between younger- and older-adult women may be linked to a lower-energy “bottom out” point, i.e. the tissues reach maximal deformation early in the impact phase, resulting in more energy transmission to the skeletal structures(Choi, Russell et al. 2014). Changes in hip flexion and abduction angle during impact may reduce the depth of soft tissue available for energy absorption (Levine, Minty et al. 2015). Further, while trochanteric soft tissue has been found to dissipate the energy of an impact to the hip by 50-78% in normal-weight older adults, this still leaves quantities of energy and loads transmitted to the proximal femur above the fracture threshold of some older adults (Robinovitch, McMahon et al. 1995). While a linear, two-dimensional mass-spring model may provide a basic assessment of the capabilities of force attenuation properties, it is more likely that the three-dimensionality and complex geometry of the anatomical structures plays a much larger role than can be captured with such a model.

Soft tissue overlying impacting structures has also been associated with decreased pressure over critical anatomical elements. In a study of impacts to the palm, while peak force and peak pressure were both associated with BMI, soft tissue thickness in the palm region was not, suggesting that, for impacts to the palm, increased torso mass has a greater effect than soft tissue energy absorption (Choi and Robinovitch 2011). However, peak pressure did differ between padded (5 mm thick protective foam) and unpadded conditions and both BMI- and padding-related decreases in "danger zone" peak force (directly over the scaphoid). These "padding" elements can result in a critical shunting of pressure to more structurally stable anatomical areas (away from the scaphoid, distributed along the arch formed by the carpals), with the thickness of soft tissue positively correlated with the distance between the danger zone and location of peak pressure (Choi and Robinovitch 2011).

Similar shunting of force away from the danger zone (in this case, the greater trochanter) is observed during impacts to the hip (Choi, Hoffer et al. 2010). During impacts to the hip, a 20° anterior rotation is associated with a 30% reduction in peak pressure compared to a lateral impact, and a 35% reduction compared to a 20° posterior rotation. This difference is much greater in participants with high BMI than participants with low BMI, providing a 65% reduction in peak pressure when comparing an anteriorly-rotated impact position to a directly lateral position (Choi, Hoffer et al. 2010). Differences between BMI groups range from 50-75%, with differences greatest at the anteriorly-rotated position, and smallest at the lateral position (Choi, Hoffer et al. 2010).

However, beyond BMI, it is unclear how more specific elements of body composition (e.g. depth of adipose and muscular components over the greater trochanter), impact configuration or skeletal geometry (e.g. pelvis height) affect the pressure distribution and other impact dynamics during impact. While more general information about body composition is helpful in predicting which BMI group will have the greatest rate of hip fractures, a more complex investigation would help explain the mechanisms behind the phenomenon.

2.5.3.3 Effective (System) Stiffness

In a complex system such as the pelvis, there are several components that contribute to a single estimate of pelvic stiffness. Skeletal components, including the femur, sacrum and pelvis, have several joints of variable stiffness. The ilium, ischium and pubis, as described in Section 2.2, have rigid, relatively immovable joints to one another. Semi-rigid joints exist at the pubic symphysis and the sacroiliac joint, the stiffness of which is controlled by the cartilage and ligaments that support them. The femur is connected to the pelvis at the flexible hip joint with several ligaments, with cartilage covering both the pelvic and femoral surfaces of the joint, and the acetabular labrum. Finally, though bone is commonly thought of as rigid, the structure of the pelvis and proximal femur are fairly flexible (Beason, Dakin et al. 2003). Soft tissue components also contribute to total pelvic stiffness. While the greater trochanter is not directly overlaid by muscle, it is surrounded by muscular attachments (e.g. *gluteus maximus*), and non-muscular, thick fascia band of the iliotibial tract. Adipose and skin tissue, as well as the fluid-filled trochanteric bursa, fill the balance of the thickness of tissue covering the proximal femur.

Based on the basic relationship between the properties of a linear spring,

$$\boldsymbol{k = AE/L} \tag{2.2}$$

the stiffness of a spring is dependent on its cross-sectional area (A), elastic material properties (E) and change in length (L). Variables L and A may be related to elements of body composition such as skeletal geometry and soft tissue thickness. The skeletal components are likely to have much stiffer elastic properties than the trochanteric soft tissue or connecting ligaments, and is likely the source of only a small amount of deflection within the system.

These components collectively contribute to the effective stiffness of the pelvis. The effective stiffness of the pelvis can be described in the general form,

$$\boldsymbol{k_{total} = (k_{skeletal} \cdot k_{soft\ tissue})/(k_{skeletal} + k_{soft\ tissue})} \tag{2.3}$$

which includes both soft tissue and skeletal components as a simplified model, shown graphically in . Based on this equation, the effective stiffness of the pelvis is dominated by the more compliant component—in this case, the soft tissue. However, this model is based on theoretical relationships between simple springs; its validity for the representation of the materially and structurally complex components of the pelvis during impact has not been tested. Despite this limitation, this model does highlight that (at least) two extremely different components must be included in the same simplified model.

Current estimates of effective pelvic stiffness derived using a pelvis release technique (Robinovitch, Hayes et al. 1991) place estimates of the variable at a mean of 70,000 kN/m (Robinovitch, Hayes et al. 1991; Laing and Robinovitch 2010; Levine 2011; Levine, Bhan et al. 2013), however, several components contribute to a 20,000-150,000 N/m range in estimates of pelvic stiffness. Using a linear estimate of pelvic stiffness based on experimental force and deflection data), males typically have lower effective pelvic stiffness (34,271 (9464) N/m) than females (25,194 (6126) N/m).

However, of critical importance to understanding the mechanics of these impacts, it is currently unknown how anatomical structures contribute to effective stiffness. While a general model (Figure 2.5) has been established, estimates for the stiffness of each component has not. Specifically, data regarding the displacement of soft tissues, rotation of the femur, movement of the bony components of the pelvis, or compliance of the ligaments of the pelvis would help make more accurate patient-specific estimates from medical images, as well as develop more easily scalable general models.

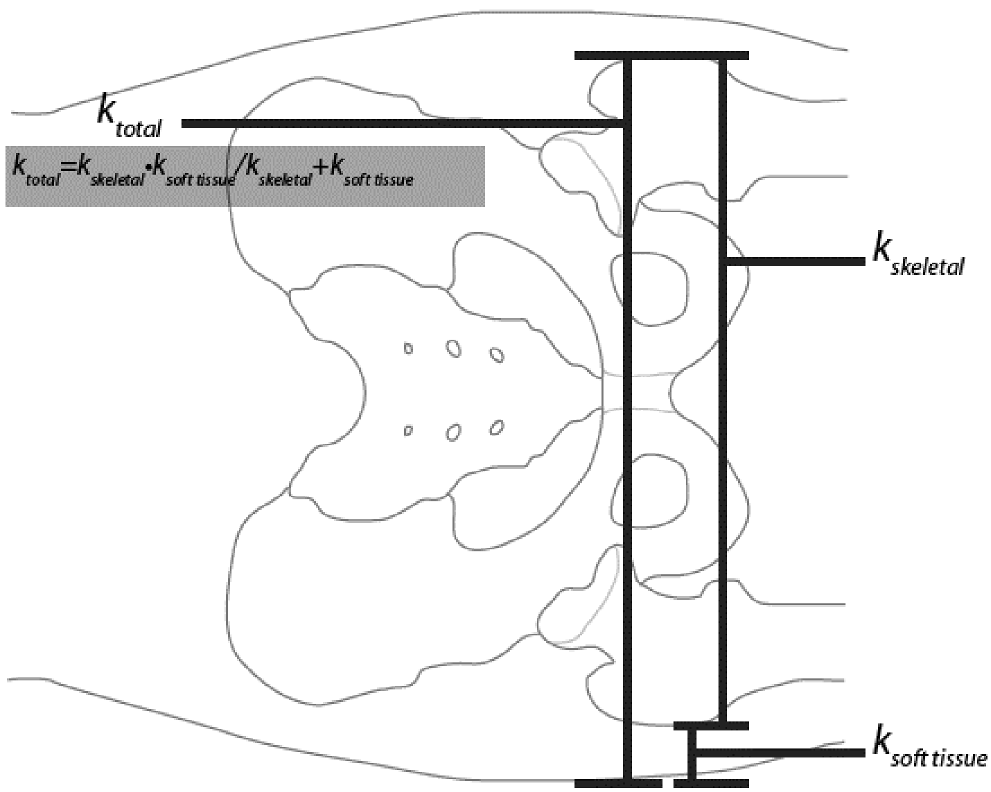

Figure 2.5 Simplified schematic of stiffness components during a lateral hip impact

Effective pelvic stiffness is a term that describes the stiffness of the pelvis and surrounding soft tissues, as a system, during impact. The two major components of this system are $k_{skeletal}$ and $k_{soft\ tissue}$. The skeletal component, $k_{skeletal}$ is much stiffer, and has been found in previous studies to not be force-dependent (Robinovitch, Hayes et al. 1991; Laing and Robinovitch 2010). The second component, $k_{soft\ tissue}$, is associated with much lower stiffness values, and varies non-linearly with force.

2.6 Methods of Assessing Loading and Load Distribution During Falls

Given the ethical and technical challenges of studying falling and impact mechanics in real-world scenarios, *in vivo, in vitro* and *in silico* methods are used to estimate the loads applied to, and distributed within the pelvis during a fall in a controlled setting.

2.6.1 Analysis of falls in real-life scenarios

Analysis of falls in real-life scenarios are a technical challenge for several reasons. First, the environment in which the falls occur (such as a long-term care (LTC) facility) is large, and is not optimal for the collection of kinematic or kinetic information. Successfully-captured real-life falls are typically limited to two-dimensional, low-quality surveillance video which is limited by orthogonality with the environment and falling subject, the ability to properly scale kinematic data, and the duration of the event relative to the sampling frequency of the types of systems used. Limited locations for cameras and interference of walls, furniture and other people or objects in the environment also contribute as limitations. Data storage is of particular concern for wearable sensors such as accelerometers, and trading a low sampling frequency for longer data collection sessions can result in poor data quality (Kangas, Vikman et al. 2009; Kangas, Vikman et al. 2012). Both visual and sensor-based methods can be negatively affected by body composition (Kangas, Vikman et al. 2009; Kangas, Vikman et al. 2012). Specifically, even a minimal amount of soft tissue allows translation between sensors or markers and the rigid (skeletal) landmarks of interest; this soft tissue artifact is amplified in impact scenarios and with increased depth of soft tissue (Leardini, Chiari et al. 2005; Bisseling and Hof 2006; Peters, Galna et al. 2010). These issues are accentuated when typical clothing (e.g. long pants, sweaters, shoes) obscure observation of joint location, interact with wearable sensors, or limit sensor placement. There are also ethical concerns by LTC residents, family members, visitors and staff regarding privacy and compliance with instrumentation or intervention use (Chan, Estève et al. 2012). While improvements in wearable sensors represents a potential future direction for analysis of dynamics of actual falls, fall simulation and modeling represent methods of analysis which can be employed with currently-available technology in a highly-controlled environment.

2.6.2 *In Vivo* fall simulation

Experimental simulated falls with live participants in impact studies are limited by ethical restrictions in order to prevent injury to participants and require a limited number of either low height, low-energy impacts, or impacts utilizing protective equipment such as crash mats or wearable padding. The first restriction reduces external validity of the impact data, while the second reduces the quality of the kinetic data collected when conclusions regarding unpadded scenarios are desired. Few current fall simulation paradigms are capable of incorporating both realistic falling characteristics (i.e. impact velocity and falling configuration) with high quality kinetic data, yet both of these elements are critical for predicting which falls will result in traumatic injury. A summary and comparison of currently-employed methods is presented in Table 2.1.

Currently reported analysis of studies employing these techniques primarily report only vertical impact components (i.e. no shear), and are mainly limited to characterization of the frontal plane responses of the pelvis. In a preliminary study (Appendix 1), we have developed a descriptive data set of falling and impact configurations from 50 older adults in an LTC setting. Only 6% of fallers fell in a "straight down" direction, and only one of these involved a lateral impact configuration. In addition to these findings, and what is currently known about the circumstances preceding falls in older adults (section 2.5.1) and impact configurations (Section 2.5.2.2), it is apparent that there are factors to consider in addition to purely vertical falling (i.e. orientation and initial velocity components) and impact characteristics (i.e. shear ground reaction forces). Additionally, there are anatomical variations in fracture tolerance, and differing fracture locations in response to loading vector application point and direction (Section 2.4). However, even in studies which include fall-simulation paradigms with other-than-vertical components (e.g. the inverted pendulum of tether release and voluntary falls from kneeling height), few have included impact characteristic results from non-vertical axes.

Additionally, of the eighteen studies cited in Table 2.1, only three (Choi, Hoffer et al. 2010; Bhan, Levine et al. 2013; Levine, Bhan et al. 2013) include participants with body composition outside a "normal" range (i.e. outside a BMI range of 22-28 kg/m^2). However, 37.1% of older adult men, and 33.6% of women over 65 have a BMI greater than 30 kg/m^2 (Flegal, Carroll et al. 2010), and there have been documented differences in injury patterns between BMI groups (Armstrong, Spencer et al. 2011; Compston, Watts et al. 2011; Armstrong, Cairns et al. 2012; Madigan, Rosenblatt et al. 2014). Three of the studies include martial arts practitioners (Groen, Weerdesteyn et al. 2007; Groen, Weerdesteyn et al. 2008; Weerdesteyn, Groen et al. 2008) who have been trained in, and regularly utilize protective measures to reduce injury during a fall, and likely have faster reaction times to fall stimuli and greater strength and power in response to an impending impact. Therefore, participants currently studied may not represent the older adult population at greatest risk for injury.

Table 2.1 Comparison of Currently Employed *In Vivo* Simulated Fall Techniques

Fall Simulation Paradigm	Description	Mean Impact Velocity	Primary Outcomes	Benefits	Limitations
Pelvis release (Robinovitch, Hayes et al. 1991; Robinovitch, Hayes et al. 1997; Choi, Hoffer et al. 2010; Laing and Robinovitch 2010; Bhan, Levine et al. 2013; Levine, Bhan et al. 2013)	The pelvis of the participant is supported in a side-lying position by a sling a set height above a force plate. The sling is released, allowing the pelvis to impact the force plate	0 (impending impact) – 1 m/s	Vertical impact characteristics of the pelvis within the frontal plane: peak force; non-linear stiffness and damping responses; distribution of loads between “effective pelvis” (EP) and rest of body; natural frequency of the EP; energy absorption of trochanteric soft tissues	Highly repeatable and controllable paradigm. “Isolation” of the pelvis allows characterization of the primary region of interest	Mainly limited to directly lateral impacts and frontal plane behavior of the pelvis. The completely vertical impact paradigm may not realistically mimic impact characteristics of a real-life fall.
Voluntary falls from kneeling height (Sabick, Hay et al. 1999; Groen, Weerdesteyn et al. 2007; Groen, Weerdesteyn et al. 2008; Weerdesteyn, Groen et al. 2008; Van der Zijden, Groen et al. 2012)	Participants voluntary fell from kneeling height in an inverted pendulum path. After a “relaxed” self-initiation, participants were triggered by audio or visual means to employ or not employ a protective technique such as rolling, bracing, or martial arts techniques.	1 – 1.5 m/s	Differential effects of protective techniques on impact characteristics (primarily peak vertical force at the hip and other impacting segments, and segment impact timing); effect of training on employability of protective techniques	Low-energy technique with non-vertical impact components	Involves a larger psychological contribution of the participant, with the participant choosing when and how to fall in attempts to mimic real-life impact scenarios. Could be improved with a tether release component
Falls from greater-than-kneeling height in response to anticipated stimuli (Smeesters, Hayes et al. 2001)	Participants responded to obstacles (such as a trip line or translating floor) while walking. The obstacle for each trial was known ahead of time, but the exact timing or location was not, and no-obstacle “catch trials” were used to reduce anticipation. A safety mat was used	1.5 m/s	Likelihood of type of fall, and impact location frequency for each type of obstacle, and dependence on initial walking velocity; orientation of the pelvis at impact in response to differing fall type	Actual falls from standing height during realistic activity (walking at various speeds)	Lower impact velocities than similar studies indicates that participant anticipation of the stimuli may have allowed them more control over their descent. Use of mats prevents kinetic analysis
Voluntary falls from standing height (Nankaku, Kanzaki et al. 2005)	Participants self-initiated a fall from standing height in lateral, posterolateral or posterior fall directions onto a mattress.	1.85 – 2.25 m/s	Effect of muscular activation and falling direction on impact velocity	Actual falls from standing height, with mattress allowing participants to feel safe during the protocol, producing greater impact velocities	Self-initiated falls. Use of mats prevents kinetic analysis
Tether release from greater-than-kneeling height (Robinovitch, Chiu et al. 2000; Robinovitch, Inkster et al. 2003; Robinovitch, Brumer et al. 2004; Sran and Robinovitch 2008; Sarvi, Luo et al. 2014)	Participants leaned against the support of a tether, which was subsequently released. Following initiation of the fall, protective techniques such as rotation or squatting onto foam-covered surfaces	0.5 – 3.5 m/s	Energy absorption of joints during protective techniques; impact velocity changes associated with protective techniques;	Actual falls from standing height with external initiation.	Primarily an inverted pendulum style fall path. Use of mats prevents direct kinetic analysis.
Unanticipated falls (Feldman and Robinovitch 2007)	Participants were recruited to participate in a “balance competition”, but were instead exposed to balance perturbations which caused them to fall onto mats.	3 m/s	Body segment impact frequency and timing (e.g. hands vs. hip first, and interval between impacts); orientation of the pelvis at impact	Actual falls from standing height with external initiation	Use of mats prevents kinetic analysis.

2.6.3 *In Vitro* and mechanical impact simulation

Given the potential for discomfort in live human subjects, *in vitro* and mechanical surrogate impact studies are used for scenarios where multiple impacts are needed (e.g. to compare between several pieces of protective equipment), higher energy levels are required (e.g. to simulate tissue damage) or where higher levels of experimental control are required. Impacts to the hip are typically modeled with a pendulum (Casalena, Badre-Alam et al. 1998; Laing and Robinovitch 2008; Li, Tsushima et al. 2013; Choi, Cripton et al. 2015) , a pneumatically-driven seated lateral protocol (Etheridge, Beason et al. 2005), or a lateral drop tower (Beason, Dakin et al. 2003; Derler, Spierings et al. 2005; Salzar, Genovese et al. 2009). In scenarios where components of the pelvis or femur are modeled (i.e. surrogate materials rather than post mortem tissue), the elastic and viscoelastic properties of the system is simulated with springs and foam. The drop tower protocol is easily modified for impacts to other body regions such as the head (Wright and Laing 2012), spine (Arun, Yoganandan et al. 2014), or wrist (Burkhart, Dunning et al. 2011), and is the simplest method for implementation with *in vitro* specimens.

2.6.3.1 Specimen preservation

Method of specimen preservation for dynamic loading scenarios is a current topic of research in biomechanics. While use of fresh (<48 hour post mortem) tissue would likely produce more biofidelic results, this introduces the challenge of completing biosafety and familial consent, and eligibility screening, transportation, and dissection and preparation within the extremely short period between release of *rigor* mortis and tissue degradation. Ongoing research (Dunford and Kemper 2017; Wettli, Cook et al. 2017) is currently exploring implementation of cell culture media such as Dulbecco's Modified Eagle Media (glucose, salts, vitamins and amino acids), saline, Ringer's solution, and antimicrobial solutions to tissue as methods to extend this short window.

In static loading scenarios, rapidly-frozen tissue which has then been thawed and re-warmed has been used to extend the window of specimen utility. Torimitsu and colleagues (2014) found no difference between fracture load of frozen-thawed skulls compared to fresh skulls under slow (100μm/s) loading rates, while Smeathers and Joanes (1988) found <1% change in compressive stiffness and hysteresis of lumbar spine segments under static conditions (<10 cycles/s, displacement < 1mm, strain <5%). However, tissue freezing has several drawbacks. First, the freezing process has been found to disrupt collagen fibres, resulting in ice lens formation (Szarko, Muldrew et al. 2010) and increased tissue permeability (Changoor, Fereydoonzad et al. 2010) or cross-linking of collagen fibres (Maiden and Byard 2015). This results in change in elastic properties such as tissue stiffness, failure load and energy to failure in unpredictable directions for both tensile and compressive loading protocols (Matthews and Ellis 1968; Gottsauner- Wolf, Grabowski et al. 1995; Leitschuh, Doherty et al. 1996; Moreno and Forriol 2002; Giannini, Buda et al. 2008; Venkatasubramanian, Wolkers et al. 2010; Maiden and Byard 2015), and even the observed mineral content of bone due to temperature-modulated biochemical changes in the tissue matrix (Moreno and Forriol 2002). Second, the freeze-thaw process is linked with substantial tissue dehydration, regardless of the rehydration process (Venkatasubramanian, Wolkers et al. 2010). This is in turn linked to substantive changes in viscoelastic properties, such as creep or system damping (Bass, Duncan et al. 1997). Viscoelastic properties of soft tissue appears to be strongly dependent on freezing rate (Chan and Titze 2003) (similar to fresh tissue when rapidly frozen with liquid nitrogen vs. a standard chest freezer), which is a factor beyond the control of researchers outside of a typical medical research setting.

Embalming methods also have mixed results. This section will focus on the more commonly available formalin-based embalming method rather than Thiel embalming. Wilke et al. (1996) showed an up to 80% decrease in specimen range of motion with formaldehyde fixation of calf spines compared to fresh specimens. Goh et al. (1989) demonstrated a decrease in energy absorption of 50% between embalmed and unembalmed cat long bones (femora and humeri). Nazarian et al (2009) found a 23% decrease in viscoelastic properties of formalin-fixed bone vs. fresh bone, a greater change than for frozen and thawed tissue. Finnie (2015) notes an increase in tissue mass directly after the embalming protocol, but notes that the effect is diminished after a period of three weeks. However, while Bourgouin and colleagues (2012) found an increase in stress at the end of the elastic region of the loading curve for embalmed vs. fresh intestine samples, they found no difference in strain or Young's Modulus. Additionally, the effects were most substantial for the outer (exposed) layers of tissue, and may be similar to the dehydration effect associated with thawed specimens. Topp et al. (2012) found no difference in stiffness, failure load between embalmed and fresh-frozen bone, and van Haaren et al. (2008) found no difference in torsion, bending stiffness, energy absorption or failure load between embalmed (>1 year) or fresh-frozen goat long bones. Finally, the profile (overall shape) of the mechanical response has been reported as similar between fresh and formalin-fixed specimens (Bourgouin, Bège et al. 2012; Rouleau, Tremblay et al. 2012); therefore, the comparison between the results of the *in vivo* and *in vitro* studies become particularly important.

2.6.4 Modeling approaches

As presented in sections 2.5.2 and 2.5.3 there are several individual and situational components to impacts, such as compressible, or deflectable tissue, or complex impact configurations which require considering when selecting complex modeling strategies. The two main challenges in modeling impacts to the hip are representing the behavior of the tissue (i.e. the anisotropic and viscoelastic properties), as well as capturing the geometric behavior (i.e. how the pelvis deflects against, and conforms to the impacting surface); these two goals are highly intertwined.

2.6.4.1 Characterization of the behavior of the pelvis during impact

Impacts to the hip, as determined experimentally, begin with a non-linear rise in normal force (Figure 2.6, T1) coinciding with a similar non-linear increase in vertical deflection (the inverse of position,

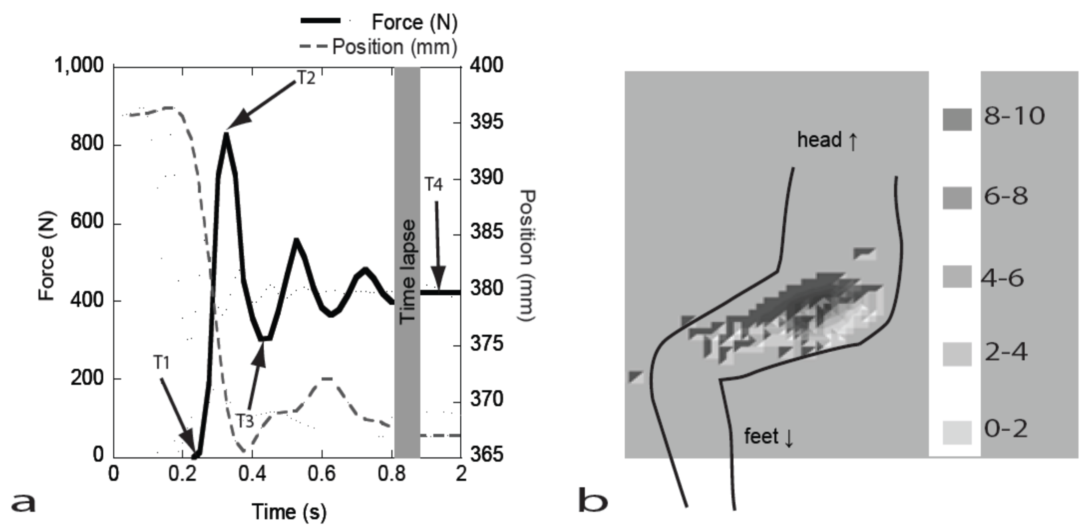

Figure 2.6 Behavior of the pelvis during impact

The force (a, solid line) and deflection (a, dashed line) resulting from a pelvis release experiment are shown. The force rises to a peak (T2) within 0.10 seconds, followed by oscillations of force (T3), eventually reaching a quiet phase (T4). Deflection follows a similar pattern, with a phase delay of up to 0.01 seconds. Contact area (b) follows a similar pattern; maximum contact area is reached, followed by oscillations of decreasing and increasing contact area until the quiet phase is reached. The pressure grayscale shows the concentration of force around the greater trochanter, with units displayed as Newtons per (0.762 x 0.508 cm) cell within a pressure plate. Figure 2.6a is described in greater detail in Figure 2.8 and Section 2.6.4.1.1

dashed line). This non-linear region is typically limited to forces less than 300 N (Laing and Robinovitch 2010), or the effective mass of the pelvis (Levine 2011). Shortly thereafter, there is a sharp, linear increase in both force and deflection, followed by peak force (T2), with an interval of 0.02-0.09 seconds between T1 and T2. Peak deflection occurs either at the same time as peak force, or up to 0.01 seconds later. There are frequently non-linearities ("shoulders") in force just prior to peak force—either small spikes less than peak force, or a decrease in the rate of increase of peak force. Following T2, both force and deflection begin a damped oscillation, with a distinct first minimum (T3), followed eventually by a quiet period (T4). Pressure is distributed along the pelvis, leg, and lower torso, concentrated at the greater trochanter and other eminent skeletal structures such as the iliac crest. Change in contact area and pressure follow a similar pattern to deflection.

These impacts can be modeled, most simply, as a single-degree-of-freedom, perfectly elastic, mass-spring model. This involves a mass (governed by the size of the pelvis) accelerating towards the impact surface, with a single, linear elastic stiffness (k). In the case of a perfectly elastic system, the force due to the acceleration of the mass will equal the restorative force of the spring (conserving the energy of the system) such that the greater the stiffness of the system, the less deflection is allowed, and vice versa. Relative to a rigid (or infinitely stiff) impacting object, the compliance modeled reduces the peak force observed during impact simulations, while the mass is unchanged. Therefore, determination of k, and the method of incorporating stiffness into the model is critical for both creating accurate predictions of peak forces as well as understanding the mechanisms underlying how impact forces are absorbed and distributed to prevent injury to the proximal femur. Expanding on this are the Standard Linear Solid (SLS), Hertzian Contact (HC) and Volumetric Contact (VC) shown schematically below, (Figure 2.7). For simplicity, when the impact of the pelvis is described in general terms (e.g. in sections 2.6.4.1-2.6.4.2), a mass-spring model will be assumed.

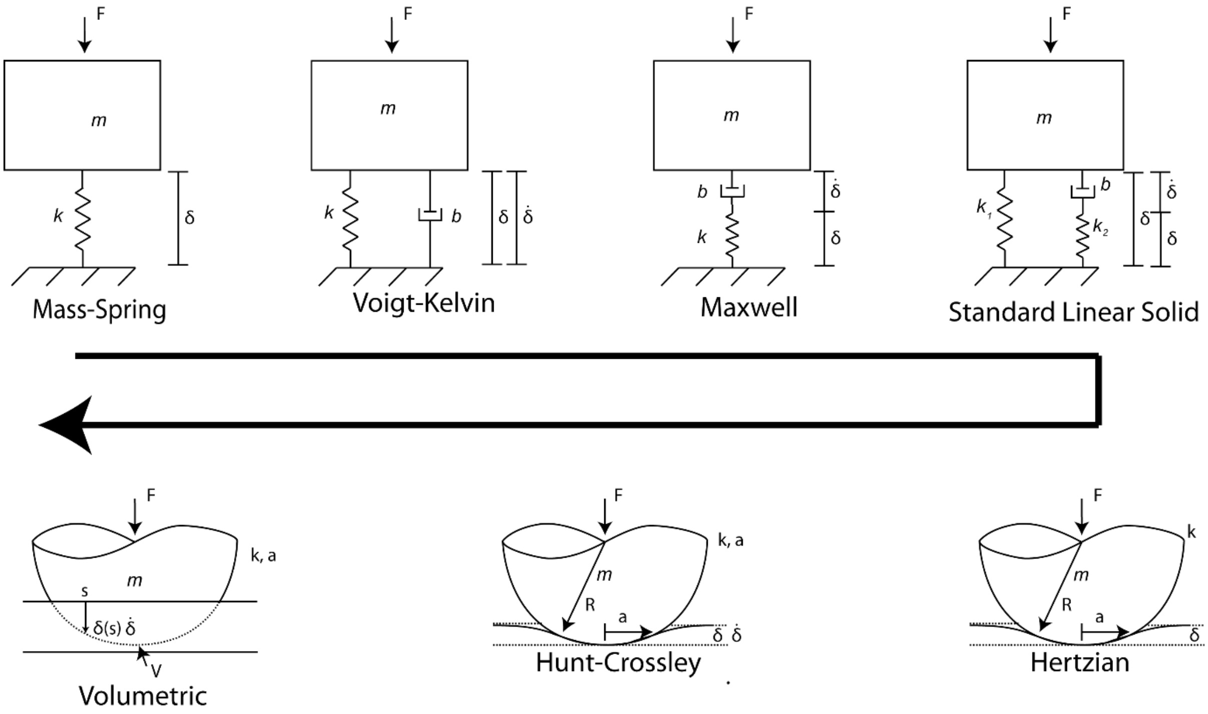

Figure 2.7 Model Schematics for the Mass-Spring, Voigt, Maxwell, Standard Linear Solid, Hertzian, Hunt-Crossley and Volumetric Contact Models

The contact between the pelvis and the impact surface (i.e. the floor) can be modeled with a variety of theoretical models, discussed in greater detail within the text. The top-row models are based on a Hookean-spring model, and can be used to model the point contact between the two structures. The second row expands on these models to follow Hertzian, rather than Hookean spring theory, while the most complex model, the Volumetric contact model, follows Winkler elastic foundation theory, in which stress is distributed unevenly across a deformable foundation. Complexity increases following the black arrow.

2.6.4.1.1 Vibration and Force-Deflection Response of the Pelvis System During Initial Impact

There are two major methods for the determination of effective pelvic stiffness. Initially, a vibration-based method of pelvic stiffness (Figure 2.8) was used, with the assumption that the pelvis responds like an undamped, linear spring during impact, with a single stiffness component (Robinovitch, Hayes et al. 1991; Robinovitch, McMahon et al. 1995). The vibration-based method simplifies data collection and analysis, because it only requires force data, and not data about the motion of the pelvis during impact. For this approach, the period of oscillation of force following impact,

$$T = 2 * (T_{min} - T_{max}) \tag{2.4}$$

is used to characterize the natural frequency of the system,

$$\omega_n = 2\pi T \tag{2.5}$$

with the effective stiffness (k_{vibe}) determined by the relationship,

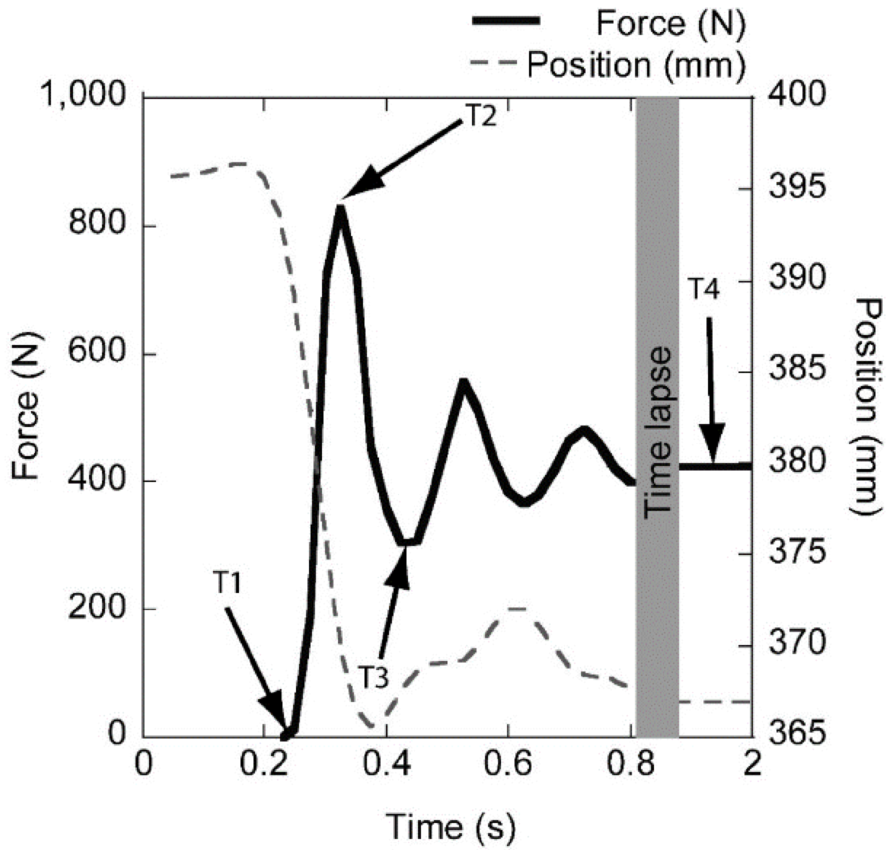

Figure 2.8 Vibration Analysis Method of Estimating Effective Pelvic Stiffness

Data points associated with the start of the impact (T1: T_{imp}, F_{imp}, D_{imp}), peak force (T2: T_{max}, F_{max}, D_{max}), minimum of the first force oscillation following impact (T3:T_{min}, F_{min}), and final resting pelvis (T4: T_{rest}, F_{rest}) are indicated. The half period of oscillation between T2 and T3 is selected to represent the post-impact behavior of the pelvis. These timepoints are used to calculate the duration of the full period of oscillation, natural frequency and stiffness, described in greater detail in the text.

$$\boldsymbol{k_{vibe} = \omega_n{}^2 m} \tag{2.6}$$

where m is the effective mass of the pelvis at rest, determined by the division of the force of the pelvis at rest (F_m) by gravity (g),

$$\boldsymbol{m = F_m}/\mathrm{g} \tag{2.7}$$

The force-deflection method was later employed (Laing and Robinovitch 2010), and incorporates a variety of modeling methods, described below. This method requires both force and deflection data, and assumes deflection of the pelvis only within the frontal plane. A comparison of three methods of estimating pelvic stiffness is shown in Figure 2.9. Briefly, time-varying force data points are plotted against their paired deflection data points, between T_{imp} and T_{max}. Using a least-squares regression approach, a curve is fit to the data, with an intercept of zero. The function associated with the polynomial is then differentiated to produce an estimate of stiffness. Previously explored functions used to characterize effective pelvic stiffness using this method include linear, 2nd order non-linear, and piece-wise (or biphasic) non-linear methods with 2nd order non-linear initial impact segments, followed by a linear region at higher impact loads (Laing and Robinovitch 2010; Levine, Bhan et al. 2013). Similar non-linear and biphasic methods have also been used to describe cartilage under compression (Mow, Kuei et al. 1980; Argatov 2013). The authors of these investigations noted that the non-linear and biphasic methods capture structural and material differences within the tissues tested, and may, but are not necessarily, linked with the viscoelastic behavior of the tissues. Additionally, biphasic methods can include differing contact model types (e.g. a mass-spring model for initial contact, and a Maxwell model at higher load conditions) to represent the differing materials and structures influencing that portion of the force-deflection curve

The method of determination of pelvic stiffness has a significant effect on the accuracy of predicted peak forces for both normal-BMI, (Laing and Robinovitch 2010) and participants with BMI below 22 or above 24 kg/m^2, (Levine, Bhan et al. 2013) participants. Based on the vibration-response of the pelvis, prediction of pelvic stiffness is accurate to within 2% (Robinovitch, Hayes et al. 1997), however, more recent research has found that this method is highly dependent on BMI , and only accurate for those outside a normal BMI range, on average, to within 33% (Levine, Bhan et al. 2013). Conceptually, there are two drawbacks of the vibration-analysis approach. First, because of the energy absorption of viscoelastic tissues, the impact is not purely elastic. Therefore, the ratio of the duration of the initial loading period relative to the fundamental period of oscillation is high; this results in poor characterization of the damping of the system based on post-impact oscillation (Gilardi and Sharf 2002). Second, the contributions of multiple components during impact must be acknowledged; a single natural frequency is a challenge to identify from pelvis impact data due to the interference of multiple signals. In contrast, a simplified linear force-deflection method has been found to be a better predictor of peak force, with average peak force prediction accuracy of within 25% (Levine, Bhan et al. 2013) for participants with BMI <22 or >24, as well as within 13.9% for

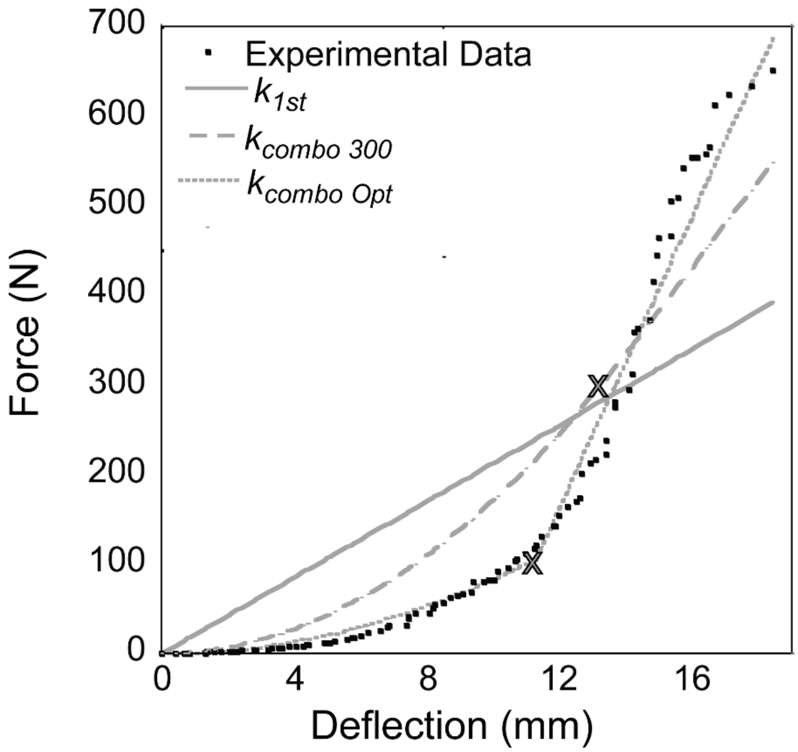

Figure 2.9 Force-deflection Stiffness Estimation Methods

Three force-deflection stiffness estimation methods are represented above, all produced using a least-squares regression fit to experimental data. For k_{1st}, this is represented by a linear red line. For $k_{combo\ 300}$ and $k_{combo\ opt}$, a linear region exists at higher levels of force, to the right of the transition point, marked by an 'x', while a non-linear region exists to the left of the transition point. For $k_{combo\ 300}$, the transition point was held constant across participants, while for $k_{combo\ opt}$, the transition was selected based on the experimental data. Effective pelvic stiffness can be compared within the linear region of each method, with k_{1st} typically producing the lowest estimate of pelvic stiffness, while $k_{combo\ 300}$ and $k_{combo\ opt}$ produce higher estimates of pelvic stiffness.

normal-BMI participants (Laing and Robinovitch 2010). This method captures a single value for effective pelvic stiffness, consistent across impact velocities. However, the differing contributions of each anatomical component cannot be separated. A simplified linear method, therefore, is appropriate for developing normative values for effective pelvic stiffness, but not developing individual pelvic stiffness estimates based on personal body characteristics, and does not help explain how body composition and impact configuration affect impact mechanics.

2.6.4.2 Single-Degree-of-Freedom Models

Models based on Hooke's law of contact dynamics form the simplest class of impact models, and incorporate a mass and spring in a one-dimensional point contact model. The resulting force applied to the proximal femur is a function of *k* and the amount of deflection of the spring (x),

$$\boldsymbol{F_s = kx} \tag{2.8}$$

where *k* is defined by either the vibration response, or the force-deflection relationship (such as Young's modulus) of the system (Section 2.6.4.1.1). In an ideal situation in which the energy of the system is conserved as elastic energy, F_s is equal to the force applied.

In the case of the impacting pelvis, the deflection would mainly be associated with the depth of soft tissue overlying the hip in a direction parallel to the normal force. Therefore if it is assumed that soft tissue stiffness is relatively consistent between people (Choi, Russell et al. 2014), the thickness of soft tissue is critical for predicting peak forces during an impact. For females of a normal adult BMI (18.5 – 24.9), there is a negative correlation between soft tissue thickness and *k* (R^2 = 0.828), peak force normalized to body weight (R^2 = 0.500) and positive correlation between soft tissue thickness and time to peak force (R^2 = 0.644) (Levine, Bhan et al. 2013).

However, there are several limitations of the simple mass-spring model. It has been consistently found that the correlation between measured soft trochanteric soft tissue thickness and impact dynamics is weak (Robinovitch, Hayes et al. 1991), particularly for study participants outside of the normal BMI range (Levine, Bhan et al. 2013), and is more accurate below 2 m/s impact velocity than above this threshold (Robinovitch, Hayes et al. 1997). This limits the applicability of the model for the prediction of injury risk based on individual body composition characteristics and within the range of impact velocity that is more likely to result in injury. Further, the simple mass-spring model assumes a linear relationship between force and deflection, with deflection occurring along only one axis; in contrast, the water-rich soft tissues undergo little pure compression. When impacted, the soft tissues displace laterally, an effect which isn't captured within the mass-spring model. The simple linear-elastic model contains no damping components, whereas biological tissues are viscoelastic. Finally, this model predicts continuous oscillation of force following impact. According to current understanding of hip fractures, the initial impact characteristics are more critical than the post-impact oscillations, however, more accurate representation of the degradation of impact energy may also be helpful in predicting and understanding impacts to biological tissues. To summarize, the simple mass-spring model has been fairly effective when used to predict peak forces during impacts, but does not represent or contribute to the understanding of biological tissues as individual components.

2.6.4.2.1.1 Modeling of Viscoelastic Components in a Mass-Spring Model

The viscoelasticity of biological materials is represented by dampers in the Voigt, Maxwell, and Standard Linear Solid models. Rather than a simple, linear relationship between the force applied to a structure and the resulting deflection, the damper accounts for the viscous fluid components of biological tissues. Mechanically, the damper serves as a source of energy dissipation; because of this, models including damping components provide better predictions of the step response of impacts to the hip following the first half-period of oscillation (Robinovitch, Hayes et al. 1997). Of the three configurations, the Voigt model is most commonly used for modeling hip impacts (Kim and Ashton-Miller 2009; Luo, Nasiri Sarvi et al. 2014; Sarvi and Luo 2015), particularly for modeling soft tissues (Choi, Russell et al. 2014). This approach is also used for by Muksian and Nash (1976) and Rosen and Arcan (2003) to model displacements of body segments during vibrational seat movement. A variation of the Voigt model is also used for some tissues in FE models of impacts to the pelvis, replacing the Hookean spring with a hyperelastic spring such as the Mooney-Rivlin material (Majumder, Roychowdhury et al. 2007). The step response for the Voigt model is,

$$\boldsymbol{F_s = kx + b\dot{x}} \tag{2.9}$$

where, again, *k* represents spring stiffness, and *x* the amount of deflection in the system. These models are also time dependent (velocity, $\dot{x}$) and include a damping component (*b*).

Each of these models, however, has limitations. The Voigt model inaccurately predicts an unrealistic instantaneous force at impact, and under predicts peak force at higher impact characteristics (Robinovitch, Hayes et al. 1997). Because the damper in the Voigt model is in parallel with the spring, it dominates the initial impact characteristics; poor characterization of the damper will therefore result in poor prediction of peak force and time to peak force (Roy and Carretero 2012). In contrast, the in-series damper of the Maxwell model causes a creep effect, but is more accurate in prediction of initial loading rate (Robinovitch, Hayes et al. 1997). The combination of both parallel and in-series dampers in the Standard Linear Solid model prevents the unrealistic instantaneous force, and predicts peak force within a mean of 3%. However, the Voigt, Maxwell and Standard Linear Solid models did not perform better than the simple mass-spring model. The author of this comparison suggests that these models are highly sensitive to characterization of their respective spring and damping components, which were based on experimental results with a synthetic pelvis. This leaves a clear gap for the exploration of realistic, yet mathematically simplistic, damping effects based on actual biological impact data.

2.6.4.3 Hertzian Contact Models

Models based on Hertz theory (Hertz 1882; Hertz 1896; Johnson 1985; Hirokawa 1991; Fregly, Bei et al. 2003; Gefen 2007) extend the simplistic mass-spring model by replacing the simple linear spring geometry with three-dimensional radius and contact area components (Figure 2.10). Additionally, rather than a simple deflection term, assuming compression of a linear spring, a more complex definition of the interaction of the impacting bodies includes terms for the dimensions of spheres which model each body, as well as a depth of interaction rather than simple deflection. The depth of

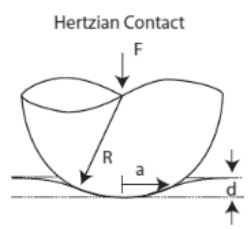

Figure 2.10 Schematic of the Basic Hertzian Contact Model

Models based on Hertz theory assume that deflection, or depth of interaction (*d*) is accompanied by change in contact area (*a*), which is defined by the radii (R_1, R_2) of the interacting bodies, or in the case of a sphere and a plane, one radius (*R*). This model is limited by the challenge of incorporating viscoelastic material properties, and assumes that contact force is distributed evenly along the contact surface (i.e. there is no conformation or local pressure peak).

interaction term differs from a simple deflection term in that it is defined by the spherical nature of the contacting bodies, i.e, in the equation governing the relationship between force and the properties of the contacting bodies,

$$\boldsymbol{F_s = k|x|^p} \qquad (2.10)$$

where p=3/2 if the contacting spheres are linearly elastic, implying a direct relationship between deflection (*x*) and contact area. In the case of the contact between a sphere (such as the general shape of the pelvis) and a plane (e.g. a non-compliant floor), *k* can be determined experimentally by fitting a curve to force and displacement data. Analytically, *k* is defined by material and geometric properties:

$$\boldsymbol{k = \frac{4}{3\pi\left(E_i^* + E_j^*\right)} R_i^{1/2}} \qquad (2.11)$$

dependent on the radius (*R*) of the impacting object, where *E** refers to the elastic properties of the system, including elastic modulus (*E*) and Poisson's ratio (*v*) of the indenter (*i*) and plane (*j*),

$$\boldsymbol{E^* = \frac{1-v_l^2}{\pi E_l} \frac{1}{E^*} = \frac{1-v_i^2}{E_i} + \frac{1-v_j^2}{E_j}} \qquad (2.12)$$

in which v_l and E_l are Poisson's ratio and Young's modulus, respectively, of *i* and *j* (Gonthier 2007). In this way, the non-linear deflection behavior may be accounted for.

During impacts to the pelvis, the soft tissues are displaced along the impact surface rather than simply compressing. From the mathematical description, above, a model based on Hertz theory could incorporate both material properties and geometric relationships which are more representative of the biological behavior. Rather than the simple mass-spring model, which assumes that changes in pelvic dimension occur only along the normal axis, incorporation of Poisson's ratio and geometric relationships (i.e. the three-dimensional shapes of the interacting components) allow a defined relationship between depth of interaction and displacement along the contact surface. Simply, a specific depth of interaction cannot be reached without a corresponding lateral displacement; this relationship is dependent on the applied force, the material properties (*v, E*) of the interacting bodies, and the geometric properties of the interacting bodies. Because of this interrelationship of geometry and material properties, a Hertzian model can also be used to estimate pressure and shear stress (Padture 2001).

While a Hertzian model has not yet been used to represent the impact of the pelvis during a fall, it has successfully been used in the biomechanical fields of soft tissue pressure injuries (i.e. bed sores) (Gefen and Haberman 2007), and has been widely used in the development of knee (Hirokawa 1991; Fregly, Bei et al. 2003; Machado, Moreira et al. 2012; Madeti, Rao et al. 2014) and hip (Sanders and Brannon 2011; Zdero, Bagheri et al. 2014) replacement prostheses.

However, this model also has limitations which reduce its applicability to biological impacts. The first concern is that this model handles typically impacts assuming only a normal direction of force application, neglecting any frictional or rolling contributions. Second, the model requires the assumption of non-conformity, i.e., that only a small portion of each body is involved in the contact, which can be defined by a single point. Additionally, Hertzian contact theory assumes symmetrical and evenly distributed loads, which limits applicability to continuous surface contact with no local maxima of pressure (Sanders and Brannon 2011). Finally, when compared with experimental pelvis impact data, force, deflection and contact area did not interact as specified in Equations 2.10 – 2.12, potentially due to the viscoelasticity of the materials involved (Bhan 2014). With the exception of further expansions upon the basic Hertzian contact model (such as the Hunt-Crossley model which incorporates damping components), viscoelastic energy dissipation (and therefore a dynamic solution) cannot be accounted for.

2.6.4.4 Volumetric contact models

The volumetric contact model (VC, Figure 2.11) was developed to account for major limitations of point-contact models (Boos and McPhee 2010). First, rather than a limited centroid of contact where the opposing applied and normal forces act, the VC can be used when contact area between two surfaces represents more than a minimal portion of the circumference of either body. Secondly, the VC accounts for conformation between the interacting bodies rather than assuming that no conformation has occurred. Third, the volumetric contact model can handle energy dissipation (via inclusion of dampers) and handles anisotropic materials better than HC models (which assume isotropic, elastic materials) (Boos and McPhee 2013).

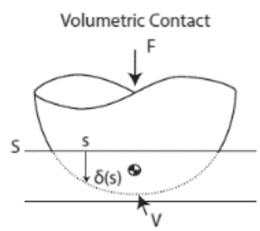

Figure 2.11 Schematic of the Volumetric Contact Model

The Volumetric Contact Model expands upon Hertz theory by allowing conforming interactions between the contacting bodies. The level of interaction is defined by the volume of interference (*V*) and depth of penetration *δ(s)*, allowing a geometrically-defined pressure distribution.

The relationship between force (F) and the impacting segment geometric and material properties is given by:

$$\boldsymbol{f_s = k_v V(1 + a v_{cn})} \tag{2.13}$$

Where the geometric term to describe the volume of interference between the impacting objects is given by:

$$\boldsymbol{V = \int_s \delta(s) dS = \int_V dV} \tag{2.14}$$

where *S* is the planar contact surface between the interacting bodies, *δ(s)* is the depth of penetration at point *s*. Volumetric stiffness (k_v) is estimated experimentally by measuring the load and displacement of the indenter (in this case, the pelvis) using a gradual (quasi-static) increase in force. This reduces the damping effects of the material, allowing the simplified equation to solve for k_v,

$$\boldsymbol{F_{QS} = k_v V} \tag{2.15}$$

with V determined from the depth of penetration of the body (δ),

$$\boldsymbol{V = \frac{\pi}{3}\delta^2(3r - \delta)} \tag{2.16}$$

The hysteretic damping factor, a, is dependent on impact velocity and the coefficient of restitution (e). a is estimated by comparing the quasi-static experimental measurements to a set of dynamic experiments,

$$\boldsymbol{F_{damped} = F_{QS}(1 + a v_{cn})} \tag{2.17}$$

which is dependent on the velocity (v_{cn}) of the centroid of the volume (n) in the normal direction.

However, the VC has had limited implementation in biomechanical research (Millard, Kubica et al. 2011; Koop and Wu 2013; Shourijeh and McPhee 2014), particularly in the cases of impacts and fall-related injuries. Investigation of this model type for fall-related impacts to the hip may provide promising results for its incorporation into other situations where complex anatomical geometry and materials highlight the oversimplification of standard biomechanical modeling methods.

2.6.4.5 Finite Element Models

Another strategy for modeling impacts to the hip has been finite element (FE) modeling (see literature by Cody et al., Hayes, et al., Keyak et al., Kim et al., and Majumder et al.) including both skeletal and soft tissue components. While these models can be highly patient-specific, they have varying levels of success in matching actual hip fracture risk (Majumder, Roychowdhury et al. 2007; Majumder, Roychowdhury et al. 2008; Keyak, Sigurdsson et al. 2011; Kim, Hsieh et al. 2013). A commonly cited limitation of these models is that not enough is known about the experimental behavior of the skeletal and soft tissue elements in impact conditions, or how to appropriately dimension the soft tissue components. Because so many individual elements are required to build the model, it can be challenging to appropriately represent the anisotropy and viscoelasticity within the tissues (Majumder, Roychowdhury et al., 2007). FE models can be limited by their computational expense, which limits the number of body segments included in the impact (particularly, limiting simultaneous contact of multiple components), the selection of kinematics preceding the modeled impact, and the direction and location of load application. This limits the inertial contribution of other body segments, and limits the realism of the impact scenario (Majumder, Roychowdhury et al., 2007). Therefore, appropriate FE (and other method) models cannot be constructed without greater knowledge of how the skeletal and soft tissue components of the pelvis react mechanically to impacts. Particularly with the advance of FE software and medical imaging techniques, patient-specific FE models may be part of the future of hip fracture prediction; however, other models are currently more utilitarian for understanding impact dynamics and how the pelvis behaves as a system during a fall to the hip.

2.7 Literature summary and specific questions to be addressed

Current methods of hip fracture prediction in clinical practice use primarily non-biomechanical methods to predict a mechanical outcome. While these models may identify a portion of older adults at high risk of fracture associated with fall-related injury, there are limitations to current methods. Most critically, these methods rely on simplified relationships between body size and composition (typically height and weight) and fracture risk, despite evidence from mechanistic and population-based studies linking body composition with more variable mechanical and epidemiological risk. Simply, body mass index is too general a surrogate for the force attenuation and distribution effects associated with body composition, but it is unclear from a biomechanical perspective which elements of body composition are linked with these effects, and to what magnitude. These issues are particularly clear when considering fallers who are at risk for suffering a fragility fracture without having been identified as at risk by current models. The second major limitation is that, from a mechanical perspective, fracture risk is dependent on the load applied to the bone, as well as the load tolerance; however, only load tolerance is typically considered in epidemiological models through assessment of bone mineral density. However, there are several factors to consider from a biomechanical approach, such as the way a person falls (i.e. velocity, configuration, orientation) and how these loads are affected by their body composition and skeletal geometry.

A biomechanical model could provide a better method of identification of individual and falling configuration components which contribute to high-risk impacts, and prevention of high-risk impacts through exercise- and engineering-based interventions. Additionally, incorporation of mechanistic evidence for current epidemiological models, as well as additional epidemiological research regarding mechanically-driven components may improve prediction of fracture risk for those who are excluded based on current diagnostic methods. The following elements have been identified as key gaps in the literature regarding fall-related injuries to the hip.

First it is currently unknown how specific elements of body composition (e.g. adiposity, soft tissue depth) affect how loads are applied and distributed during impacts to the hip. Further, it is unclear how these characteristics might be linked to elastic and viscoelastic components of mechanical models which could be used to predict force attenuation and distribution. Study 1 addresses the direct links between body composition elements and impact dynamic outcomes using *in vivo* fall simulation protocols with young, healthy volunteers, while Study 2 uses these relationships to drive development of model parameters based on individual body composition and size. The model accuracy of the models in recreating the experimental loading profile is then assessed and compared in Study 3.

Second, it is unknown how internal anatomical components contribute to effective stiffness during impact, particularly over a variety of impact configurations. In order to address these gaps in the literature, Study 4 explores this gap using *in vitro* techniques to delve further into identifying individual characteristics which may be linked to injury outcome and model performance

Finally, while there have been investigations using a variety of fall simulation protocols, it is unknown how these simulated impact methods compare to one another or interact with elements of body composition to attenuate or redistribute forces at the hip. Study 5 explores these gaps using *in vivo* fall simulation protocols with young, healthy adult volunteers to characterize these relationships and identify future directions for modeling approaches.

Chapter 3, Study 1: Force Attenuation and Distribution during Impacts to the Hip are Affected Differentially by Elements of Body Size and Composition

Chapter 3 consists of a study collected for, and presented in part at the 2014 Canadian Obesity Student Meeting, June 18th-21st, 2014 and the 7th World Congress of Biomechanics, July 6-11, 2014. Briefly, this study compares impact characteristics during a pelvis release experiment with a complex set of elements of body composition that have been proposed as mechanically relevant to impact characteristics and risk of fall-related injury.

3.1 Introduction

Theories regarding the mechanics of hip fracture suggest that hip fracture risk is reduced when applied loads are attenuated by trochanteric soft tissue via energy absorption, reduction of stiffness and load distribution (Cummings and Nevitt 1994; Hayes, Myers et al. 1996). This theory is used to highlight soft tissue as a protective factor responsible for lower epidemiological risk of fracture in fallers with high BMI (Johansson, Kanis et al. 2014). In experimental studies, there is a link between soft tissue thickness and impact outcomes, however, these results are of mixed strength (Robinovitch, Hayes et al. 1991; Robinovitch, McMahon et al. 1995; Etheridge, Beason et al. 2005).

A 71 N decrease in peak force for a 1 mm increase in trochanteric soft tissue (Robinovitch, McMahon et al. 1995) has been used to estimate attenuated force following a lateral impact to the hip. However, in epidemiological outcomes, soft tissue thickness is predictive of fracture risk in women (Bouxsein, Szulc et al. 2007) but not men (Nielson, Bouxsein et al. 2009), though estimated attenuated force was lower for controls than fracture cases in both studies. Further, it has been noted that this method estimates greater force attenuation than peak force for fallers with high trochanteric soft tissue thickness (Sarvi and Luo 2015). Deflection-based estimates of pelvic stiffness do not differ between extremely different (<22 or >28 kg/m^2) body mass index groups despite differences in peak force, normalized to the effective mass of the pelvis (Levine, Bhan et al. 2013). The relationship between soft tissue thickness and reduction of load at the hip may be more complex than simply absorbing energy through one-dimensional compression. It is likely that applied loads are distributed by soft tissue rather than simply absorbed.

Under low-velocity compression, weight extremes (underweight and obesity) have been cited as an independent risk factor for soft tissue injury (Elsner and Gefen 2008; Kottner, Gefen et al. 2011; Lyder, Wang et al. 2012). Differing mechanisms have been proposed, with adipose contribution to increases in both cushioning and mass, mirroring arguments regarding the effect of trochanteric soft tissues on impacts to the hip; these investigations may provide insight into load distribution during impact conditions. Elsner and Gefen (2008) found that pressure within the ischial tuberosity-seat interface increased slightly with simulated increases in BMI, along with substantially increased compressive strain of the internal tissues and change in location of peak strain (greater directly under the ischial tuberosity for high BMI); these changes were exacerbated when simulated increased BMI was coupled with decreased muscle volume. Load distribution is also dependent on interactions with the underlying skeletal structures. A skeletal component with a wider simulated radius of curvature is associated with greater low-velocity compressive soft tissue injury than one with a narrower radius of curvature (Linder-Ganz and Gefen 2009). However, structures with a narrower radius of curvature are associated with greater initial instantaneous tissue stress (Linder-Ganz and Gefen 2009). These studies involved quasi-static loading over prolonged duration; it is unclear whether the load distribution effects are similar during dynamic conditions and loading rates associated with a fall from standing height.

In summary, while existing work supports existing theories regarding soft tissue attenuation of impact loads, current understanding of the relationships is not clear enough to explain experimental results with participants outside a normal BMI range, nor is the current relationship clearly supported by epidemiological outcomes. Second, while load distribution by the gluteal soft tissues has been explored in static conditions, it is unclear how the mechanism may change under dynamic conditions.

Therefore, the primary goal of this study is to explore whether there is a relationship between contact area, pressure and peak force during impact, and body composition.

We hypothesized that:

1. Due to the energy associated with mass, peak force would be positively related to body size (i.e. total mass, lean mass, fat mass, etc).
2. System deflection will be positively correlated with measures of soft tissue, more specifically, total fat mass and trochanteric soft tissue thickness (TSTT).
3. High thickness of trochanteric soft tissues would increase contact area between the pelvis and impact surface, resulting in positive associations with contact area and negative associations with peak pressure).

4. Because soft tissue mass is unevenly distributed, and non-rigidly linked, we expected stronger relationships between impact characteristics and local hip-specific elements of body size / composition during the pelvis release protocol than global body size (e.g. hip circumference vs. overall body height).

3.2 Methods

This study involved two separate collection sessions with participants. The first involved simulated falls to measure impact dynamics; initial body composition assessment was also collected at this time. A second session was used to measure additional body composition parameters via dual x-ray absorptiometry (DXA). The two sessions occurred within two weeks of each other to minimize potential time-related changes in body composition between the two sessions.

3.2.1 Participants

Nineteen females provided informed consent and participated in this study. Approval of the methodology was provided by the Office of Research Ethics at University of Waterloo (ORE# 18715). Participant recruitment focused on developing a cohort with a wide variety of body types and body composition characteristics, as illustrated in Table 3.1.

Table 3.1 Recruited Participant Characteristics

	Mean (SD)	**Maximum**	**Minimum**
Age (years)	24.4 (3.1)	31	20
Height (m)	1.68 (0.07)	1.79	1.56
Mass (kg)	66.0 (11.5)	87.0	50.0
BMI (kg/m^2)	23.7 (3.8)	33.1	18.4
Waist-Hip Ratio	0.80 (0.05)	0.87	0.67
Body Fat (%)	29.9 (11.8)	60.5	17.2
TSTT (cm)	3.9 (1.1)	6.68	2.0

Young adult participants (<35 years) were recruited because of their lower risk of osteoporosis-related injury compared to their older adult counterparts. Exclusion criteria included musculoskeletal injury in the past year preventing completion of the protocol, lifetime fracture history of the hip, pelvis or spine, fear of falling, pregnancy, previous high doses of radiation or other health conditions which would make participation unsafe. Two participants reported history of sacroiliac joint laxity, but did not differ significantly in either skeletal geometry, body composition or impact characteristic results from the rest of the cohort. All participants provided written informed consent.

3.2.2 Body Composition Assessment

Participants underwent a health screening in order to determine their eligibility for this study. Specific exclusion criteria for this portion of this study included: pregnancy, history of reactions to imaging gels or easy bruising, or recent medical procedures involving the hip or pelvis.

Participant mass was measured with a scale to the nearest 0.5 kg. Hip circumference was measured with a flexible tape measure to the nearest 0.5 cm at the level of the greater trochanter. Transverse-plane TSTT was assessed via ultrasound (minimum precision 0.17 cm; C60x, 2-5 MHz transducer, M-Turbo Ultrasound, SonoSite, Inc., Bothell, WA) in a side-lying position, similar to that expected during the impact phase of the fall simulations (Figure 3.1). While other transducers (e.g. a linear array) provide better image resolution, there is a large variability in soft tissue depth over the greater trochanter; therefore the curved-array transducer, with a scan depth of up to 15 cm, was appropriate across the entire study cohort. For each participant, a calibration frame was collected, using a built-in 2D caliper within the SonoSite image processing software. The ALARA (As Low As Reasonably Achievable) principle was used to limit potential thermal and mechanical sources of tissue damage (AIUM 2008). Because soft tissue is easily compressible, care was taken to strike a balance between tissue compression and clarity of image.

Whole-body DXA images were collected by a Medical Radiation Technologist (MRT) using a Discovery QDR Series linear X-ray fan-beam bone densitometer with motorized C arm and table (Hologic, Inc. Bedford, MA, USA). The device was phantom calibrated prior to each session and has a level of precision of 3.2% for fat mass and 2.2% for lean mass in obese individuals, and 2.1 and 1.5% for lean individuals (Galgani, Smith et al. 2011). Images were digitized using Hologic APEX Software Version 3.2. Discovery QDR W Series (Hologic, Inc. Bedford, MA, USA). Participants dressed in a hospital gown, and removed all jewelry and other metal objects. During the image collection, the participant rested in a standardized position on the bed of the DXA scanner. The procedure, which took approximately three minutes to complete, involves one high- and one low-energy x-ray in a piecewise scan of the entire body, which are stitched together to form a composite image by the software. The MRT then segmented the images into standard compartments (Figure 3.2, solid white lines) and prepared a whole body and segmental tissue composition report for each

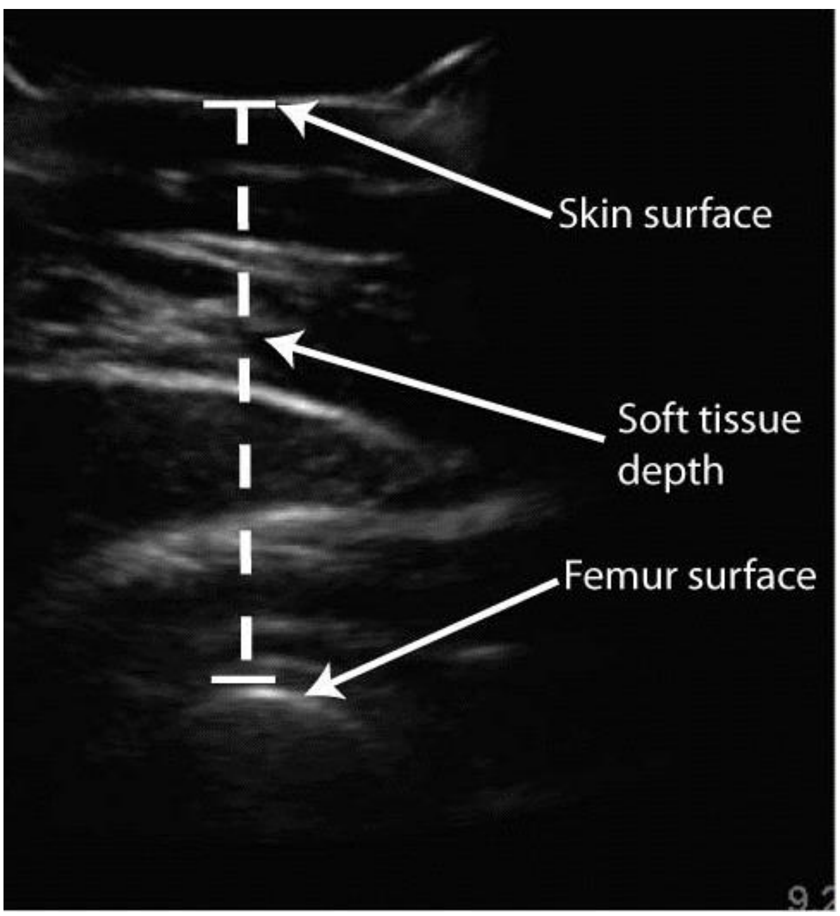

Figure 3.1 Ultrasound image of soft tissue overlying the greater trochanter

A transverse plane image of the greater trochanter, with the participant in a side-lying position. An interference marker identifies the skin surface in this figure, while the femur surface was identified as the deepest anatomical structure the ultrasound waves were capable of penetrating. Trochanteric soft tissue depth was defined as the shortest distance between the skin surface and the femur surface.

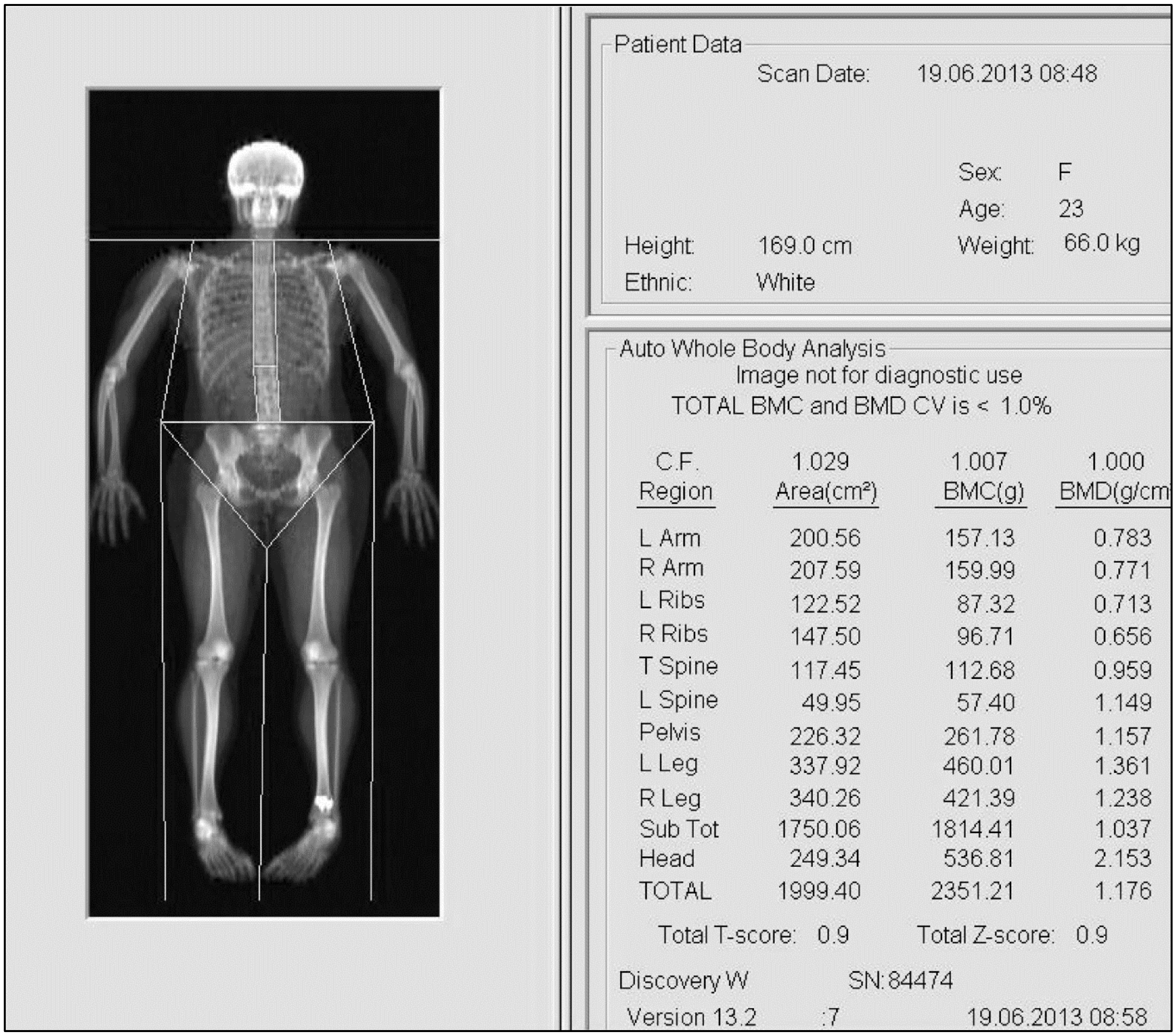

Figure 3.2 Full body DXA image and analysis results within the Hologic software

Preliminary analysis of the DXA image by the MRT. The body of the participant is segmented (white lines), and a whole body and segmental analysis sheet is produced for each participant, including total and segmental fat mass, lean mass, total mass.

participant. We extracted total percent body fat (*BF*), the total fat and lean mass ($Mass_{fat}$, $Mass_{lean}$), the fat and lean mass of the right leg ($Mass_{leg\_fat}$, $Mass_{leg\_lean}$), Fat Mass Index (BMI_{fat}) and Lean Mass Index (BMI_{lean}).

3.2.3 Instrumentation and experimental impact protocol

A lateral pelvis release protocol (Robinovitch, Hayes et al. 1991; Robinovitch, Hayes et al. 1997; Choi, Hoffer et al. 2010; Laing and Robinovitch 2010; Bhan, Levine et al. 2013; Levine, Bhan et al. 2013) with a drop height of 5 cm was employed (creating an impact velocity of ~1m/s). During the protocol, the pelvis of the participant was supported by a thin, nylon sling (Figure 3.3), connected to an electromagnet (model DCA-400T-24C, AEC Magnetics, Cincinnati, Ohio, USA) via a set of length-adjustable ropes, which is in turn affixed to the ceiling. The participant held her arms away from the pelvis (crossed across the chest or underneath the head to reduce the chance of marker occlusions), with 45° of hip flexion, and 90° of knee flexion. The participant was instructed to relax their core and extremity muscles in order to reduce muscle tension as a potential confounding variable (Bhan, Levine et al. 2013; Levine, Bhan et al. 2013; Bhan, Levine et al. 2014). After the participant reported they were both 'relaxed' and 'ready' to begin a trial, the magnet was disengaged by the investigator following a delay of 1-3 seconds, allowing the participant's pelvis to impact the force platform. The participant was warned that this event would occur, but was blinded to the timing of the event. Following each trial, the participant was given a brief rest (between one and five minutes) to allow tissue recovery. The participant was asked to stand quietly or kneel, minimizing the contact between the impacted hip and any surface (e.g. floor, chair, etc.). Three trials were collected.

A force plate (OR6-7, Advanced Medical Technology, Inc., Watertown, Massachusetts, USA) was situated beneath the sling for the pelvis release experiments. Time-varying force data was collected at a rate of 1500 Hz. A rigid pressure plate (RSscan International, Olen, Belgium) was affixed to the force plate with double-sided tape. Pressure data was collected at the maximum sampling rate of 500 Hz over the 4096 sensel area (each 0.762 by 0.508 cm, resistive sensors). Motion of the pelvis was tracked using an Optotrak Certus system with First Principles software

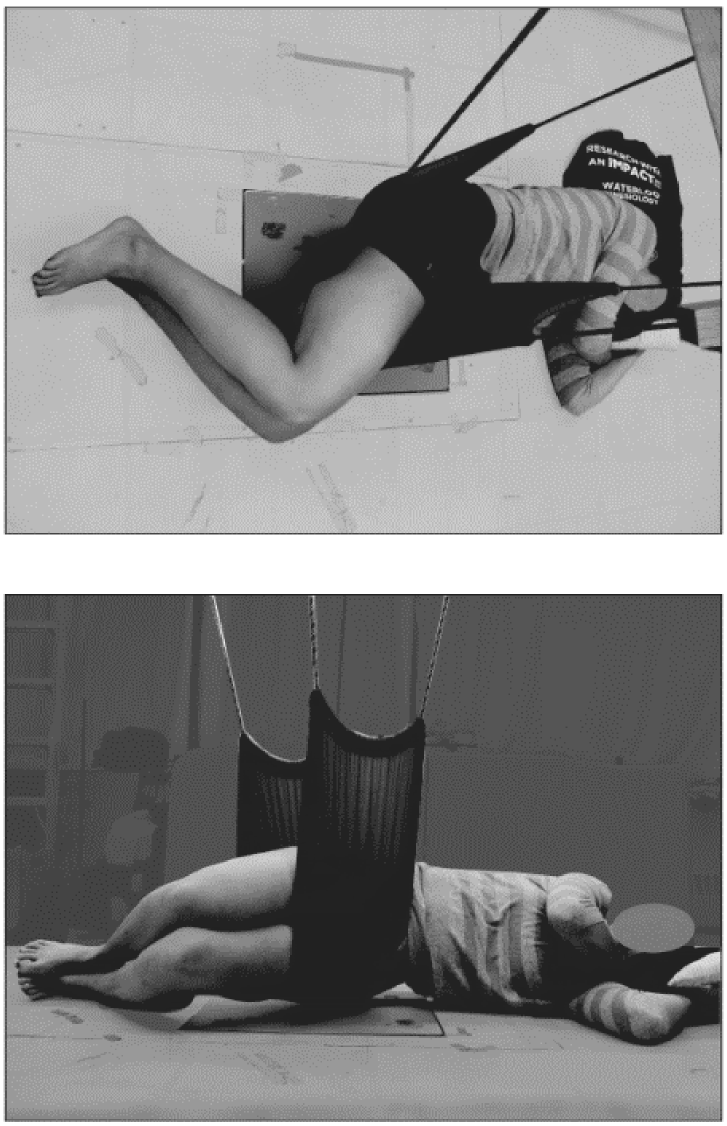

Figure 3.3 Support sling for the pelvis release protocol

A thin nylon sling was connected to an electromagnet (affixed to the ceiling) via a set of length-adjustable ropes. The sling is centered over a force plate which tracks time-varying force data. An Optotrak Smart Marker (not shown) was placed on the skin of the participant overlying the right greater trochanter. The configuration of the participant was adjusted prior to each trial, using the following protocol: First, the sling was raised so that the pelvis was suspended above the force plate the appropriate height for the trial. The participant was asked to position their arms near their head, and flex their knees (90°) and hips (45°). Finally, once the flexion angles were confirmed, the height of the pelvis was finely adjusted to the required height.

(Northern Digital, Waterloo, Ontario, Canada), with one Optotrak Smart Marker placed on the skin overlying the right greater trochanter to track the frontal plane deflection of the pelvis during impact.

3.2.4 Image treatment, signal conditioning and data reduction

Ultrasound images, and digital signals from the experimental impact protocol, were analyzed using customized Matlab (R2016a, Mathworks, Natick, Massachusetts, USA) routines.

3.2.4.1 Ultrasound Image Analysis

The ultrasound images were analyzed within a custom Matlab routine. The software within the M-Turbo device produces an image with square pixels, simplifying the calibration process. To calibrate the image, the in-software caliper function was used to draw a horizontal and a vertical line, both of 2 cm in length, within an image. One calibration frame was collected for each potential scan depth, and these frames were used to establish pixel-to-centimeter conversion values. Each of the trochanteric ultrasound images was then analyzed. A line tool was used to determine the pixel locations of the endpoints of the interference marker, and XY pixel locations were linearly interpolated between the endpoints. The curvature of the greater trochanter was traced, with an XY pixel location output for the entirety of the curve. The resultant distance between each point on the interference marker and each point on the femur surface was calculated; the soft tissue thickness is defined as the shortest possible resultant line.

3.2.4.2 Impact experiment - signal conditioning

Briefly, the filtering of impact data and methods of selection of cut-off frequencies have been the subject of debate. Impact events occur rapidly--in the case of this data set, a time-to-peak-force of 0.02-0.09 s would be expected. Implementation of a low-pass filter would, therefore, potentially over-smooth the impact event, reducing the impact peaks. Because this the focus of this study is peak values, we did not filter any time-varying signals.

3.2.4.2.1 Identification of key kinematic, kinetic and event timing variables within experimental impact data

Each trial was analyzed separately, and the trial results were averaged within each subject. An automated point-selection routine was developed to determine key data coordinates for further analysis. Each trial was segregated by defining an initial quiet (unloaded) region (Figure 3.4, prior to T1; $F_{initial}$, $D_{initial}$), the beginning of impact (when force exceeds two standard deviations of the mean in the quiet region preceding impact, Figure 3.4, T1; T_{imp}, F_{imp}), peak force (Figure 3.4, T2; T_{max}, F_{max}, P_{peak}, CA_{peak}, D_{peak}), and a final resting value (Figure 3.4, T4; T_{end}, F_{end},). Bias ($F_{initial}$, $D_{initial}$) was subtracted from F_{max} and D_{peak}; this step was not necessary for CA_{peak} and P_{peak} because the level of initial noise did not exceed the threshold for sensel activation. Effective mass ($Mass_{effective}$) was equal to T_{end}, representing the mass of the pelvis system and peripheral structures contributing to its mass during the impact and at rest. Across participants, maximum axial rotation of the pelvis relative to the ground during the pelvis release protocol was measured (via a marker cluster affixed to the sacrum in a separate study) as 9.2° during the pelvis release protocol; this maximal rotation would induce a potential error of less than 15%. That is, for a participant with a pelvis width of 30 cm, the vertical height of the sacral cluster at maximum rotation would be 13.0 cm (vs. 15 cm in a perfectly upright position) with an observed decrease in deflection of 0.038 cm over an expected deflection of 3 cm (i.e 2.962 cm observed deflection rather than 3 cm).

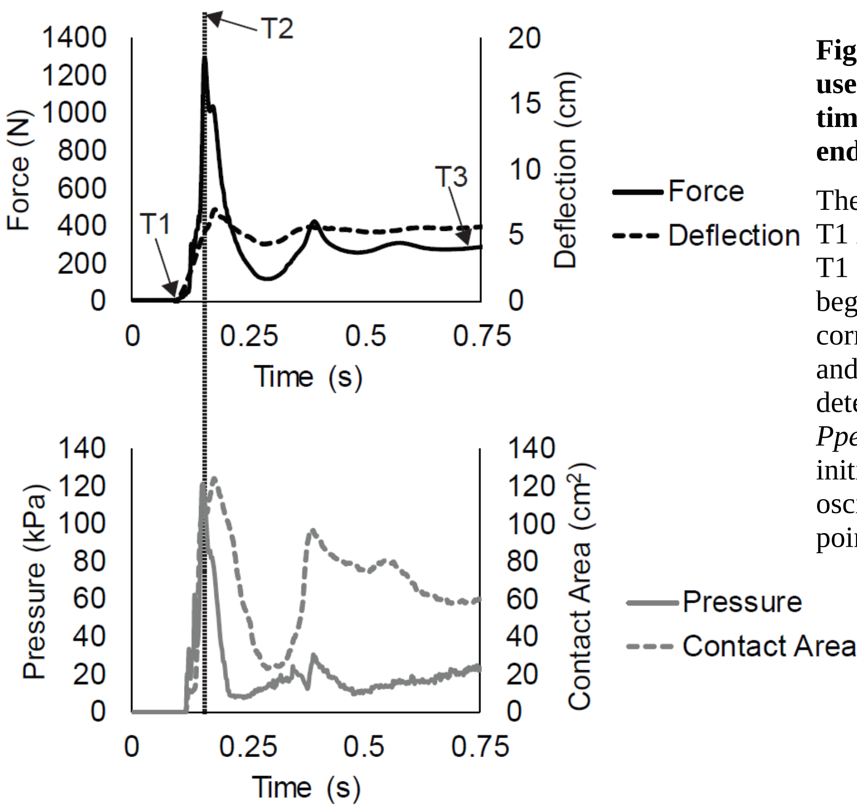

Figure 3.4 Critical timepoints used to define impact initiation, time of peak force and trial endpoint

The region prior (to the left of) T1 is the unloaded, quiet region. T1 corresponds with the beginning of impact, while T2 corresponds with the peak force, and is the timepoint selected for determination of D_{max}, CA_{max} *and Ppeak*. Interval T1-T2 is the initial loading phase. Force oscillates until a final resting point, T3.

3.2.5 Statistical Analysis

Statistical analysis was performed with a software package using an α of 0.05 (SPSS version 22, Chicago, USA). With *a priori* power analysis, a sample of 13 was determined to be sufficient for this study (α=0.05, β=0.95, r=0.500, G*Power version 3.1.9.2, Universität Düsseldorf, Düsseldorf, Germany). Pearson product-moment correlations (one-tail) were used to assess the strengths of relationships between body composition variables and impact characteristics. The hypotheses and specific independent and dependent variables are presented in Table 3.2 and Table 3.3. Independent and dependent variables were normally distributed for outcomes in this study.

Regarding hypothesis 4, the results of the Pearson product-moment correlation were further compared between "local" and "global" body composition characteristics, in pairs (Table 3.3). An *a priori* threshold for improvement was defined as an increase in r-square value of 0.05 or more.

Table 3.2 Independent-Dependent variable sets for hypothesis tests

Hypothesis	Dependent Variable	Independent Variables
1	F_{max}	$Mass_{total}$, BMI, $Mass_{effective}$, $Mass_{fat}$, $Mass_{lean}$, $Mass_{leg\_fat}$, $Mass_{leg\_lean}$, BMI_{fat}, BMI_{lean}
2	D_{peak}	$TSTT$, $Circ_{Hip}$, BF, $Mass_{fat}$, $Mass_{lean}$, $Mass_{leg\_fat}$, $Mass_{leg\_lean}$, BMI_{fat}, BMI_{lean}
3	CA_{peak}, P_{peak}	$TSTT$, $Circ_{Hip}$, BF, $Mass_{fat}$, $Mass_{lean}$, $Mass_{leg\_fat}$, $Mass_{leg\_lean}$, BMI_{fat}, BMI_{lean}

Table 3.3 Dependent-Global Independent-Local Independent Variable Sets

Dependent Variable	Global Independent Variable	Local Independent Variables
F_{max}	$Mass_{total}$ DXA_{lean_mass}	$Mass_{effective}$ $Mass_{leg\_lean}$
$D_{peak,}$ $CA_{peak,}$ P_{peak}	DXA_{fat_mass}	$Mass_{leg\_fat}$ $TSTT$

3.3 Results

For reference, descriptive statistics of the impact characteristics are presented below in Table 3.4.

Regarding the first hypothesis, peak force was significantly positively correlated with all indices of overall body size, except BMI_{fat} (Table 3.5; Figure 3.5). Stronger correlations were found between total ($Mass_{total}$, BMI) and lean mass indices ($Mass_{lean,}$ $Mass_{leg\_lean,}$ BMI_{lean}) than with fat mass indices ($Mass_{fat,}$ $Mass_{leg\_fat,}$ BMI_{fat}). $Mass_{total}$ alone explained 50.7% of the variance.

Regarding the second hypothesis, deflection was positively correlated with indices of adiposity (BF, $Mass_{fat,}$ $Mass_{leg\_fat,}$ BMI_{fat}), but not indices of lean mass ($Mass_{lean,}$ $Mass_{leg\_lean,}$ BMI_{lean},Table 3.6, Figure 3.6). The strongest relationship with D_{peak} was with $Mass_{leg\_fat}$, explaining 69.0% of the variance. However, more easily accessible measures, such as $Circ_{hip}$ explained as much as 52.6% of the variance.

CA_{peak} and P_{peak} were also correlated (CA_{peak} positively, P_{peak} negatively) only with indices of adiposity, but not lean mass (Hypothesis 3). All three variables were additionally correlated with $Circ_{hip}$. *TSTT* was consistently predictive of all three dependent variables (D_{peak} 51.2%, CA_{peak} 59.0%, P_{peak}, 59.8% variance explained) and was the single strongest correlate with P_{peak}. *BF* was the best performing variable for CA_{peak} (60.8%).

Regarding the fourth hypothesis, we found that an additional 16.2% of variance was explained for F_{max} with $Mass_{effective}$ relative to $Mass_{total}$, however, there was no improvement of $Mass_{leg\_lean}$ compared to $Mass_{lean}$. $Mass_{leg\_fat}$ improved the variance explained for D_{peak} (10.2%) and CA_{peak} (5.4%) but not P_{peak}.

Table 3.4 Impact characteristics

				Dependent variable correlations, r (p)		
	Maximum	**Minimum**	**Mean (SD)**	D_{max}	CA_{max}	P_{peak}
F_{max} (N)	1672.3	848.0	1267.4 (47.8)	0.476 (0.073)	0.318 (0.092)	-0.095 (0.709)
D_{peak} (cm)	3.13	0.91	1.68 (0.68)		0.813 (<0.001**)	-0.474 (0.087)
CA_{peak} (cm^2)	247.6	62.2	135.4 (47.7)			-0.318 (0.185)
P_{peak} (kPa)	1258.7	266.1	541.3 (253.9)			

* correlations significant at p<0.05, ** correlations significant at p<0.01

Table 3.5 Participant characteristics correlated with F_{max}

Variable	r	r^2	p
$Mass_{total}$	0.712	0.507	<0.001**
$Mass_{effective}$	0.818	0.669	<0.001**
BMI	0.521	0.271	0.011*
BMI_{fat}	0.401	0.161	0.039*
BMI_{lean}	0.510	0.260	0.015*
$Mass_{fat}$	0.497	0.247	0.018*
$Mass_{lean}$	0.713	0.508	<0.001**
$Mass_{leg\_fat}$	0.592	0.350	0.005**
$Mass_{leg\_lean}$	0.692	0.479	<0.001**

* correlations significant at p<0.05, ** correlations significant at p<0.01

Table 3.6 Correlations with D_{peak}, CA_{peak} and P_{peak}

Variable	D_{peak} r	D_{peak} r^2	D_{peak} p	CA_{peak} r	CA_{peak} r^2	CA_{peak} p	P_{peak} r	P_{peak} r^2	P_{peak} p
TSTT	0.716	0.512	0.002**	0.768	0.590	<0.001**	-0.773	0.598	0.002**
$Circ_{hip}$	0.725	0.526	0.001**	0.466	0.217	0.022*	-0.471	0.221	0.024*
BF	0.738	0.545	0.001**	0.780	0.608	<0.001**	-0.529	0.230	0.014*
$Mass_{fat}$	0.767	0.588	<0.001**	0.705	0.497	<0.001**	-0.490	0.240	0.023*
$Mass_{lean}$	0.016	0.000	0.478	-0.206	0.042	0.206	-0.005	0.000	0.492
$Mass_{leg\_fat}$	0.831	0.690	<0.001**	0.742	0.551	<0.001**	-0.535	0.268	0.025*
$Mass_{leg\_lean}$	-0.093	0.009	0.371	-0.234	0.055	0.175	-0.007	0.000	0.489
BMI	0.679	0.461	0.005**	0.520	0.270	0.023*	-0.473	0.224	0.048*
BMI_{fat}	0.766	0.587	<0.001**	0.735	0.540	0.001**	-0.529	0.280	0.015*
BMI_{lean}	0.110	0.021	0.348	-0.102	0.010	0.343	-0.160	0.026	0.270

** correlations significant at p<0.05, ** correlations significant at p<0.01*

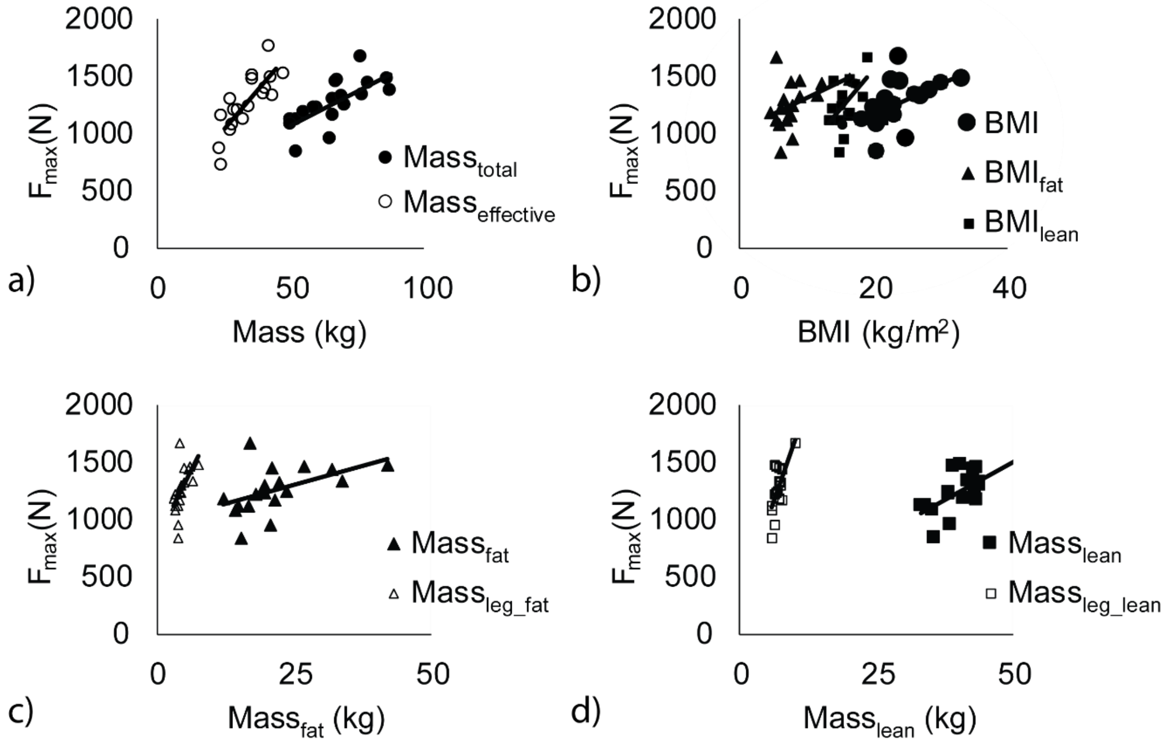

Figure 3.5 Participant characteristics correlated with F_{max}
including global and local estimates of mass (a), total and compositional BMI (b), global and local estimates of fat mass (c) and lean mass (d)

All independent variables investigated correlated with F_{max}. F_{max} was most strongly correlated with $Mass_{total}$, $Mass_{effective}$ (a) and $Mass_{lean}$, (d) and less strongly correlated with BMI (b) and indices of adiposity ($Mass_{fat}$, $Mass_{leg\_fat}$, c).

In this, and all following figures, circles (○) represent general body characteristics, squares (□) are specific to lean mass, triangles (△) are specific to fat mass. Filled elements are global characteristics, open elements are local characteristics. Solid lines indicating trends have been included for significant correlations.

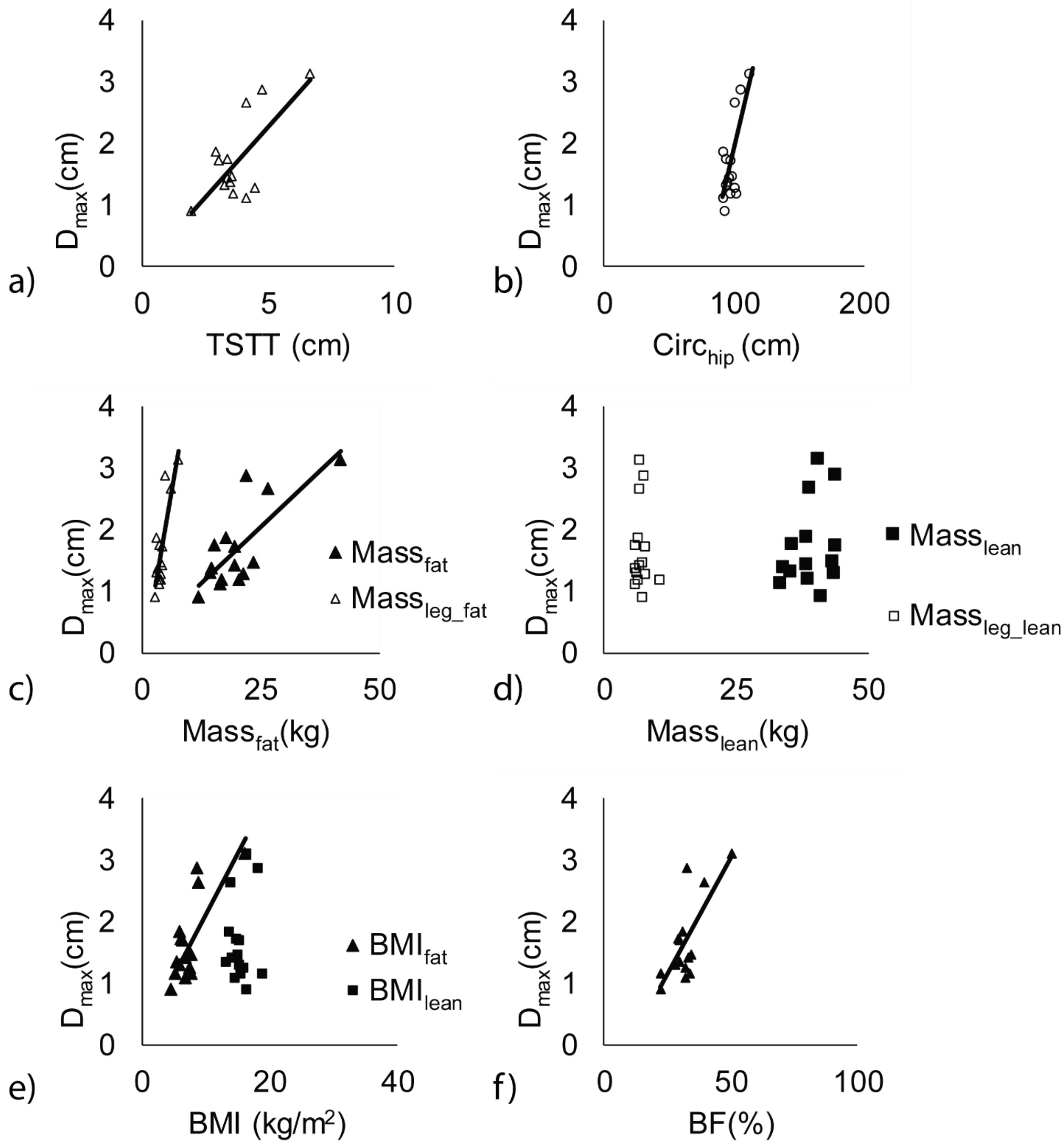

Figure 3.6 Scatterplots of *D_{peak}* vs. participant characteristics including
a) TSTT, b) *$Circ_{hip}$*, c) global and local estimate of fat mass, d) global and local estimate of lean mass, e) total and compositional BMI, and f) percent body fat.
Only indices or direct measures of adiposity were correlated with D_{peak}. D_{peak} was most strongly correlated with $Mass_{fat}$, $Mass_{leg\_fat}$, $Circ_{hip}$ *STT* and BMI_{fat}, however, *BF* also explained greater than 50% of the variance in D_{peak}.

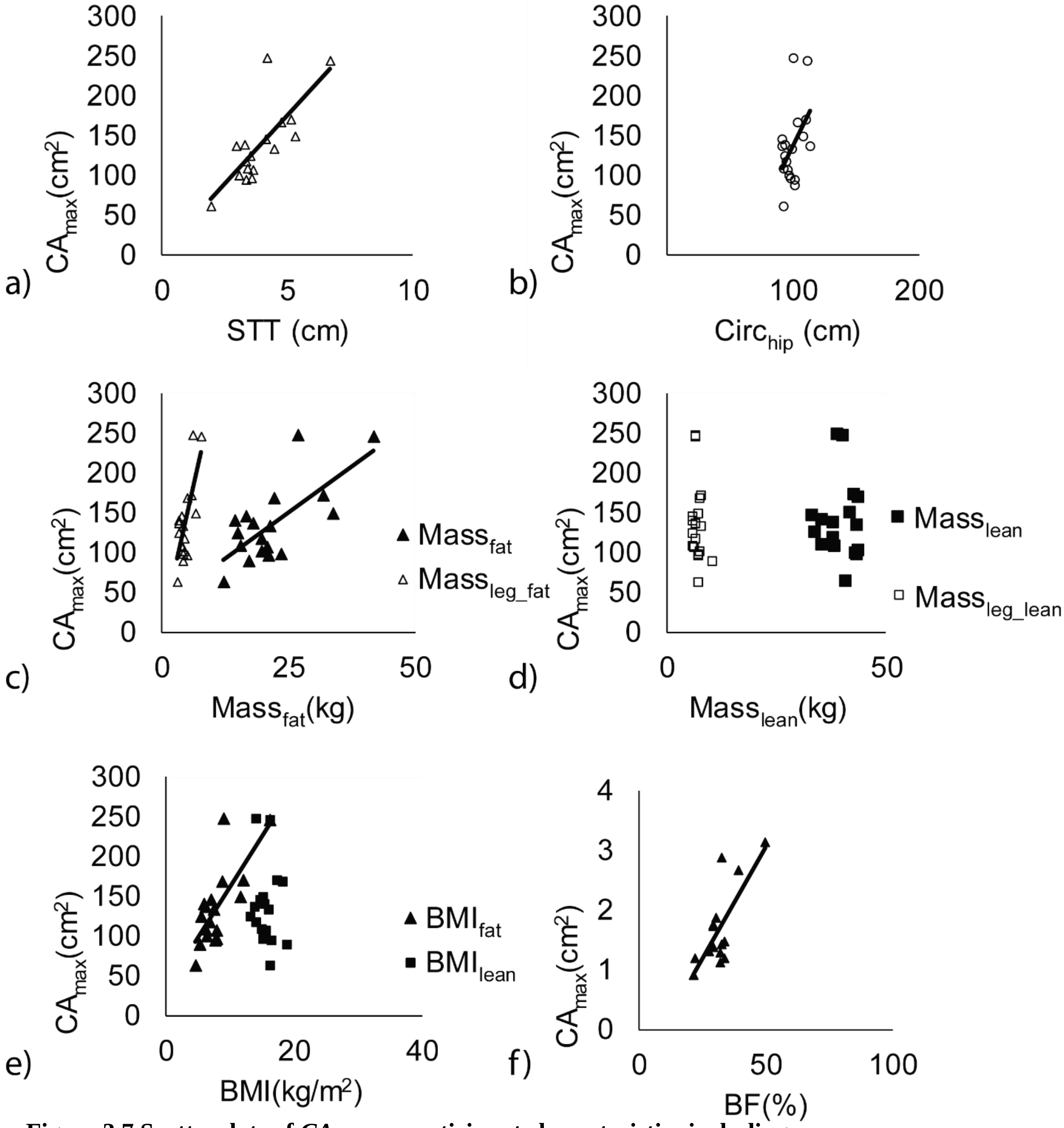

Figure 3.7 Scatterplots of CA_{peak} vs. participant characteristics including a) TSTT, b) $Circ_{hip}$, c) global and local estimate of fat mass, d) global and local estimate of lean mass, e) total and compositional BMI, and f) percent body fat.

Only indices or direct measures of adiposity were correlated with CA_{peak}. $CA_{peak}$was most strongly correlated with BF, STT, $Mass_{fat}$, $Mass_{leg\_fat}$, and BMI_{fat}, and more weakly related to $Circ_{hip}$.

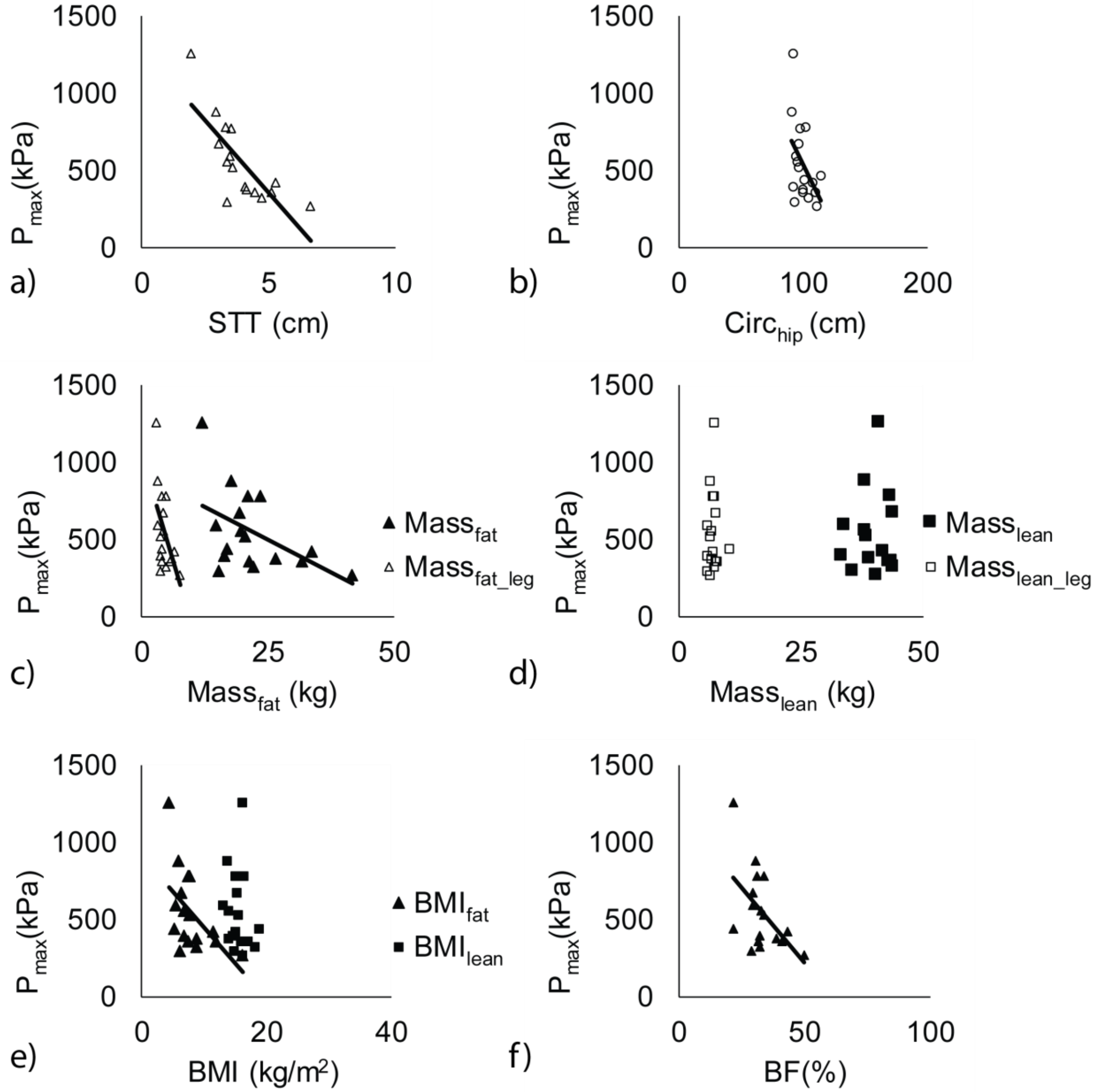

Figure 3.8 Scatterplots of P_{peak} vs. participant characteristics including a) TSTT, b) *Circ*$_{hip}$, c) global and local estimate of fat mass, d) global and local estimate of lean mass, e) total and compositional BMI, and f) percent body fat.

Only indices or direct measures of adiposity were correlated with P_{peak}. P_{peak} was most strongly correlated with *STT* and *BF*, and more weakly correlated with BMI_{fat}, $Circ_{hip}$, $Mass_{fat}$ and $Mass_{leg\_fat}$.

Table 3.7 Comparison of Local vs. Global Body Composition Variable Relationships with Outcome Variables

Dependent Variable	Global Independent Variable	r^2	Local Independent Variables	r^2	Improvement
F_{max}	$Mass_{total}$	0.507	$Mass_{effective}$	0.669	0.162*
	$Mass_{lean}$	0.508	$Mass_{leg\_lean}$	0.479	---
D_{peak}	$Mass_{fat}$	0.588	$Mass_{leg\_fat}$	0.690	0.102*
			TSTT	0.512	---
CA_{peak}	$Mass_{fat}$	0.497	$Mass_{leg\_fat}$	0.551	0.054*
			TSTT	0.590	0.093*
P_{peak}	$Mass_{fat}$	0.240	$Mass_{leg\_fat}$	0.268	0.028
			TSTT	0.598	0.358*

* Represents a significant improvement over the global variable, defined by an increase in r^2 of 0.05 or better

3.4 Discussion

The goal of this study was to explore relationships between contact area, pressure and peak force during impact with respect to body composition. We found clear differences between the variables associated with F_{max} compared to D_{peak}, CA_{peak}, and P_{peak}. F_{max} was strongly related to overall body size and lean mass. D_{peak}, CA_{peak}, and P_{peak} were strongly related to indices of adiposity and soft tissue thickness. We found that more than 50% of the variance for all four dependent variables could be explained by one of two independent variables: $Mass_{total}$ (for peak force) and *TSTT* (for peak contact area, pressure and deflection). Several local body composition variables were more strongly related with the dependent variables than the paired global body composition variables. Collectively, these findings provide important new insights into role body composition factors on impact dynamics during lateral falls on the hip.

It has been a long-standing hypothesis that peak forces are attenuated by soft tissues overlying the hip primarily through a two-dimensional energy absorption mechanism (Robinovitch, Hayes et al. 1991; Robinovitch, McMahon et al. 1995; Laing and Robinovitch 2010; Levine, Bhan et al. 2013). However, in this study, we found that F_{max} was most strongly related to lean mass (50.8% of variance) and not fat mass (24.7% of variance. This supports our first hypothesis. The greater trochanter and lateral aspect of the pelvis are primarily surrounded by fat, not lean tissue; in this study, the mean (SD) right leg fat content was 37.9 (6.3)%. Despite this, F_{max} appears to be more strongly related to the initial energy of the system ($1/2mv^2$) rather than the energy absorption of the soft tissues. This follows the findings of Bhan and colleagues (2014) that showed an increase in energy absorption between participants with low- and high-BMI, but not between male and female participants of the same BMI during a similar pelvis release protocol. Females have greater trochanteric TSTT than males at the same BMI (Levine, Minty et al. 2015), yet did not experience the associated greater energy absorption. Peak forces, therefore, were strongly driven by overall mass, particularly lean mass, and the added mass associated with increased body fat may have a limited influence on peak force during an impact to the hip.

In contrast, P_{peak}, or what could be described as the localized force in the "danger zone" was strongly related to *TSTT*, as was CA_{peak}, supporting hypothesis three. These outcomes were not related to any lean mass component. This contrasts findings from simulated static, long-duration loading of the pelvis, during which simulated reduced lean mass was associated with greater pressure between the pelvis and contact surface (Elsner and Gefen 2008), though not as strong of an effect as simulated reduced soft tissue mass. This difference may be due, in large part, to the local anatomy of the lateral hip. The lateral aspect of the greater trochanter is primarily surrounded only by adipose tissue, and serves only as an attachment point for the muscles in the region. This narrow location is most the most likely anatomical location corresponding to P_{peak}, and would explain the dependence on fat mass rather than lean mass. However, the proximal femur excluding the greater trochanter, and lateral pelvis are surrounded by muscle; lean mass may have a larger effect on load distribution within regions distal to the greater trochanter. Other loading regions may have substantial effects on injury outcomes, particularly with respect to pelvis and subtrochanteric fractures. Future work should clarify whether the differences in effect of tissue type on load distribution depend on local anatomical differences, loading rate, or a combination of both factors. Additionally, the relationship between hip fracture risk and P_{peak} has only been theorized. Determining the link between load distribution and fracture outcomes would clarify whether our highly localized P_{peak}, or a load distribution region with a larger surface area, is more predictive of hip fracture. Therefore, while body size is the largest driver of total impact force and the influence of body composition is more limited, when moving from a global to local load distribution perspective, the opposite is true—mass drives the energy input to the system, while body composition drives energy redistribution away from the central contact point.

The associations we observed between *STT* and metrics of both load distribution (CA_{peak}, P_{peak}) and local energy absorption (D_{peak}) provide novel insights into impact dynamics during lateral pelvic impacts. This supports hypothesis two and three. D_{peak} and CA_{peak} were strongly correlated (r=0.824, p<0.001), however, the magnitude of D_{peak} was, on average, only 25.5 (6.5)% as large as the radius of CA_{peak}. , Additionally, D_{peak} reached only 45.6 (12.1)% of TSTT. Oomens et al. (2003) found a maximum soft tissue deflection of 25% over the ischial tuberosity, and local compressive strain concentrations within muscle and adipose components directly overlying skeletal landmarks. This lends support to alternative theories regarding pelvis-ground contact mechanics. First, low system D_{peak} or component compressive strain supports the theory that the primary behavior of soft tissues during an impact is not one-dimensional elastic compression, and maximum strain limitations within the soft tissues may increase localized stress. Second, soft tissue reached maximum compression at a low proportion of TSTT. Adipose tissue contains glycerol, a viscous liquid, along with water; the soft tissues overlying the hip may therefore follow basic principles of fluid dynamics rather than elastic behavior of springs. Rather than being compressed, the tissue maintains volume throughout the impact, but is displaced away from the greater trochanter at a rate dependent on the impact velocity. The loading period of a pelvis release is <0.1 s (Laing and Robinovitch 2010; Levine, Bhan et al. 2013). At a loading rate of 2 m/s and indentation duration of 0.002 s, only 25-50% of stress-relaxation in porcine gluteus muscle occurs within 0.1 s (Palevski, Glaich et al. 2006); with identical conditions, stress-relaxation in ovine adipose tissue is substantially slower (Gefen and Haberman 2007). Further, compressive strain rates greater than 0.5%/s, the viscoelastic component contributes more than 50% of the total stress in porcine skeletal muscle (Van Loocke, Lyons et al. 2008). The viscoelastic effect on limiting compression and shear flow, and increasing stress within the soft tissues is, therefore, likely substantial over the duration of the loading period.

We found that local body composition characteristics explained substantially more variance than global characteristics. These results have implications for modeling of pelvis impacts, as well as implementation in clinical injury prediction models. Specifically with regards to peak pressure, *TSTT* provided a 35.8% improvement over $Mass_{fat}$, highlighting the importance of local system characteristics on localized impact dynamics. $Mass_{effective}$ and *TSTT* were the strongest overall correlates with F_{max} and D_{peak}, P_{peak}, and CA_{peak}. However, $Mass_{total}$ and *BF* may be more easily obtainable characteristics within a clinical setting than effective mass and *TSTT*. A relationship linking $Mass_{effective}$ and $Mass_{total}$, as well as *BF* with *TSTT* may improve performance of the global characteristics when included in load prediction models. Additionally, *TSTT* was associated with an 11% improvement in r^2 over BMI for deflection, and better than 100% improvement over BMI for CA_{peak} and P_{peak}. This, along with clear differences in effects of lean mass and fat mass on force magnitude and distribution outcomes, points towards the importance of a model which incorporates a separate estimate of lean and fat mass.

This study was associated with several limitations. In this study, we only included female participants due to the greater representation in hip fracture epidemiology (Cawthon 2011) and the greater variation in pelvis tissue composition in females compared to males (Levine, Minty et al. 2015). However, the general results likely extend to male fallers as well: total mass, particularly lean mass, is related to peak force during an impact to the hip, while fat mass is related to load distribution. We also only measured external forces and load distribution. It is unclear whether the compressive strain concentrations identified by Oomens et al (2003) contribute to localized stiffness and loading at the greater trochanter during loading rates used in this study. It would be valuable to investigate the effect on load distribution at the floor-pelvis interface on internal loading of the proximal femur and pelvis. Finally, we only explored bivariate correlations in this study and did not correct the significance level for multiple comparisons. The goal of this study was to provide evidence for the individual mechanical behavior of the tissue types, as well as identify key, streamlined links between individual elements of body size or composition that could be included in an individualized model or population-based clinical test for fracture risk. However, it is unclear how the factors measured in this study interact, and how the interactions or interdependence of multiple components could be incorporated in such models. Interactions of the dependent variables, such as stiffness (i.e. force vs. deflection) may clarify how body size and composition interact beyond peak force, deflection, contact area and pressure outcomes.

In summary, we found that impact dynamics related to hip fracture were strongly related to individual characteristics, providing support for the development of subject-specific lateral pelvis impact load prediction model. Peak force was most strongly related to mass, while peak pressure, contact area and deflection were most strongly related to the quantity of adipose tissue overlying the hip. There was substantially lower compression than load distribution, and maximum compression was achieved at less than half TSTT. Considering the anatomy of the pelvis viscoelastic components likely have a substantial effect over the impact duration. This points towards the development of a three-dimensional, viscoelastic load distribution model as an improvement over the one-dimensional force attenuation model, subsequently explored in Studies 2 and 3.

Chapter 4, Study 2: Parameter Identification for a Multibody Approach to Predicting Impact Characteristics During Lateral Impacts to the Hip

Chapter 4 discusses development and analysis of the model parameters. The work in this chapter supports comparison of model performance in Study 3

4.1 Introduction

Fall-related hip fractures are responsible for over 30% of injury-related hospitalizations in community-dwelling older adults, and nearly 60% of older adults in residential care, representing a high proportion of the $2 billion annual fall-related hospitalization and rehabilitation costs in Canada (Stinchcombe, Kuran et al. 2014). From a mechanical perspective, the risk of hip fracture is dependent on the ratio of applied load to tissue tolerance, known as the factor of risk (Hayes, Piazza et al. 1991) or load-strength ratio. However, widely used models to predict hip fractures have primarily focused on the tissue tolerance perspective (Kanis, Hans et al. 2011; Leslie, Berger et al. 2011; Lewiecki, Compston et al. 2011; Hippisley-Cox and Coupland 2012). While these models represent a significant advancement in prediction and prevention of fracture, they are based on population-level parameters and outcomes—relationships which are sensitive to change as the population evolves (Luo 2016). Finally, it is challenging to mechanistically link clinical risk factors included in these models, such as tobacco consumption, to fracture outcomes. Further understanding of the mechanics of impacts to the hip may improve prediction of hip fractures.

One approach to predicting the mechanical behavior of impacts to the hip is multibody modeling. Previous attempts at this approach have focused on simple models comprised of a mass and spring, or mass spring and damper (Robinovitch, Hayes et al. 1991; Robinovitch, Hayes et al. 1997; Laing and Robinovitch 2010; Luo, Nasiri Sarvi et al. 2014; Sarvi and Luo 2015). It is primarily hypothesized that the stiffness and damping components of these models are driven by factors such as the thickness of compliant trochanteric soft tissue (TSTT) and the stiff skeletal structures. However, these models predict impact characteristics less accurately for experimental participants outside a normal BMI range than for those within a BMI range of 21-24 kg/m^2 (Levine 2011; Levine, Bhan et al. 2013). Additionally, TSTT alone has mixed effectiveness in predicting hip fracture cases (Bouxsein, Szulc et al. 2007; Nielson, Bouxsein et al. 2009)—the mechanical behavior of individual-specific components, such as TSTT during impacts is unclear. Trochanteric soft tissues have been linked to distribution of loads during an impact to the hip (Study 1; Appendix 2; Laing and Robinovitch 2008; Choi, Hoffer et al. 2010). More complex models including geometric components, such as those based on Hertzian spring theory (Hertz and Hunt-

Crossley models) and the Volumetric contact model, may better replicate this load distribution, but include a greater range of parameters. While all of these models would have greater external validity and utility if they were to be linked to individual body size or composition parameters, this relationship has not yet been characterized.

Therefore, the overall purpose of this study was to characterize stiffness and damping parameters during a controlled impact to the hip during a simulation of a lateral fall. Within this framework, the primary goal was to determine: 1) if the model parameters differed between sexes or groups divided by TSTT, and, 2) if model parameters could be directly linked to body size (e.g. height, pelvis width) or body composition (e.g. TSTT, percent body fat) characteristics which could be used to develop regression equations to predict model parameters. We hypothesized that

1. stiffness and damping parameters would be different between sex and TSTT groups, more specifically, that stiffness parameters would be lower, and damping parameters greater in females and participants with greater TSTT,
2. that differences in TSTT groups would be associated, such that stiffness would be positively correlated, and damping negatively correlated with TSTT, and

in support of developing multiple-regression equations for model parameters,

3. other body size or composition elements will be correlated with stiffness or damping parameters, with the direction of relationship based on the conceptual link between the model parameter and body size or composition element (e.g. positive for hip circumference and Volumetric interference volume).

4.2 Methods

Forty-six healthy participants (<35 years, 24 female) consented to participate in this study (Table 4.1). Participant recruitment focused on developing a cohort with a wide variety of body composition. Exclusion criteria included musculoskeletal injury in the past year preventing completion of the protocol, lifetime fracture history, fear of falling, or other health conditions which would make participation unsafe. Participant mass (*mass*) was measured with a scale to the nearest 0.5 kg. Hip circumference ($Circ_{hip}$) was measured with a flexible tape measure at the level of the greater trochanter, and body height (*H*) and skeletal pelvis width (from right to left anterior superior iliac spine, *PW*) with a rigid meter stick, to the nearest 0.5 cm. Skinfold calipers were used to estimate percent body fat (*BF*, (Jackson and Pollock 1978; Jackson, Pollock et al. 1978; Jackson, Pollock et al. 1979)). Transverse-plane TSTT was assessed via ultrasound (minimum precision 0.17 cm; C60x, 2-5 MHz transducer, M-Turbo Ultrasound, SonoSite, Inc., Bothell, WA) in a side-lying position, similar to that expected during the impact phase of the fall simulations. Participants were grouped into low-, mid- and high-TSTT groups based the following criteria: males low <3 cm, mid 3.1-4 cm, high >4.1 cm; females low <3.5, mid 3.6-5, high >5 cm. These thresholds represent low- (<18.5 kg/m2), moderate (18.6-25 kg/m2) and high- (>25.1 kg/m2) BMI older adults (unpublished data).

Table 4.1: Mean (SD) participant anthropometric characteristics for participants with complete data

		N	Height (m)	Mass (kg)	BMI (kg/m^2)	TSTT (cm)
Females						
	Low	4	1.65 (0.07)	56.0 (7.4)	20.6 (1.6)	2.90 (0.35)
STT	Mid	5	1.67 (0.03)	66.1 (11.0)	23.6 (3.4)	4.38 (0.29)
	High	6	1.67 (0.04)	86.2 (24.1)	31.0 (7.0)	6.97 (2.31)
Males						
	Low	6	1.81 (0.07)	75.9 (10.4)	23.1 (2.0)	2.33 (0.46)
STT	Mid	6	1.80 (0.07)	84.2 (7.5)	26.1 (2.7)	3.37 (0.28)
	High	5	1.78 (0.09)	89.4 (10.8)	28.2 (2.2)	4.96 (1.22)

TSTT represents trochanteric soft tissue thickness. BMI represents body mass index

4.2.1 Experimental Protocol

Participants underwent a three-trial pelvis release experiment protocol, preceded by two modified quasi-static pelvis release experiments (Figure 4.1). Both protocols involved the lateral aspect of the left hip impacting a pressure plate (4096 resistive sensors, each 0.762 by 0.508 cm, sampled at 500 Hz; FootScan, RSScan, Olen, Belgium) overlying a force plate (sampled at 3500 Hz; OR6-7, AMTI, USA). The force

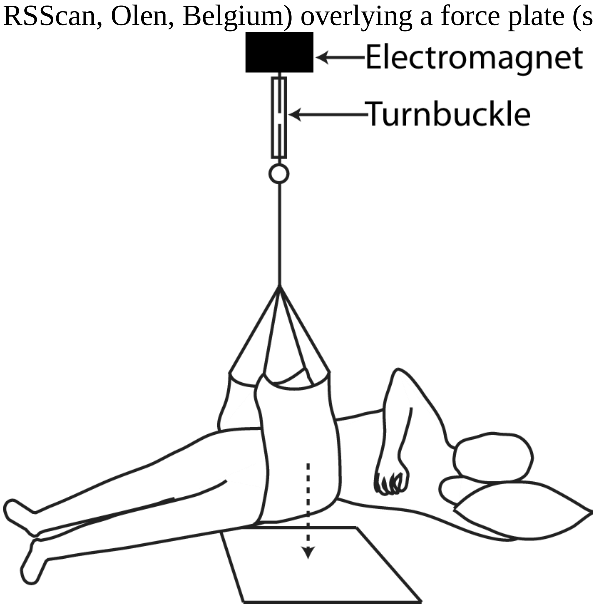

Figure 4.1 Initial position of the participant during the pelvis release protocol

The pelvis of the participant was suspended in a sling, supported by a set of ropes connected to a turnbuckle and an electromagnet. During the quasi-static experiments, the turnbuckle was used to slowly lower the sling. During the dynamic pelvis release experiments, the electromagnet was release to allow the sling to release rapidly and allow the pelvis of the participant to impact the force plate.

and pressure plates were spatially aligned and temporally synchronized using a motion capture system (Optotrak Certus, Northern Digital, Inc., Waterloo, ON). Motion of the pelvis and left thigh were tracked using three-dimensional motion capture (Optotrak Certus, Northern Digital, Inc., Waterloo, ON) at the maximum sampling rate (300 Hz) for the number of markers used. More specifically, the pelvis cluster was firmly affixed to the skin overlying the sacrum and L5 lumbar vertebrae—this region of the pelvis is overlaid by a relatively low level of soft tissue relative to other regions of the pelvis, and was selected to minimize soft tissue artifact during the impact. Digitized markers were used to estimate motion of the right and left anterior superior iliac spine and posterior superior iliac spine, along with the left lateral and medial femoral condyle to allow confirmation of consistent position of the pelvis and femurs during the protocol.

For both quasi-static and dynamic protocols, the pelvis of the participant was supported by the sling, which was designed to not directly contact the tissues between the iliac crest (superior border) and mid thigh (inferior border). The upper body of the participant was supported by a pillow, while the feet rested on a mat, both outside the contact area of the force plate. The hips of the participant were flexed to 45° and knees were flexed to 90°. For the quasi-static protocol, the pelvis was raised to a height where the soft tissues over the left hip were barely not contacting the impact surface. The participant was instructed to remain as still as possible, while the sling was lowered incrementally using the turnbuckle at a rate of <0.5 cm/min to create a negligible-velocity scenario. For the dynamic trials, the sling was raised so that the soft tissues over the left hip were 2 cm above the impact surface. When the participant reported that they were "relaxed and ready", the electromagnet was released, allowing the pelvis to impact the impact surface.

Two trials of quasi-static data were available for only 36 of the participants. The data sets for the remaining 10 participants were unavailable due to inconsistent data quality. For participants for whom the quasi-static data set was unavailable, the primary cause was noise in the vertical position of the pelvis. The procedure for the quasi-static trials was prolonged (up to 15 minutes per trial) and uncomfortable for some participants; this resulted in active movement of the pelvis, such as wiggling, activation of the muscles near the left greater trochanter to reduce pressure directly over the bony prominence, or other strategies to reduce prolonged pressure and discomfort to the impacting hip region. These active movements resulted in vertical motion of the pelvis exceeding the expected motion from the turnbuckle, or (less frequently) reduction in force from that expected based on the mass of the participant. Two or more trials of dynamic data was only available for 37 of the participants. Missing data in these cases was due to marker occlusion between the start of impact and peak force. In total, we had fourteen male and seventeen female participants with full datasets for further analysis.

4.2.2 Signal Processing

We used a customized MATLAB routine (MathWorks, Natick, MA) to process the time-varying signals. All data points collected were included in the quasi-static analysis. For the dynamic trials, an automated point-selection routine was developed to truncate the data for further analysis. Each trial was segregated by defining an initial quiet (unloaded) region ($F_{initial,} D_{initial}$), the beginning of impact (when force exceeded two standard deviations of the mean within $F_{initial}$: T_{imp}, $F_{imp,}$ D_{imp}), and peak force (T_{max}, $F_{max,}$ D_{max}). Bias ($F_{initial}$) was subtracted from all F_{max}

Force and position data were then resampled to 500 hz to maximize the number of data points within the region of interest and match the sampling frequency of the pressure plate. The resampling procedure implemented a zero-lag least-squares linear-phase finite impulse response filter with a Kaiser-Bessel window followed by a spline interpolation. This procedure induced an mean (SD) absolute change in peak force of 0.55 (1.18)% from the unfiltered peak values.

Time-varying vertical position of the pelvis cluster was subtracted from the position of the cluster at T_{imp} to produce positive deflection (δ) values. The contact profile (*CP*) associated with each quasi-static or dynamic data frame was further processed: first, peak pressure magnitude (P_{peak}, $P_{peak\_location}$) was determined as the sensel with the greatest magnitude within the *CP*. Second, the *CP* was converted to a binary matrix, and an iterative algorithm was used to include active sensels within a three-sensel radius of sensels concurrent with $P_{peak\_location}$. The final *CP* was used to mask distal and proximal body segment contacts to determine Contact Area (*CA*). Contact area (CA) was calculated as the sum of all active sensels at a given time, multiplied by the sensel area (0.387 cm^2). Time-varying volume of interaction (V) between the floor and pelvis was calculated following Boos (2011) as:

$$V_t = \frac{\pi}{3}{\delta_t}^2[(3r) - \delta_t] \qquad (4.1)$$

With *r*, a constant representing the radius of interaction of the pelvis and floor at the time of maximum system deflection (i.e. compression):

$$r = \sqrt{CA_{max}/\pi} \qquad (4.2)$$

Time-varying force, deflection, and volume area were truncated to the points between T_{imp} and T_{max}). Impact velocity (*v*) was confirmed for the pelvis over the two data points directly preceding T_{imp} .

4.2.2.1 Stiffness and Damping Components

Stiffness (*k*) and damping (*a* for VG, *b*, for HC and VO) were characterized separately for each model based on the force and corresponding deflection or volume data from the quasi-static and characterization data sets. The general formula for each model is as follows:

Table 4.2 Model normal force formulae

Model	Formula	
MS	$F_N = k_{MS}\delta$	(4.3)
HZ	$F_N = k_{HZ}\delta^{3/2}$	(4.4)
VG	$F_N = k_{VG}\delta + b_{VG}\dot{\delta}$	(4.5)
HC	$F_N = k_{HC}\delta^{3/2} + a_{HC}\delta^{3/2}\dot{\delta}$	(4.6)
VO	$F_N = k_{VO}V(1 + a_{VO}\dot{\delta})$	(4.7)

For the mass-spring model, k_{MS} was characterized using a least-squares curve-fitting approach using paired dynamic force and deflection data points between the start of impact (T_{imp}) and peak force (T_{max}) (Figure 4.2, red line). Stiffness for HZ (k_{HZ}) followed the same approach, with a non-linear curve satisfying the theoretical exponent (p) of 3/2 (Figure 4.2, cyan line).

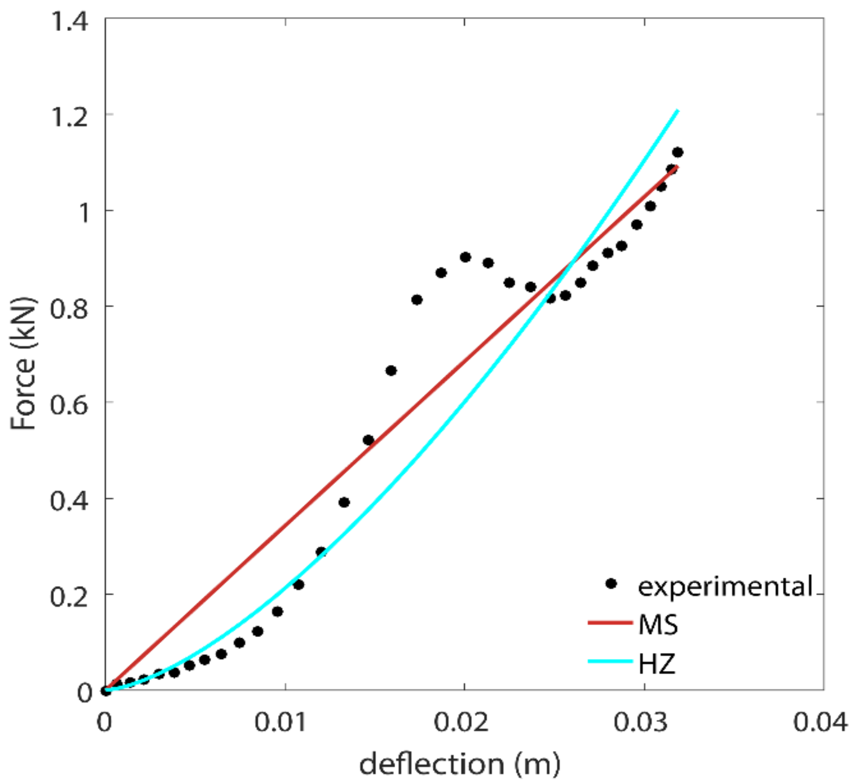

Figure 4.2 Least-squares curve fits for estimation of MS and HZ stiffness components

The experimental dynamic data (dots) is fit with a linear (MS, red) or nonlinear (HZ, cyan) curve, minimizing the least-squares error between the curve fit and the experimental data.

For models including stiffness and damping components, models were characterized with the assumption that deflection was distributed equally between the components. Therefore, stiffness estimates for the Voigt (k_{VG}), Hunt-Crossley (k_{HC}) and Volumetric (k_{VO}) were determined using a least-squares fit to the quasi-static data set to determine the system stiffness independent of velocity (Figure 4.3a,b). For VG, k_{VG} was characterized using a linear fit to paired force and deflection data; k_{HC} was characterized following the same approach with a non-linear curve satisfying the theoretical exponent of 3/2. For VO, k_{VO} was characterized using a linear-fit to paired force and volume data.

For models including damping, the total restorative force is the sum of the effects of the spring (dependent on deflection or change-of-shape) and damping (dependent on rate-of-deflection or rate-of-change-of-shape) components, with both elements undergoing the same instantaneous magnitude of deflection. The stiffness parameters were used to estimate load based on the stiffness component and deflection (*VG*, *HC*) or volume (*VO*), indicated by the coloured dots in Figure 4.3 (panel c,d). The difference (F_{diff}) between the experimental dynamic force and the force predicted using only the stiffness component was used to develop a cost function to solve for damping parameters (b_{VG}, a_{HC}, a_{VO}) using a least-squares approach.

The final curves fit to the data for all models are presented in Figure 4.3

Table 4.3 Cost functions for viscoelastic models

Model	Formula	
VG	$$c_{damp} = \sum_{t_{imp}}^{t_{max}} \left(F_{dyn}^{t} - F_{QS}^{t} - b_{VG}\dot{\delta}\right)^2$$	(4.8)
HC	$$c_{damp} = \sum_{t_{imp}}^{t_{max}} \left(F_{dyn}^{t} - F_{QS}^{t} - a_{HC}\delta^{3/2}\dot{\delta}\right)^2$$	(4.9)
VO	$$c_{damp} = \sum_{t_{imp}}^{t_{max}} \left(F_{dyn}^{t} - F_{QS}^{t}(1 + a_{VO}\dot{\delta})\right)^2$$	(4.10)

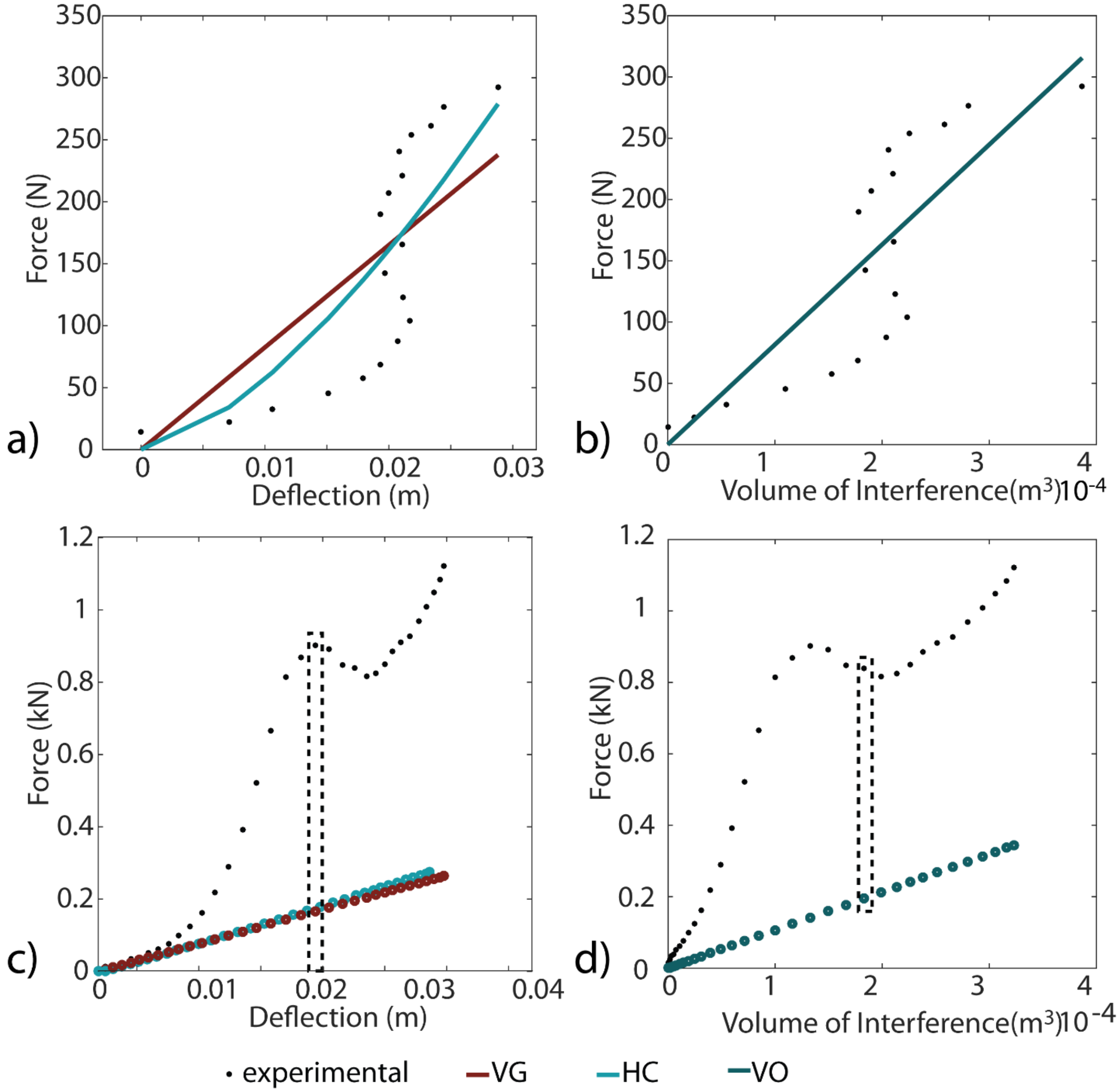

Figure 4.3 Characterization of velocity-independent stiffness and velocity-dependent damping components

The experimental quasi-static data (a, b, dots) was fit with a linear (VG, burgundy, VO, dark teal) or nonlinear (HC, teal) curve, minimizing the least-squares error between the curve fit and the experimental data. The stiffness parameters were used to estimate the force generated by the stiffness components only (i.e. velocity independent) based on the deflection or volume in the dynamic trial (c,d, coloured dots). The difference between the experimental (F_{dyn}) and estimated (F_{QS}) force (F_{diff}) was then fit using a least-squares method for each model to determine the damping component. The instantaneous rise in force (panels a,b between 100-250 N) is likely an artifact of muscle activation or wiggling during the trial, as discussed in section 4.2.1.

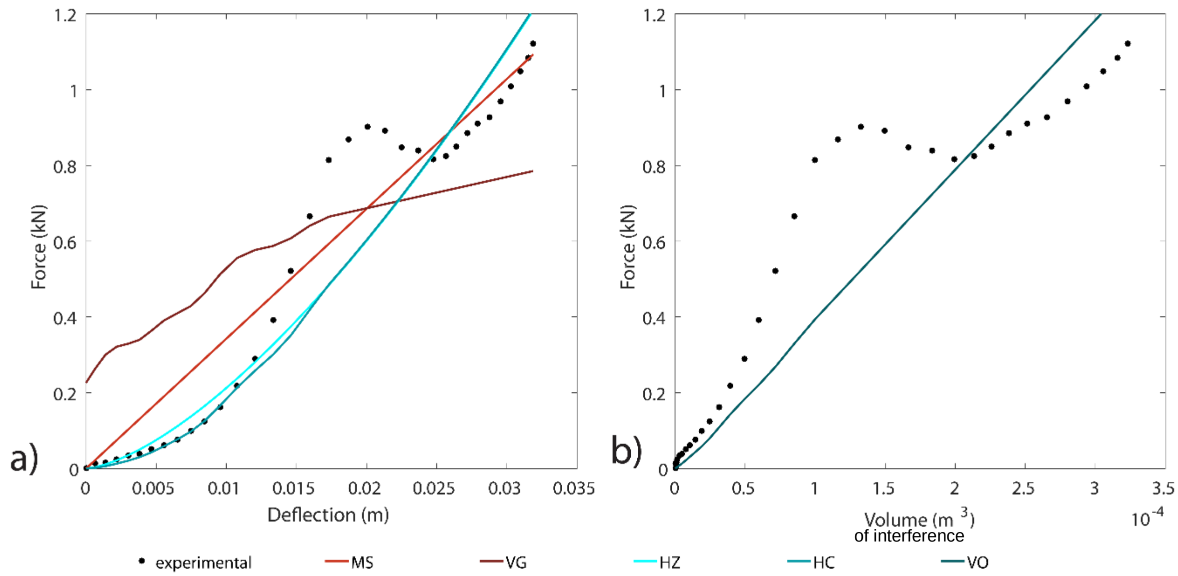

Figure 4.4 Demonstration of curve fit to experimental data for MS, HZ, VG, HC and VO

The experimental data (dots) is shown along with the final curve fit for each model, consisting of a stiffness (MS, HZ) or stiffness and damping (VG, HC, VO) component.

4.2.3 Statistical analysis

All statistical analysis was performed using a software package (SPSS version 21, Chicago, USA) using an α of 0.05 to signify statistical significance. Regarding the first hypothesis, a two-way analysis of variance (ANOVA) was used to compare sex and TSTT group (both between-subjects factors) on the model parameters (k_{MS}, k_{HZ}, k_{VG}, k_{HC}, k_{VO}, b_{VG}, a_{HC}, a_{VO}). Regarding the second hypothesis, Pearson product-moment correlation (one-tail) was used to assess the strength of relationship between TSTT and the stiffness and damping parameters. Regarding the third hypothesis, Pearson-product moment correlation (one-tail) was used to characterize the relationship between other body size and composition elements (*height, body mass, TSTT, pelvis width, hip circumference and body fat (%)*) and model parameters. Finally, for each parameter, multiple linear regression was performed based on the results of hypotheses 1-3 using a forced-entry method. In cases where dependent predictors were both correlated with the dependent variable (e.g. TSTT and body fat, BMI and mass), the strongest of the correlates was selected for inclusion in the regression protocol. For the correlations and regressions, if a sex difference was observed within the ANOVA results, correlations and regressions were performed separately for males and females. With *a priori* power analysis, a sample of 13 was determined to be sufficient for this study (α=0.05, β=0.95, r=0.500, G*Power version 3.1.9.2, Universität Düsseldorf, Düsseldorf, Germany).

A sample of 54 participants was required for the ANOVA procedures (α=0.05, β=0.95, d=0.5, G*Power version 3.1.9.2, Universität Düsseldorf, Düsseldorf, Germany), however, we did not reach this level of recruitment. If a TSTT group difference was observed within the ANOVA results, and there appeared to be discontinuities between groups (i.e. it would not be appropriate to characterize one or more groups with a single regression), correlations and regressions were performed separately for each TSTT group. Independent variables were normally distributed for outcomes in this study.

4.3 Results

Quality of fit for each model is presented in Appendix 4.

Regarding the first hypothesis, there were no sex-TSTT interactions for any model parameter (Table 4.4). The Hunt-Crossley stiffness estimate (k_{HC}) differed between sexes (91.6% greater for males than females, Figure 4.6b) but not TSTT groups. The volumetric stiffness estimate, k_{VO} differed between TSTT groups (higher for high-TSTT participants) but not sexes (Figure 4.6c). There was no difference between sexes or TSTT groups for k_{MS} (Figure 4.5a), k_{HZ} (Figure 4.5b), or k_{VG} (Figure 4.6a). Damping coefficient b_{VG} was 1.4-fold higher for males vs. females , but was not influenced by TSTT (Figure 4.7a). In contrast, damping coefficients a_{VO} and a_{HC} did not differ between sex (*HC*, Figure 4.7b; *VO*, Figure 4.7c) or TSTT groups.

Regarding the second hypothesis, k_{VG}, k_{HC} and b_{VG} were not linked to any body size or composition element. TSTT was most strongly negatively correlated with k_{VO} (r^2=0.587, p<0.001, Figure 4.5d). *BF* was negatively correlated with k_{MS} (r^2=0.112, p=0.046, Figure 4.6c) and k_{HZ} (r^2=0.157, p=0.017, Figure 4.6d). *PW* was negatively correlated with a_{HC} (r^2=0.123, p=0.038, Figure 4.6d) and a_{VO} (r^2=0.157, p=0.039, Figure 4.7e). Full correlation results are presented in Table 4.5 and Appendix 4.

Final regression equations and single parameter values (in cases where parameters were not correlated with body size or composition measures) are presented in Table 4.6. All final models were single-predictor models, and inclusion of secondary predictors did not improve the predictive capability or residual errors against a minimum r^2 improvement threshold of 0.05 or better.

Table 4.4 Summary of ANOVA results for Hypothesis 1

Dependent Variable	Factor	Pair	F	t	p
k_{MS}	TSTT X sex		0.1		0.368
	TSTT		0.7		0.496
	Sex		3.6		0.065
k_{HZ}	TSTT X sex		0.2		0.856
	TSTT		1.0		0.370
	Sex		1.9		0.181
k_{VG}	TSTT X sex		0.4		0.660
	TSTT		0.0		0.976
	Sex		2.6		0.119
k_{HC}	TSTT X sex		0.0		0.968
	TSTT		0.5		0.640
	Sex		8.2		0.010*
k_{VO}	TSTT X sex		0.8		0.467
	TSTT		16.2		<0.001**
		High vs. low		4.4	<0.001**
		High vs. medium		4.5	0.001**
	Sex		1.9		0.185
b_{VG}	TSTT X sex		0.1		0.968
	TSTT		0.6		0.548
	Sex		6.2		0.019*
a_{HC}	TSTT X sex		0.2		0.791
	TSTT		1.1		0.339
	Sex		0.9		0.341
a_{VO}	TSTT X sex		0.4		0.642
	TSTT		0.7		0.487
	Sex		1.5		0.231

** comparison significant at $p<0.05$; ** comparison significant at $p<0.01$*

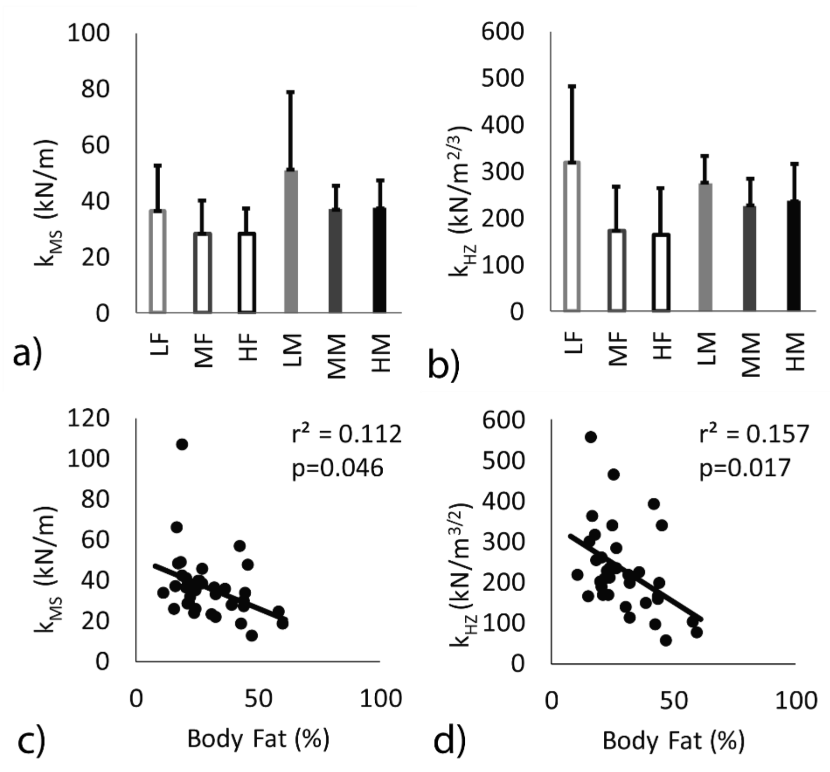

Figure 4.5 Groupwise differences and strongest correlations for k_{MS} and k_{HZ}

Only models with elastic components only are included in this figure. There were no significant interactions between sex and TSTT group for k_{MS} (a) or k_{HZ} (b), nor were there significant main effects of sex or TSTT group. However, both stiffness estimates were significantly negatively correlated with *BF* (c,d).

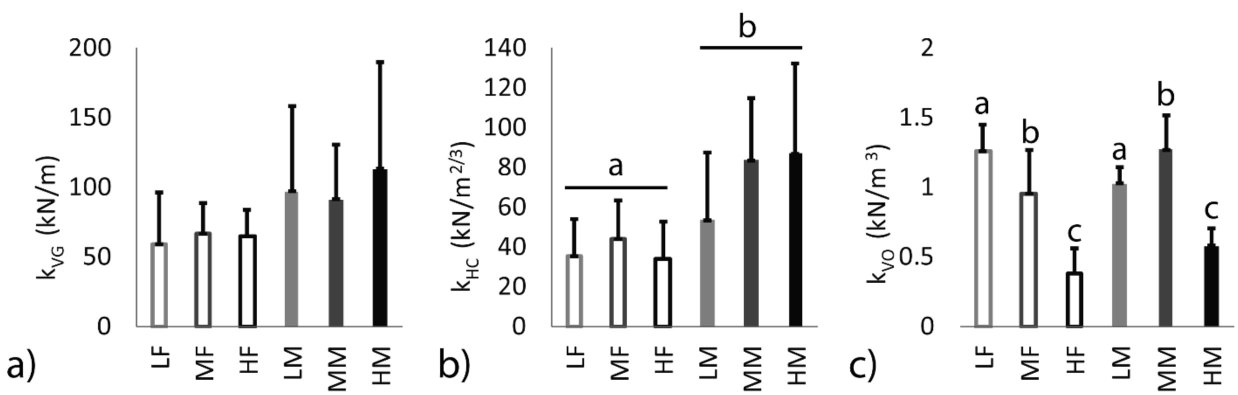

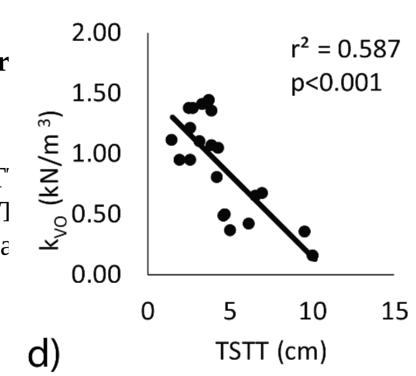

Figure 4.6 Groupwise differences and strongest correlations for k_{VG}, k_{HC} and k_{VO}

Stiffness components for viscoelastic models are included in this figure. There were no significant interactions between sex and TST group for k_{VG}, k_{HC} or k_{VO}. There were no main effects of sex or TST for k_{VG} (a), however, there was a main effect of sex for k_{HC} (b) and a main effect of TSTT group for k_{VO} (c) that was captured by a significant linear correlation (b).

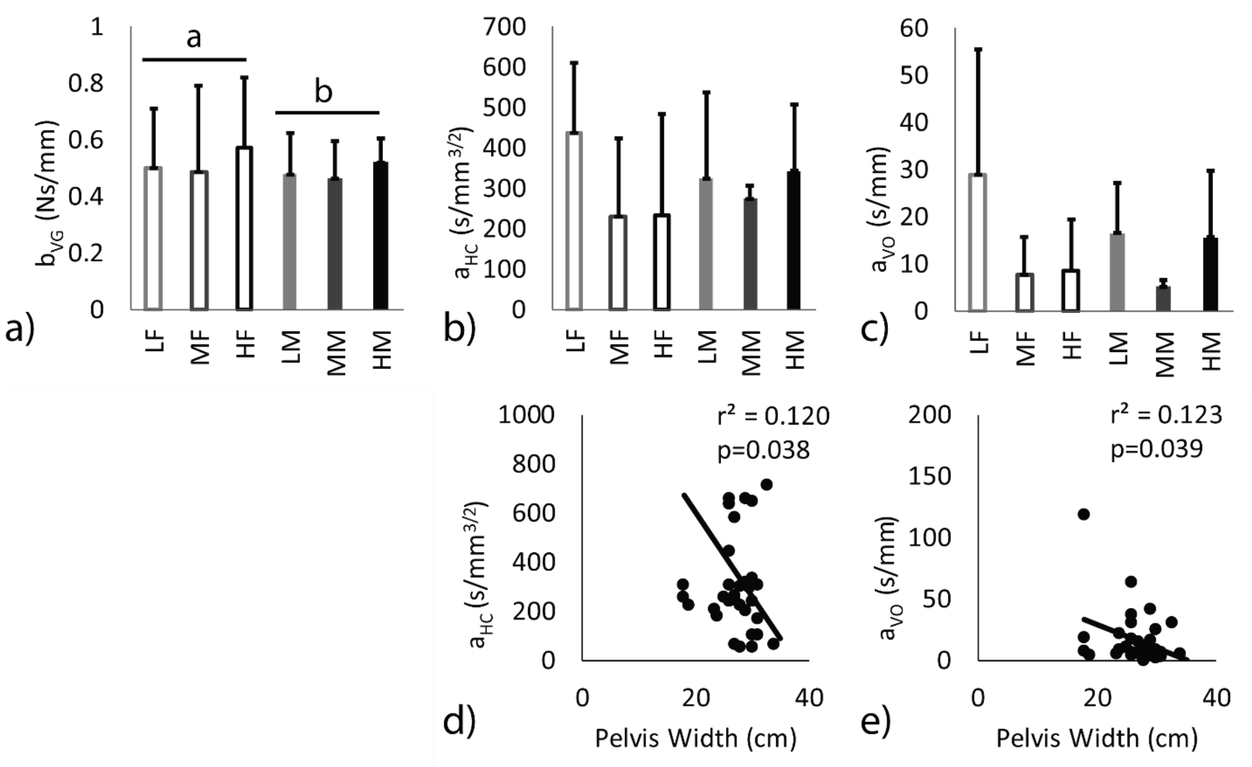

Figure 4.7 Groupwise differences and strongest correlations for b_{VG}, a_{HC} and a_{VO}

There were no significant interactions between sex and TSTT group for b_{VG}, a_{HC} or a_{VO}. There was a main effect of sex for b_{VG} (a). There were no main effects of sex or TSTT for a_{HC} (b) or a_{VO} (c), however, both damping parameters were negatively correlated with pelvis width (d, e). In characterization of a_{VO} (e), one participant had particularly high damping (a female with low TSTT and narrow, 18 cm pelvis, 1.2×10^5 s/m); when removed, the relationship between pelvis width and a_{VO} became non-significant. No other body size or composition element was related to a_{VO}.

Table 4.5 Bivariate correlation results for model parameters with body size and composition elements

Parameter		***Height (m)***		***Body Mass (kg)***		***BMI (kg/m^2)***		***TSTT (cm)***		***Pelvis Width (cm)***		***Hip Circumference (cm)***		***Body Fat (%)***	
		r	**p**	**r**	**p**	**r**	**p**	**r**	**p**	**r**	**p**	**r**	**p**	**r**	**p**
k_{MS}	*All*	0.153	0.367	-0.047	0.783	-0.149	0.380	-0.199	0.237	-0.044	0.794	-0.306	0.070	-0.335	0.046*
k_{HZ}	*All*	0.017	0.921	-0.247	0.140	-0.313	0.059	-0.297	0.075	-0.176	0.297	-0.366	0.028*	-0.397	0.017*
k_{VG}	*All*	0.309	0.071	0.149	0.392	0.001	0.995	0.025	0.885	-0.110	0.529	0.031	0.860	-0.102	0.562
k_{HC}	*Males*	-0.079	0.788	0.296	0.304	0.438	0.117	0.296	0.304	-0.138	0.638	0.301	0.296	0.119	0.686
	Females	-0.048	0.861	-0.313	0.238	-0.282	0.291	-0.222	0.392	0.018	0.947	-0.300	0.259	-0.081	0.765
k_{VO}	*All*	0.099	0.670	-0.596	0.004**	-0.690	0.001**	-0.766	<0.001**	-0.523	0.015*	-0.634	0.002**	-0.679	0.001**
b_{VG}	*Males*	-0.180	0.489	0.203	0.434	0.386	0.125	0.434	0.082	0.037	0.887	0.010	0.971	0.349	0.170
	Females	0.210	0.387	0.044	0.859	0.005	0.983	-0.045	0.853	-0.099	0.686	-0.151	0.549	0.017	0.947
a_{HC}	*All*	-0.071	0.682	-0.200	0.243	-0.202	0.238	-0.169	0.324	-0.347	0.038*	-0.213	0.220	-0.191	0.271
a_{VO}	*All*	-0.156	0.370	-0.244	0.158	-0.202	0.245	-0.101	0.566	-0.351	0.039*	-0.024	0.894	-0.111	0.532

** correlations significant at p<0.05, ** correlations significant at p<0.01*

Table 4.6 Final model parameters and regression equations for determining model parameters based on individual characteristics

Parameter		Males	Females	r^2	p
	MS	*(-305*BF)+42700N/m*	*(-305*BF)+42700N/m*	0.112	0.046
	HZ	*(-3450*BF)+326000* $N/m^{3/2}$	*(-3450*BF)+326000* $N/m^{3/2}$	0.158	0.017
k	*VG*	*8270 N/m*	*8270 N/m*		
	HC	*7110* $N/m^{3/2}$	*3710* $N/m^{3/2}$		
	VO	*(-14.1*TSTT)+1570* N/m^3	*(-14.1*TSTT)+1570* N/m^3	0.123	0.039
	VG	*727 Ns/m*	*519 Ns/m*		
b, a	*HC*	*(-1980*PW)+69000* $s/m^{3/2}$	*(-1980*PW)+69000* $s/m^{3/2}$	0.554	0.001
	VO	*(-34200*PW)+1290000 s/m*	*(-34200*PW)+1290000 s/m*	0.575	<0.001

4.4 Discussion

In this study, we aimed to characterize stiffness and damping parameters for five models, and link these experimentally-determined parameters to individual body size and composition parameters. Based on previous findings (Robinovitch, Hayes et al. 1991; Levine, Bhan et al. 2013), we hypothesized that these parameters may differ substantially between sex or body composition groups. We found that the volumetric stiffness estimate varied between TSTT groups, however, this could be characterized as a simple linear relationship. The Voigt and Hunt-Crossley stiffness estimates, and Voigt damping coefficient differed between males and females, but were otherwise unrelated to individual characteristics measured in this study. Finally, stiffness estimates for the Mass-Spring and Hertz models were negatively linked to body fat, while Volumetric and Hunt-Crossley damping coefficients were negatively correlated with pelvis width.

This study adds to the understanding of the behavior of TSTT on force attenuation and distribution. The leading theories regarding the link between body composition and hip fracture rates, from the applied loads perspective, suggest that pelvic stiffness is directly related to absorption or distribution of energy by the trochanteric soft tissues (Robinovitch, Hayes et al. 1991; Robinovitch, McMahon et al. 1995; Beck, Petit et al. 2009; Laing and Robinovitch 2010; Levine, Bhan et al. 2013). While we did not find that TSTT was linearly correlated with the majority of our stiffness parameters, TSTT was negatively correlated with k_{VO}, and k_{HC} was lower for females (greater TSTT) than males. These stiffness parameters were determined via quasi-static trials where only soft tissue compression was considered. TSTT therefore has a strong link to rate-independent distribution of loads. A more global measure, *BF*, was negatively correlated with k_{MS} and k_{HZ}, which contrasts our findings in Study 1 that impact dynamics were more closely linked to local, rather than global body composition characteristics. However, *BF*, as quantified in this study using calipers, may capture differences in elastic modulus rather than dimension, which may be more variable than the thickness of the tissue. System stiffness, for a linear model such as the mass-spring, can be characterized as:

$$k = \frac{ae}{l} \tag{4.11}$$

which demonstrates the dependence of observed stiffness on both material and dimensional properties. A local estimate of fat, such as percent leg fat (determined via DXA in Study 1) may be more strongly linked to k_{MS} and k_{HZ}. Additionally, in Study 1 we found that TSTT was more strongly linked to pressure, or localized force, than total force applied to the hip during a lateral impact-- k_{MS} and k_{HZ} may not characterize this distribution effect. Only in k_{VG} did we find no link between TSTT and stiffness. In this case, k_{VG} did not appear to be related to any measured body size or composition parameter; however, mean value (8270 N/m) was within the range of soft tissue stiffness previously reported (Makhsous, Venkatasubramanian et al. 2008; Choi, Russell et al. 2014) at the hip and in the inferior gluteal region, both cases in which the compressive soft tissue stiffness was independent of tissue thickness. Finally, we did not observe any differences for stiffness parameters between males and females, except for k_{HC}, despite having previously found higher k_{MS} for males than females (Levine, Bhan et al. 2013). However, TSTT was not included in this previous study—it is unclear whether this previous observation was directly related to a difference in stiffness between males and females, or whether the two groups may have had different magnitudes of TSTT. Therefore, stiffness (as characterized in this study) in simplified compression scenarios may be less dependent on tissue thickness, and instead dependent on factors affecting the elastic modulus of the tissue, such as aging or tissue hydration. Links between model stiffness parameters and individual characteristics may be improved with a more dimensional metric to quantify the quantity of trochanteric soft tissue, such as volume.

Model damping appeared to have little to do with TSTT or body composition, and was instead negatively influenced by skeletal pelvis width (distance between right and left ASIS). For *VG*, this was captured by increased damping for males (i.e. a narrower pelvis) than females, mirroring previous results (Robinovitch, Hayes et al. 1991). For *HC* and *VO*, we found a similar effect, captured as a significant negative correlation between damping coefficient and pelvis width. Observed damping within the pelvis, therefore, may have little to do with the thickness soft tissues, and more to do with the skeletal components and contents—i.e. the soft tissues may be viscoelastic, but from a system perspective, the damping characteristic is dominated by the skeletal component. One explanation is that the skeletal pelvis is itself composed of viscoelastic material, surrounding pelvic organs which are also composed of viscoelastic tissue and contain fluids. A larger pelvis would not only contain more viscoelastic bone material, but would also provide greater volume for pelvic organs. A second possible explanation is the anatomical complexity of the skeletal pelvis--the effect may be an artifact of time-varying stiffness within the pelvis which reflects the generation and dissipation of stress within the complex structure (Majumder, Roychowdhury et al. 2008). However, a third explanation is that, particularly for *HZ* and *VO*, the damping effect is bound by the geometry of the pelvis, given that pelvis width likely correlates with pelvis height and depth (forming a boundary for contact area or volume). The boundary limits the displacement of fluids within the pelvis, resulting in increased pressure on the contained fluids and a stronger viscous effect. These multiple explanations warrant further exploration through *in vitro* and *in silico* methods to control and simulate the potential effects.

This leads into limitations of this study. First, we used young, healthy adults to characterize the parameters. The pelvis release protocol is typically performed only with participants <35 years in the interest of safety (Robinovitch, Hayes et al. 1991; Laing and Robinovitch 2010; Bhan, Levine et al. 2013; Levine, Bhan et al. 2013; Bhan, Levine et al. 2014). However, Choi and colleagues (2015) demonstrated an age-related decrease in both stiffness and damping of trochanteric soft tissues via sonography. Additionally, age-related deterioration of the collagen network within bone results in decreased stiffness of the skeletal components (Wang, Shen et al. 2002), and decreased bone mineralization results in decreased storage and loss modulus (Wang and Feng 2005). Therefore, experimentation with young adults may result in overestimation of stiffness and damping parameters. Second, it is unclear what effect the structure of the skeletal pelvis and the pelvic contents have on the parameters characterized in this study. In this study, we focused on a lumped system perspective, and by characterizing the system as a whole we are unable to draw conclusions as to the contributions of individual skeletal and soft tissue components to the total system behavior. Additionally, we assumed the forces measured could be attributed solely to the effective mass of the pelvis. Robinovitch et al. (1995) found that less than 15% of impact force was distributed to peripheral structures (torso, legs) during a lateral impact to the hip. While we ignored the contributions of these components to the results of the study, their effects are likely limited. During the quasi-static trials, it is likely that the load applied to the pelvis due to gravity was not large enough to induce substantial stress on the skeletal structures. Stiffness estimates derived from the quasi-static trials were similar to those reported by Choi and colleagues (2015) for the trochanteric soft tissues alone. Therefore it is likely that during the quasi-static trials we were only able to characterize the stiffness of the soft tissue components and not the entire pelvis system. This limitation could be resolved in a future study by applying a higher load to the pelvis in the frontal plane via a jig rather than simply allowing the pelvis to rest on the ground. Further work towards refinement of parameters based on individual characteristics could be developed through *in vitro* and *in silico* (particularly finite element or curved beam modeling) methods to facilitate incorporation of these anatomical components. Third, it is unclear from the current study why some parameters differed between males and females and others did not. It is likely that these differences are linked to differences in trochanteric soft tissue thickness (typically around 30% lower for males than females; Levine, Minty, et al., 2015; 30.8% lower in this study) and underlying skeletal geometry (not studied in this thesis) rather than material differences between males and females. Future research may clarify whether the difference observed is truly an effect of sex or whether it can be attributed to quantifiable individual factors such as soft tissue thickness. In this study, we only explored bivariate correlations in this study and did not correct the significance level for multiple comparisons. The goal of this study was to provide simplified links between individual characteristics and model parameters. We found that these parameters were most strongly linked to a few consistent factors (body fat, particularly trochanteric soft tissue thickness, sex, and pelvis size), therefore, the influence of multiple comparisons is likely limited. Finally, we did not evaluate the unloading phase of the impact. While analysis of system unloading would provide insight into the dissipation of energy, it is unclear whether the observed forces during the unloading phase can be attributed to the damping components, or motion of the participants (e.g. rolling of the pelvis or muscle activation) directly after impact. A more controlled protocol employing a jig (previously discussed) may provide a better loading protocol to assess the unloading phase.

These results provide a stronger mechanistic link between individual body size and composition, and parameters to define the contact dynamics of a lateral impact to the hip. We found that trochanteric soft tissue thickness was linked to stiffness components, though more strongly to impact force distribution than attenuation. Damping was negatively correlated to pelvis width, which highlights the viscoelastic components of the bone, as well as the potential importance of the structural behavior of the pelvis. Finally, we were able to generate regression equations to predict an initial set of parameters to develop a multibody model of an impact to the pelvis.

Chapter 5, Study 3: Comparison of the Accuracy of Hip Impact Contact Models

Study 3 compares the differences in model performance between five models, focusing on the effects of including viscoelastic and geometric components. Development and analysis of the model parameters are discussed more thoroughly in Study 2. This work was presented, in part, at the 12th Ohio State Injury Biomechanics Symposium, June 5-7, 2016, and the 19th Biennial Meeting of the Canadian Society for Biomechanics, July 19-22, 2016.

5.1 Introduction

Fall-related injuries form up to 85% of injury-related hospitalizations in adults over the age of 65, and the mortality rate associated with falls increased by 65% from 2003 to 2008 (Stinchcombe, Kuran et al. 2014). Hip fractures alone are responsible for 40-60% of these cases (Stinchcombe, Kuran et al. 2014), and are independently associated with a nearly 30% one-year mortality rate (Cenzer, Tang et al. 2016). Current tools to estimate injury risk in older adults focus on bone strength and fractures which are categorized as osteoporotic, such as the hip and spine. However, falls involve impacts to multiple body regions (Choi, Wakeling et al. 2015), many of which are associated with a high mortality rate (Ioannidis, Papaioannou et al. 2009; Evans, Pester et al. 2015). Therefore, a stronger strategy to reduce fall-related mortality and disability might involve the estimation of injury risk across several body regions. A multibody systems approach allows rapid estimation of loading magnitude and distribution between multiple body segments. However, the mechanical behavior of each segment must be characterized.

Within the dynamics approach, impacts to the hip have typically been modeled as a simple single-degree-of-freedom (SDF) model, consisting of a mass and spring, or mass, spring and damper following Hooke's law of contact dynamics (Robinovitch, Hayes et al. 1991; Robinovitch, Hayes et al. 1997; Laing and Robinovitch 2010) (Figure 2.7). This approach is based on the assumption that the soft tissues overlying the hip (trochanteric soft tissue thickness, TSTT) act in a primarily two-dimensional energy absorption mechanism. SDF models with linear stiffness and damping parameters have been associated with underprediction of time to peak force across velocity conditions, underprediction of peak force at high impact velocity and overprediction of peak force at low impact velocity (Robinovitch, Hayes et al. 1997). To counteract these errors and more strongly mimic the initial rise of force at impact, Laing et al. (2010) implemented non-linear (2^{nd} order) stiffness estimates, which matched the initial rise of force more closely, but substantially overpredicted peak force. Additionally, this more complex stiffness estimate was not explicitly linked to behavior of standard Hookean (or more complex) models. In

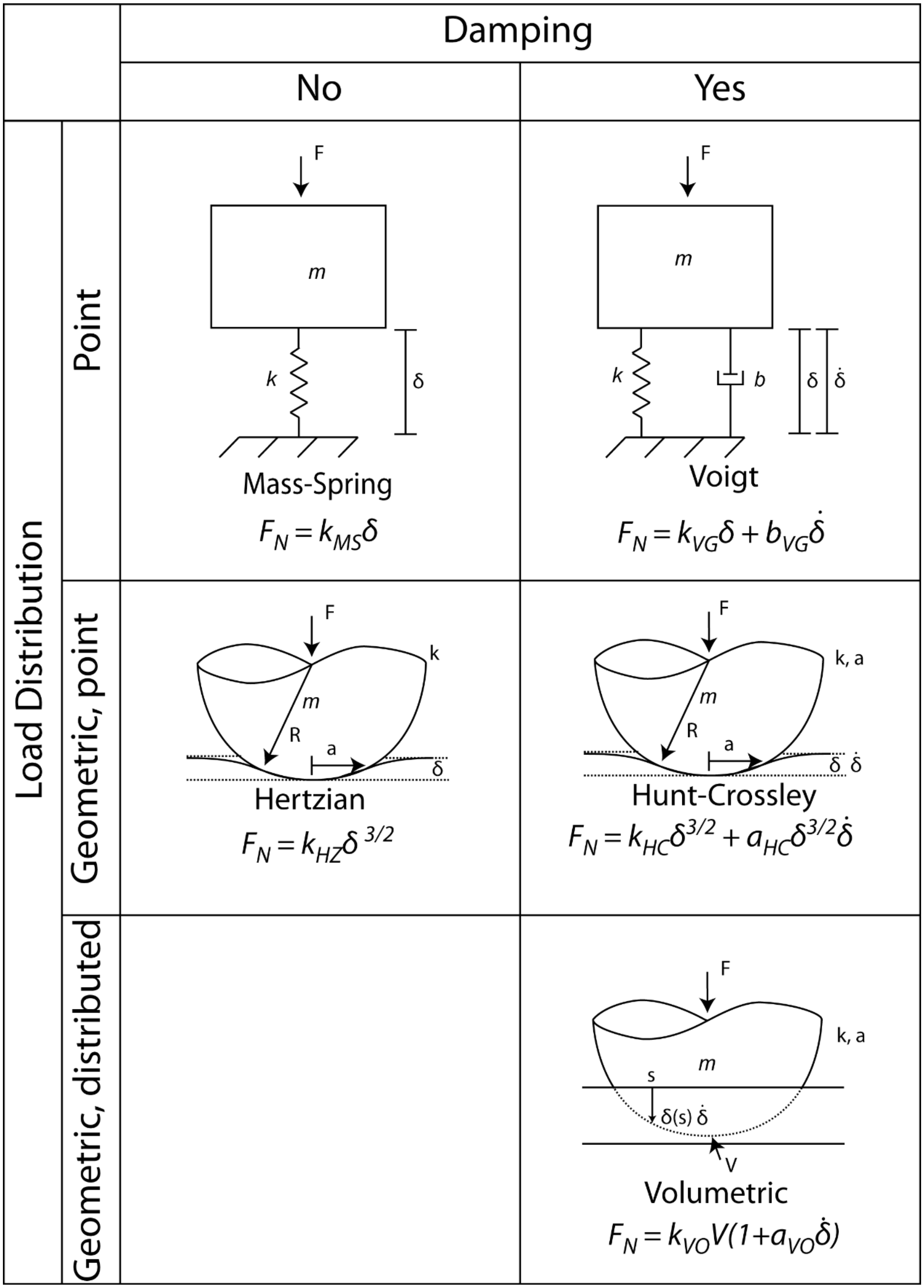

Figure 5.1Model Schematics and normal force formulae for the MS, VG, HZ, HC and VO

Study 1 and Appendix 2, soft tissue was linked to load distribution in addition to lower peak forces. However, load distribution is not accounted for in SDF models. While simple to develop parameters for, and rapid to implement, errors identified in existing models support the idea that it may be too drastic a simplification to characterize the pelvis system as a one-dimensional model.

In contrast, models based on Hertz contact theory or Volumetric models incorporating three-dimensional geometry of the interacting bodies (i.e. the pelvis system and the floor) have the potential to better explain the non-linear loading response (Laing and Robinovitch 2010) of the pelvis during an impact, as well as link this response to the spatial distribution of loading associated with TSTTs. In addition to increasing predictive capability of fracture prediction tools, more complex models may provide better understanding of the interactions between the pelvis and compliant protective devices such as safety floors (Laing, Tootoonchi et al. 2006) and hip protectors (Robinovitch, Evans et al. 2009). The Hertz model, and the derivative Hunt-Crossley model (Hunt and Crossley 1975) involve non-linear spring and damping components, both with exponents of $^{3}/_{2}$ reflecting a sphere-on-plane contact. These models simulate a scenario where deformation (and therefore stress) is concentrated in, and influenced by the area of contact between the interacting bodies. However, the Hertz and Hunt-Crossley models are limited to scenarios where the contact area is low relative to the surface area of the interacting bodies, and cannot handle scenarios where interacting bodies are conforming prior to impact (e.g. a pelvis and a hip protector). The Volumetric contact model answers this by employing spring and damper parameters dependent on the geometry of the bodies rather than simplified non-linear components. However, it is untested whether the inclusion of geometric parameters will improve prediction of impact characteristics during an impact to the hip.

Finally, for both Hookean and Hertzian systems, inclusion of damping components has the potential to improve model biofidelity. In static scenarios, both the mass-spring and Hertz models have been successfully employed in biological systems (Fregly, Bei et al. 2003; Gefen 2007). Robinovitch et al. (1997) found weaker performance for viscoelastic models than elastic models. However, the primary limitation of a model excluding damping components is the continuous oscillation of force following impact, representing a complete return of spring potential energy to the body in the form of kinetic energy. Biological systems behave viscoelastically due to high levels of fluid within the tissues—i.e. the tissue exhibits velocity-dependent resistance to deformation, which results in energy dissipation and decreased post-impact oscillation. This is particularly important as velocity increases, exhibited by poor performance of the mass-spring model at impact velocities exceeding 2 m/s (Robinovitch, Hayes et al. 1997). The performance improvement provided by the addition of damping components, and in particular, the interaction of damping and geometric components, has not yet been tested for fall-related impacts.

Therefore, the primary goal of this study was to determine the improvement in model performance based on the addition and interaction of a) damping, and b) geometric components. The Voigt (VG) and Hunt-Crossley (HC) and Volumetric (VO) models were used to demonstrate the effect of damping, while the Hertzian (HZ) and HC models were used to demonstrate the effect of geometric considerations. The MS served as the comparator model with neither damping nor geometric components. We hypothesized that geometry and damping will interact, with HC and VO performing substantially better than VG or HZ, and MS performing substantially worse.

5.2 Methods

Forty-six healthy participants (<35 years, 24 female) consented to participate in this study Table 5.1. Participant recruitment focused on developing a cohort with a wide variety of body composition. Exclusion criteria included musculoskeletal injury in the past year preventing completion of the protocol, lifetime fracture history, fear of falling, or other health conditions which would make participation unsafe. Participant mass (*mass*) was recorded to the nearest 0.5 kg. Hip circumference ($Circ_{hip}$) was measured with a flexible tape measure at the level of the greater trochanter, and height (*H*) and pelvis width (from right to left anterior superior iliac spine, *PW*) with a rigid meter stick, to the nearest 0.5 cm. Skinfold calipers were used to estimate percent body fat via a seven-site method (*BF*, (Jackson and Pollock 1978; Jackson, Pollock et al. 1978; Jackson, Pollock et al. 1979)). Transverse-plane TSTT was assessed via ultrasound (minimum precision 0.17 cm; C60x, 2-5 MHz transducer, M-Turbo Ultrasound, SonoSite, Inc., Bothell, WA) in a side-lying position, similar to that expected during the impact phase of the fall simulations. Participants were grouped into low-, mid- and high-TSTT groups based the following criteria: males low <3 cm, mid 3.1-4 cm, high >4.1 cm; females low <3.5, mid 3.6-5, high >5 cm. These thresholds represent low- (<18.5 kg/m2), moderate (18.6-25 kg/m2) and high- (>25.1 kg/m2) BMI older adults (unpublished data).

Table 5.1: Mean (SD) participant anthropometric characteristics. STT represents trochanteric soft tissue thickness. BMI represents body mass index

		N	Height (m)	Mass (kg)	BMI (kg/m^2)	TSTT (cm)
				Females		
	Low	7	1.64 (0.05)	54.7 (6.4)	20.1 (1.6)	2.84 (0.31)
TSTT	Mid	10	1.66 (0.06)	65.9 (12)	23.7 (3.2)	4.20 (0.38)
	High	7	1.65 (0.07)	86.6 (22)	32.0 (8.4)	6.93 (2.12)
				Males		
	Low	8	1.80 (0.07)	72.5 (11.5)	22.4 (2.3)	2.28 (0.50)
TSTT	Mid	8	1.80 (0.07)	84.5 (6.4)	26.1 (2.3)	3.44 (0.27)
	High	6	1.87 (0.08)	90.0 (9.7)	28.5 (9.7)	5.29 (1.36)

5.2.1 Experimental protocol

Participants underwent a three-trial pelvis release experiment protocol, which involved the lateral aspect of the left hip impacting a force plate (500 Hz; OR6-7, AMTI, USA), with a 0.05 m initial displacement of the pelvis. During the protocol, the pelvis of the participant was supported by the sling, which was designed to not directly contact the tissues between the iliac crest (superior border) and mid thigh (inferior border). The upper body of the participant was supported by a pillow, while the feet rested on a mat, both outside the contact area of the force plate. The hips of the participant were flexed to 45° and knees were flexed to 90°.The sling was raised so that the soft tissues over the left hip were 5 cm above the impact surface. When the participant reported that they were “relaxed and ready”, the electromagnet was released, allowing the pelvis to impact the impact surface.

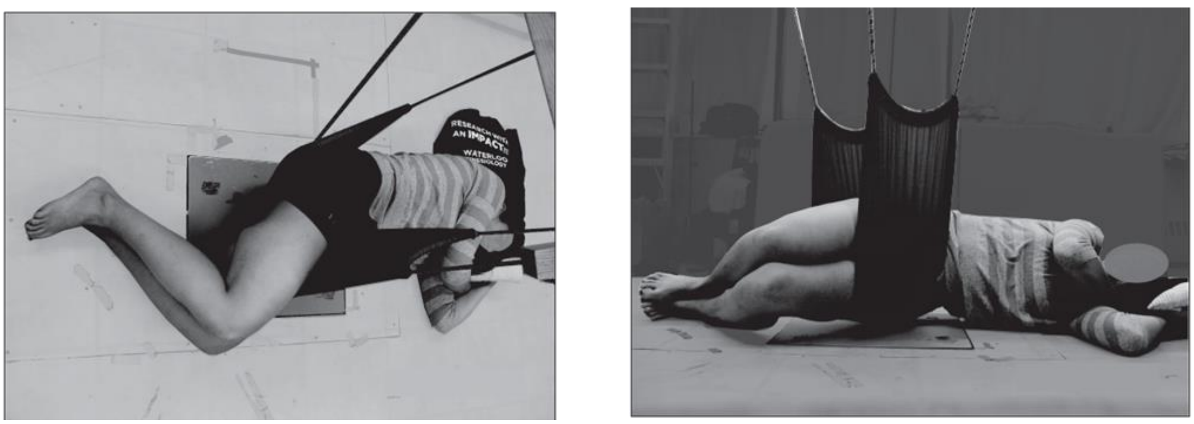

Figure 5.2 Initial position of the participant during the pelvis release protocol

The pelvis of the participant was suspended in a sling, supported by a set of ropes connected to a turnbuckle and an electromagnet. During the quasi-static experiments, the turnbuckle was used to slowly lower the sling. During the dynamic pelvis release experiments, the electromagnet was release to allow the sling to release rapidly and allow the pelvis of the participant to impact the force plate.

5.2.2 Signal Processing

We used a customized MATLAB routine (MathWorks, Natick, MA) to process the time-varying signals. An automated point-selection routine was developed to truncate the data for further analysis. Each trial was segregated by defining an initial quiet (unloaded) region ($F_{initial}$), the beginning of impact (when force exceeds two standard deviations of the mean within $F_{initial}$: T_{imp}, F_{imp}), peak force (T_{max}, F_{max}), and the first minimum of force following F_{max} (T_{min}, F_{min}). Bias ($F_{initial}$) was subtracted from all force values. Time to peak (*TTP*) was estimated as the difference between T_{imp} and T_{max}. The impulse was calculated between T_{imp} and T_{min} as:

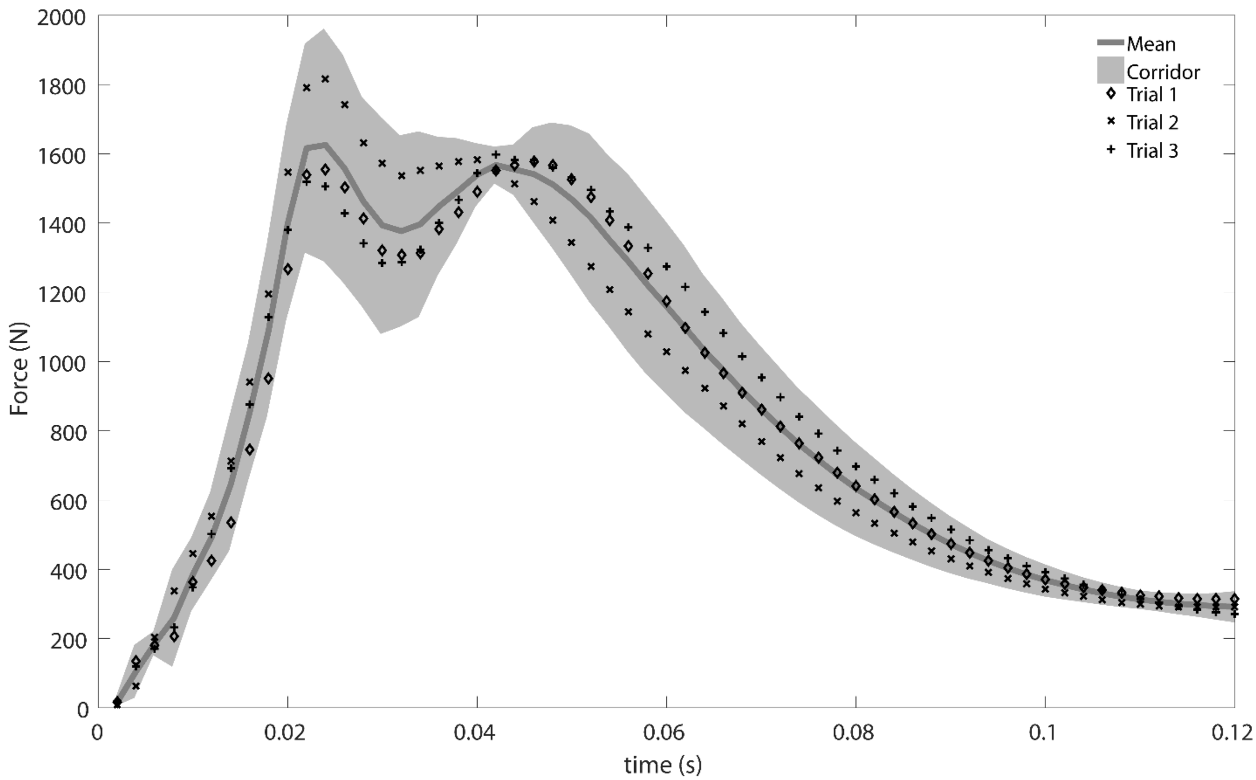

Figure 5.3 Experimentally-determined loading response corridors
Trial data (markers) were used to develop a time-varying mean (grey line) and two-standard-deviation corridor (grey band) for comparison.

$$I = \int_{T_{imp}}^{T_{min}} F_t dt \tag{5.1}$$

A force corridor for model validation was established based on experimental data between T_{imp} and T_{min} (Figure 5.3, grey band). The corridor is established as a two-standard-deviation (i.e. 95% confidence interval) deviation from the mean (grey line) of the experimental data (trial markers). .

5.2.3 Characterization of impact dynamics and definition of model parameters

The parameter characterization process is discussed in greater detail in Study 2. Briefly, in this linked study, deflection and contact area of the pelvis was quantified during the impact phase of the pelvis release protocol using a different initial height (2 cm vs. 5 cm). The resulting force, deflection and volume data curves were fit using a least-squares approach in order to characterize stiffness and damping parameters (Figure 5.4).

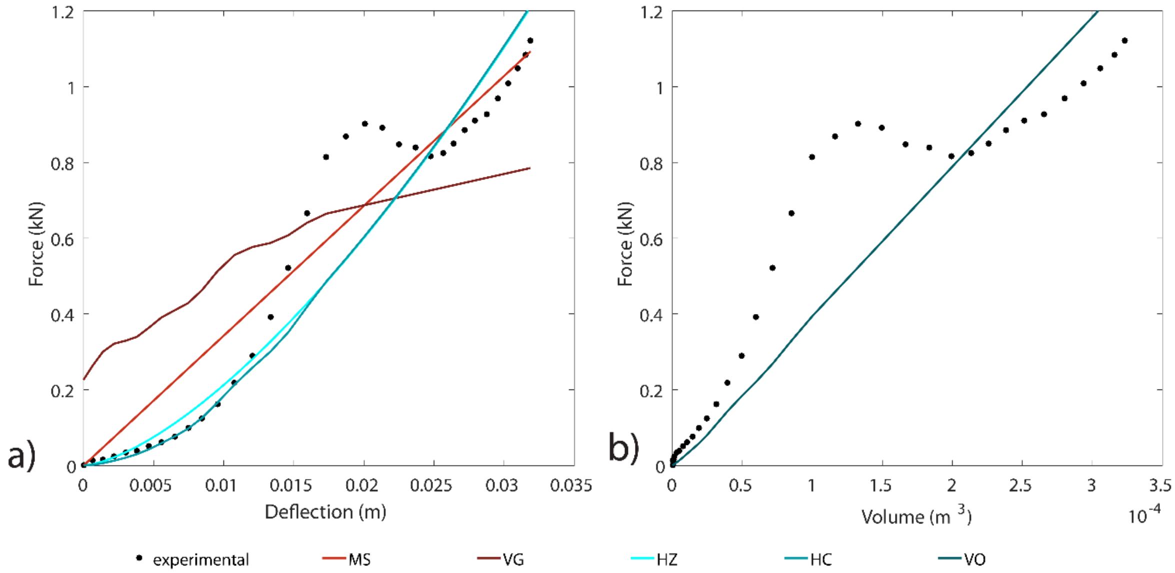

Figure 5.4 Demonstration of final curve fit to experimental data for MS, HZ, VG, HC and VO

The experimental data (dots) is shown along with the final curve fit for each model, consisting of a stiffness (MS, HZ) or stiffness and damping (VG, HC, VO) component.

Table 5.2 Model parameters

Parameter		Males	Females
Effective Mass		*m_{total}/2 kg*	*m_{total}/2 kg*
Pelvis Diameter		*($Circ_{hip}/\pi$) m*	*($Circ_{hip}/\pi$) m*
k	*MS*	*(-304.8*BF)+42699.7 N/m*	*(-304.8*BF)+42699.7 N/m*
	HZ	*(-3452.7*BF)+326489.1 N/$m^{3/2}$*	*(-3452.7*BF)+326489.1 N/$m^{3/2}$*
	VG	*8270 N/m*	*8270 N/m*
	HC	*7110 N/$m^{3/2}$*	*3710 N/$m^{3/2}$*
	VO	*(-14.1*TSTT)+1567 N/m^3*	*(-14.1*TSTT)+1567 N/m^3*
b, a	*VG*	*727.1 Ns/m*	*519.1 Ns/m*
	HC	*(-1983.9*PW)+69039.7 s/$m^{3/2}$*	*(-1983.9*PW)+69039.7 s/$m^{3/2}$*
	VO	*(-34177.5*PW)+1285708.3 s/m*	*(-34177.5*PW)+1285708.3 s/m*

5.2.4 Model simulation

Models were simulated in MapleSim (Version 6.4, Maplesoft, Waterloo, ON), a symbolic multibody modeling software package. An initial centre-of-mass displacement of 0.05 m (matching experimental initial conditions) and constant acceleration (α) due to gravity ($g=9.81\ m/s^2$) was used for all models. In cases where the simulated pelvis is not in contact with the ground, the movement of the simulated pelvis is in a state of free fall. Normal force equations for each model are presented in Table 5.3; these formulae are implemented when only the simulated pelvis is in contact with the ground. Centre of mass displacement (δ) is calculated as vertical deflection from the initial contact point. A fixed time-step 2nd order Runge-Kutta solver was used to approximate solutions to the ordinary differential equations.

Table 5.3 Model normal force formulae

Model	Formula	
MS	$F_N = k_{MS}\delta$	(5.2)
HZ	$F_N = k_{HZ}\delta^{3/2}$	(5.3)
VG	$F_N = k_{VG}\delta + b_{VG}\dot{\delta}$	(5.4)
HC	$F_N = k_{HC}\delta^{3/2} + a_{HC}\delta^{3/2}\dot{\delta}$	(5.5)
VO	$F_N = k_{VO}V(1 + a_{VO}\dot{\delta})$	(5.6)

5.2.5 Model evaluation

Models were evaluated based on a within-subjects basis relative to the reference curve in Figure 5.3 for the criteria presented in Table 5.4 and discussed below.

Table 5.4: Model evaluation criteria

Component	
Err_{max}	The difference between the maximum of the reference curve and the maximum of the simulated curve, as a percent error
Err_{TTP}	The difference in T_{imp}-T_{max} interval between the reference curve and simulated curve, as a percent error
Err_{imp}	The difference in impulse between the reference curve and simulated curve, as percent error
Err_{corr}	The number of simulated data points falling outside the 2 SD corridor, expressed as a percent error (Figure 5.5)

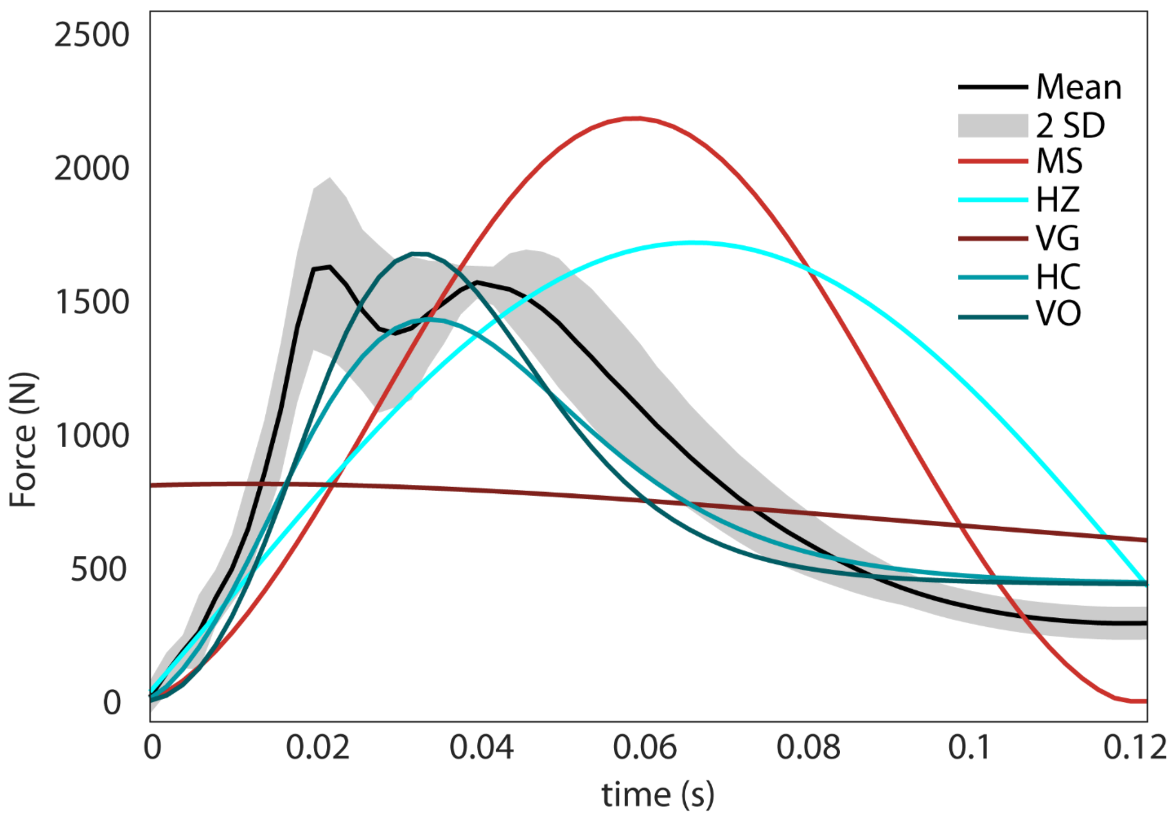

Figure 5.5 Demonstration of time-varying model performance within the 2 SD (95% CI) corridors

Models were compared against the experimental data (black line, grey band) between the initiation of impact and first minimum following peak force. Models were compared on performance in replicating peak force, time to peak force, impulse, and the percentage of predicted data points within the experimental corridor.

Additionally, a binary outcome, Err_{out} was used to determine whether the maximum force predicted by the model was within two standard deviations of experimental peak force (i.e. a score of 1 for predicted force outside of the experimental range, and a score of 0 for predicted force within the experimental range). A composite score (the percent of predictions outside the experimental range) across all participants was calculated as Err_{out}/N. Finally, the root-mean-squared error (Err_{RMSE}) was calculated for each model

5.2.6 Statistical Analysis

Statistical analysis was performed using a software package (SPSS version 21, Chicago, USA) using an α of 0.05 as criterion for statistical significance. Outcomes (Err_{max}, Err_{TTP}, Err_{imp}, Err_{corr} and Err_{RMSE}) were compared across all five models (MS, HZ, VG, HC and VO) via ANOVA, with model type treated as a repeated measure, and TSTT and sex as between-subjects factors. Finally, model performance for all outcomes (Err_{max}, Err_{TTP}, Err_{imp}, Err_{corr}, Err_{RMSE} and Err_{out}) were compared against MS, the comparator model; a decrease in absolute error of 5% was considered a substantial functional improvement. Differences in model performance for all criteria is reported and compared in percentage points. Independent and dependent variables were normally distributed for outcomes in this study.

5.3 Results

Performance outcomes differed between models across all criteria (Table 5.5), with a disordinal interaction between sex and model for Err_{corr}. Model performance did not otherwise differ between males and females or TSTT groups. Comparing peak force prediction, Err_{max} differed between all models except for MS and VO; errors were large and positive for MS and VO, large and negative for VG, and more moderate for HZ and HC (Table 5.5, Table 5.6, Figure 5.6a). HZ and HC provided the best improvement over MS, with 31.9% and 39.3% (Table 5.7). Time to peak force prediction performance was similar and moderate for VG and HC, significantly larger and positive for MS and HZ, and larger and low for VO Table 5.5, Table 5.6, Figure 5.6b). Time to peak force improvement compared to MS was equal for VG and HC, both at 64.0% (Table 5.7). Differences in Err_{corr} performance between models were more substantial for males than females. For males, Err_{corr} HC performed significantly better than any other model (Table 5.5, Table 5.6, Figure 5.6c), however, performance compared to MS was better for both HC (20.7% improvement) and VO (9.3% improvement, Table 5.7). For females, Err_{corr} performance was better for HC than VG or VO only (Table 5.5, Table 5.6, Figure 5.6d). While HC provided improvement over MS according to our test of substantial functional improvement (7.6%, Table 5.7), we found no statistical difference using ANOVA between MS and HC due to high between-subjects error. Err_{imp} performance was similar and low for VG and VO, 4.5-6.6% higher for HC, and 26.0-41.8% higher for MS and HZ (Table 5.5, Table 5.6, Figure 5.6e). All four models (HZ, VG, HC and VO) performed better than MS for Err_{imp} (Table 5.7). Err_{out} performance differed between all models, with HZ performing best, followed by HC, VO, MS and VG (Table 5.7, Figure 5.6f). Finally, performance for Err_{RMSE} differed between models, with errors significantly better for HC than all other models (Table 5.5, Table 5.6, Figure 5.6g).

Table 5.5 Summary of ANOVA results

Dependent Variable	Factor	F	p
	Model X TSTT X Sex	1.9	0.106
	Model X TSTT	2.8	0.025*[1]
	Model X Sex	2.0	0.136
Err_{max}	TSTT	0.8	0.462
	Sex	2.6	0.115
	Model	301.6	<0.001**
	Model X TSTT X Sex	1.3	0.290
	Model X TSTT	4.8	0.005**[1]
	Model X Sex	9.5	0.001**[1]
Err_{TTP}	TSTT	1.3	0.298
	Sex	1.0	0.319
	Model	54.4	<0.001**
	Model X TSTT X Sex	0.8	0.587
	Model X TSTT	0.5	0.717
	Model X Sex	3.4	0.033*[2]
Err_{corr}	TSTT	0.6	0.580
	Sex	2.5	0.124
	Model, males	12.1	<0.001**
	Model, females	4.5	0.014*
	Model X TSTT X Sex	1.1	0.367
Err_{imp}	Model X TSTT	0.8	0.543
	Model X Sex	1.5	0.226
	TSTT	0.1	0.908
	Sex	0.8	0.361
	Model	48.8	<0.001**
Err_{RMSE}	Model X TSTT X Sex	0.5	0.728
	Model X TSTT	0.8	0.571
	Model X Sex	1.5	0.225
	TSTT	2.2	0.134
	Sex	3.8	0.061
	Model	14.3	<0.001**

** Significant comparison at p<0.05 ** Significant comparison at p<0.01 1. ordinal interaction 2. disordinal interaction*

Table 5.6 Pairwise comparisons between models for significant model error differences

Model		Err_{max}		Err_{TTP}		Err_{corr}, males		Err_{corr}, females		Err_{imp}		Err_{RMSE}	
		MD[1]	**p**	**MD**	**p**	**MD**	**p**	**MD**	**p**	**MD**	**p**	**MD**	**p**
MS	HZ	31.8	<0.001**	-20.4	<0.001**	-0.7	0.695	-1.2	0.628	-9.2	<0.001**	77.6	0.001**
	VG	92.9	<0.001**	65.7	<0.001**	-0.9	0.828	5.8	0.163	-41.3	<0.001**	149.4	0.001**
	VO	6.9	0.095	92.8	<0.001**	-9.4	0.042*	2.0	0.604	-39.1	<0.001**	72.1	0.076
	HC	50.1	<0.001**	67.3	<0.001**	-20.5	0.001**	-7.4	0.085	-34.5	<0.001**	236.2	<0.001**
HZ	MS	-.1.8	<0.001**	20.4	<0.001**	0.7	0.695	1.2	0.528	9.2	<0.001**	-77.6	0.001**
	VG	61.1	<0.001**	86.1	<0.001**	-0.2	0.949	6.9	0.044*	-32.1	<0.001**	71.8	0.017*
	VO	-24.9	<0.001**	113.2	<0.001**	-8.8	0.025*	3.2	0.350	-29.8	<0.001**	-5.5	0.900
	HC	19.2	<0.001**	87.7	<0.001**	-19.8	<0.001**	-6.2	0.108	-25.3	<0.001**	158.7	<0.001**
VG	MS	-92.9	<0.001**	-65.7	<0.001**	0.9	0.828	-5.8	0.163	41.3	<0.001**	-149.4	0.001**
	HZ	-61.1	<0.001**	-86.1	<0.001**	0.2	0.949	-6.9	0.032*	32.1	<0.001**	-71.8	0.017*
	VO	-86.0	<0.001**	27.1	0.002**	-8.6	0.001**	-3.7	0.021*	2.2	0.560	-77.3	0.092
	HC	-42.8	<0.001**	1.6	0.874	-19.6	<0.001**	-13.1	0.020*	6.8	0.004**	86.9	0.002**
VO	MS	-6.9	0.095	-92.8	<0.001**	9.4	0.042*	-2.0	0.604	39.1	<0.001**	-72.1	0.076
	HZ	24.8	<0.001**	-113.2	<0.001**	8.8	0.025*	-3.2	0.350	29.8	<0.001**	5.5	0.900
	VG	86.0	<0.001**	-27.1	0.002**	8.6	0.001**	3.7	0.094	-2.2	0.560	77.3	0.092
	HC	43.2	<0.001**	-25.5	<0.001**	-11.1	0.001**	-9.4	<0.001**	4.5	0.243	164.1	<0.001**
HC	MS	-50.1	<0.001**	-67.3	<0.001**	20.5	0.001**	7.4	0.085	34.5	<0.001**	-236.2	<0.001**
	HZ	-18.3	<0.001**	-87.7	<0.001**	19.8	<0.001**	6.2	0.108	25.3	<0.001**	-158.7	<0.001**
	VG	42.8	<0.001**	-1.6	0.874	19.6	<0.001**	13.1	<0.001**	-6.8	0.004**	-86.9	0.002**
	VO	-43.2	<0.001**	25.5	<0.001**	11.1	0.001**	9.4	<0.001**	-4.5	0.243	-164.1	<0.001**

** Significant comparison at p<0.05 ** Significant comparison at p<0.01 1. Mean difference, in percentage points*

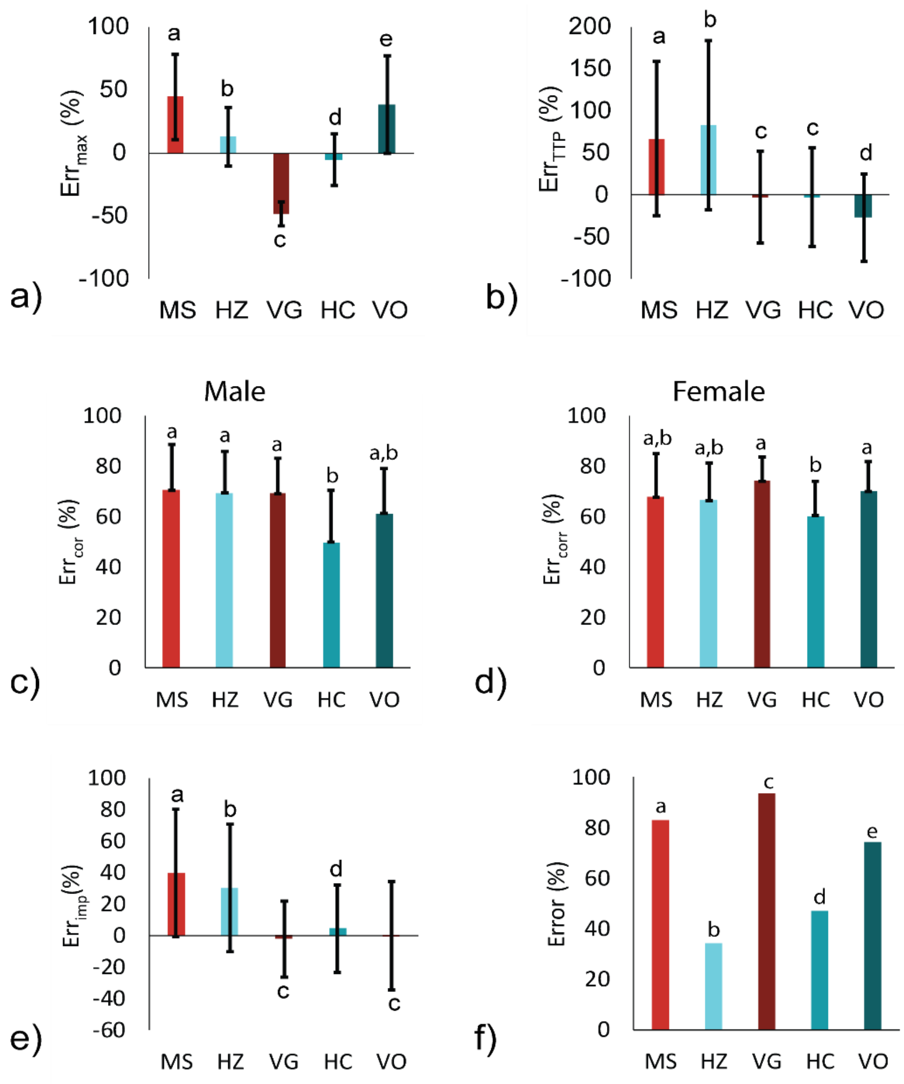

Figure 5.6 Model absolute and directional performance for peak criteria

Model performance varied, with HC consistently performing within the most accurate group across criteria. A geometry-damping interaction revealed a directional effect of damping and magnitude effect of geometry on Err_{max} (a), while the timing improvement introduced by damping components in Err_{TTP} (b) carried through to better performance in Err_{imp} (e). Err_{corr} performance differed between males (c) and females (d), but was generally best for HC compared to other models. Performance for Err_{out} (f) was improved by inclusion of geometric components, however, this did not extend to improved performance of VO. Quality of fit, Err_{RMSE} was substantially improved for HC compared to all other models (g). Homogeneous subsets, based on pairwise comparisons, are indicated with letters (a, b . . .).

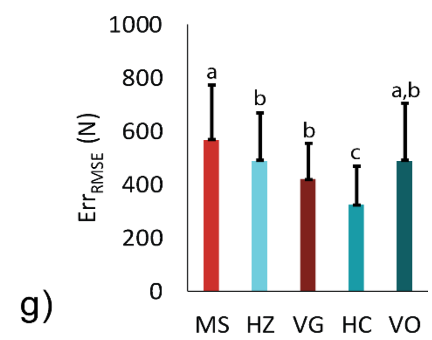

Table 5.7 Improvement over MS, in percentage points

	HZ	VG	HC	VO
Err_{max}	31.9*	-3.4	39.3*	6.3*
Err_{TTP}	-16.2	64.0*	64.0*	40.1*
Err_{corr}, *males*	1.0	1.4	20.7*	9.3*
Err_{corr}, *females*	1.3*	-6.2	7.6*	-2.1
Err_{imp}	9.2*	37.2*	35.2*	39.3*
Err_{out}	48.9*	-10.6	36.1*	8.5*
Err_{RMSE}	13.6*	26.1*	42.7*	13.8*

5.4 Discussion

In this study, we aimed to determine what level of complexity, through inclusion of damping and geometric components, was required to replicate the impact phase of a fall to the hip in a controlled, experimental setting. Geometry had a stronger effect than damping on prediction of peak force, however, damping had a stronger effect on timing, which carried through to performance in replication of the impact impulse, as well as performance in matching the 95% CI experimental corridors and root mean squared error. We found that the Hunt-Crossley model performed consistently well across all five criteria.

Damping had a substantial effect on Err_{TTP}, highlighting the importance of the viscoelastic nature of the pelvis system on loading rate. VG provided a 64.0% improvement over MS, while HC provided an 86.1% improvement over HZ. This is a reflection of the sharper rise to peak force demonstrated by HC vs HZ in Figure 5.5, where the velocity-dependent components influenced a much sharper rise to peak force. This is carried forward in stronger prediction of the impact impulse and in the strength of the Hunt-Crossley model for replication of the experimental corridor. In Chapter 4, we demonstrated that total system deflection during a pelvis release experiment was, on average, only 45.6% of TSTT. The loading period of a pelvis release is less than 0.1 s (Laing and Robinovitch 2010; Levine, Bhan et al. 2013), but the stress-relaxation period of soft tissues in the hip region is substantially longer (Palevski, Glaich et al. 2006; Gefen and Haberman 2007). The soft tissues are likely loaded at a greater rate than the force can be dissipated, resulting in greater stress generation (i.e. higher peak forces and lower system deformation). Additionally, the viscous components are supported by the clear hysteretic nature of an impact to the hip, seen in the low magnitude of force oscillations following peak force in Study 1 and Study 2. However, large variance in Err_{TTP} for VG (Figure 5.6c), along with the poor characterization of VG in Figure 5.5 demonstrates that success of inclusion of damping components varies greatly between subjects. This may be improved through further exploration of what individual characteristics (such as viscoelasticity of the skeletal components) are responsible for accurate estimation of damping parameters.

In contrast, geometry primarily influenced error related to peak force, reflecting the distribution of loading away from a single contact point. This demonstrates agreement with previous studies (Study 1, Appendix 2) which showed that soft tissues were strongly related to the magnitude of load distribution (demonstrated through contact area), which was in turn linked to overall reduction in peak force. However, there was limited improvement in performance across evaluation criteria for the geometrically more complex volumetric model. In contrast, the Hunt-Crossley model performed within the best subset for four out of six criteria, and a substantial functional improvement over MS for all criteria. One explanation for this is the added challenge of characterizing additional parameters for VC (i.e. the diameter of the sphere representing the pelvis) or a mismatch between the geometry of the pelvis during the impact phase and the sphere-on-plane representation. In a supporting study (Appendix 2), we found that there was substantial deviation from a circular contact profile for participants, particularly those with low TSTT. The sensitivity of VC to variation to deviance from the expected contact profile has not yet been tested, and a different interference geometry (e.g. cylinder-on-plane rather than sphere-on-plane) may be warranted.

A second explanation is the difference in distribution of contact pressure between HC and VC (Figure 5.7). There is substantial localization of force within the contact profile (Choi, Hoffer et al. 2010; Laing and Robinovitch 2010) which is likely better recreated by the Hunt-Crossley model than the Volumetric model. Understanding of the individual characteristics which control this phenomenon (possibly the projection of the proximal femur away from the pelvis, into the pelvis-floor interface) would provide value into predicting how these loads are distributed. Shourijeh and McPhee (2015) developed a hyper-volumetric model (a volumetric model with a hyperelastic, or non-linear foundation) of the foot, citing the large deformation of the soft tissue as their rationale (i.e. the soft tissue pad is more deformable than standard engineering materials). While this may be a fruitful approach for a lateral hip impact scenario, it is unclear whether the improvement would be worth the additional cost of parameter development and computation, considering the positive performance of the simpler Hunt-Crossley model.

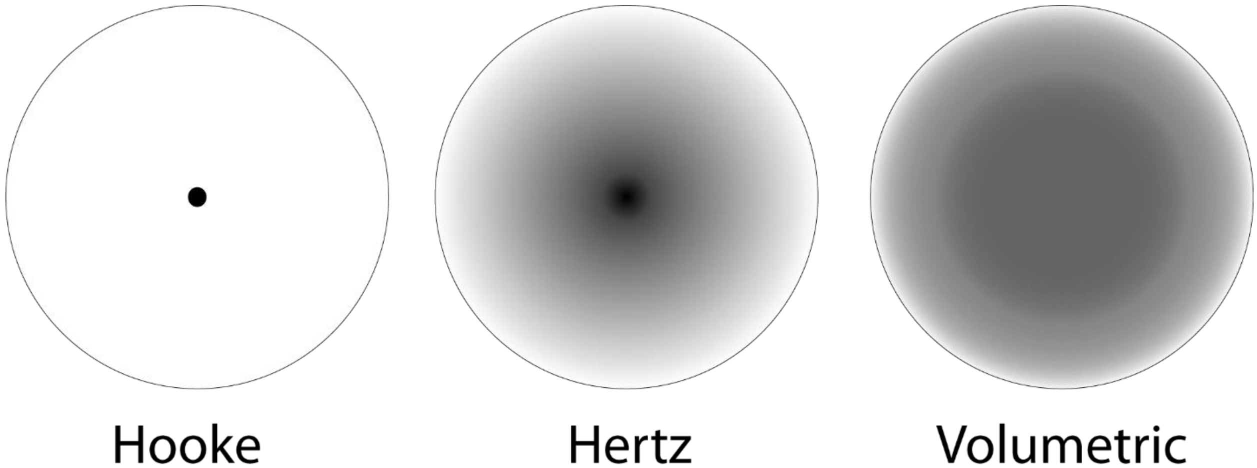

Figure 5.7 Distribution of contact stress for models

For models based on Hookean theory (MS, VG), pressure is assumed to be applied at a single central point. For models based on Hertz theory (HZ, HC), pressure is concentrated at a single central point. In the volumetric model, pressure is distributed away from the central contact point, dependent on the depth of interaction between the sphere and plane.

When considering load application in finite element models (or other modeling paradigms considering the internal distribution of loads within the proximal femur and pelvis), this information regarding load distribution is valuable. The models developed here can be used to generate a subject-specific spatial matrix of force inputs for detailed finite element models, such as those developed by Majumder et al. (Majumder, Roychowdhury et al. 2004; Majumder, Roychowdhury et al. 2007; Majumder, Roychowdhury et al. 2008; Majumder, Roychowdhury et al. 2008; Majumder, Roychowdhury et al. 2013) and Luo and colleagues (Luo, Ferdous et al. 2011; Ferdous and Luo 2015; Sarvi and Luo 2015; Sarvi and Luo 2015; Sarvi and Luo 2015; Nasiri and Luo 2016; Kheirollahi and Luo 2017). That is, partitioning stress along the modeled components in a matrix based on a pressure distribution of a Hertzian spring may be more biofidelic than assuming a point load at the greater trochanter, or assuming loading based on the hemispherical volume of the pelvis. Additionally, modification of pressure distribution based on individual TSTT may improve subject-specific finite element models. This may improve understanding of localized stress within anatomical components, and may explain how anatomical components are responsible for the loading response.

From a factor-of-risk perspective, accurate estimation of total impact force during falls to the hip is critical for predicting hip fracture. In this study, we were able to predict applied loads within a mean (SD) of 5.4 (20.7)% for the Hunt-Crossley model; however, the model, in its current implementation, is limited to a directly lateral impact to the hip, with an impact configuration similar to the pelvis release body configuration. Bouxsein et al. used a mass-spring model to estimate TSTT-attenuated peak force for hip fracture cases and older adult faller controls. They found that this method of distinguishing fracture cases from controls was effective for women (Bouxsein, Szulc et al. 2007), but not men (Nielson, Bouxsein et al. 2009), highlighting limitations of implementing a simplified contact model. Incorporation of an impact model considering damping and geometry may improve epidemiological, or population-level prediction of risk. Van der Zijden and colleagues (2017) developed a regression model, based on body mass, hip acceleration and shoulder angle, to predict impact forces to the hip within 5%. However, this model could only explain 46-63% of the variance in impact force, and had limited mechanistic support. Additionally, the model is largely dependent on hip acceleration and shoulder angle (identified as an indicator of energy dissipation through the upper limb), the neuromechanics and impact dynamics of which are unclear, and it is unclear how externally valid the model would be to impact configurations beyond those in the model training data set. Additionally, the authors point out that the model is likely not generalizable to fallers who are not trained judokas, highlighting the sensitivity to control of descent and distribution of energy to other body segments. Using a three-link (torso, thigh, shank) whole-body dynamics model with a Voigt impact model, Sarvi and Luo (2015) developed an individual-specific, mechanistic model of falls from standing height, finding a substantial effect of TSTT and obesity or underweight on fall force estimates. When validating the model with experimental data (Sarvi, Luo et al. 2014), error in peak force estimation was similar to magnitude of error for VG in this study; however, our results show that replication of the loading response may be improved by changing the impact model to a Hunt-Crossley formulation, particularly in replicating the loading response within experimental corridors during the impact phase. Incorporation of a stronger contact model would improve performance of multi-level modeling of falls.

Our findings add to the body of evidence supporting geometry-based models for biomechanical purposes. Hertzian models have previously been successfully used to simulate deep tissue injuries resulting from prolonged sitting (Gefen 2007), as well as cartilaginous joints under static conditions (Eberhardt, Lewis et al. 1991; Hirokawa 1991). Queen et al. (2003) used a Hertzian model to simulate soccer heading, reporting that soccer ball dimension moreso than inflation pressure (i.e. stiffness) had a significant effect on heading kinematics, particularly contact duration, but did not discuss the potential of a viscoelastic component. Lintern et al. (2015) successfully implemented a Hunt-Crossley model within the OpenSim framework to simulate brain trauma during an infant shaking paradigm. Shourijeh and McPhee (2015) and Lopes et al. (2016) found a substantial improvement in ground reaction force prediction (shear and vertical) using a volumetric model to simulate foot contact during level gait compared to a point-contact model. The results of this study highlight the importance of inclusion of damping components in geometric models of impacts to biological systems.

Limitations of the current work support development of a stronger model for the prediction of loading magnitude and distribution between body segments. First, though we included overall corridor performance in this study, we did not determine which regions were associated with good or bad concordance between the experimental and simulated data. Qualitatively, there is an inflection point (Figure 5.8) in the majority of experimental data which was a region of poor concordance between the experimental and modeled force curves. This may represent a change in the dominant anatomical or system components (e.g. a soft-tissue-dominated phase followed by a skeletal-tissue-dominated phase). Accordingly, a model with a multiphase response may better represent this region if users consider this phase to be of clinical importance. Third, in this study, we only simulated the normal force during a directly lateral impact to the hip. Further development of the model should include more complex impact configurations; this highlights a potential benefit of the Volumetric model over simpler models. It is possible to include resistance to tangential rolling, along with tangential friction between the pelvis and floor within the Volumetric model. Both of these may be important in simulating impact scenarios with greater lateral motion. Finally, we characterized and validated our model parameters at low (but clinically-relevant (Choi, Wakeling, et al., 2015) impact velocities. The force-deflection response of the pelvis is potentially non-linear, i.e. at higher impact velocities, stiffness and damping characteristics may differ. Validation at higher impact velocities, as well as within an implementation of a factor-of-risk based epidemiological model would be of value to determine whether the improved performance of the Hunt-Crossley model extends to injurious

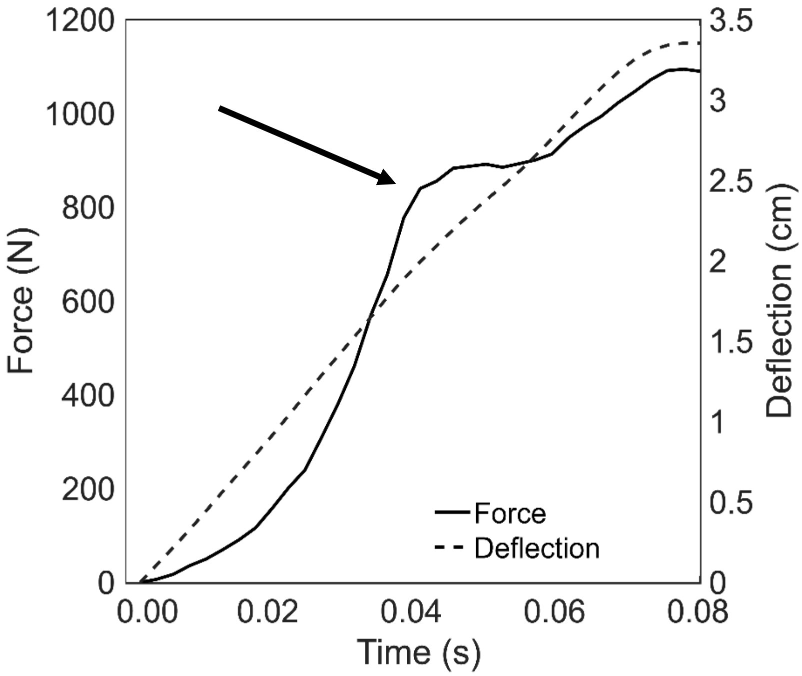

Figure 5.8 Nonlinearity in the force and deflection data during the initial impact phase

During the initial phase of the impact, the loading response (solid line) is typically non-linear. Loading responses typically include a "shoulder region" (black arrow) which was not captured by any of the models in this study. In contrast, the deflection response (dashed line) is primarily linear.

falling scenarios. Additionally, model performance varied between participants, however, we did not analyze whether errors were linked to individual characteristics such as sex or anthropometrics. Future work should clarify whether errors can be linked to specific groups of participants or sets of individual characteristics, which may help refine methods of quantifying anthropometry or characterization of parameters.

In summary, in this study we compared a selection of contact models with geometric and damping components. We found that the geometric components had a stronger effect on prediction of peak force, while the damping components had a stronger effect on timing characteristics. However, both factors interacted to influence impulse and corridor rating, which are both dependent on both timing and magnitude of loading. The Hunt-Crossley model clearly performed the best within this study, and is relatively simple and quick to implement—therefore, this may be the strongest contender for modeling approaches.

Chapter 6, Study 4: *In Vitro* Determination of the Anatomical Sources of Pelvic Stiffness Components

Chapter 6 focuses on in vitro *experiments to describe the influence of anatomical components and hip-pelvis position on deflection within the hip and pelvis during impact. It should be noted that this thesis chapter represents exploratory work, which will inform ongoing projects with larger samples sizes.*

6.1 Introduction

While it has been established that pelvic stiffness is a critical component of energy absorption during impacts to the hip (Lauritzen and Askegaard 1992; Bhan, Levine et al. 2013), and that differences in pelvic stiffness exist between sexes and BMI groups (Levine 2011; Levine, Bhan et al. 2013), skeletal and soft tissue sources of these differences have only been theorized. Potential sources include adipose tissue, muscle tissue, ligament laxity or damage, and movement of the femur within the hip joint. However, a primary limitation of the *in vivo* pelvis release experiment is that the motion of the pelvis is tracked as a whole, rather than segmentally, and typically via a single marker or limited marker set. Using these approaches, it is difficult to determine the anatomical sources of pelvic stiffness. Additionally, use of live participants limits the impact velocity that can be collected to 1 m/s to reduce the discomfort to the participant. Because of this, non-linearities in patterns of kinetic impact variables (such as peak force and pelvic stiffness) have not been investigated at even average impact velocities observed during falls from standing height (~3 m/s). Viscoelasticity of biomaterials, and a "bottoming out" effect (Serina, Mote et al. 1997), could potentially decrease energy absorption at these higher impact velocities.

The pelvis and femur is an anatomically complex system, and freedom of motion of each component contributes to deflection of the pelvis during impact.. The bones involved during an impact to the hip are the femur, ilium, ischium, pubis and sacrum. These bones are held together by ossification (e.g. the three components of the pelvic girdle) and ligaments (e.g. the posterior sacroiliac ligaments connecting the sacrum to the pelvic girdle, or the ischiofemoral ligament connecting the ischium to the femur). The joints within this system have varying levels of flexibility, depending on their purpose and injury history. The sacroiliac joint allows approximately 8° of sagittal plane motion of the pelvic girdle relative to the sacrum, and 4-8 mm of translation in all directions (Smidt, Wei et al. 1997), motions which are limited collectively by four sacroiliac ligaments, bilaterally (Eichenseer, Sybert et al. 2011). The majority of angular motion in the pubic symphysis is within the transverse plane (60%), but is less than 1° in all directions (Birmingham, Kelly et al. 2012). Less than 2 mm of superior translation of one side over the other is normal, though the translation increases in women who have been pregnant (Garras, Carothers et al. 2008). In total, the pelvis (including the femur) can typically tolerate 17.6% compressive strain laterally (Beason, Dakin et al. 2003). There are also muscular connections between the bones to provide control over relative position, though only *tensor fascia lata* is directly lateral to (i.e. covering) the greater trochanter. In actual falls of older adults, roughly sagittal plane movement of the knee was observed, with the knee on the impacting side free (not contacting any other body part) in 33% of cases, contacting the floor in 43% of cases and contacting the contralateral knee in 23% of cases (Choi, Cripton et al. 2015).However, no study to date has reported on the motion of individual skeletal pelvis components during a lateral impact, which may give insight into what components are responsible for apparent effective pelvic stiffness.

All of these structures listed above are surrounded by adipose, layers of fascia, and skin. Trochanteric soft tissue thickness has been reported to range from 1.5 – 10 cm in depth (Robinovitch, Hayes et al. 1991; Maitland, Myers et al. 1993; Lauritzen 1997; Dufour, Roberts et al. 2012; Choi, Russell et al. 2014; Levine, Minty et al. 2014). While the exact composition of trochanteric soft tissue thickness (within a transverse plane) varies by transducer perspective and how muscles wrap relative to the landmarks of interest, one investigation places the makeup at 90% muscle, 6% fat, and 4% skin (Choi, Russell et al. 2014). However, trochanteric soft tissue thickness in another investigation was mainly influenced by sex (27% lower for males than females) and hip position (27% greater at 30° extension than quiet standing; 16% greater at 60° flexion than quiet standing), and not significantly affected by muscle activation (Levine, Minty et al. 2014). In consideration of the volume (or deflectable thickness) and low elastic modulus of adipose and muscle, these tissues likely have a large contribution to effective pelvic stiffness, but how the redistribution of loads by these tissues might affect the structures within the skeletal pelvis is unclear.

The goal of this study was to characterize the sources (and associated magnitudes) of frontal plane deflection of under unpadded (musculoskeletal components only) and padded (cadaveric tissue pad, “trochanteric adipose pad”, abbreviated as TAP) conditions. In this study, I described (1) peak total force, and deflection across the Greater Trochanter, Anterior Superior Iliac Spine, Iliac Wing, Lateral Apex of the Pelvic Ring and Pubic Symphysis, and (2) changes to these outcomes under conditions and without a trochanteric adipose pad, and finally (3) failure location and mechanism for each specimen.

6.2 Methods

Participants in this study were donors to the University of Waterloo School of Anatomy, compliant with the regulations and standards associated with the School of Anatomy for post-mortem donation. Additionally, we excluded donors with unilateral or bilateral hip replacement, or obvious pre-mortem femur, pelvis or lumbar spine deformity. All specimens were embalmed with a formaldehyde solution (65% Anydrous alcohol, 20% propylene glycol, 3.75% formaldehyde (37%), 5% phenol, 4.25% Dettol, 0. 75% Sodium acetate) prior to dissection and testing.

Table 6.1 Post-mortem human donor characteristics

Code	Sex	Age	Tap thickness (cm)	Femur length (GT to lateral femoral condyle, cm)	Right hemipelvis width (ASIS to L5 midline) (cm)
14089	Female	95	1.0	37.7	10.0
14090	Female	82	0.99	37.3	10.1
14091	Male	78	1.0	39.3	12.9

6.2.1 Dissection process and specimen preparation

The experiments were performed with the pelvis sectioned from the rest of the body, superiorly through the L4 lumbar spine segment, and inferiorly through the right knee joint (Figure 1). The left femur was removed, along with soft tissues lateral to the left obturator foramen, to the periosteal surface to allow potting of the left side of the pelvis. The trochanteric adipose pad (TAP) was removed, extending as deep as possible without compromising the underlying musculoskeletal structures, approximately 20 cm anteriorly, posteriorly, superiorly and inferiorly from the greater trochanter. The depth of the TAP was measured using calipers and tagged to indicate anatomical orientation. The TAP was stored in an airtight container, fixed in solution (90% water, 7.5% glycerol, 1.5% sodium acetate, 1.3% Dettol). Muscle and surrounding fascia was left intact, including the inguinal ligament. The contents of the pelvic ring (e.g. bladder, rectum, uterus) were removed, along with neurovascular structures as needed to view musculoskeletal landmarks.

The left side of the specimen was fixed in a custom steel containment fixture (internal dimensions relative to the pelvis, 18 cm anterior-posterior, 26 cm superior-inferior, and 10 cm medial-lateral, Figure 6.1) such that the frontal plane of the pelvis was parallel to the side walls of the fixture. Stainless steel wire (18-gauge) was used to limit motion of the pelvis, and non-exothermic dental plaster (Denstone®, Miles, South Bend, IN, USA) was used to pot the specimen to a depth of the medial border of the obturator foramen. The entire containment fixture was in turn affixed to a load cell (sampled at 20,000 Hz; Model 925M113, Kistler Instrument Corporation, Amherst, NY, USA), in turn affixed to a solid base. Tissues were conditioned periodically (in approximately 15 minute intervals) with a moistening fluid (Dettol 1.3%, Sodium Acetate 1.5%, Glycerol 7.5%, Water 90%).

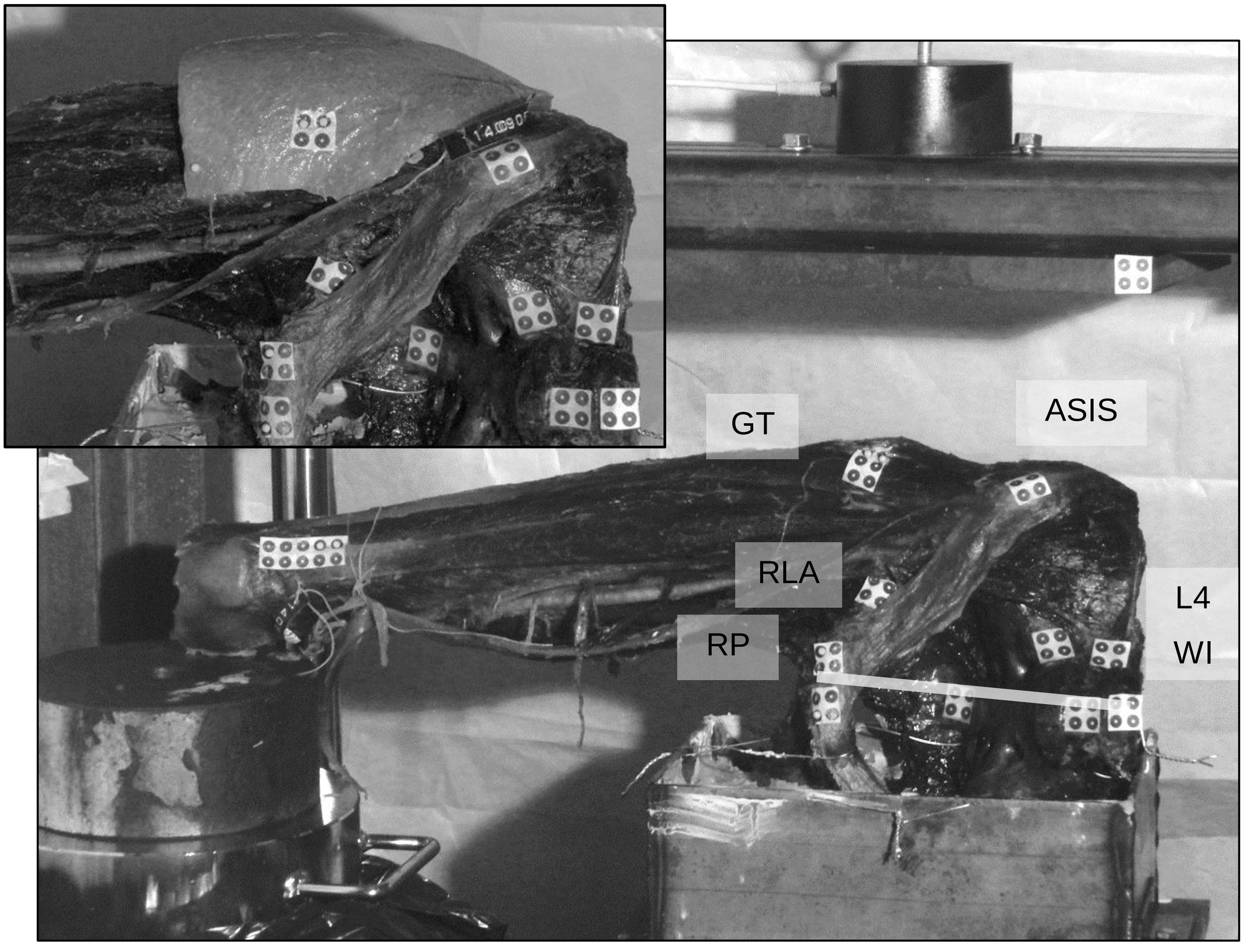

Figure 6.1 Orientation of the pelvis for the testing protocol

The pelvis and right femur of PMHS 14090 is shown, affixed within a steel containment fixture, which is in turn affixed to a load cell. The support on which the femur is resting in the photo was removed during testing, and was used for stabilization between trials. Each of the anatomical landmarks is overlaid with a planar marker, each with a minimum of four tracking markers, spaced 1 cm apart. The inlay shows the positioning of the TAP; the two steel pins placed through the marker are used to ensure consistent placement of the TAP. It should be noted that because the placement of the TAP obscures motion of the GT, motion of the GT will be reported only for the unpadded condition.

The white shaded line indicates the deflection baseline, which was determined for each timepoint. The baseline is formed by the midpoint of the right and left pubic symphysis and the midline of the L4 body. The baseline is shown in clearer detail in Figure 6.3. Marker locations of the GT, ASIS, lateral apex of the pelvic ring (RLA), wing of the ilium at L4 (WI) and right pubic symphysis (RP)

6.2.2 Instrumentation

A custom, low-friction drop tower (Figure 6.2), instrumented with a load cell, electromagnetic release (model DCA-400T-24C, AEC Magnetics, Cincinnati, Ohio, USA) was used along with a planar steel impact plate to impact the pelvis (total carriage weight, 38 kg). Frontal plane pelvis motion was

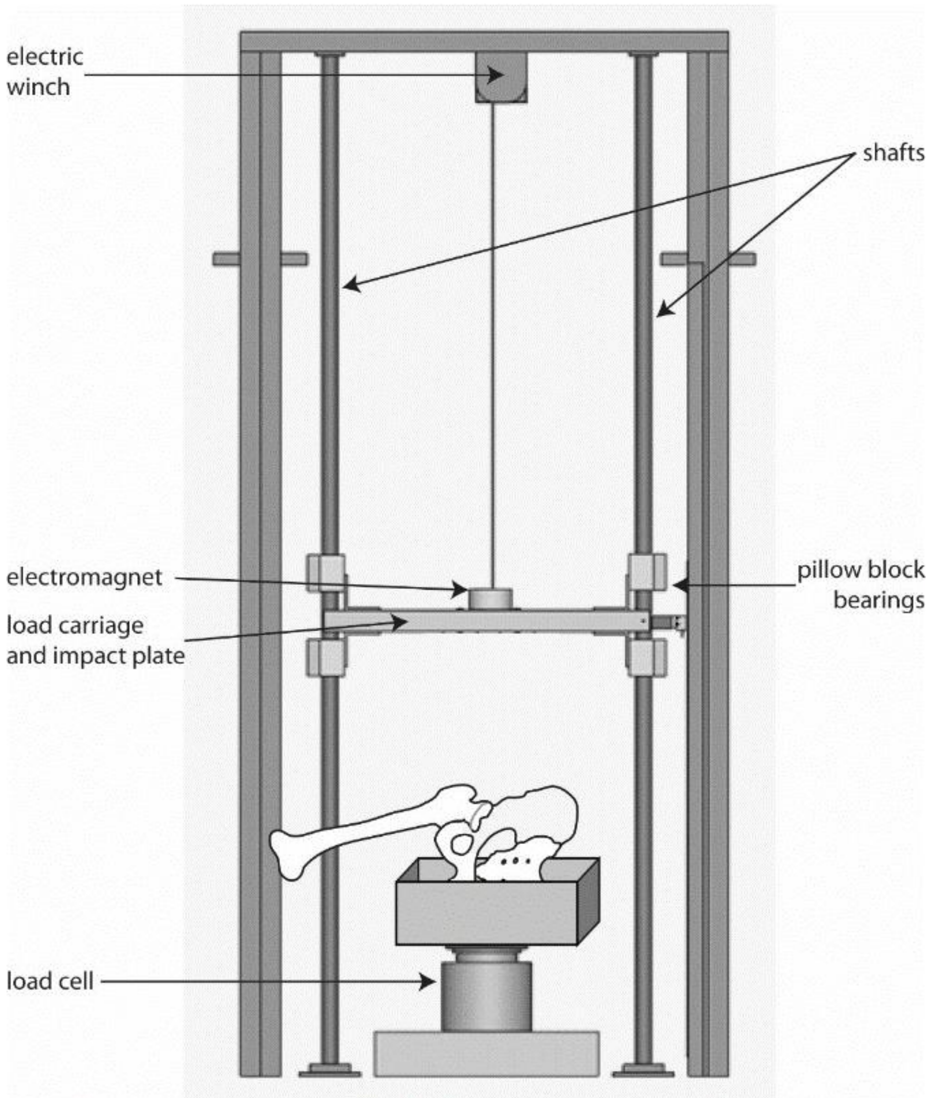

Figure 6.2 Pelvis drop tower

The pelvis drop tower consists of two frictionless shafts, along which a carriage slides vertically. A steel impact plate contacted the pelvis. The pelvis was affixed within a custom steel fixture, which is in turn affixed to the load cell. The initial height of the carriage and electromagnet is controlled via an electric winch. *Figure courtesy Frederick Goh.*

captured using a 2D high speed video camera (1250 frames per second, S-PRI, AOS Technologies, Cheshire, CT).

Adhesive motion tracking markers were adhered directly to the specimen (Figure 6.1), and attached so that they were oriented parallel to the plane of view of the camera. Markers were placed at the distal end of the right femur, right anterior superior iliac crest (ASIS), right apex of the greater trochanter (from the anterior view), lateral apex of the pelvic ring, right and left edges of the pubic symphysis, the wing of the ilium lateral to the L4 and L5 bodies, and the centres of the L4 and L5 bodies (Figure 6.1). A marker was also placed on the skin surface overlying the greater trochanter when the TAP was in position; however, it should be noted that because the placement of the TAP obscures motion of the GT, motion of the GT will be reported only for the unpadded condition.

6.2.3 Experimental protocol

Dynamic trials were collected in impact-velocity blocks (i.e. all 0 cm trials were performed first, followed by all 1.5 cm trials, and so on) until specimen failure, with the carriage raised to 0 cm (impending impact, a minimal height above the specimen, associated with an impact velocity of ~0.2 m/s), 1.5 cm (~0.55 m/s), 5 cm (~1 m/s) and 12 cm (~1.5 m/s), with two trials per combination of height and pad condition. Low-velocity trials were completed first in order to maximize the number of trials likely to be completed prior to specimen failure, similar to other studies with an *a priori* endpoint of specimen failure (Beason, Dakin et al. 2003; Etheridge, Beason et al. 2005). Within each velocity block, the condition order (i.e. TAP vs. unpadded) was randomized. The specimen and high-speed video were examined visually after each impact to assess tissue damage.

6.2.4 Signal Conditioning and Data Reduction

High-speed videos were temporally synchronized with the load cell data within MiDAS DA (Xcitex, Cambridge, MA), and image conditioned (correction for image brightness, contrast). Planar calibration and tracking was performed for each anatomical landmarks in ProAnalyst software (Xcitex, Cambridge, MA). All specimens had calibration values between 12 – 13 pixels per centimeter, resulting in a precision of approximately 0.08 cm. For all comparisons between the padded conditions compared to the unpadded condition, 0.08 cm was used as a threshold to detect change.

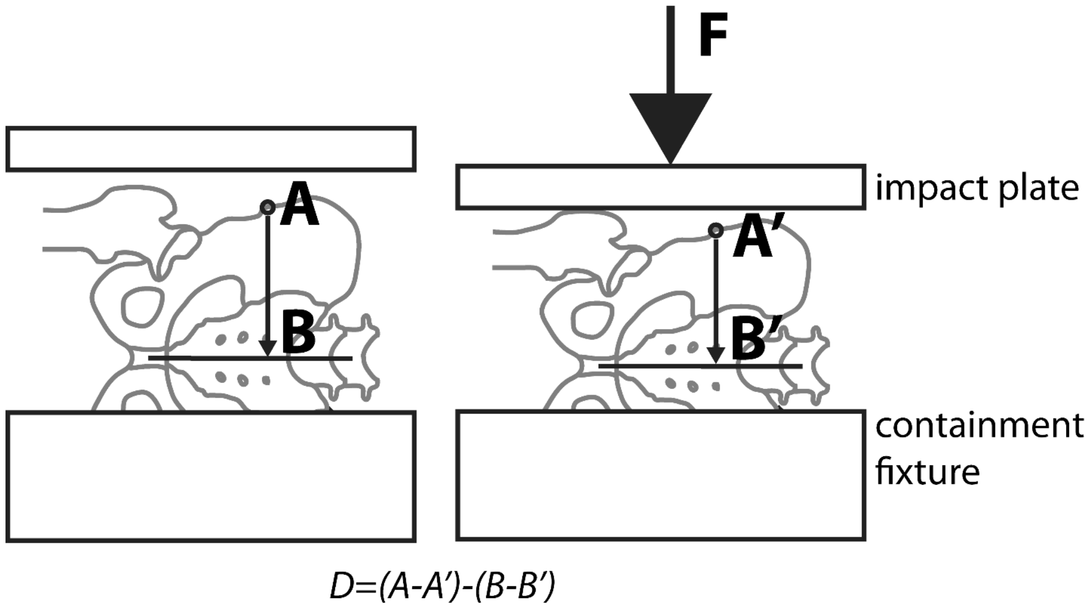

Figure 6.3 Demonstration of the method of calculating landmark deflection

The deflection of each landmark was calculated with reference to the baseline (solid horizontal line) formed by the midpoint of the pubic symphysis and the midline of the L5 body. The position of the landmark at each timepoint (A') is subtracted from the initial position (A). The position of the baseline point corresponding with the horizontal position of the landmark at each timepoint (B') is subtracted from the initial position (B). The time-varying bias (B-B') is then subtracted from the gross deflection (A-A').

The vertical planar position of each anatomical component was used to determine the time-varying deflection within each anatomical component of the pelvis relative to the midline baseline formed by the markers identifying the Pubic Symphysis and L4 and L5 spinal bodies (Figure 6.3). First, gross deflection was calculated as the time-varying vertical change in position for each landmark from the initial position of that landmark. The gross deflection was then corrected for total pelvis motion by subtracting the time-varying deflection of the baseline.

An automated point-selection routine was developed to determine key data coordinates for further analysis. Each trial was segregated by defining an initial unloaded region (Figure 6.4, prior to T1; $F_{initial}$, $D_{initial}$), the beginning of impact (when force exceeds two standard deviations of the mean in the quiet region preceding impact, Figure 6.4, T1; T_{imp}, F_{imp}), peak force (Figure 6.4, T2;T_{max}, F_{max}, D_{max}). Bias ($F_{initial}$) was subtracted from F_{max}. Finally, a deflection initiation delay (D_{delay}) was calculated as the difference in time between T_{imp} and the timepoint at which initial deflection was observed for each landmark.

Data was reduced by calculating the mean across specimens within each velocity and condition, including only trials for which no specimen damage was observed. Because of the low number of specimens available for the study, only descriptive statistics and not statistical comparisons (i.e. analysis of variance) are reported in this chapter. Regarding the first goal of the study, I reported total peak force range and time to peak force, as well as the total component deflection and deflection initiation delay for both padded and unpadded conditions, at each velocity. Regarding the second goal, I quantified a percent change for each outcome between padded and unpadded conditions. Finally, regarding the third goal, I reported the failure location and mechanism for each specimen.

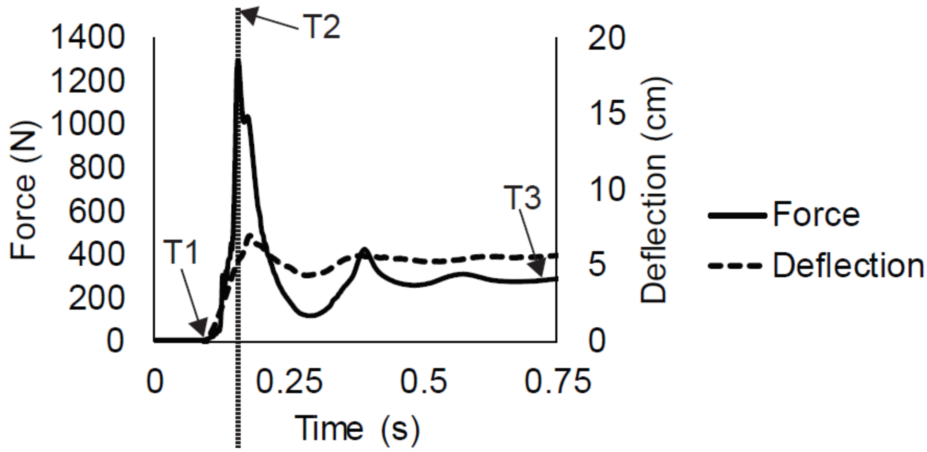

Figure 6.4 Critical timepoints

The region prior (to the left of) T1 is the unloaded, quiet region. T1 corresponds with the beginning of impact, while T2 corresponds with the peak force, and is the timepoint selected for determination of D_{max}, CA_{max} and P_{max}. Interval T1-T2 is the initial loading phase. Force oscillates until a final resting point, T3.

6.3 Results

For trials not resulting in specimen damage, peak forces ranged from 636– 4287 N, increasing between the impending impact condition (mean (SD) unpadded 1135 (405) padded, 875 (216) N) and the highest impact velocity (unpadded, 4060 (145) N; padded, 3945 (417) N; Figure 6.5a). Time to peak force was greater and more variable during the impending impact velocity (unpadded, 0.032 (0.014) s; padded, 0.053 (0.017) s), but was more similar across the higher impact velocities (across 0.55-1 m/s, unpadded, 0.019 (0.004) s; padded, 0.020 (0.006) s; Figure 6.5b). Average force attenuation provided by the trochanteric adipose pad condition compared to the unpadded condition was greater during the impending impact condition (22.9%), but limited at greater impact velocity (across 0.55-1 m/s, <1%, Figure 6.5a).

Deflection of the impact plate (i.e. total hemi-pelvis deflection) ranged from 0.31 – 1.77 cm for trials not resulting in specimen damage (2.4-13.7% hemipelvis width, Figure 6.6a). Deflection of individual components across all impact velocities are reported in Table 6.2. Mean deflection was similar between GT, lateral apex of the pelvic ring and the wing of the ilium (~0.2 cm), greater for the ASIS (~0.4 cm), and lower for the right pubic symphysis (<0.1 cm). The Lateral Apex of the Pelvic Ring provided the single highest deflection during non-damaging trials (Table 6.2), but more moderate deflection on average. Maximum deflection of the GT and wing of the ilium also exceeded 1 cm. Deflection of the right pubic symphysis reached the change threshold during only one trial; deflection during other trials was minimal (Figure 6.6f).

Deflection generally increased with increasing impact velocity, across all locations (Figure 6.6), up to 330% Inclusion of the TAP decreased deflection at anatomically superior structures (ASIS, Figure 6.6d; wing of the ilium (Figure 6.6e) and increased deflection at the lateral apex of the pelvic ring, Figure 6.6c). Variability in deflection generally increased during conditions when the TAP was included vs. unpadded conditions. However, interaction between padding condition and impact velocity altered the effectiveness of the TAP. Inclusion of the TAP decreased deflection of the ASIS 69.5% during the impending impact condition, however, this decrease was reduced to 17% for the 0.75 and 1 m/s conditions. Similarly, for the wing of the ilium, effectiveness reduced from 103% deflection decrease at the lowest impact velocity to 49% decrease at the highest velocity. Deflection of the lateral apex of the pelvic ring was greater during padded trials than unpadded trials at all impact velocities except 0.55 m/s, where the two conditions produced similar deflection of the lateral apex.

The time delay between force initiation and deflection initiation (D_{delay}) decreased up to 80% with increasing impact velocity for all anatomical landmarks (from 0.0043 to 0.009 s, Figure 6.7). D_{delay} magnitude and mean response to the padding condition was similar between structures within the pelvis, but was more variable for anatomically superior structures (ASIS, wing of the ilium) than inferior structures (ring lateral apex, pubic symphysis).

Table 6.2 Component Deflection

Component	Mean (SD) across velocity conditions (cm)	Maximum (cm)
Greater Trochanter	0.21 (0.31)*	1.01*
Pelvic Ring Lateral Apex	0.25 (0.25)*	1.13*
ASIS	0.43 (0.31)*	1.08*
Wing of Ilium, L4	0.21 (0.23)*	0.60*
Right Pubic Symphysis	-0.01 (0.04)	0.09*

* represents deflection greater than the *a priori* change threshold based on the resolution of the high-speed video

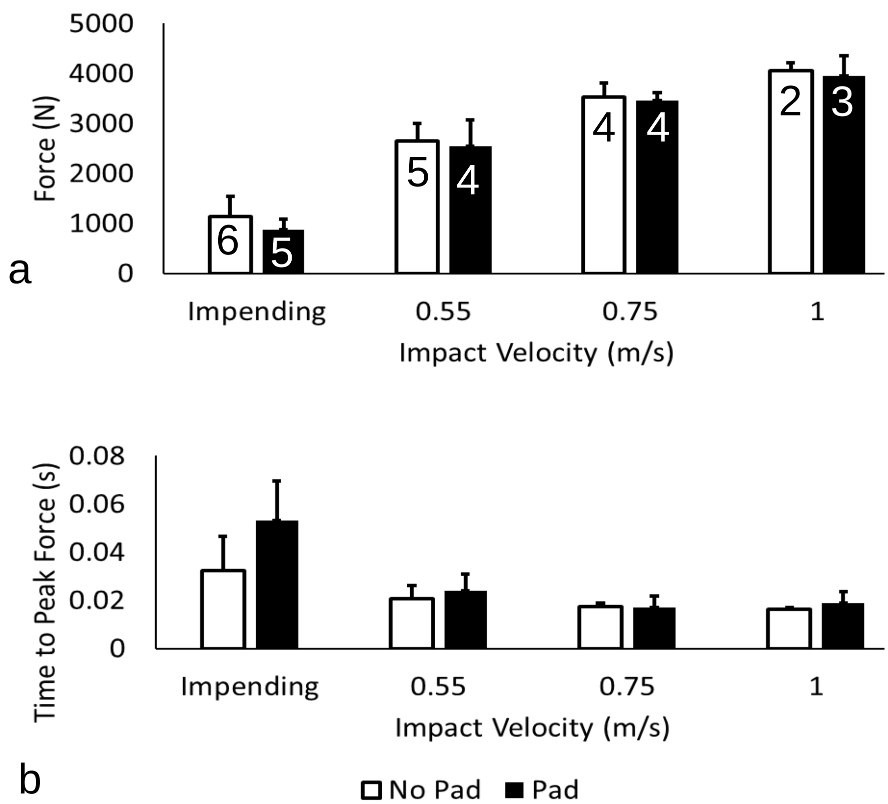

Figure 6.5 Peak force, force attenuation and duration of loading Peak force increased with increasing impact velocity (a), and the padded condition provided little force attenuation at higher impact velocity. Similarly, time to peak force decreased with increasing impact velocity (b), and the padded condition provided a substantial increase in time to peak force only for the impending impact condition. *Numbers of trials (reflecting specimen damage) included for each condition are indicated by the numeral overlying the bars in pane a.*

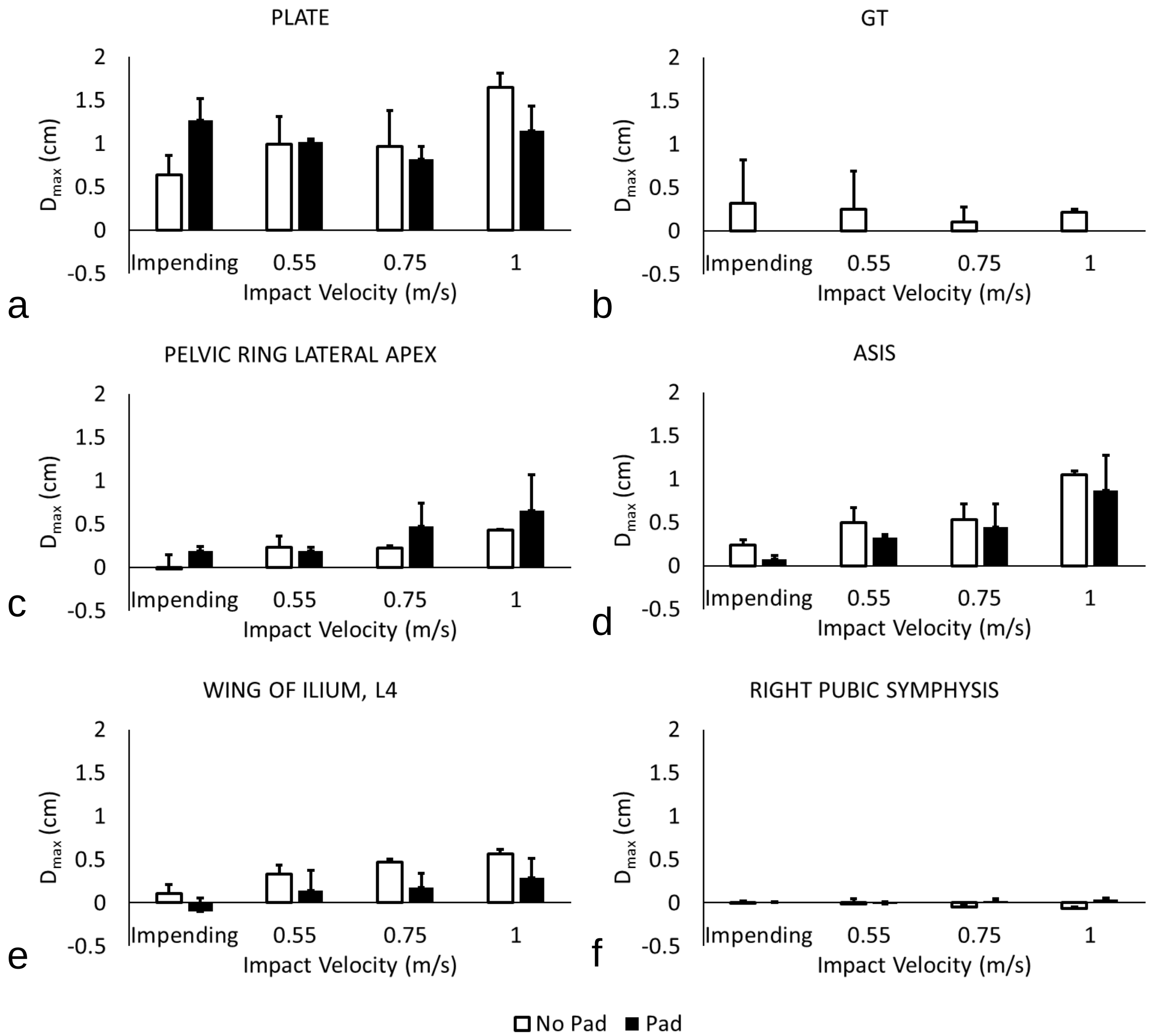

Figure 6.6 Deflection at time of peak force
Deflection of the plate during the unpadded condition increased with impact velocity (a), but not during the padded condition. Deflection of the GT (b) did not appear to follow any clear trends with regards to impact velocity. Deflection of the lateral apex of the pelvic ring (c) increased substantially with both impact velocity and inclusion of the TAP, compared to the unpadded condition. Deflection of the ASIS (d) and wing of the ilium (e) increased with increasing impact velocity, but decreased during padded vs. unpadded conditions. Deflection of the right pubic symphysis was minimal and did not appear to have any trends regarding impact velocity or inclusion of the TAP.

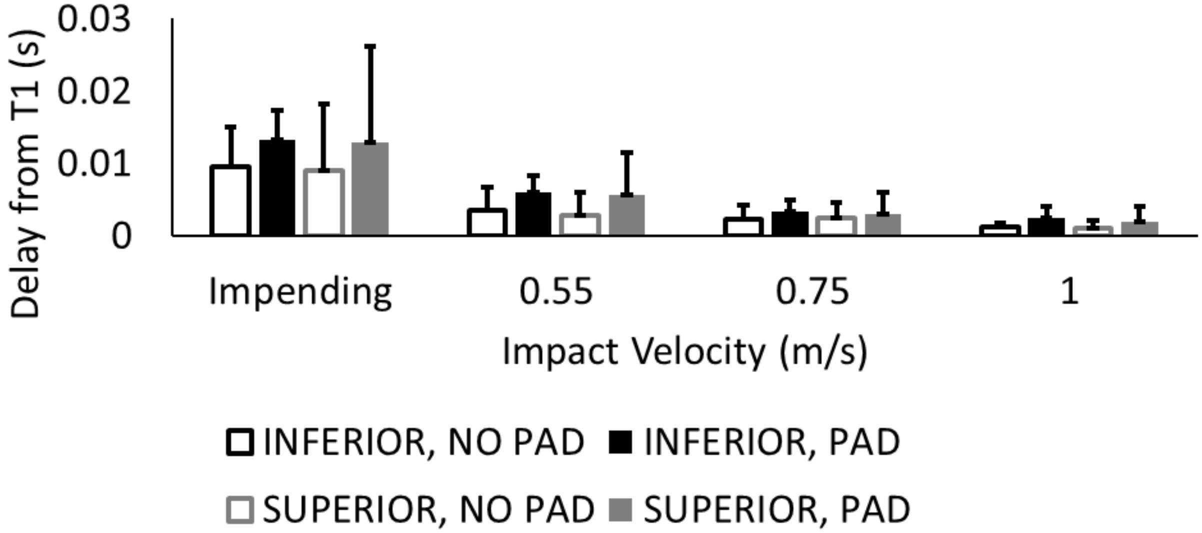

Figure 6.7 Time delay between force initiation (T1) and deflection initiation

While deflection delay was similar across structures, and the TAP increased deflection delay for both superior (wing of ilium, ASIS) and inferior (ring lateral apex, right pubic symphysis) structures, the delay was more variable for superior structures than inferior structures. This implies that the loading pathway may be more consistent through inferior structures, which are located more proximally to the point of external load application.

6.3.1 Specimen fracture patterns

Specimen 14089 failed during the 21st trial, a no pad condition, with an impact velocity of 1 m/s and a peak force of 3947.9 N. No damage was observed in the femur. The lesion locations were determined based on analysis of the trial video (Figure 6.8a,b) and manual compression and distraction of the specimen (Figure 6.8c-h). During the fracture, the superior pelvis (ilium) rotated anteriorly relative to the inferior pelvis (ischium, pubis), generating tension on the anterior surface. The primary injury was medial to the acetabulum, slightly inferior to the iliopubic eminence, and not apparent without dissection. The lesion spanned the entire width of the pubis, but was not deep, and except for a 2 mm^2 gap, required manual distraction to be observed (Figure 6.8c). Corresponding damage to the anterior margin of the acetabulum was also observed, with approximately 6 mm of the margin visibly damaged (Figure 6.8d,e). A second lesion, a gap between the pubic symphysis, was also observed (Figure 6.8f). However, the pubic symphysis was devoid of the normal cartilage—this may have been an ante mortem injury. This constellation of injuries (fracture of the anterior pubic ramus and dislocation of the pubic symphysis) is observed, according to orthopaedic reports, when the pelvis is compressed along with rapid external rotation of the femur against the acetabulum (Tile, Helfet et al. 2003). No external rotation of the femur was noted during load application, however, the load may have been directed through the femur towards the anterior margin of the acetabulum.

Specimen 14090 failed during the 9th trial, a padded condition, with an impact velocity of 0.55 m/s and a peak force of 1638.8 N (Figure 6.9a, b). During the fracture, the right ilium rotated posteriorly while the left (potted) ilium and sacrum remained vertical, causing the ilium to displace posteriorly from the sacrum under lateral compression. Similar to Specimen14089, the lesion was not apparent without deep dissection. After removing the overlying muscle fibres, there were no visible fractures, however, there was a lesion of the anterior sacroiliac and interosseous sacroiliac ligaments spanning the entire height of the sacroiliac joint (Figure 6.9c-e). The articular surfaces of the sacrum and ilium appeared to be fairly smooth, which is associated with sacroiliac instability (Rosatelli, Agur et al. 2006). No damage was observed at the pubic symphysis or to the sacral body.

Specimen 14091 failed during the 25th trial, a padded condition with an impact velocity of 1.5 m/s and a peak force of 3853.3 N (Figure 6.10a, b). During the fracture, the right anterior superior iliac crest rotated posterolaterally as tension was released along the iliac fossa. Damage to the ilium was visible prior to deep dissection, and included tears to fibres of the iliacus (Figure 6.10c). Damage to the iliac fossa was substantial, and included a major, unstable fracture 7.25 cm in length (Figure 6.10d), as well as a stable fracture (intersecting at 30° to the major fracture) of 7.0 cm in length, and several small lesions, <1cm in length, to the cortex of the ilium (Figure 6.10e). Iliac wing fractures are associated with >1 cm lateral displacement of the iliac crest, with loading directed through the ilium rather than the acetabulum. During the potting process, specimen 14091 shifted within the potting fixture, which, combined with a relatively short femoral neck, resulted the point of load application shifting towards the ilium. Five out of six trials preceding the fracture trial (all at 1 m/s impact velocity) resulted in >1 cm deflection of the ASIS.

None of the specimens in this study suffered any damage to the proximal femur.

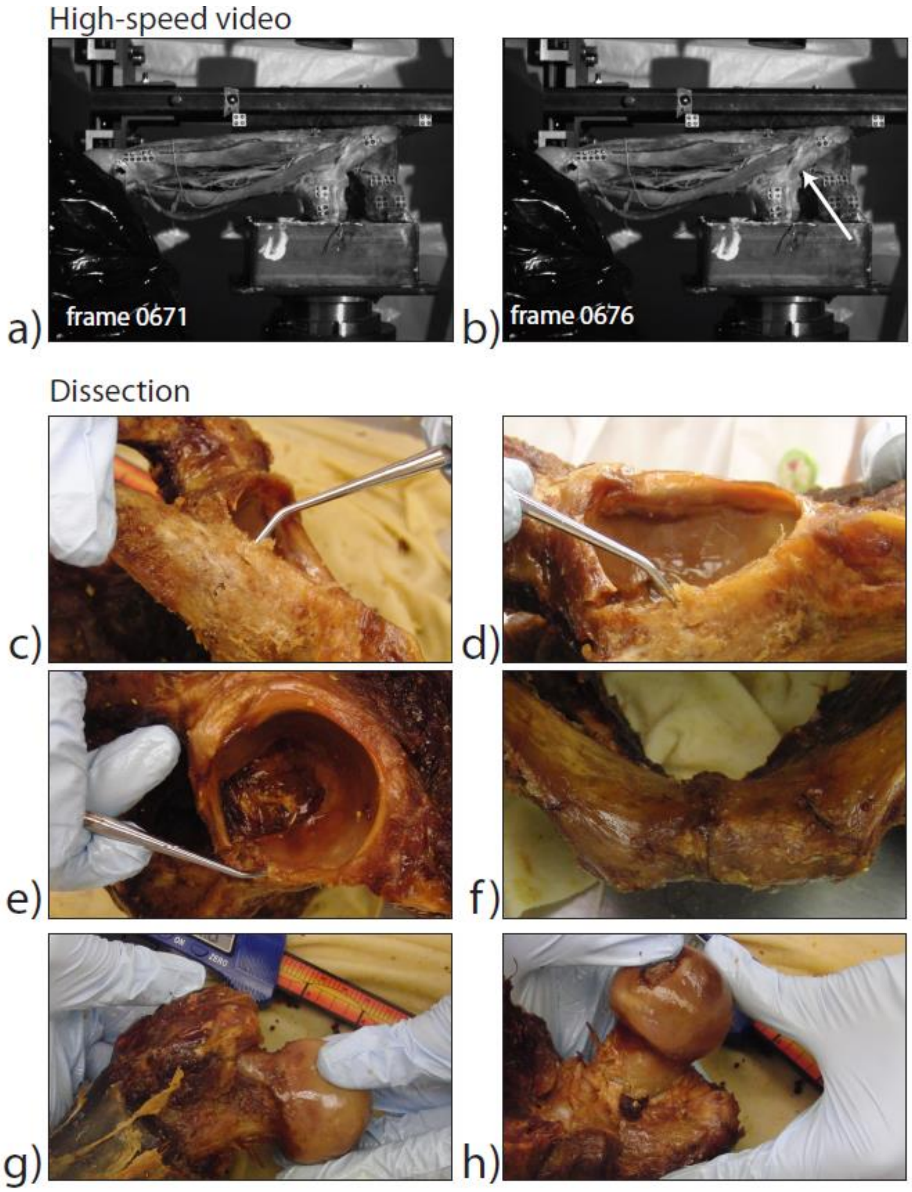

Figure 6.8 High-speed video stills and dissection of PMHS 14089

Video frames of the loaded specimen pre-fracture (a) and post-fracture (b), with the arrow indicating the area of movement during the injury. During the fracture, the superior pelvis (ilium) rotated anteriorly relative to the inferior pelvis (ischium, pubis), resulting in a fracture (c, shown with distraction) inferior to the iliopubic eminence, which carried laterally to the margin of the acetabulum (d) and corresponded to damage to the margin of the acetabulum (e). There was notable incomplete anterior separation of the pubic symphysis (f), and the cartilage typically found in this joint was absent. There was no noted damage to the femur (g, h).

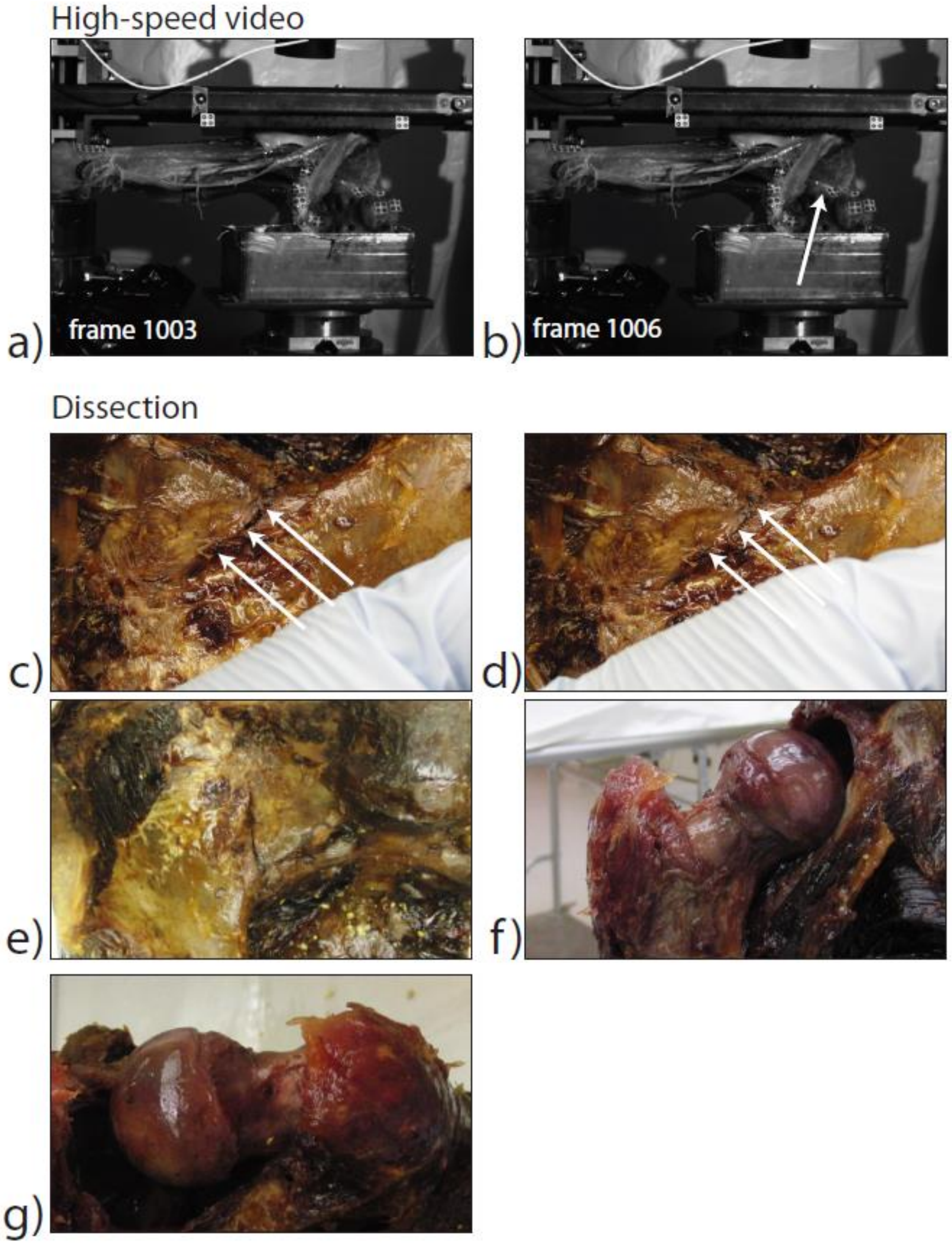

Figure 6.9 High-speed video stills and dissection of PMHS 14090

Video frames of the loaded specimen pre-fracture (a) and post-fracture (b), with the arrow indicating the area of movement during the injury. During the fracture, the right ilium rotated posteriorly while the left (potted) ilium and sacrum remained vertical, causing the ilium to displace posteriorly from the sacrum. The lesion at the sacroiliac joint is shown superiorly under distraction (c) and compression (d), with the depth of the ligament injury indicated by the arrows. The damage is presented from an anterior view (e). There was no noted damage to the femur (f, g).

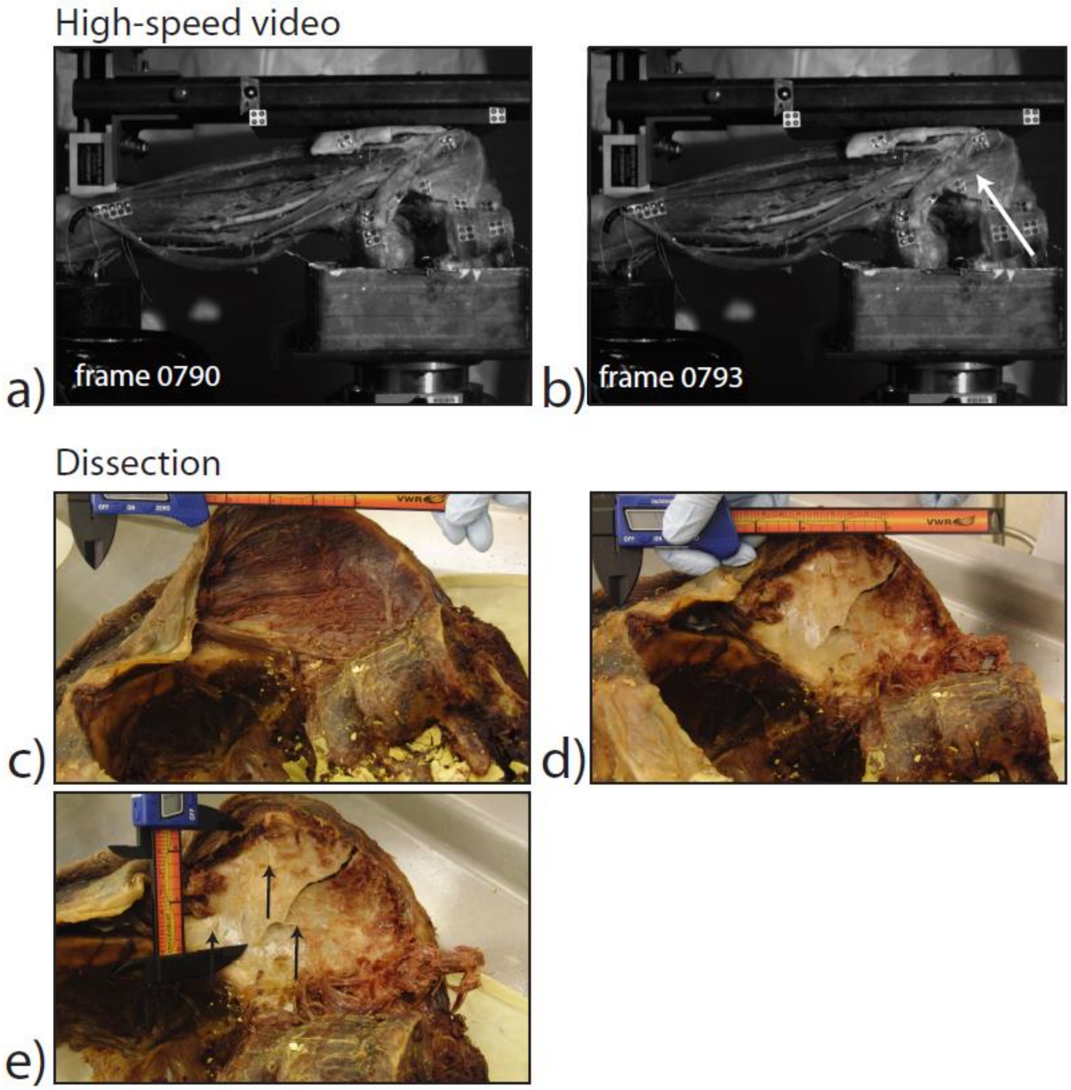

Figure 6.10 High-speed video stills and dissection of PMHS 14091

Video frames of the loaded specimen pre-fracture (a) and post-fracture (b), with the arrow indicating the area of movement during the injury. During the fracture, the right anterior superior iliac crest rotated posterolaterally as tension was released along the iliac fossa. Damage to the fibres of iliacus were observed (c). After removal of iliacus, there was a substantial fracture (d), an incomplete secondary fracture (e, indicated by the calipers), and several small lesions to the cortex of the ilium (e, arrows). There was no noted damage to the femur (not pictured).

6.4 Discussion

The goal of this study was to characterize the sources of pelvis frontal plane deflection in response to a lateral load applied to the hip. In this study, specimens underwent applied loads of up to 4287 N; two specimens failed at nearly 4000 N, while the third failed at only 1600 N. Several anatomical structures experienced greater than 0.5 cm of deflection during the protocol, including the greater trochanter, the lateral apex of the pelvic ring, the ASIS, and the wing of the ilium. The greatest deflection within the pelvis occurred at the ASIS, lateral apex of the pelvic ring, and wing of the ilium near L4, while the pubic symphysis was more stable. Motion of the greater trochanter did not appear to be linked with impact velocity, while motion of other components followed patterns based on impact velocity and padding conditions. Initiation of deflection occurred later when the TAP was in position, while deflection delay was more variable for superior pelvis structures than structures more proximal to the femur. Generally, the results of this study provide insight into the internal loading pathway of the pelvis during lateral impacts to the hip, which in turn supports understanding of the anatomical sources of pelvic stiffness.

In the current cases, we found trends associated with our two alternate loading scenarios. While the effects on peak force were low and diminished with higher impact velocity, inclusion of the TAP appears to redistribute strain away from the ASIS and iliac wing, and increase deflection of the lateral apex of the pelvic ring. Additionally, inclusion of the TAP increased the loading delay for landmarks within the pelvis, and in particular, induced a more variable delay for the ASIS and wing of the ilium. The lateral apex of the pelvic ring is typically just medial to the acetabulum (the location of the head of the femur), and therefore sensitive to motion of the femur. This indicates that inclusion of the TAP may have centralized loading rather than distributing the load, as hypothesized, and that loading pathways may be more variable during padded conditions. Additionally, because the deflection delay was longer for the landmarks within the pelvis, this increased the proportion of the impact period where stress was primarily directed through the proximal femur and acetabulum, rather than other pelvis structures. However, our current cohort had particularly low TAP thickness, compared to the expected 1.5-10 cm (Choi, Russell et al. 2014; Levine, Minty et al. 2014); it is unclear whether these trends would be maintained in a larger cohort.

We observed injuries consistent with epidemiological reports and previous studies involving lateral compressive loading directed through the hip. The incidence of pelvis fractures has rapidly risen since the 1970's (Kannus, Palvanen et al. 2005), and the population and causation of pelvis fractures has shifted from young adults in automotive accidents to adults over 80 years of age resulting from falls (83% of cases) (Guggenbuhl, Meadeb et al. 2005; Kannus, Palvanen et al. 2005). This incidence shift is likely due to improvements in automotive safety, as well as improvement in medical imaging and diagnosis of pelvis fractures (Scheyerer, Osterhoff et al. 2012; Studer, Suhm et al. 2013), i.e. the rate of diagnosis for stable pelvis fractures has improved, though the actual injury rate may not have changed. Abrassart and colleagues observed that 20% of iliac wing fractures were the result of falls (2009). Pelvis fractures in older adults are associated with similar rates of morbidity to hip fractures. Nearly all diagnosed pelvis fractures require hospitalization, however treatment is typically conservative and non-surgical (Studer, Suhm et al. 2013). The one-year mortality rate of pelvis fractures is approximately 18.5% (Studer, Suhm et al. 2013). Lateral compression injuries to the pelvis are rarely associated with vascular injuries (Schmitt, Zürich et al. 2014). Injuries to specimens 14089 and 14090 were relatively stable, and required substantial dissection and manipulation to detect. No sharp bone edges were observed within the pelvis—there would likely be no vascular damage in these scenarios. Injury to specimen 14091 resulted in a more substantial fracture, which though overlaid with iliacus, was fairly close to the position of the external iliac artery; therefore, this injury may have resulted in vascular trauma. Iliac wing fractures represent <10% of all pelvis fractures, and are most commonly associated with comorbidity to the bowel and gluteal and iliac arteries (Abrassart, Stern et al. 2009). Therefore, the injuries observed for Specimen 14089 and 14090 were low-severity, but relevant fracture patterns, which may or may not have reached threshold for diagnosis, while the injury observed for Specimen 14091 was more substantial, and may have required surgical intervention.

One contrast in this study to previous reports is the dominance of single-location injuries. Pennal and colleagues (1980) hypothesized that pelvis injuries typically occur in clusters, i.e. an anterior-posterior or right-left injury cluster. This hypothesis was driven by understanding of arch mechanics—i.e. as tensile stress is generated along the concave surface of the arch, stress is also generated on the convex surface of the arch, displaced from the area of direct load application. This concept has driven description and understanding of the mechanisms responsible for pelvis injury, such as the Young and Burgess classification system (Burgess, Eastridge et al. 1990). Under similar loading configuration, but substantially higher energy[1], Beason et al. (2003), found similar injury locations to those in this study, but in right-left pairs (e.g. fracture of the right and left superior rami, along with additional fractures on the right (impacted) side). We observed only anterior or posterior pelvis injuries independently, and no left-side injuries. Contemporary reports find that single-location injuries are more common, and cite improvement in CT scan resolution, radionuclide bone scanning and diagnostic criteria for the change in rate (Guggenbuhl, Meadeb et al. 2005; Scheyerer, Osterhoff et al. 2012). Therefore, low-energy impacts to the pelvis, such as those resulting from a fall, may more frequently be associated with low-severity single-location injuries rather than traditional high-energy paired injury patterns.

We did not observe any damage to the proximal femur during any of our tests with this cohort. The fracture tolerance of the proximal femur under lateral loading simulating a fall has been reported to be as low as 2100 – 2500 N, on average (Lotz and Hayes 1990; Keyak 2000; Heini, Franz et al. 2004); 65% of our tests exceeded 2100 N, while 58% exceeded 2500 N. There are several possible explanations for this discrepancy. First is the orientation of the femur relative to the acetabulum (i.e. the loading boundary). In isolated femur testing, the femur is typically oriented laterally with a 30° inclination angle of the femoral neck, a fixed boundary at the greater trochanter, and the load applied to the head of the femur (or, conversely, a fixed boundary at the head of the femur and load application at the greater trochanter as in Manske et al. (2006)). In contrast, the head of the femur in this study was fixed only in the acetabulum by anatomical structures—this allowed the femur to rotate within the acetabulum. This limits the repeatability of the loading scenario (as evidenced by greater variability in the greater trochanter results), but may be a more biofidelic protocol. Second, the skeletal pelvis is a high-stiffness energy absorbing structure. Isolated testing of the femur restricts frontal plane deflection against a rigid boundary. Inclusion of the pelvis in the system introduces a low, but critical amount of deflection, resulting in transfer of energy (and injury) from the femur to the pelvis. In the loading protocol for this study, the femur was allowed to rotate freely, however the pelvis was firmly affixed within the containment structure. This contrast may

[1] In this study, we used an indenter mass of 38 kg, with a maximum impact velocity of 1.5 m/s, for an estimated kinetic energy of 419.4 J. Beason et al., used an indenter mass of 13.4 kg, with an impact velocity of 4.49 m/s, for an estimated kinetic energy of 1325.1 J.

have resulted in greater risk of fracture to the pelvis than the femur. Further work regarding faller characteristics and falling configuration during real-world events may help explain whether this discrepancy in mechanical testing results is representative of injury mechanisms, and what protocols might be employed in the future to improve biofidelity.

In the current state, this study has several limitations. First, the number of specimens included in this cohort was limited—an initial cohort of five was anticipated, however, one specimen was lost due to mould growth, and one specimen was excluded due to extreme bone fragility observed during the dissection process. However, the current analysis of this study will inform a future study with an additional nine specimens, a similar cohort size to other studies with similar goals and protocols (Beason, Dakin et al. 2003; Etheridge, Beason et al. 2005). In this study, we found the majority of strain, as evidenced by both deflection and injury results, was directed through the lateral portion of the iliac wing, and the pelvic ring, particularly around the region of the lateral apex of the pelvic ring. It may be worthwhile in future studies to evaluate motion of these anatomical semilandmarks in greater resolution. Additionally, in this study, we found a biphasic loading curve (discussed previously in Study 3) in 16 out of 33 impact trials, at impact velocities between 0.55-1 m/s. Visual analysis of the loading and deflection curves revealed that the biphasic transition point (Figure 6.11, dashed line, grey highlighted region) closely matched the deflection behavior of the wing of the ilium at L4 (grey line). While it is not necessarily intuitive that a decrease in deflection would be causatively linked to a decrease of force (without damage of the structure), further analysis of this phenomenon may reveal an anatomical or mechanical control for both features. While the rationale for this study focused on demonstrating how individual anatomical components contribute to stiffness of the pelvis system during a lateral impact (Study 2, Study 3), we were unable to characterize localized stiffness within this study. However, deflection is a major component of the force-deflection stiffness relationship, and reflects the load applied to the system. With the current methodology, we were only able to characterize a single loading vector for the entire system rather than determine localized loading and estimate anatomical component stiffness. However, it may be possible to estimate localized stiffness through structural or finite element modeling approaches.

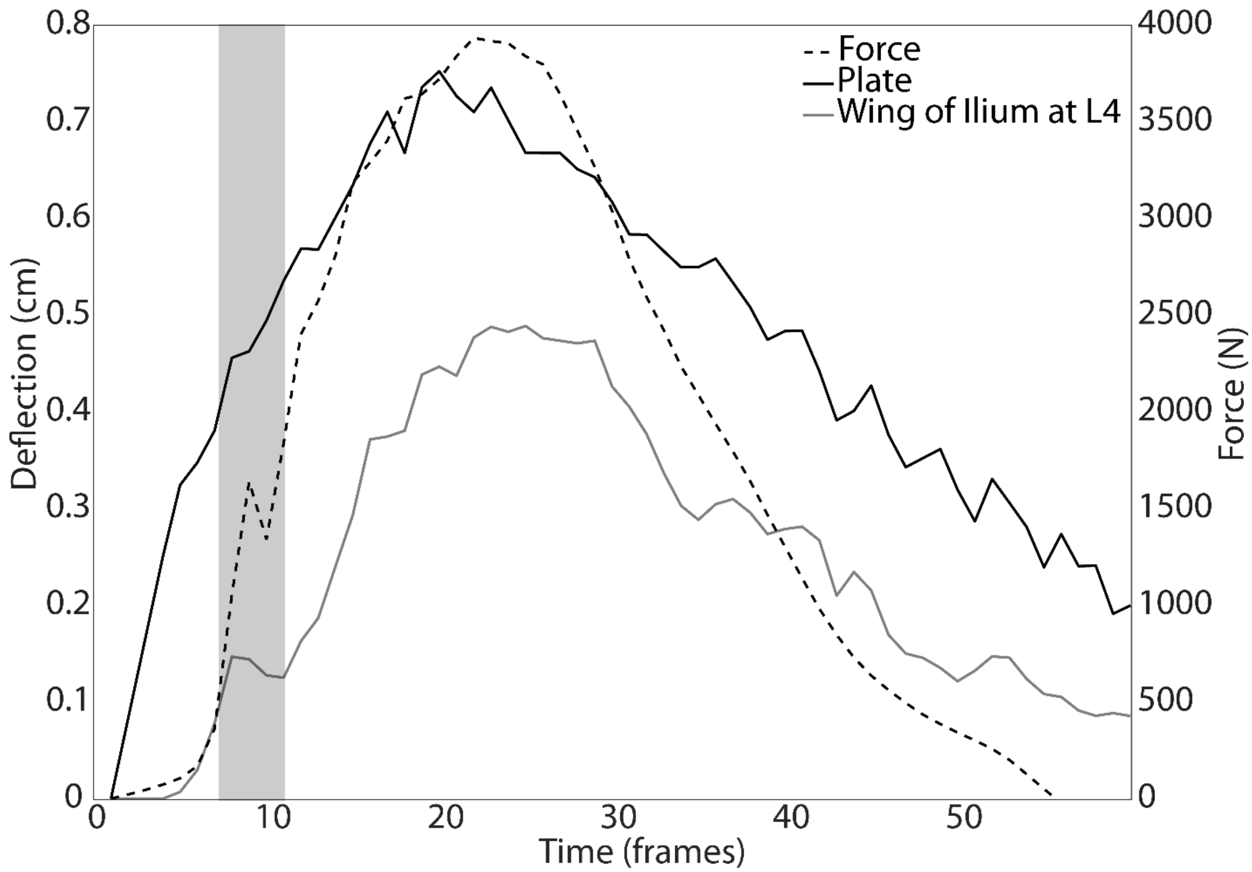

Figure 6.11 Demonstration of the biphasic loading behavior

A biphasic loading curve was observed for 16 out of 33 non-fracture trials. The biphasic transition point is highlighted in grey. For all of the trials with a biphasic loading curve, the transition point in the loading curve (black dashed line) corresponded with a momentary decrease in deflection in the wing of the ilium at L4 (grey solid line).

Further, in this study we were limited to including formaldehyde-embalmed specimens. Tissue fixation is a complex methodological consideration, particularly for impact testing. First, while use of fresh (<48 hour post mortem) tissue would likely produce more biofidelic results, this introduces the challenge of completing biosafety and familial consent, and eligibility screening, transportation, and dissection and preparation within the extremely short period between release of *rigor* mortis and tissue degradation. Second, frozen and thawed tissue is considered an inappropriate alternative for dynamic testing, primarily due to damage to the collagen structures, and redistribution or removal of water which affects the viscoelastic properties of the specimen (Maiden and Byard 2015). The freeze-thaw process is associated with collagen damage from ice lens formation (Szarko, Muldrew et al. 2010) or cross-linking of collagen fibres, resulting in increased strength and stiffness (Maiden and Byard 2015), along with substantial tissue dehydration. This corresponds with a variable direction of change in soft tissue stiffness, failure load, and energy to failure (Gottsauner- Wolf, Grabowski et al. 1995; Leitschuh, Doherty et al. 1996; Giannini, Buda et al. 2008; Venkatasubramanian, Wolkers et al. 2010; Maiden and Byard 2015). Effects of formaldehyde on cadaveric tissues are also mixed, however, the embalming process involves pressurized displacement of blood and interstitial fluid volume with embalming fluid. Wilke et al. (1996) showed an up to 80% decrease in specimen range of motion with formaldehyde fixation of calf spines compared to fresh specimens. Goh et al. (1989) demonstrated a decrease in energy absorption of 50% between embalmed and unembalmed cat long bones (femora and humeri). However, while Bourgouin and colleagues (2012) found an increase in stress at the end of the elastic region of the loading curve for embalmed vs. fresh intestine samples, they found no difference in strain or Young's Modulus. Additionally, the effects were most substantial for the outer (exposed) layers of tissue, and may be similar to the dehydration effect associated with thawed specimens. Topp et al. (2012) found no difference in stiffness, failure load between embalmed and fresh-frozen bone, and van Haaren et al. (2008) found no difference in torsion, bending stiffness, energy absorption or failure load between embalmed (>1 year) or fresh-frozen goat long bones. Effects of both freeze-thaw and embalming on dynamic characteristics are both likely influenced by the hydration levels of the tissue.

We attempted to maintain a consistent level of hydration throughout the protocol with moistening fluid, and the TAP was stored in moistening fluid when not positioned on the specimen, in order to minimize these effects on our rate-dependent timing outcomes (time to peak force, deflection delay). The use of embalmed specimens may limit the applicability of this study to predicting magnitude of pelvis deflection in actual falls, however, the relative deflection of each individual anatomical landmark is likely not affected by the embalming process. Total system deformation ranged from 2-13.7% in this study, which is similar to reported maximum pelvis deformation ranges of 8-32% in specimens with substantially greater trochanteric soft tissue thickness (Viano, Lau et al. 1989; Cavanaugh, Walilko et al. 1990; Matsui, Kajzer et al. 2003; Etheridge, Beason et al. 2005). We also found similar injury patterns to other studies with lateral pelvis and femur-pelvis impact loading protocols using fresh or fresh-frozen specimens (Viano, Lau et al. 1989; Cavanaugh, Walilko et al. 1990; Beason, Dakin et al. 2003; Matsui, Kajzer et al. 2003; Etheridge, Beason et al. 2005; Salzar, Genovese et al. 2009) and modeled simulations (Song, Trosseille et al. 2006; Majumder, Roychowdhury et al. 2007), suggesting that distribution of stress is not affected by the fixation process. Finally, there is a wealth of comparable literature which employed embalmed specimens reporting impact dynamics of the proximal femur and/or pelvis (e.g. Lochmüller, Groll et al., 2002; Manske, Liu-Ambrose et al. 2006; Pulkkinen, Jämsä et al. 2008; Gnat, Spoor et al. 2013), to which the results of this study may be compared more directly than had fresh tissue been employed.

Finally, the loading protocol employed in this study may not be representative of the majority of falling configurations. However, in this study, our goal was to understand the anatomical sources of deflection, linked to the directly lateral loading of the pelvis in Study 1, and models of pelvis impacts in Studies 2 and 3. Similar to Study 1, we found a strong link between trochanteric soft tissue and total system deflection, and were additionally able to demonstrate that the soft tissue may affect the distribution of loading within the pelvis as well as on the floor-pelvis interface. In Study 2, we found that trochanteric soft tissue was linked to model damping components, while in this study, we found that inclusion of TAP resulted in increased deflection delay for anatomical landmarks within the pelvis. While not directly a viscoelastic effect, this may contribute to the observed force-deflection behavior of the pelvis which can be characterized as viscoelastic (i.e. the mathematical model describing the anatomical effect and the mechanical effect are similar, even if the mechanical effect does not directly characterize the anatomical effect). Finally, Study 3, we found that the loading profile of the pelvis during a lateral impact included a biphasic feature which was not captured with the single-phase models we implemented. In this study, we were able to link that to motion of the ilium, which may help drive future research to explain the mechanisms controlling deflection of the pelvis under dynamic conditions. Finally, directly lateral loading of the pelvis has been a classical primary mode of force application for fall-related hip fractures (Robinovitch, Hayes et al. 1991). However, this study, as well as others with similar experimental and modeled lateral loading protocols (Viano, Lau et al. 1989; Beason, Dakin et al. 2003; Etheridge, Beason et al. 2005; Song, Trosseille et al. 2006; Majumder, Roychowdhury et al. 2007) have found no hip fractures with this loading mechanism, only injuries to the pelvis, despite applied loads above the fracture threshold of the proximal femur (Lotz and Hayes 1990; Keyak 2000; Heini, Franz et al. 2004). This lends support to the theory of the pelvis as an "energy absorbing" structure during a lateral impact, i.e. that when the femur is loaded laterally through the greater trochanter, the load is redistributed to the pelvis, which deflects, allowing greater total force to be sustained by the pelvis-femur system rather than the proximal femur alone. Future studies which aim to simulate loading protocols with greater biofidelity and potential for hip fracture rather than pelvis injury should include a posterolateral loading protocol. This loading direction is associated with greater impact velocity (Nankaku, Kanzaki et al. 2005) and peak pressure (Choi, Hoffer et al. 2010) *in vivo*, as well as reduced load tolerance (Pinilla, Boardman et al. 1996), and may be more likely to result in hip rather than pelvis fracture.

In this study, we aimed to describe frontal plane deflection of key anatomical landmarks, as well as describe how motion of these landmarks changed when the trochanteric adipose pad was placed *in situ* compared to an unpadded condition. As evidenced by injury patterns, we were able to recreate a biofidelic loading protocol. We found that the majority of deflection occurred at the anterior superior iliac spine (or lateral portion of the ilium). However, when the trochanteric adipose pad was included, more deflection was directed towards inferior structures, such as the lateral apex of the pelvic ring. Finally, we found that inclusion of the trochanteric adipose pad induced longer time to peak force, as well as a delay in deflection of pelvis (versus femur) landmarks, which likely has influenced on the loading impulse and energy absorption of these structures. These details regarding deflection of pelvic structures provide novel insight into loading pathways within the pelvis, as well as point towards anatomical regions to investigate in greater detail in a future study.

Chapter 7, Study 5: The Relationship Between Experimental Fall Simulation Protocol, Individual Body Composition and Impact Characteristics

Chapter seven is an in vivo *comparison of the impact characteristics of three simulated fall techniques, with the goal of investigating whether the relationships between individual body composition characteristics and impact characteristics reported in Study 1 hold across more complex impact configurations. The results of this study were presented, in part, at the 19th Biennial Meeting of the Canadian Society for Biomechanics, July 19-22, 2016, and the 40th Annual Meeting of the American Society of Biomechanics, August 2-5, 2016.*

7.1 Introduction

Impact configuration has been identified as a key determinant of injury risk (Cummings and Nevitt 1989), with characteristics such loading direction, distribution, and anatomical exposure to loading key to predicting how falling patterns influence injury mechanics. However, falls to the hip are more commonly simplified to a one-dimensional model, where the vertical elements are the primary components of interest (Robinovitch, Hayes et al. 1997; Dufour, Roberts et al. 2012; Sarvi and Luo 2015). In experimental falling studies simulating impacts to the hip (discussed in detail in Section 2.6.2), seventeen out of nineteen report only vertical impact force and velocity, and exclude shear components. However, real falls can rarely be simplified to this extent. In a study of falling and impact configurations of 50 older adults in a long-term care setting (Appendix 1), only 6% of fallers fell in a "straight down" direction, and only one of these involved a lateral impact configuration. Walking or standing and introducing motion (reaching, turning or initiating walking) are all common activities preceding falls (Robinovitch, Feldman et al. 2013; Choi, Wakeling et al. 2015) which would introduce rotational and translational motion to the impact configuration. However, even in studies which include fall-simulation protocols with other-than-vertical components (e.g. the inverted pendulum of tether release and voluntary falls from kneeling height), few have included non-vertical impact characteristics.

Additionally there have been documented differences in injury patterns between BMI groups (Armstrong, Spencer et al. 2011; Compston, Watts et al. 2011; Armstrong, Cairns et al. 2012; Madigan, Rosenblatt et al. 2014), and 37.1% of older adult men, and 33.6% of women over 65 have a BMI greater than 30 kg/m^2 (Flegal, Carroll et al. 2010). Yet only three fall simulation studies (Choi, Hoffer et al. 2010; Bhan, Levine et al. 2013; Levine, Bhan et al. 2013) include participants with body composition outside a “normal” range (i.e. outside a BMI range of 22-28 kg/m^2). Three fall simulation studies (Groen, Weerdesteyn et al. 2007; Groen, Weerdesteyn et al. 2008; Weerdesteyn, Groen et al. 2008) used to support injury-avoidance falling training (Smulders, Weerdesteyn et al. 2010) include young, healthy martial arts practitioners who have been trained in, and regularly utilize protective measures to reduce injury during a fall. Therefore, participants currently studied may not represent the older adult population at greatest risk for injury.

Finally, it is unclear how falling configuration and body composition interact to affect load direction and distribution during simulated falls. Increased trochanteric soft tissues may reduce normalized peak forces (Levine, Bhan et al. 2013), along with pressure localized at the “danger zone”, directly over the proximal femur (Choi, Hoffer et al. 2010). However, high soft tissue thickness is tied to an increase in mass, which is linked to greater absolute peak forces (Levine, Bhan et al. 2013). This effect may be amplified in falling configurations where the torso is oriented more directly over the hip. In contrast, falling configurations where the distal thigh or abdomen are in contact with the ground may reduce pressure in the hip region—but especially in fallers with enough soft tissue to substantially increase contact area.

Therefore, the overall goal of this study was to investigate the potential influence of falling configuration and body composition on impact dynamics during a lateral fall. We hypothesized (1) different fall simulation protocols (FSPs) would produce different impact dynamics profiles (vertical force, shear force, peak pressure and contact area) at the hip. In greater detail, we expected

(a) Peak vertical forces would be similar between protocols.

(b) Shear forces would be greater for the kneeling and squat release than pelvis release.

(c) Contact area would be similar between protocols.

(d) Peak pressure would be lower during pelvis and squat release (protocols with greater hip flexion) than kneeling release.

Further, we expected, (2) Impact dynamics will differ between participants of differing TSTT groups. To expand, contact area will be higher, and peak pressure will be lower in high-TSTT participants, demonstrating the force distribution effect of soft tissue, while shear and vertical forces will be lower in high-TSTT fallers, demonstrating the force attenuation effect of soft tissue.

7.2 Methods

Forty-four healthy participants (<35 years, 23 female) consented to participate in this study (Table 1). Participant recruitment focused on developing a cohort with a wide variety of body composition. Exclusion criteria included musculoskeletal injury in the past year preventing completion of the protocol, lifetime fracture history, fear of falling, or other health conditions which would make participation unsafe. Transverse-plane TSTT was assessed via ultrasound (minimum precision 0.17 cm; C60x, 2-5 MHz transducer, M-Turbo Ultrasound, SonoSite, Inc., Bothell, WA) in a side-lying position, similar to that expected during the impact phase of the fall simulations. Participants were grouped into low-, mid- and high-STT groups based the following criteria: males low <3 cm, mid 3.1-4 cm, high >4.1 cm; females low <3.5, mid 3.6-5, high >5 cm. These thresholds represent low- (<18.5 kg/m^2), moderate (18.6-25 kg/m^2) and high- (>25.1 kg/m^2) BMI older adults (unpublished data).

Table 7.1: Mean (SD) participant anthropometric characteristics.

		N	Height (m)	Mass (kg)	BMI (kg/m^2)	TSTT (cm)
Females						
	Low	7	1.62 (0.04)	54.0 (6.1)	20.4 (1.7)	3.0 (0.4)
STT	Mid	9	1.66 (0.06)	64.6 (10.3)	23.2 (2.8)	4.3 (0.4)
	High	7	1.66 (0.07)	85.8 (20.6)	31.5 (7.9)	6.9 (2.0)
Males						
	Low	8	1.80 (0.07)	72.5 (11.5)	22.4 (2.3)	2.3 (0.5)
STT	Mid	7	1.79 (0.08)	83.4 (10.9)	26.1 (3.2)	3.5 (0.5)
	High	6	1.77 (0.08)	92.1 (9.7)	28.7 (2.9)	4.9 (0.3)

TSTT represents trochanteric soft tissue thickness. BMI represents body mass index

7.2.1 Experimental Protocol

Each participant completed eighteen fall simulation trials, consisting of six blocks of trials, each block consisting of one Pelvis Release, one Kneeling Release and one Squat Release protocol (Figure 1), in randomized order. Blocks 1-3 were “training trials”, allowing for participant adaptation to the protocol; Blocks 4-6 were used for characterizing biomechanical outcomes. All protocols involved the lateral aspect of the left hip impacting a pressure plate (4096 resistive sensors, each 0.762 by 0.508 cm, 500 Hz; FootScan, RSScan, Olen, Belgium) overlying a force plate (3500 Hz; OR6-7, AMTI, USA). The force and pressure plates were spatially aligned and temporally synchronized using a motion capture system (Optotrak Certus, Northern Digital, Inc., Waterloo, ON).

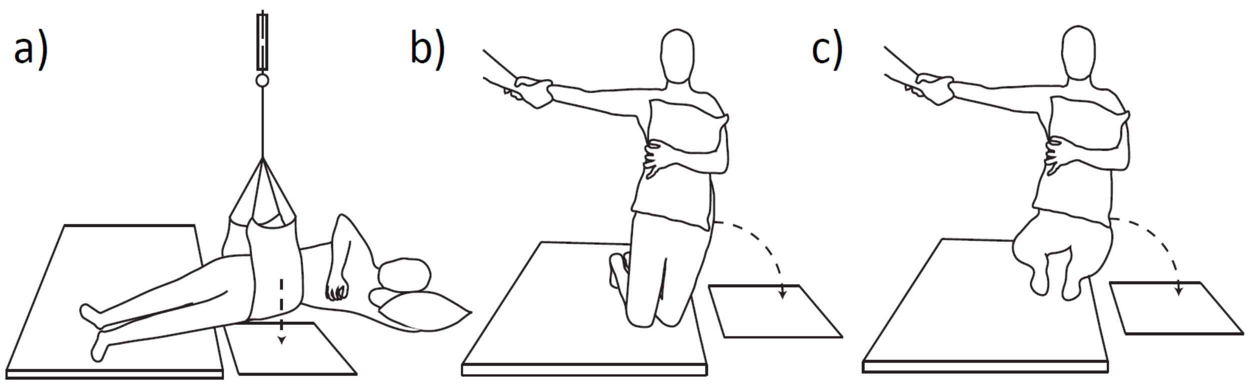

Figure 7.1 Initial position and motion path of the Pelvis (a), Kneeling (b), and Squat Release (c).

The protocols were selected as they represent different fall scenarios observed in older adults (Kangas 2011; Kangas, Vikman et al. 2012; Robinovitch, Feldman et al. 2013; Choi, Wakeling et al. 2015), and primarily involve differing motion paths of the pelvis. A controlled, vertical motion is produced during Pelvis Release, while Kneeling Release produces vertical and lateral motion in an inverted pendulum path (Groen, Weerdesteyn et al. 2007; Groen, Weerdesteyn et al. 2008; Weerdesteyn, Groen et al. 2008; Van der Zijden, Groen et al. 2012), and Squat Release typically has more lateral than vertical motion. For the Pelvis Release, the upper body of the participant was supported by a pillow outside the contact area of the force plate. For the Kneeling Release and Squat Release, the participant held a pillow throughout the trial to prevent bracing with their arms during the impact. The Pelvis Release protocol is highly controlled, and represents a scenario where the faller rotates into a horizontal position before impacting the hip directly laterally (Robinovitch, Hayes et al. 1991; Robinovitch, Hayes et al. 1997; Choi, Hoffer et al. 2010; Laing and Robinovitch 2010; Bhan, Levine et al. 2013; Levine, Bhan et al. 2013). The Kneeling Release reflects a scenario where the faller impacts the knee prior to rotating to impact the hip (Sabick, Hay et al. 1999; Groen, Weerdesteyn et al. 2007; Groen, Weerdesteyn et al. 2008; Weerdesteyn, Groen et al. 2008; Van der Zijden, Groen et al. 2012). The Squat Release is a novel protocol which reflects a scenario where the faller flexes the knee, hip and ankle during the descent phase prior to rotating laterally to impact the hip. Greater kinematic details for all three protocols are presented in Appendix 4.

In greater detail, for the initial position for Pelvis Release, hips were flexed to 45°, knees were flexed to 90°, and the pelvis was raised in a thin nylon sling using a turnbuckle until the soft tissues overlying the hip were 5 cm above the pressure plate. The participant was instructed to reduce the muscle tension in their body; when the participant reported that they were "relaxed and ready", the electromagnet supporting the sling was released, allowing the pelvis of the participant to impact the pressure plate. For Kneeling and Squat Release, the participant was supported in the initial position by the researcher, was instructed to lean until their weight was supported by their left side, self-release, and fall "like a pendulum". For Kneeling Release, the initial position was hips were flexed to 0°, knees were flexed to 90° and the lower leg was in contact with the starting mat. For Squat Release the initial position was a heel-lifted Squat, with maximal thigh-calf contact and an upright torso. A minimum of one minute of rest was provided between each trial, during which the participant was asked to stand or kneel without contact between the ground and trochanteric or gluteal soft tissues. A two-dimensional video camera sampling at 30 frames per second (EXILIM High Speed, Model EX-FC100, Casio Computer Co., Tokyo, Japan) was used to collect qualitative data for each trial. Detailed comparisons of the kinematics of each fall simulation protocol are presented in Appendix 4.

7.2.2 Signal Processing and Data Reduction

We used a customized MATLAB routine (MathWorks, Natick, MA) to process the time-varying signals. Briefly, the filtering of impact data and methods of selection of cut-off frequencies have been the subject of debate. Impact events occur rapidly--in the case of this data set, a time-to-peak-force of 0.02-0.09 s would be expected (Robinovitch, Hayes et al. 1997; Laing and Robinovitch 2010; Levine, Bhan et al. 2013), with a corresponding natural frequency of 30-160 Hz (Levine, Bhan et al. 2013) . It is challenging, therefore, to select an appropriate low-pass cut-off frequency which is appropriate across participants (i.e. does not over-smooth the impact event for some participants, reducing the impact peak) and impacts, yet also appropriately filters out environmental noise within the same frequency range such as electrical, building vibration and jackhammer noise To conserve peak force values, we therefore did not filter force prior to determining the peak force value.

An automated point-selection routine was developed to determine key data coordinates for further analysis. Each trial was segregated by defining an initial unloaded phase ($F_{initial\_vertical}$, $F_{initial\_shear}$), the beginning of impact (when force exceeds two standard deviations of the mean in the unloaded region preceding impact, T_{imp}, F_{imp}) and peak force (T_{max}, $F_{vertical}$). All following peak variables were calculated at T_{max}, the timepoint of maximum vertical force. F_{shear} was calculated as the resultant of the two shear vectors in the plane of the impact surface at T_{max}. Bias ($F_{initial\_vertical}$, $F_{initial\_shear}$) was subtracted from $F_{vertical}$ and F_{shear}. The contact profile (*CP*) associated with T_{max} was further processed: first, peak pressure magnitude (P_{peak}, $P_{peak\_location}$) was determined as the sensel with the greatest magnitude within the *CP*. Second, the *CP* was converted to a binary matrix, and an iterative algorithm was used to include active sensels within a three-sensel radius of sensels concurrent with $P_{peak\_location}$. The final *CP* was used to mask distal and proximal body segment contacts to determine Contact Area (*CA*).

7.2.3 Statistical Analysis

All statistical analysis was performed using a software package (SPSS version 21, Chicago, USA) using an α of 0.05. A sample of 45 participants was required for the ANOVA procedures (α=0.05, β=0.95, d=0.54, G*Power version 3.1.9.2, Universität Düsseldorf, Düsseldorf, Germany). Both hypotheses were tested using two factor (FSP, TSTT-group) mixed-model ANOVA for each impact dynamics outcome ($F_{vertical}$, F_{shear}, P_{peak}, *CA*). FSP was treated as a repeated measure, and TSTT-group as a between-subjects factor. When Mauchly's test indicated violations of sphericity for repeated measures, a Greenhouse-Geisser adjustment was employed. Pairwise comparisons using a Bonferroni correction were employed when significant main effects of FSP or TSTT-group were observed. Independent and dependent variables were normally distributed for outcomes in this study.

7.3 Results

Vertical forces ranged from 447-3625 N. $F_{vertical}$ was associated with a significant main effect of FSP but not TSTT, and no significant interaction between FSP and TSTT was observed (Table 7.2, Figure 7.3). Pairwise comparisons indicated significantly lower peak forces during Pelvis Release (mean (SD) 1430 (326) N) compared to Kneeling Release (2114 (603) N) or Squat Release (2001 (702) N).

Shear forces ranged from 24-443 N, and were affected by a significant interaction between TSTT group and FSP , Figure 7.3). However, there was a clear main effect of FSP for all three TSTT groups. The Squat Release produced significantly higher shear forces (211 (98) N) than the other protocols (Pelvis Release, 115 (53) N; Kneeling Release 108 (55) N).

Peak pressure ranged from 307-9992 kPa, and was associated with a significant main effect of fall simulation protocol but not TSTT group (Table 7.2, Figure 7.5). There was no significant interaction between FSP and TSTT. Peak pressure was greater during Kneeling Release (1557 (991) kPa) than Pelvis Release (1212 (489) kPa), and greater during Squat Release (2690 (2474) kPa) than Kneeling Release or Pelvis Release.

Finally, contact area ranged from 24-364 cm^2. Significant main effects were observed for both TSTT group and FSP for CA, however, there was no interaction between the two factors (Table 7.2, Figure 7.4). Contact area was lower for low-TSTT fallers (116 (41) cm^2) than medium- (164 (57) cm^2) or high-TSTT (193 (62) cm^2) fallers, and lower during Pelvis Release (147 (61) cm^2) than Kneeling Release (159 (54) cm^2) or Squat Release (166 (45) cm^2.

Table 7.2 Summary of main effects, interactions, and significant pairwise comparisons

Dependent Variable	Factor	Significant Pairwise Differences	F	T	p
F_{max}	STT x FSP		0.9		0.498
	STT		36.4		<0.001**
	FSP		2.7		0.083
		Pelvis vs. Kneeling		-7.2	<0.001**
		Pelvis vs. Squat		-6.6	<0.001**
F_{shear}	STT x FSP		3.8		0.008**
	STT		6.3		0.004**
	FSP		39.7		<0.001**
		Squat vs. Pelvis		7.8	<0.001**
		Squat vs. Kneeling		7.0	<0.001**
P_{peak}	STT x FSP		0.9		0.464
	STT		1.2		0.318
	FSP		10.1		0.000**
		Kneeling vs. Pelvis		2.3	0.028*
		Squat vs. Kneeling		2.7	0.010*
		Squat vs. Pelvis		3.8	0.001**
CA	STT x FSP		2.3		0.065
	STT		9.0		0.001**
		Low vs. Medium		-2.7	0.010*
		Low vs. High		-4.2	<0.001**
	FSP		3.9		0.025*
		Pelvis vs. Kneeling		-3.5	0.001**
		Pelvis vs. Squat		-4.0	<0.001**

** Significant comparison at p<0.05 ** Significant comparison at p<0.01*

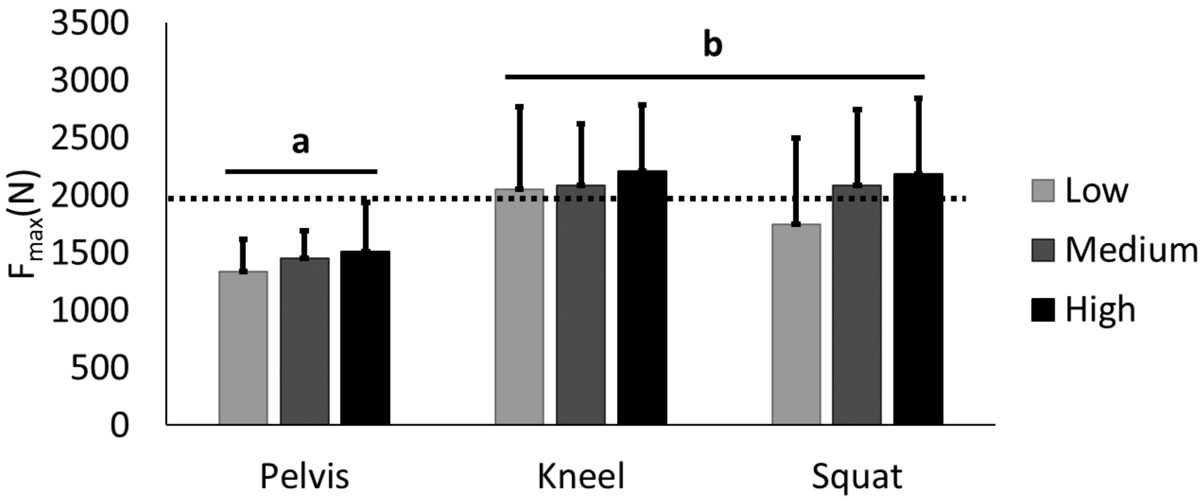

Figure 7.3 Main effect of fall simulation protocol on $\boldsymbol{F_{vertical}}$

Peak vertical forces were 32.3% lower for Pelvis Release (a) compared to Kneeling Release (b), and 28.5% lower compared to Squat Release (b). No main effects were observed for STT group and no STT-FSP interactions were observed. The average femur fracture tolerance for older adult women (Bouxsein, Coan et al. 1999) is plotted as a dashed line.

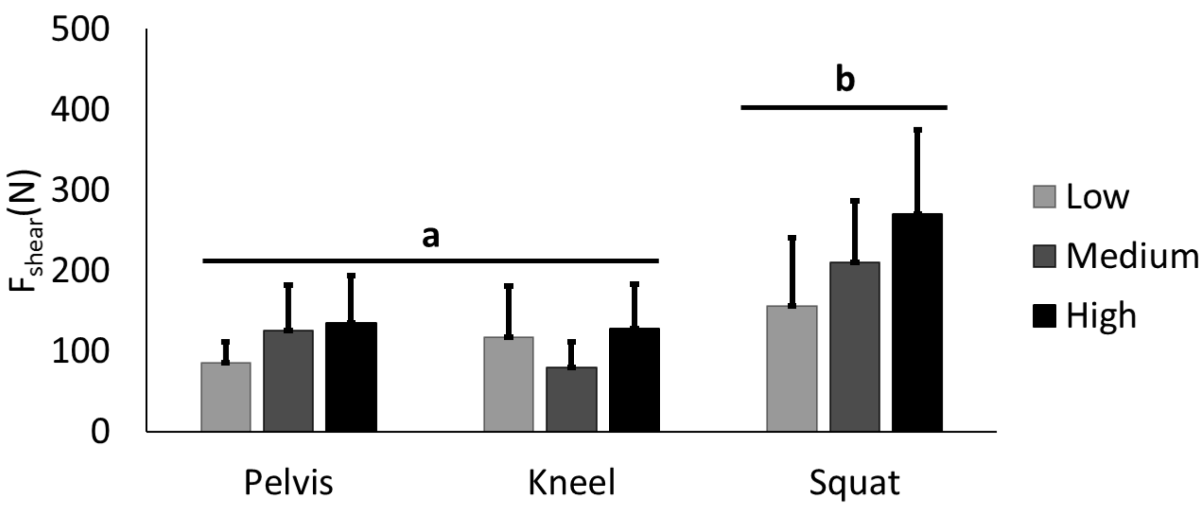

Figure 7.2 Interaction effect of STT group and fall simulation protocol on $\boldsymbol{F_{shear}}$

Peak shear forces were affected by a significant TSTT-FSP interaction, however there was a clear main effect of FSP, with Squat Release (b) producing significantly higher shear forces than Pelvis or Kneeling Release (a). There was a significant main effect of TSTT, however the effect was inconsistent between protocols.

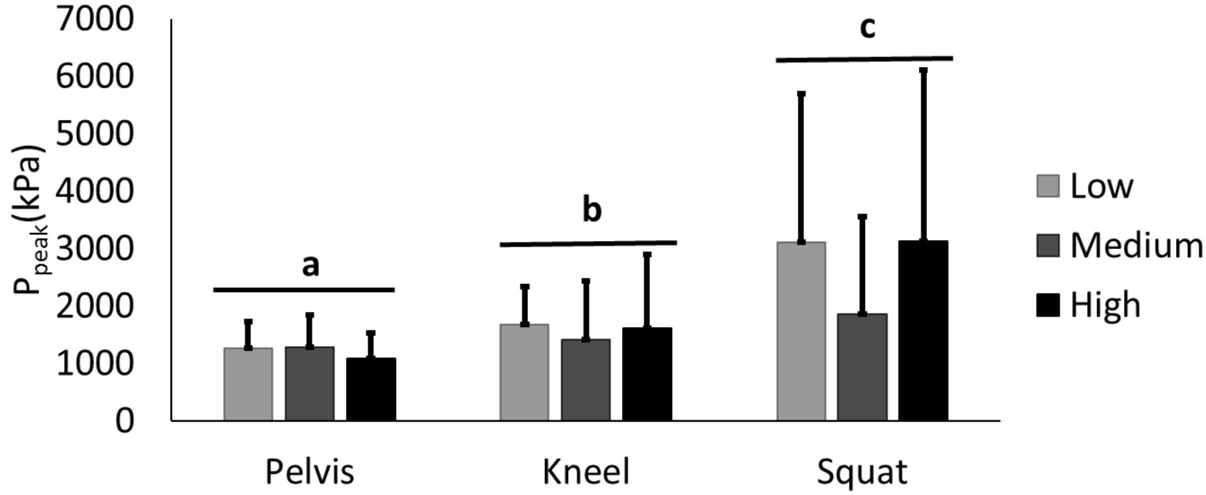

Figure 7.5 Main effect of fall simulation protocol on *P_{peak}*

Peak pressure was affected by a main effect of FSP, with no main effect of TSTT or TSTT-FSP interaction. Squat release was linked with the highest peak pressure (c), followed by Kneeling Release (b) and Pelvis Release (a)

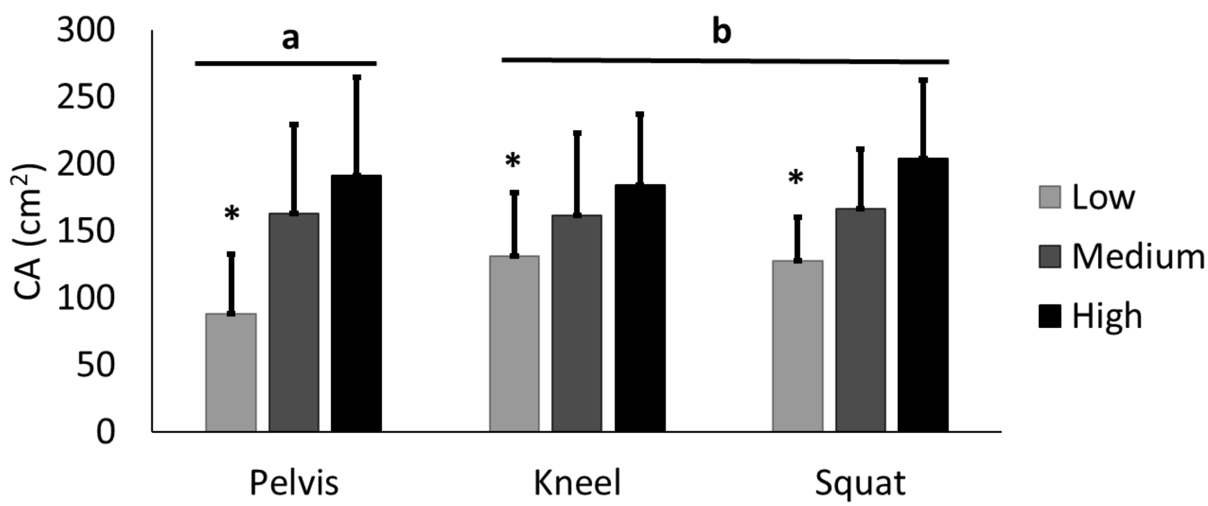

Figure 7.4 Main effects of TSTT group and fall simulation protocol on *CA*
CA was influenced by a significant main effect of both TSTT and FSP, however, there was no interaction between FSP and TSTT. CA was lower for low-TSTT participants (*) than medium- or high-TSTT participants, and lower during the Pelvis release (a) than Kneeling or Squat release (b)

7.4 Discussion

The goal of this study was to compare how impact dynamics were affected by falling configuration and TSTT. Regarding the first hypothesis, we found that falling configuration had a significant effect on vertical and shear force, peak pressure and contact area, with Kneeling Release producing the greatest vertical force, Squat Release producing the greatest shear force and pressure, and Pelvis Release producing the lowest contact area. Regarding the second hypothesis, soft tissue thickness also had a significant effect on contact area, with low-TSTT participants producing smaller contact profiles than medium- or high-TSTT fallers. Only one interaction was observed between TSTT group and fall simulation protocol—group differences in shear force were greatest during Squat Release, smaller during Pelvis Release and not significant during Kneeling Release. These results provide novel insights into how load magnitude and distribution is affected by both impact configuration and body composition.

The effects of FSP on impact dynamics we observed provide important insights into the effects of falling characteristics on hip fracture risk. We found a substantial effect of fall simulation

Figure 7.6 Backwards rotation during the Squat Release Protocol

Still frames from planar video during a Squat Release trial. The participant initiated the Squat Release protocol laterally, but rotated posterolaterally during the impact phase. Some participants began rotating posterolaterally shortly after trial initiation, while others began the rotation during the impact phase.

protocol on all four outcome variables. The greatest differences were found for P_{peak} and F_{shear}, with Squat Release producing 70-120% greater peak pressure and 84-96% greater shear forces than the other protocols. Both of these factors are significant contributions to understanding the variability in injury risk within otherwise homogenous groups of fallers. In the simplest estimation, pressure is the ratio of vertical force to contact area. However, the increase in P_{peak} for Squat Release exceeded what would be predicted based on $F_{vertical}$ and CA. Visual analysis of videos of each trial revealed that most participants rotated backwards during the Squat Release protocol (Figure 7.6). Posterolateral impact configurations have previously been linked with greater peak pressure, particularly for fallers with low BMI (Choi, Hoffer et al. 2010). The estimate of P_{peak} was also substantially localized (i.e. the contact area of one sensel vs. a contact area with a radius of 1.25 cm (Laing and Robinovitch 2008; Choi, Hoffer et al. 2010)—it is currently unknown what characterization of P_{peak} (i.e. in what anatomical regions, and how localized) is related to injury risk. Second, F_{shear} nearly doubled for Squat Release compared to Pelvis or Kneeling Release. This is likely linked to impact velocity in the shear direction (lower for Pelvis Release, Appendix 4). Additionally, during the Squat Release protocol, participants have active control over the ankle, knee and hip, while the foot remains in contact with the starting mat—extension of these joints against friction during the impact phase contributes to greater shear force. Overall, these shear forces were low—8.0, 5.1 and 10.5% of vertical forces during Pelvis, Kneel and Squat release, respectively. However, shear forces influence the direction of loading, which has a substantial effect on fracture risk. A change in load vector direction from directly vertical through the femoral neck to 20° inferior decreases load tolerance of the proximal femur by approximately 5%, while the same degree of deviation in the posterior direction decreases load tolerance by nearly a third (Keyak, Skinner et al. 2006). In this study, shear angles were directed 19 (53)° more posteriorly during kneeling release and 11.0 (41.0)° more anteriorly during squat release than pelvis release, however, this metric was sensitive to variance and calculated only in the global coordinate system relative to the point of peak pressure (i.e. not within the local coordinate system of the femur). In sum, the effects of impact configuration on local loading at the hip and shear force likely have a substantial consequence for injury risk.

Differences in peak vertical force and contact area between protocols were less drastic—29-32% lower $F_{vertical}$, and 7-11% lower CA for Pelvis Release than Squat Release or Kneeling Release. Similar impact velocity between protocols (Appendix 4) is likely a driving factor for smaller differences in vertical force between protocols. Impact configuration is a consideration for both $F_{vertical}$ and *CA*. These differences are likely due to the contribution of the head, arms and torso to effective mass (Appendix 4; van den Kroonenberg, Hayes et al. 1996; Sarvi Luo et al. 2014). Load sharing between the pelvis and distal structures during the Pelvis Release protocol has been reported as approximately 15% (Robinovitch, Hayes et al. 1997), however, when the Pelvis Release is performed with an upright torso position, forces at the hip increase by an average 36% due to the contribution of the head, arms and torso to the effective mass of the pelvis (Robinovitch, Hayes et al. 1997). While hip orientation angle is associated with a change in apparent TSTT directly over the greater trochanter (Levine, Minty et al. 2015), radial displacement of soft tissue away from the location of peak pressure appears to be more dependent on quantity of TSTT rather than configuration at impact. Volume of trochanteric soft tissue is likely similar between impact configurations.

We observed varying strength of effects of TSTT for F_{max} and $F_{shear.}$ we did not observe a main effect of TSTT group on $F_{vertical}$, despite having previously found a strong effect of BMI on vertical force during the pelvis release protocol (Study 1; Levine, Bhan et al. 2013). Within the TSTT groups, there were participants of varying BMI and mass (e.g. within the high-TSTT females, there was one member with a BMI of 24.1 and mass of 64 kg, closer to the means of the medium-TSTT females; within the low-TSTT males, there was a member with a BMI of 25.1 and mass of 81 kg, closer to the means of the medium-TSTT males). It may be more valuable to compare normalized (to effective mass) peak force, or energy absorption between groups to quantify the force attenuation between groups. Similarly, while TSTT had a significant effect on F_{shear}, the effect was inconsistent between protocols. There may be factors related to the energy of the impact which may be important links with shear forces during a fall. In addition to effective mass, taller fallers may have greater initial pelvis height during Kneeling release, whereas the initial height during Pelvis release is fixed, and the initial height during Squat release is dependent on squat depth. Other factors of participant control (hesitation, strength, power, adaptation) may affect shear forces moreso than vertical forces, which are driven more by effective mass and initial vertical pelvis height.

Differences *in CA* were greater for low- compared to medium- and high-TSTT participants, suggesting there may be ceiling effect for improvement in load distribution. In comparison to Study 1, we observed a similar increase in *CA* with increase in TSTT; however, no participant in the previous study had STT greater than 7 cm, and no participant had *CA* greater than 250 cm^2, similar to the ceiling observed in this study. While trochanteric soft tissues may contact surrounding the area, the force at these distal regions may be below the threshold of detection for the RSScan plate. Laing et al (Laing and Robinovitch 2008) found that <30% of total hip impact force is distributed beyond a radius of 5 cm from the greater trochanter, while Choi and colleagues (Choi, Hoffer et al. 2010) reported that less than 9% of force is distributed to a radius of 20 cm in fallers with high BMI (>25 kg/m^2), while less than 2% of force is distributed to this radius in fallers with low BMI (<25 kg/m^2). Load distribution may be limited by skeletal pelvis size (both as the more rigid component of the pelvis system, as well as the container for the mass concentration of organs), which is less variable between participants. In this study, male participants had a mean (SD) pelvis depth (anterior superior iliac spine to posterior superior iliac spine) of 13.6 (2.2) cm and pelvis height (iliac crest to greater trochanter) of 15.8 (7.7) cm, and female participants had pelvis depth of 13.3 (1.4) and pelvis height of 13.4 (4.2), for an average skeletally-driven contact area of approximately 200 cm^2.(80% of the 250 cm^2 ceiling). This may add to the explanation of the limited effect of fat tissue on force attenuation (Study 1), as well as the limited difference in normalized peak forces between females of differing BMI groups (Levine, Bhan et al. 2013).

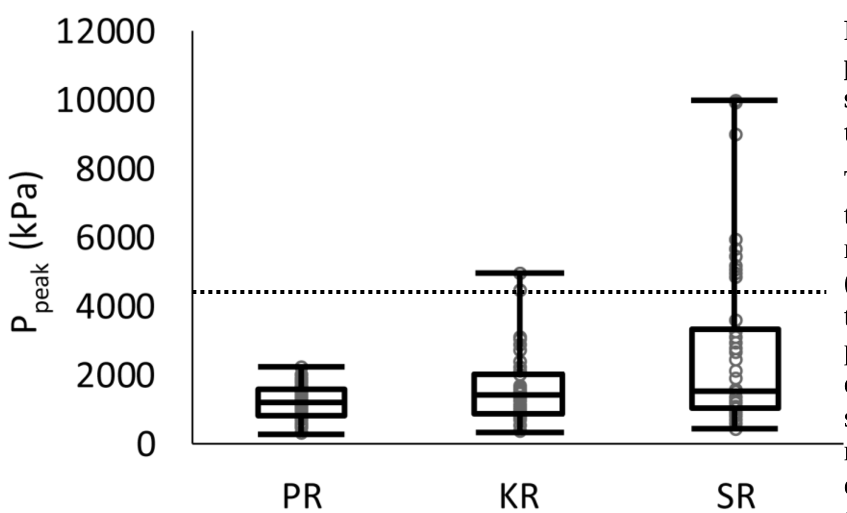

Figure 7.7 Box and whisker plot demonstrating the separation of the outlying trial means

The first quartile, median and third quartile (box) and minimum and maximum (whisker) are ploted along with the trial means for each participant (grey circle), demonstrating separation of some trial means from the narrow quartile bands. The dashed line indicates a threshold of 4461 kPa.

Additionally, while P_{peak} during Pelvis Release was similar to that previously reported (Choi, Hoffer et al. 2010), P_{peak} did not differ between our TSTT groups, in contrast to a 266% increase in P_{peak} for participants with low BMI compared to participants with high BMI reported by Choi et al. The combined effect of mass and TSTT associated with BMI may have a greater effect on load distribution than TSTT alone. This is confirmed in our data – when categorized by BMI (in low-, medium- and high- BMI groups as in Levine, et al., 2013), we found significant main effects of BMI for $F_{vertical}$ ($F_{(2,29)}$=9.1, p=0.001), F_{shear} ($F_{(2,29)}$=7.8, p=0.001), and CA ($F_{(2,29)}$=8.2, p=0.001). However, the relationship between BMI and P_{peak} ($F_{(2,29)}$=0.8, p=0.445) was still more complex. Post hoc analysis of the distribution for P_{peak} revealed that, while 90% of mean FSP outcomes had P_{peak} below 4461 kPa, ten Squat Release trial means and two Kneeling Release trial means had P_{peak} values exceeding this boundary. P_{peak} was consistent between the trials comprising each mean. When these outliers were removed, P_{peak} was 55.4% higher for participants with low BMI compared to participants with high BMI (t(31)=2.2, p=0.038), however, the same effect was not seen between low- and high-STT participants even when outliers were removed ($F_{(2,26)}$=2.1, p=0.141). This is in contrast to Study 1, where we found that peak pressure during the Pelvis Release protocol was significantly correlated with TSTT (r^2=0.598, p=0.002) for female participants. However, participants in Study 1 were, on average, 2 cm taller, and had less soft tissue (as demonstrated above with differences in contact area). Therefore, faller characteristics not captured in the current study, such as skeletal anatomy[2], may interact with TSTT to influence impact characteristics than soft tissue thickness; this represents an avenue for future exploration.

Regarding implications for hip fracture risk, the results of this study indicate that falling configuration may have a more substantial effect on the applied loads component of injury risk than soft tissue thickness. In particular, the falling configuration associated with Squat Release may present a high-risk scenario in terms of localized force and loading direction. Posterolateral falls, similar to those simulated by the Squat Release, are associated with greater peak pressure (Choi, Hoffer et al. 2010) and higher impact velocity (Nankaku, Kanzaki et al. 2005). Further work should quantify what interactions of anatomy, faller behavior and impact mechanics are responsible for the

[2] Secondary analysis found a significant effect of relative femur length (i.e. femur length divided by total height, t(44)=2.7, p=0.011) and with participants in the outlier group having longer femurs, as well as longer femurs relative to pelvis width (t(44)=2.7, p=0.010). These factors may potentially be linked with other risk factors for hip fracture, such as hip axis length.

increase in P_{peak} for this falling scenario. However, TSTT also had a substantial effect on *CA* and a small, but significant interaction effect with falling configuration for F_{shear}. Additionally, we found significant main effects of BMI group for all four outcome variables. Transverse plane measurement may not be the most relevant characterization of TSTT to predict impact characteristics at the hip--three-dimensional characterization of trochanteric soft tissue, or separate characterization of lean and adipose tissue may more effectively highlight group differences.

This study has several limitations. In this study, we constrained participants from using their arms to brace during the fall simulations to control the effects of load distribution to distal body segments in order to provide a better comparison between protocols. However, in a real falling scenario, hand or arm contact with the ground previous to, or simultaneous with, hip contact would distribute loads away from the hip for impact configurations consistent with the Kneeling and Squat Releases. However, the timing of these impacts is variable (Choi, Wakeling et al. 2015), and bracing is a less effective strategy for older adults compared to younger adults due to reaction time and power generation (Sran, Stotz et al. 2010). Second, we included only young, healthy adults. Age-related changes in trochanteric soft tissue characteristics (Choi, Russell et al. 2014) and control of the descent phase of the fall may have an effect on the magnitude of differences for the outcomes in this study. We did not include electromyography in this study due to technical challenges with electrode cables during the fall simulation, therefore we are unable to determine whether activation of the musculature

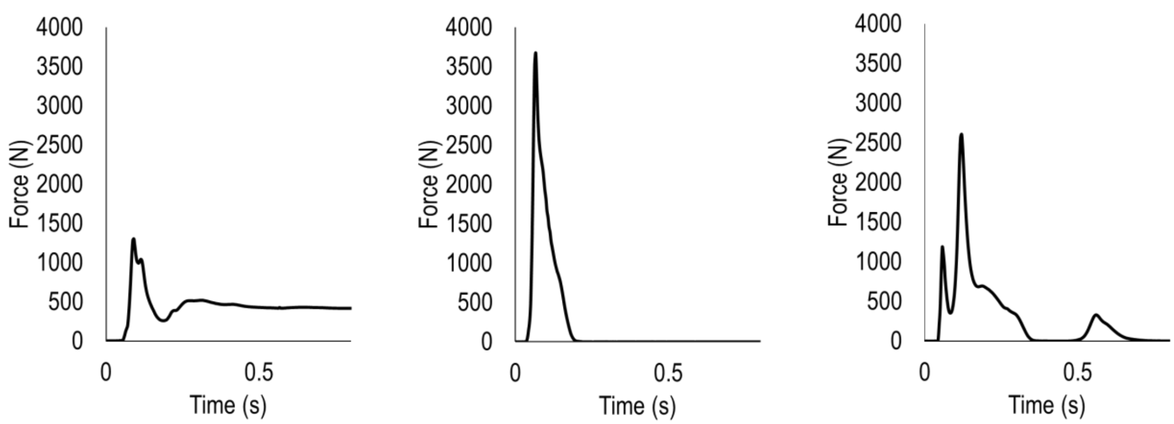

Figure 7.8 Demonstration of time-varying loading response during a Pelvis (a), Kneeling (b) and Squat Release (c)

In this study, we focused on the impact characteristics at peak force. However, a overview of the time-varying nature of the protocols demonstrates potential for future investigations focusing on differences in loading impulse and loading waveform.

around the hips differed between protocols or participants. In a recent study, Pretty and colleagues (2017) found that during a pelvis release protocol, peak force and contact area increased during a "muscle-contracted" protocol vs. a relaxed protocol, however the differences were less than 20%. Future investigations may provide insight into whether muscle activation strategies differ between protocols, and what effects these may have, in combination with impact configuration, on impact dynamics. Finally, in this study we only investigated outcomes at the time of peak vertical force. However, each protocol also has time-varying characteristics (Figure 7.8) in the domains investigated in this study (force, contact area, pressure) as well as kinematic differences that likely influence magnitude and distribution of loading during the protocols. Key elements to focus on in future studies include the loading impulse and consistency of the loading waveform, which may give insight into participant strategies during the protocols.

To summarize, we found that impact characteristics during a simulated fall to the hip were strongly affected by fall simulation method. However, these outcomes were also influenced to a smaller extent by participant soft tissue thickness. Future work should characterize the contribution of faller behavior, such as muscle activation or bracing, skeletal anatomy, and peak pressure location to injury risk.

Chapter 8 Thesis Synthesis and Conclusions

8.1 How do individual body size or body composition characteristics relate to impact dynamics during a lateral fall?

The primary goal of this thesis was to link individual faller characteristics, such as sex, body size and body composition, with impact dynamics during a lateral fall on the hip. In Study 1 (Figure 8.1) we found strong links between overall body size and peak force during a simulated lateral fall. We also found that distribution of those loads was affected by the adiposity of the faller, and that local body size and composition characteristics had stronger relationships to peak force than global characteristics. Trochanteric soft tissue thickness was strongly linked to peak pressure, contact area and deflection. In Study 4, we found that inclusion of trochanteric soft tissue vs. musculoskeletal components only, changed load distribution within the pelvis, as well. However, in Study 5, we found no link between TSTT and pressure. Participant TSTT-peak pressure relationships for both studies are

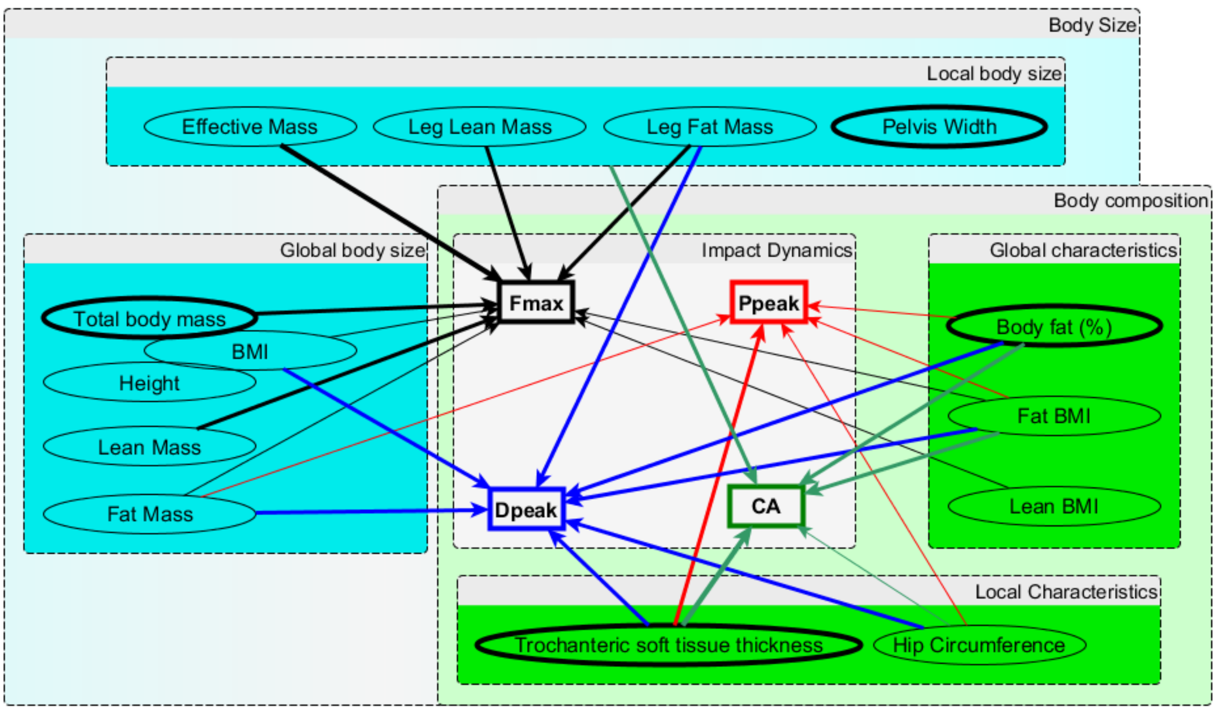

Figure 8.1 Relationship between individual characteristics and impact dynamics

In Study 1, we found that overall body size, particularly body mass, and localized mass at the pelvis and leg were related to peak force. Indices of adiposity, particularly body fat and TSTT were strongly linked to load distribution and deflection. Bolded lines represent significant relationships at p<0.01, while solid lines indicate significant relationships at p<0.05. Bolded individual characteristics (ovals) were incorporated into final models in Study 2 and Study 3.

displayed in Figure 8.2. Out of 59 participants between both studies, 44 fit into the linear model relating TSTT to peak pressure, which explains 59.8% of the variance in peak pressure. The remaining 15 participants, all members of Study 5, are highlighted in grey—these participants spanned both sexes, and all TSTT groups. It is unclear from the current studies why these participants do not fit into the main model, however, we hypothesized that this may be related to underlying skeletal structures previously identified as predictors of hip fracture, such as hip axis length (Broy, Cauley et al. 2015). Further, in Study 1 we found that total pelvis deflection was less than 50% of TSTT, and across studies 1, 4 and 5, we found no link between TSTT and peak force. In contrast, TSTT was strongly linked to contact area in both Study 1 and 5, the shape of force distribution (Appendix 2), and damping characteristics in Study 2. In the studies in this thesis, we included only a linear measure of TSTT; given the clear link between the trochanteric soft tissues and load distribution (i.e. a three-dimensional behavior vs. a one-dimensional force attenuation), a more dimensional assessment of the volume of trochanteric soft tissue may be warranted.

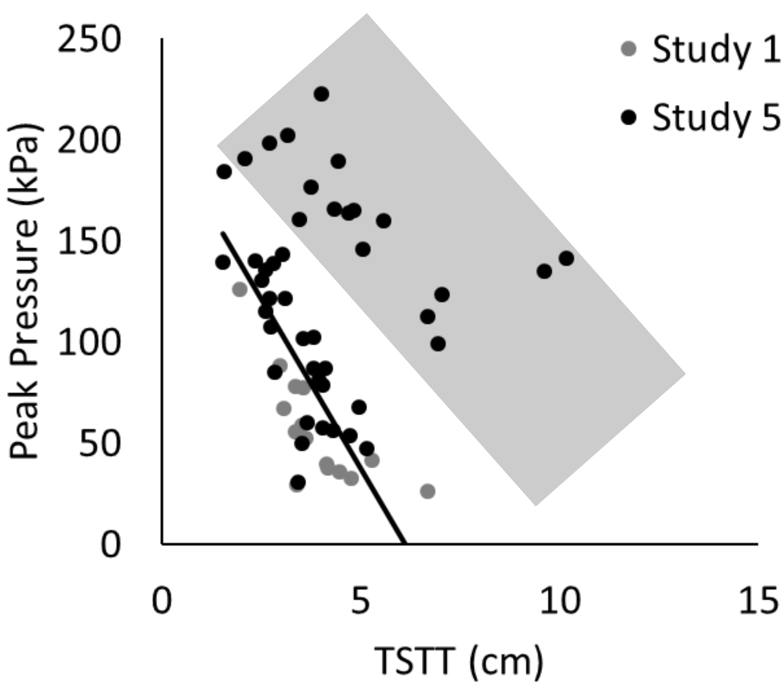

Figure 8.2 Graphical display of relationship between TSTT and peak pressure

Participants from Study 1 (grey) and Study 5 (black) are plotted to demonstrate the relationship between TSTT and pressure. Participants in the grey band do not fit within the model (black line) to describe the TSTT-peak pressure relationship from Study 1. It is unclear from the current studies why these participants do not fit the model, however, this discrepancy may be explained in future studies by the underlying skeletal structure, or skeletal-TSTT relationship.

These results extend current understanding of the links between individual body size and composition characteristics and impact dynamics. First, peak loads are strongly driven by overall mass. However, in a modification of previous hypotheses, TSTT had a limited effect on total force attenuation, but a strong effect on localized force (i.e. pressure), in some participants. Therefore, hypotheses regarding the effect of TSTT on normal force attenuation are supported, only localized in regions of high pressure. Second, there is a strong relationship between TSTT and force distribution, particularly with regards to contact area. However, for some fallers, identified as outliers, this load distribution may not be effective at reducing pressure over the greater trochanter. Underlying skeletal structures may interact with TSTT to influence peak pressure more directly, and should be a focus of future investigations.

8.2 Can we incorporate individual characteristics in a mechanistic hip impact model?

In Study 2, we noted that a major drawback of current fracture prediction models was the lack of mechanistic links between population-level predictive components and fracture outcomes. This drawback limits implementation of these injury risk prediction models to populations (older adults) with individual characteristics (e.g. low body weight, epidemiologically linked to low bone mass) in common injury scenarios. This can lead to confirmation bias or opportunistic screening for fracture risk—40-50% of older adults with osteoporotic fractures receive inadequate screening and treatment prior to their injury, with age (both too old and too young), and male sex as risk factors for inadequate screening (Blecher, Wasrbrout et al. 2013). Further, rates of osteoporotic fractures are not static—rates of osteoporotic pelvis fractures are rising (Kannus, Palvanen et al. 2000), and while osteoporotic fractures have declined in Europe, Oceania and North America, they have increased in South America and Asia (Cauley, Chalhoub et al. 2014). Luo (2016) cited time-varying changes in population characteristics, such as height, as a major drawback in development of statistical injury models. However, this thesis provides evidence regarding the mechanistic links between individual characteristics and modeled and experimental outcomes related to predicting injury risk.

In Study 2, we were able incorporate individual characteristics into model parameters for a multibody modeling approach. We found that stiffness parameters were most strongly related to body fat and TSTT. For point contact models, stiffness was more strongly related to body fat, which may reflect the material properties of adipose tissue. For geometric models, TSTT was more strongly related, which again highlights the importance of TSTT in distributing loads three-dimensionally rather than simply attenuating force from a one-dimensional perspective. Damping was more closely related to pelvis size. This likely reflects the viscoelasticity of the underlying skeletal structures, as well as the skeletal structures as a boundary for the fluids contained in the soft tissues (i.e a smaller pelvis will more tightly limit flow away from the pelvis). In Study 3, we compared the resulting models, and found that the Hunt-Crossley, with both geometric and viscoelastic components, predicted peak force within (on average) 6%.

However, conceptually the Volumetric model still has several potential benefits over the HC model. First, the Hertz-based model is limited to impacts where the contact area is low relative to the geometry of the contacting bodies, and second, the two bodies must not be conforming at the point of impact (Gilardi and Sharf 2002; Boos and McPhee 2010). The first of these assumptions may be violated in cases where, due to high levels of TSTT, there is substantially greater contact area than that observed in the cohort used to develop parameters for the models in this study. While we did not observe greater errors for the HC model for participants in our high TSTT group, which ranged up to 10.2 cm, this effect may be exaggerated for older adults due to the decrease in TSTT compressive stiffness associated with aging (Choi, Russell et al. 2014). The second assumption may be violated in the case of wearable protective equipment, such as hip protectors, which introduce conformation of two interacting surfaces at the point of impact. Therefore, further development of the Volumetric model may not only improve its predictive capability, but may also be warranted in order to improve the external validity of the modeling approach proposed in this study.

We also identified several limitations to the model in its current implementation, which lead into future development points. First, there may be a multiphase loading response of the pelvis during impact. This may be directly linked to motion of individual anatomical components (Study 4), including a “bottoming-out” effect of the trochanteric soft tissues or skeletal structures such as the wing of the ilium. Second, it is unclear how the model will perform in the prediction of more complicated falling configurations. It may be beneficial to implement the Hunt-Crossley model in replacement of the Voigt model in a multilevel falling model (Sarvi and Luo 2015), however, further work may be required to characterize parameters to support non-normal velocity and forces. Third, we are unable to characterize the inflection point of the loading curve identified in Figure 5.8 with our current modeling strategy, nor is it clear what mechanisms are responsible for this loading response. While shear loading between distal body segments (torso, legs) has previously been demonstrated to have a limited effect on peak force magnitude (Robinovitch et al., 1997), however it is uncertain whether the distal segments contribute to finer characteristics in the loading response curve. Additionally, we have demonstrated in Study 4 that the inflection point may be linked to motion of the wing of the ilium relative to the midline of the pelvis, however, it is unclear what mechanisms drives this behavior. Future work should determine whether this inflection point is of clinical or mechanistic importance, and attempt to incorporate it in future modeling strategies. Ultimately, this approach could be used to develop a more globally applicable individualized model to predict, or forensically analyze, simulated low-energy impacts. This model could follow strategies of currently existing approaches, such as the Global Human Body Models Consortium (GHBMC), which focuses on automotive crash simulations, or be incorporated into an existing software framework, such as OpenSim.

Additionally, reflecting back to current population-based methods of fracture prediction, the results of this thesis also provide avenues for improvement. Stronger understanding of the mechanistic links between individual characteristics can help drive epidemiological research regarding factors identified in this study (e.g. TSTT) and actual fracture outcomes to create better predictors for models such as FRAX. Additionally, incorporation of more accurate contact models may provide better estimates of TSTT-linked force attenuation for probabilistic population-level estimates of hip fracture risk (Martel 2017).

8.3 What happens when we simulate the impact phase of the fall using different fall simulation protocols?

Building on the limitations in Studies 1 and 3, we compared common and novel methods of simulated falls in a laboratory environment. In Study 5, we found that fall simulation protocols had a substantial effect on peak force magnitude and distribution. Despite similar vertical impact velocity, the Keeling and Squat Release were associated with greater vertical forces, likely reflecting the effective mass of the torso during the impact phase. The Squat Release was linked to 84-96% higher shear forces compared to Kneeling or Pelvis Release, which can be attributed to shear velocity at impact. Peak pressure was also increased for the Squat Release, by 70-120%, which we hypothesized may be an effect of posterior rotation, as well as potential underlying skeletal structure in a posterolateral impact configuration. In a supplementary study (Appendix 2) we found that fall simulation protocol had an effect on not only the contact area during impact, but also the shape of the distribution—this information could be used to drive inputs into internal load-prediction models (e.g. a finite-element strategy) for fracture risk, as well as understanding lower-energy injuries such as bruising patterns.

Further work should explore participant strategies and neuromuscular control during the impact phase. While a large body of work focuses on the loss-of-balance phase of falls, there is still much to quantify regarding control and configuration during the impact phase of falls to explain how load magnitude and distribution are modified by faller strategy. Better understanding of faller strategy, and individual factors contributing to impact configuration (e.g. strength and power, mass distribution, skeletal geometry and neurocognitive factors such as reaction time and ability to generate an appropriate response) will help drive more effective identification of high-risk fallers and improve fall prevention training programs.

8.4 From a clinical perspective, what are the most critical research findings?

From a fracture-risk screening perspective, current statistical models, such as FRAX or CAROC, may be improved through the inclusion of biomechanically-related components. In addition to an estimate of fracture tolerance (i.e. BMD) and overall size (height, weight), prediction of fracture may be refined by inclusion of an individual characteristic related to load distribution. Refinement of the TSTT measurement protocol, and perhaps inclusion in a DXA-based fracture risk assessment would be ideal, however, assessment of overall total body fat may be more accessible to a greater number of potential fallers. Given that body size has been previously positively correlated with bone mineral density, but high body fat has been linked to poor bone quality (discussed in greater detail in Section 2.4), body size and composition appear to play a strong role from both the applied loads and fracture tolerance perspectives of the Factor of Risk method of fracture risk assessment. Therefore, incorporation of both body size and composition components may improve prediction of fracture risk. Inclusion of a Hunt-Crossley-based attenuated peak force prediction may improve epidemiological implementation of the factor-of-risk approach to injury prediction over previous mass-spring approaches (Bouxsein, Szulc et al. 2007; Nielson, Bouxsein et al. 2009; Dufour, Roberts et al. 2012).

In Studies 1 and 5, we found strong and differing mechanistic links between lean body mass, fat body mass and impact dynamics. In Studies 2 and 3, we demonstrated that these individual characteristics were linked to mechanical behavior from a contact-mechanics perspective and their inclusion resulted in improvements of up to 65 percentage points over current simple mass-spring models which incorporate fewer individual characteristics. In contrast, more general estimates of body size and composition, such as BMI, were linked in a more limited manner, or in some cases not linked, to impact characteristics. Assessing the problem from a Factor of Risk perspective, the addition of specific measures of lean and fat components, as well as a potentially more accurate model including load distribution, would likely improve assessment of the applied loads portion of the equation. Future research regarding the potential costs and benefits of the added complexity from a population-level perspective is warranted.

The results of this thesis support current prevention strategies for fall-related-injury prevention, as well as help drive future intervention research strategies. From a fall-training perspective, it is clear that impact configuration has a substantial effect on impact dynamics—perhaps more so than individual characteristics. Fall-training programs should consider the impact phase of falls in addition to preventing the loss of balance, however, more work is required to more clearly understand the dynamics of this phase. For example, Moon and Sosnoff (2017) recommend, based on a meta-analysis of fall-landing strategies, a squatting strategy for backwards falls. However, in Study 5, we found that during a lateral fall, some participants rotated to a higher-risk posterolateral impact configuration. Therefore, the squatting technique may not be universally appropriate injury-avoidance strategy. However, individual characteristics also have a strong influence on impact dynamics. Peak force was strongly driven by overall body size and lean mass—factors which cannot be changed (e.g. height) or may be detrimental to reduce. Body fat was linked to load distribution, and in some cases, reduction in loading at the location of peak pressure, or the "danger zone" over the proximal femur. Interventions which effectively simulate or improve the load distribution effect of soft tissues, such as hip protectors or safety floors, are supported by the results of this set of studies, and can easily be incorporated into the computational models developed within this thesis. Additionally, better understanding of how the skeletal and soft tissues interact to influence load distribution, as discussed in Section 8.1 may help identify designs of hip protectors which are more effective for specific patients on an individualized basis.

8.5 Summary of Contributions

In sum, the research in this thesis provide the following contributions:

1. Improved understanding of the contributions of overall body size, specifically total body mass, lean mass, and mass attributed to the pelvis system, to peak force magnitude during a lateral impact to the hip.
2. Expanded evidence of the effects of trochanteric soft tissues (or more generally, body fat) to the distribution of loads during a lateral impact to the hip rather than one-dimensional attenuation of force.
3. Comparison of impact characteristics between traditional and novel fall simulation protocols
4. Analysis of the interaction between fall simulation protocol and body composition to affect load magnitude and distribution.
5. Development and initial verification and validation of a geometric and viscoelastic modeling approach for simulation of impacts to the hip.
6. Insight into the deformation of structures within the pelvis system and hypotheses and recommendations for future investigation into the contributions of individual anatomical components to the overall behavior of the pelvis system.

Global Summary: The Take-Home Statement

In this thesis, we compared the effects of different individual characteristics and falling configuration on impact dynamics during falls impacting the lateral pelvis. We found that peak force was related to body size and impact configurations where the torso was oriented in a way which added to the effective mass of the pelvis. Load distribution at the floor-pelvis interface, as well as within the pelvis, are both affected by trochanteric soft tissues. We can incorporate individual characteristics in mechanistic models of lateral impacts to the hip, which can be implemented into both individual- as well as population-level estimates of injury risk.

Bibliography

Abrassart, S., R. Stern, et al. (2009). "Morbidity associated with isolated iliac wing fractures." Journal of Trauma and Acute Care Surgery **66**(1): 200-203.

AIUM (2008). "American Institute of Ultrasound in Medicine Consensus Report on Potential Bioeffects of Diagnostic Ultrasound Executive Summary." Journal of Ultrasound in Medicine **27**(4): 503-515.

Alarcón, T., J. González-Montalvo, et al. (2011). "Activities of daily living after hip fracture: profile and rate of recovery during 2 years of follow-up." Osteoporosis International **22**(5): 1609-1613.

Alonso, J. E., D. A. Volgas, et al. (2000). "A review of the treatment of hip dislocations associated with acetabular fractures." Clinical orthopaedics and related research **377**: 32-43.

Argatov, I. (2013). "Mathematical modeling of linear viscoelastic impact: Application to drop impact testing of articular cartilage." Tribology International **63**: 213-225.

Armstrong, M. E., E. A. Spencer, et al. (2011). "Body mass index and physical activity in relation to the incidence of hip fracture in postmenopausal women." Journal of Bone and Mineral Research **26**(6): 1330-1338.

Armstrong, M. E. G., B. J. Cairns, et al. (2012). "Different effects of age, adiposity and physical activity on the risk of ankle, wrist and hip fractures in postmenopausal women." Bone **50**(6): 1394-1400.

Arun, M. W. J., N. Yoganandan, et al. (2014). "A methodology to condition distorted acoustic emission signals to identify fracture timing from human cadaver spine impact tests." Journal of the Mechanical Behavior of Biomedical Materials **40**: 156-160.

Bass, E. C., N. A. Duncan, et al. (1997). Frozen storage affects the compressive creep behavior of the porcine intervertebral disc. **22:** 2867-2876.

Beason, D. P., G. J. Dakin, et al. (2003). "Bone mineral density correlates with fracture load in experimental side impacts of the pelvis." Journal of biomechanics **36**(2): 219-227.

Beck, T. J., M. A. Petit, et al. (2009). "Does obesity really make the femur stronger? BMD, geometry, and fracture incidence in the women's health initiative-observational study." J Bone Miner Res **24**(19292617): 1369-1379.

Becker, C., L. Schwickert, et al. (2012). "Proposal for a multiphase fall model based on real-world fall recordings with body-fixed sensors." Zeitschrift für Gerontologie und Geriatrie **45**(8): 707-715.

Bell, A. L., R. A. Brand, et al. (1989). "Prediction of hip joint centre location from external landmarks." Human Movement Science **8**(1): 3-16.

Bergmann, G., F. Graichen, et al. (2004). "Hip joint contact forces during stumbling." Langenbeck's Archives of Surgery **389**(1): 53-59.

Bessette, L., L.-G. Ste-Marie, et al. (2008). "The care gap in diagnosis and treatment of women with a fragility fracture." Osteoporosis International **19**(1): 79-86.

Bhan, S. (2014). Biomechanics of Lateral Hip Impacts: the Influence of Measurement Technique and Contact Area. Kinesiology. Waterloo, ON, University of Waterloo. **Master of Science**.

Bhan, S., I. Levine, et al. (2013). "The Influence of Body Mass Index and Gender on the Impact Attenuation Properties of Flooring Systems." Journal of applied biomechanics.

Bhan, S., I. C. Levine, et al. (2014). "Energy absorption during impact on the proximal femur is affected by body mass index and flooring surface." Journal of biomechanics.

Birmingham, P. M., B. T. Kelly, et al. (2012). "The Effect of Dynamic Femoroacetabular Impingement on Pubic Symphysis Motion A Cadaveric Study." The American Journal of Sports Medicine **40**(5): 1113-1118.

Bisseling, R. W. and A. L. Hof (2006). "Handling of impact forces in inverse dynamics." Journal of biomechanics **39**(13): 2438-2444.

Blecher, R., Z. Wasrbrout, et al. (2013). "Who is at Risk of Receiving Inadequate Care for Osteoporosis Following Fragility Fractures? A Retrospective Study." The Israel Medical Association journal: IMAJ **15**(10): 634-638.

Boos, M. (2011). Validation of Volumetric Contact Dynamics Models, University of Waterloo.

Boos, M. and J. McPhee (2010). "Volumetric Contact Dynamics Models and Validation."

Boos, M. and J. McPhee (2013). "Volumetric modeling and experimental validation of normal contact dynamic forces." Journal of Computational and Nonlinear Dynamics **8**(2): 021006.

Bourgouin, S., T. Bège, et al. (2012). "Biomechanical characterisation of fresh and cadaverous human small intestine: applications for abdominal trauma." Medical & biological engineering & computing **50**(12): 1279-1288.

Bourgouin, S. p., T. Bege, et al. (2012). "Biomechanical characterisation of fresh and cadaverous human small intestine: Applications for abdominal trauma." Medical and Biological Engineering and Computing **50**(12): 1279-1288.

Bouxsein, M., B. Coan, et al. (1999). "Prediction of the strength of the elderly proximal femur by bone mineral density and quantitative ultrasound measurements of the heel and tibia." Bone **25**(1): 49-54.

Bouxsein, M., P. Szulc, et al. (2007). "Contribution of Trochanteric Soft Tissues to Fall Force Estimates, the Factor of Risk, and Prediction of Hip Fracture Risk*." Journal of Bone and Mineral Research **22**(6): 825-831.

Bouxsein, M. L., P. Szulc, et al. (2007). "Contribution of Trochanteric Soft Tissues to Fall Force Estimates, the Factor of Risk, and Prediction of Hip Fracture Risk*." Journal of Bone and Mineral Research **22**(6): 825-831.

Broy, S. B., J. A. Cauley, et al. (2015). "Fracture risk prediction by non-BMD DXA measures: the 2015 ISCD official positions part 1: hip geometry." Journal of Clinical Densitometry **18**(3): 287-308.

Burgess, A. R., B. J. Eastridge, et al. (1990). "Pelvic ring disruptions: effective classification system and treatment protocols." Journal of Trauma and Acute Care Surgery **30**(7): 848-856.

Burkhart, T. A., C. E. Dunning, et al. (2011). "Determining the optimal system-specific cut-off frequencies for filtering in-vitro upper extremity impact force and acceleration data by residual analysis." Journal of biomechanics **44**(15): 2728-2731.

Carrasco, F., M. Ruz, et al. (2009). "Changes in bone mineral density, body composition and adiponectin levels in morbidly obese patients after bariatric surgery." Obesity surgery **19**(1): 41-46.

Casalena, J. A., A. Badre-Alam, et al. (1998). "The Penn State Safety Floor: Part II--Reduction of fall-related peak impact forces on the femur." J Biomech Eng **120**(4): 527-532.

Cauley, J. A., D. Chalhoub, et al. (2014). "Geographic and ethnic disparities in osteoporotic fractures." Nature Reviews Endocrinology **10**(6): 338-351.

Cavanaugh, J. M., T. J. Walilko, et al. (1990). Biomechanical response and injury tolerance of the pelvis in twelve sled side impacts, SAE Technical Paper.

Cawthon, P. M. (2011). Gender differences in osteoporosis and fractures. Clinical Orthopaedics and Related Research. **469:** 1900-1905.

CDC (2012). Anthropometric Reference Data for Children and Adults: United States, 2007–2010. Vital Health and Statistics. U. S. D. o. H. a. H. Services, C. f. D. C. a. Prevention and N. C. f. H. Statistics. **11**.

Cenzer, I. S., V. Tang, et al. (2016). "One- Year Mortality After Hip Fracture: Development and Validation of a Prognostic Index." Journal of the American Geriatrics Society **64**(9): 1863-1868.

Chan, M., D. Estève, et al. (2012). "Smart wearable systems: Current status and future challenges." Artificial intelligence in medicine **56**(3): 137-156.

Chan, R. W. and I. R. Titze (2003). "Effect of postmortem changes and freezing on the viscoelastic properties of vocal fold tissues." Annals of biomedical engineering **31**(4): 482-491.

Changoor, A., L. Fereydoonzad, et al. (2010). "Effects of refrigeration and freezing on the electromechanical and biomechanical properties of articular cartilage." Journal of biomechanical engineering **132**(6): 064502-064502.

Cheng, X., G. Lowet, et al. (1997). "Assessment of the strength of proximal femur in vitro: relationship to femoral bone mineral density and femoral geometry." Bone **20**(3): 213-218.

Cheng, X. G., G. Lowet, et al. (1998). "Prediction of vertebral and femoral strength in vitro by bone mineral density measured at different skeletal sites." Journal of Bone and Mineral Research **13**(9): 1439-1443.

Choi, W., P. Cripton, et al. (2015). "Effects of hip abductor muscle forces and knee boundary conditions on femoral neck stresses during simulated falls." Osteoporosis International **26**(1): 291-301.

Choi, W., J. Hoffer, et al. (2010). "The effect of positioning on the biomechanical performance of soft shell hip protectors." Journal of biomechanics **43**(5): 818-825.

Choi, W., C. Russell, et al. (2014). "Age-related changes in dynamic compressive properties of trochanteric soft tissues over the hip." Journal of biomechanics.

Choi, W., J. Wakeling, et al. (2015). "Kinematic analysis of video-captured falls experienced by older adults in long-term care." Journal of biomechanics **48**(6): 911-920.

Choi, W. J., J. A. Hoffer, et al. (2010). "Effect of hip protectors, falling angle and body mass index on pressure distribution over the hip during simulated falls." Clinical Biomechanics **25**(1): 63-69.

Choi, W. J. and S. N. Robinovitch (2011). "Pressure distribution over the palm region during forward falls on the outstretched hands." J Biomech **44**(21035120): 532-539.

CIHI (2013). National Trauma Registry Report 2013: Hospitalizations for Major Injury in Canada, 2010-2011. National Trauma Registry Report: Major Injury in Canada, Canadian Institute for Health Information.

Cody, D. D., G. J. Gross, et al. (1999). "Femoral strength is better predicted by finite element models than QCT and DXA." Journal of biomechanics **32**(10): 1013-1020.

Colon-Emeric, C., K. Lyles, et al. (2007). "Prevalence and predictors of osteoporosis treatment in nursing home residents with known osteoporosis or recent fracture." Osteoporosis International **18**(4): 553-559.

Compston, J. E., N. B. Watts, et al. (2011). "Obesity Is Not Protective against Fracture in Postmenopausal Women: GLOW." The American Journal of Medicine **124**(11): 1043-1050.

Corbeil, P., M. Simoneau, et al. (2001). "Increased risk for falling associated with obesity: mathematical modeling of postural control." IEEE Transactions on Neural Systems and Rehabilitation Engineering **9**(2): 126-136.
Courtney, A., E. Wachtel, et al. (1994). "Effects of loading rate on strength of the proximal femur." Calcified tissue international **55**(1): 53-58.
Crabtree, N., H. Kroger, et al. (2002). "Improving risk assessment: hip geometry, bone mineral distribution and bone strength in hip fracture cases and controls. The EPOS study." Osteoporosis International **13**(1): 48-54.
Crabtree, N., M. Lunt, et al. (2000). "Hip geometry, bone mineral distribution, and bone strength in European men and women: the EPOS study." Bone **27**(1): 151-159.
Cummings, S. and M. Nevitt (1994). "Non-skeletal determinants of fractures: the potential importance of the mechanics of falls." Osteoporosis International **4**(1): S67-S70.
Cummings, S. R. and L. J. Melton (2002). "Epidemiology and outcomes of osteoporotic fractures." The Lancet **359**(12049882): 1761-1767.
Cummings, S. R. and M. C. Nevitt (1989). "A hypothesis: the causes of hip fractures." Journal of gerontology **44**(5): M107-M111.
de Bakker, P. M., S. L. Manske, et al. (2009). "During sideways falls proximal femur fractures initiate in the superolateral cortex: evidence from high-speed video of simulated fractures." Journal of biomechanics **42**(12): 1917-1925.
Derler, S., A. B. Spierings, et al. (2005). "Anatomical hip model for the mechanical testing of hip protectors." Medical Engineering & Physics **27**(6): 475-485.
Di Monaco, M., F. Vallero, et al. (2011). "Prevalence of sarcopenia and its association with osteoporosis in 313 older women following a hip fracture." Archives of Gerontology and Geriatrics **52**(1): 71-74.
Dufour, A. B., B. Roberts, et al. (2012). "The factor-of-risk biomechanical approach predicts hip fracture in men and women: the Framingham Study." Osteoporos Int **23**(21344243): 513-520.
Dunford, K. and A. Kemper (2017). Effect of Postmortem Time and Preservation Fluid on the Tensile Material Properties of Bovine Liver Parenchyma. 13th Annual Injury Biomechanics Symposium. Columbus, Ohio.
Eberhardt, A., J. Lewis, et al. (1991). "Normal contact of elastic spheres with two elastic layers as a model of joint articulation." J Biomech Eng **113**(4): 410-417.
Eichenseer, P. H., D. R. Sybert, et al. (2011). "A finite element analysis of sacroiliac joint ligaments in response to different loading conditions." Spine **36**(22): E1446-E1452.
El-ghazal, A., O. Basir, et al. (2009). "Farthest point distance: A new shape signature for Fourier descriptors." Signal Processing: Image Communication **24**(7): 572-586.
Elsner, J. J. and A. Gefen (2008). "Is obesity a risk factor for deep tissue injury in patients with spinal cord injury?" Journal of biomechanics **41**(16): 3322-3331.
Etheridge, B. S., D. P. Beason, et al. (2005). "Effects of trochanteric soft tissues and bone density on fracture of the female pelvis in experimental side impacts." Annals of Biomedical.
Etheridge, B. S., D. P. Beason, et al. (2005). "Effects of trochanteric soft tissues and bone density on fracture of the female pelvis in experimental side impacts." Annals of biomedical engineering **33**(2): 248-254.
Evans, D., J. Pester, et al. (2015). "Elderly fall patients triaged to the trauma bay: age, injury patterns, and mortality risk." The American journal of emergency medicine **33**(11): 1635-1638.

Feldman, F. and S. N. Robinovitch (2007). "Reducing hip fracture risk during sideways falls: evidence in young adults of the protective effects of impact to the hands and stepping." Journal of biomechanics **40**(12): 2612-2618.
Ferdous, Z. and Y. Luo (2015). "Study of hip fracture risk by DXA-based patient-specific finite element model." Bio-medical materials and engineering **25**(2): 213-220.
Finnie, J. W. (2015). "Forensic Pathology of Traumatic Brain Injury." Veterinary pathology **53**(5): 1-17.
Fjeldstad, C., A. S. Fjeldstad, et al. (2008). "The influence of obesity on falls and quality of life." Dynamic Medicine **7**(1): 4.
Flegal, K. M., M. D. Carroll, et al. (2010). "Prevalence and trends in obesity among US adults, 1999-2008." Jama **303**(3): 235-241.
Fleischer, J., E. Stein, et al. (2008). "The decline in hip bone density after gastric bypass surgery is associated with extent of weight loss." Journal of Clinical Endocrinology & Metabolism **93**(10): 3735.
Ford, C. M., T. M. Keaveny, et al. (1996). "The effect of impact direction on the structural capacity of the proximal femur during falls." Journal of Bone and Mineral Research **11**(3): 377-383.
Fregly, B. J., Y. Bei, et al. (2003). "Experimental evaluation of an elastic foundation model to predict contact pressures in knee replacements." Journal of biomechanics **36**(11): 1659-1668.
Galgani, J. E., S. R. Smith, et al. (2011). "Assessment of EchoMRI-AH™ vs. Dual-energy X-ray Absorptiometry (DXA) to Measure Human Body Composition." International journal of obesity (2005) **35**(9): 1241.
Garman, C. R., C. T. Franck, et al. (2015). "A bootstrapping method to assess the influence of age, obesity, gender, and gait speed on probability of tripping as a function of obstacle height." Journal of biomechanics **48**(6): 1229-1232.
Garman, C. R., J. M. Scanlon, et al. (2014). Effects of Age and Obesity on the Likelihood of Tripping During ANterior Load Carriage. 7th World Congress of Biomechanics. Boston, MA.
Garras, D. N., J. T. Carothers, et al. (2008). "Single-leg-stance (flamingo) radiographs to assess pelvic instability: how much motion is normal?" The Journal of Bone & Joint Surgery **90**(10): 2114-2118.
Gefen, A. (2007). "Risk factors for a pressure-related deep tissue injury: a theoretical model." Medical & biological engineering & computing **45**(6): 563-573.
Gefen, A. and E. Haberman (2007). "Viscoelastic properties of ovine adipose tissue covering the gluteus muscles." Journal of biomechanical engineering **129**(6): 924-930.
Giangregorio, L., M. Jantzi, et al. (2009). "Osteoporosis management among residents living in long-term care." Osteoporosis International **20**(9): 1471-1478.
Giannini, S., R. Buda, et al. (2008). "Effects of freezing on the biomechanical and structural properties of human posterior tibial tendons." International Orthopaedics **32**(2): 145-151.
Gilardi, G. and I. Sharf (2002). "Literature survey of contact dynamics modelling." Mechanism and Machine Theory **37**(10): 1213-1239.
Gjesdal, C., J. Halse, et al. (2008). "Impact of lean mass and fat mass on bone mineral density: The Hordaland Health Study." Maturitas **59**(2): 191-200.
Gnat, R., K. Spoor, et al. (2013). "Simulated transversus abdominis muscle force does not increase stiffness of the pubic symphysis and innominate bone: An in vitro study." Clinical Biomechanics **28**(3): 262-267.

Goh, J. C., E. J. Ang, et al. (1989). "Effect of preservation medium on the mechanical properties of cat bones." Acta Orthopaedica Scandinavica **60**(4): 465-467.
Gonthier, Y. (2007). Contact dynamics modelling for robotic task simulation, University of Waterloo.
Gottsauner- Wolf, F., J. J. Grabowski, et al. (1995). "Effects of freeze/thaw conditioning on the tensile properties and failure mode of bone- muscle- bone units: A biomechanical and histological study in dogs." Journal of Orthopaedic Research **13**(1): 90-95.
Grisso, J., J. Kelsey, et al. (1991). "Risk factors for falls as a cause of hip fracture in women. The Northeast Hip Fracture Study Group." New England Journal of Medicine **324**(19): 1326.
Groen, B., V. Weerdesteyn, et al. (2008). "The relation between hip impact velocity and hip impact force differs between sideways fall techniques." Journal of Electromyography and Kinesiology **18**(2): 228-234.
Groen, B. E., V. Weerdesteyn, et al. (2007). "Martial arts fall techniques decrease the impact forces at the hip during sideways falling." Journal of biomechanics **40**(2): 458-462.
Guggenbuhl, P., J. Meadeb, et al. (2005). "Osteoporotic fractures of the proximal humerus, pelvis, and ankle: Epidemiology and diagnosis." Joint Bone Spine **72**(5): 372-375.
Hayes, W., E. Myers, et al. (1996). "Etiology and prevention of age-related hip fractures." Bone **18**(1): S77-S86.
Hayes, W., S. Piazza, et al. (1991). "Biomechanics of fracture risk prediction of the hip and spine by quantitative computed tomography." Radiologic Clinics of North America **29**(1): 1.
Hayes, W. C., S. J. Piazza, et al. (1991). "Biomechanics of fracture risk prediction of the hip and spine by quantitative computed tomography." Radiologic Clinics of North America **29**(1): 1-1.
Heini, P. F., T. Franz, et al. (2004). "Femoroplasty-augmentation of mechanical properties in the osteoporotic proximal femur: a biomechanical investigation of PMMA reinforcement in cadaver bones." Clinical Biomechanics **19**(5): 506-512.
Hergenroeder, A. L., D. M. Wert, et al. (2011). "Association of body mass index with self-report and performance-based measures of balance and mobility." Physical therapy **91**(8): 1223-1234.
Hertz, H. (1882). "Über die Berührung fester elastischer Körper."
Hertz, H. (1896). Miscellaneous papers, Macmillan.
Hippisley-Cox, J. and C. Coupland (2012). "Derivation and validation of updated QFracture algorithm to predict risk of osteoporotic fracture in primary care in the United Kingdom: prospective open cohort study." Bmj **344**: e3427-e3427.
Hirokawa, S. (1991). "Three-dimensional mathematical model analysis of the patellofemoral joint." Journal of biomechanics **24**(8): 659-671.
Hodges, P. W., L. H. M. Pengel, et al. (2003). "Measurement of muscle contraction with ultrasound imaging." Muscle Nerve **27**(12766979): 682-692.
Hsiao, E. T. and S. N. Robinovitch (1997). "Common protective movements govern unexpected falls from standing height." Journal of biomechanics **31**(1): 1-9.
Hunt, K. and F. Crossley (1975). "Coefficient of restitution interpreted as damping in vibroimpact." Journal of Applied Mechanics, Transactions ASME **42**.
Hwang, H.-F., H.-D. Lee, et al. (2011). "Fall mechanisms, bone strength, and hip fractures in elderly men and women in Taiwan." Osteoporosis International **22**(8): 2385-2393.
Ioannidis, G., A. Papaioannou, et al. (2009). "Relation between fractures and mortality: results from the Canadian Multicentre Osteoporosis Study." Canadian Medical Association Journal **181**(5): 265-265.

Jackson, A. S. and M. L. Pollock (1978). "Generalized equations for predicting body density of men." British journal of nutrition **40**(03): 497-504.
Jackson, A. S., M. L. Pollock, et al. (1978). "Intertester reliability of selected skinfold and circumference measurements and percent fat estimates." Research Quarterly. American Alliance for Health, Physical Education and Recreation **49**(4): 546-551.
Jackson, A. S., M. L. Pollock, et al. (1979). "Generalized equations for predicting body density of women." Medicine and science in sports and exercise **12**(3): 175-181.
Jaglal, S. B., I. Weller, et al. (2005). "Population Trends in BMD Testing, Treatment, and Hip and Wrist Fracture Rates: Are the Hip Fracture Projections Wrong?" Journal of Bone and Mineral Research **20**(6): 898-905.
Johansson, H., J. A. Kanis, et al. (2014). "A Meta-Analysis of the Association of Fracture Risk and Body Mass Index in Women." Journal of Bone and Mineral Research **29**(1): 223-233.
Johnson, K. (1985). Contact mechanics. 1985, Cambridge [Cambridgeshire], New York: Cambridge University Press. xi.
Jokinen, H., P. Pulkkinen, et al. (2010). "Risk factors for cervical and trochanteric hip fractures in elderly women: a population-based 10-year follow-up study." Calcified tissue international **87**(1): 44-51.
Kangas, M. (2011). "Development of accelerometry-based fall detection."
Kangas, M., I. Vikman, et al. (2012). "Comparison of real-life accidental falls in older people with experimental falls in middle-aged test subjects." Gait & posture **35**(3): 500-505.
Kangas, M., I. Vikman, et al. (2009). "Sensitivity and specificity of fall detection in people aged 40 years and over." Gait & posture **29**(4): 571-574.
Kanis, J. A., D. Hans, et al. (2011). "Interpretation and use of FRAX in clinical practice." Osteoporosis International **22**(9): 2395-2411.
Kanis, J. A., D. Hans, et al. (2011). "Interpretation and use of FRAX in clinical practice." Osteoporosis International **22**(9): 2395-2411.
Kannus, P., P. Leiponen, et al. (2006). "A sideways fall and hip fracture." Bone **39**(2): 383-384.
Kannus, P., M. Palvanen, et al. (2000). "Epidemiology of osteoporotic pelvic fractures in elderly people in Finland: Sharp increase in 1970-1997 and alarming projections for the new millennium." Osteoporosis International **11**(5): 443-448.
Kannus, P., M. Palvanen, et al. (2005). "Osteoporotic pelvic fractures in elderly women." Osteoporosis International **16**(10): 1304-1305.
Kelsey, J. L., S. D. Berry, et al. (2010). "Indoor and outdoor falls in older adults are different: the maintenance of balance, independent living, intellect, and Zest in the Elderly of Boston Study." Journal of the American Geriatrics Society **58**(11): 2135-2141.
Keyak, J. (2001). "Improved prediction of proximal femoral fracture load using nonlinear finite element models." Medical Engineering & Physics **23**(3): 165-173.
Keyak, J., H. Skinner, et al. (2006). "Effect of force direction on femoral fracture load for two types of loading conditions." Journal of Orthopaedic Research **19**(4): 539-544.
Keyak, J. H. (2000). "Relationships between femoral fracture loads for two load configurations." Journal of biomechanics **33**(4): 499-502.
Keyak, J. H., S. Sigurdsson, et al. (2011). "Male-female differences in the association between incident hip fracture and proximal femoral strength: A finite element analysis study." Bone **48**(6): 1239-1245.

Keyak, J. H., H. B. Skinner, et al. (2001). "Effect of force direction on femoral fracture load for two types of loading conditions." Journal of Orthopaedic Research **19**(4): 539-544.

Kheirollahi, H. and Y. Luo (2017). "Understanding Hip Fracture by QCT-Based Finite Element Modeling." Journal of Medical and Biological Engineering

Kim, J.-E., M.-H. Hsieh, et al. (2013). "Childhood obesity as a risk factor for bone fracture: A mechanistic study." Obesity **21**(7): 1459-1466.

Kim, K.-J. and J. A. Ashton-Miller (2009). "Segmental dynamics of forward fall arrests: A system identification approach." Clinical Biomechanics **24**(4): 348-354.

Koo, T. K. and M. Y. Li (2016). "A Guideline of Selecting and Reporting Intraclass Correlation Coefficients for Reliability Research." Journal of Chiropractic Medicine **15**(2): 155-163.

Koop, D. and C. Q. Wu (2013). "Passive Dynamic Biped Walking—Part I: Development and Validation of an Advanced Model." Journal of Computational and Nonlinear Dynamics **8**(4): 041007.

Kottner, J., A. Gefen, et al. (2011). "Weight and pressure ulcer occurrence: a secondary data analysis." International journal of nursing studies **48**(11): 1339-1348.

Kuwahata, A., Y. Kawamura, et al. (2008). "Non-weight-bearing effect of trunk and peripheral fat mass on bone mineral density in pre-and post-menopausal women." Maturitas **60**(3-4): 244-247.

Laing, A. and S. Robinovitch (2010). "Characterizing the effective stiffness of the pelvis during sideways falls on the hip." Journal of biomechanics.

Laing, A. C., F. Feldman, et al. (2011). "The effects of pad geometry and material properties on the biomechanical effectiveness of 26 commercially available hip protectors." J Biomech **44**(15): 2627-2635.

Laing, A. C. and S. N. Robinovitch (2008). "Effect of soft shell hip protectors on pressure distribution to the hip during sideways falls." Osteoporosis International **19**(7): 1067-1075.

Laing, A. C. and S. N. Robinovitch (2008). "The force attenuation provided by hip protectors depends on impact velocity, pelvic size, and soft tissue stiffness." Journal of biomechanical engineering **130**(6): 061005.

Laing, A. C. and S. N. Robinovitch (2010). "Characterizing the effective stiffness of the pelvis during sideways falls on the hip." Journal of biomechanics **43**(10): 1898-1904.

Laing, A. C., I. Tootoonchi, et al. (2006). "Effect of compliant flooring on impact force during falls on the hip." Journal of Orthopaedic Research **24**(7): 1405-1411.

Langlois, J., M. Mussolino, et al. (2001). "Weight loss from maximum body weight among middle-aged and older white women and the risk of hip fracture: the NHANES I epidemiologic follow-up study." Osteoporosis International **12**(9): 763-768.

Lauritzen, J. and V. Askegaard (1992). "Protection against hip fractures by energy absorption." Danish medical bulletin **39**(1): 91.

Lauritzen, J. B. (1997). "Hip fractures. Epidemiology, risk factors, falls, energy absorption, hip protectors, and prevention." Dan Med Bull **44**(9151010): 155-168.

Leardini, A., L. Chiari, et al. (2005). "Human movement analysis using stereophotogrammetry: Part 3. Soft tissue artifact assessment and compensation." Gait & posture **21**(2): 212-225.

Leitschuh, P. H., T. J. Doherty, et al. (1996). "Effects of postmortem freezing on tensile failure properties of rabbit extensor digitorum longus muscle tendon complex." Journal of Orthopaedic Research **14**(5): 830-833.

Leslie, W., C. Berger, et al. (2011). "Construction and validation of a simplified fracture risk assessment tool for Canadian women and men: results from the CaMos and Manitoba cohorts." Osteoporosis International **22**(6): 1873-1883.

Levine, I. C. (2011). The Effects of Body Mass Index and Gender on Pelvic Stiffness and Peak Impact Force During Lateral Falls. Kinesiology. Waterloo, Ontario, University of Waterloo. **MSc**.

Levine, I. C., S. Bhan, et al. (2013). "The effects of body mass index and sex on impact force and effective pelvic stiffness during simulated lateral falls." Clinical Biomechanics **28**(9): 1026-1033.

Levine, I. C., L. E. Minty, et al. (2014). "Factors that influence soft tissue thickness over the greater trochanter: Application to understanding hip fractures." Clinical Anatomy.

Levine, I. C., L. E. Minty, et al. (2015). "Factors that influence soft tissue thickness over the greater trochanter: Application to understanding hip fractures." Clinical Anatomy **28**(2): 253-261.

Lewiecki, E. M., J. E. Compston, et al. (2011). "FRAX® Bone Mineral Density Task Force of the 2010 Joint International Society for Clinical Densitometry & International Osteoporosis Foundation Position Development Conference." Journal of Clinical Densitometry **14**(3): 223-225.

Lewiecki, E. M., J. E. Compston, et al. (2011). "Official Positions for FRAX® Bone Mineral Density and FRAX® Simplification: From Joint Official Positions Development Conference of the International Society for Clinical Densitometry and International Osteoporosis Foundation on FRAX®." Journal of Clinical Densitometry **14**(3): 226-236.

Li, N., E. Tsushima, et al. (2013). "Comparison of impact force attenuation by various combinations of hip protector and flooring material using a simplified fall-impact simulation device." Journal of biomechanics **46**(6): 1140-1146.

Linder-Ganz, E. and A. Gefen (2009). "Stress analyses coupled with damage laws to determine biomechanical risk factors for deep tissue injury during sitting." Journal of biomechanical engineering **131**(1): 011003.

Lintern, T., N. P. Gamage, et al. (2015). "Head kinematics during shaking associated with abusive head trauma." Journal of biomechanics **48**(12): 3123-3127.

Lochmüller, E.-M., J.-B. Zeller, et al. (1998). "Correlation of femoral and lumbar DXA and calcaneal ultrasound, measured in situ with intact soft tissues, with the in vitro failure loads of the proximal femur." Osteoporosis International **8**(6): 591-598.

Lochmüller, E., O. Groll, et al. (2002). "Mechanical strength of the proximal femur as predicted from geometric and densitometric bone properties at the lower limb versus the distal radius." Bone **30**(1): 207-216.

Lochmüller, E. M., O. Groll, et al. (2002). "Mechanical strength of the proximal femur as predicted from geometric and densitometric bone properties at the lower limb versus the distal radius." Bone **30**(1): 207-216.

Lohmann, G. P. (1983). "Eigenshape analysis of microfossils: A general morphometric procedure for describing changes in shape." Journal of the International Association for Mathematical Geology **15**(6): 659-672.

Lopes, D., R. Neptune, et al. (2016). "A superellipsoid-plane model for simulating foot-ground contact during human gait." Computer methods in biomechanics and biomedical engineering **19**(9): 954-963.

Lotz, J. C. and W. C. Hayes (1990). "The use of quantitative computed tomography to estimate risk of fracture of the hip from falls." The Journal of Bone & Joint Surgery **72**(5): 689-700.

Luo, Y. (2016). "A biomechanical sorting of clinical risk factors affecting osteoporotic hip fracture." Osteoporosis International **27**(2): 423-439.

Luo, Y., Z. Ferdous, et al. (2011). "A preliminary dual-energy X-ray absorptiometry-based finite element model for assessing osteoporotic hip fracture risk." Proceedings of the Institution of Mechanical Engineers, Part H: Journal of Engineering in Medicine **225**(12): 1188-1195.

Luo, Y., M. Nasiri Sarvi, et al. (2014). "Prediction of impact force in sideways fall by image-based subject-specific dynamics model." International Biomechanics **1**(1): 1-14.

Lyder, C. H., Y. Wang, et al. (2012). "Hospital- acquired pressure ulcers: results from the national Medicare patient safety monitoring system study." Journal of the American Geriatrics Society **60**(9): 1603-1608.

Machado, M., P. Moreira, et al. (2012). "Compliant contact force models in multibody dynamics: Evolution of the Hertz contact theory." Mechanism and Machine Theory **53**: 99-121.

Madeti, B. K., C. S. Rao, et al. (2014). "Failure analysis of ACL and Hertz contact stress in human knee." International Journal of Biomedical Engineering and Technology **16**(4): 317-328.

Madigan, M., N. J. Rosenblatt, et al. (2014). "Obesity as a Factor Contributing to Falls by Older Adults." Current Obesity Reports: 1-7.

Maiden, N. and R. Byard (2015). "Unpredictable tensile strength biomechanics may limit thawed cadaver use for simulant research." Journal of Forensic Sciences **0618**(February): 1-5.

Maitland, L. A., E. R. Myers, et al. (1993). "Read my hips: measuring trochanteric soft tissue thickness." Calcif Tissue Int **52**(8443696): 85-89.

Majumder, S., A. Roychowdhury, et al. (2004). "Dynamic response of the pelvis under side impact load–a three-dimensional finite element approach." International Journal of Crashworthiness **9**(1): 89-103.

Majumder, S., A. Roychowdhury, et al. (2007). "Simulation of hip fracture in sideways fall using a 3D finite element model of pelvis–femur–soft tissue complex with simplified representation of whole body." Medical Engineering & Physics **29**(10): 1167-1178.

Majumder, S., A. Roychowdhury, et al. (2008). "Effects of trochanteric soft tissue thickness and hip impact velocity on hip fracture in sideways fall through 3D finite element simulations." Journal of biomechanics **41**(13): 2834-2842.

Majumder, S., A. Roychowdhury, et al. (2008). "Three-dimensional finite element simulation of pelvic fracture during side impact with pelvis-femur-soft tissue complex." International Journal of Crashworthiness **13**(3): 313-329.

Majumder, S., A. Roychowdhury, et al. (2009). "Effects of body configuration on pelvic injury in backward fall simulation using 3D finite element models of pelvis–femur–soft tissue complex." Journal of biomechanics **42**(10): 1475-1482.

Majumder, S., A. Roychowdhury, et al. (2013). "Hip fracture and anthropometric variations: Dominance among trochanteric soft tissue thickness, body height and body weight during sideways fall." Clinical Biomechanics **28**(9): 1034-1040.

Makhsous, M., F. Lin, et al. (2011). "Use of MRI images to measure tissue thickness over the ischial tuberosity at different hip flexion." Clin Anat **24**(21647964): 638-645.

Makhsous, M., G. Venkatasubramanian, et al. (2008). "Investigation of soft-tissue stiffness alteration in denervated human tissue using an ultrasound indentation system." The journal of spinal cord medicine **31**(1): 88-96.

Manske, S. L., T. Liu-Ambrose, et al. (2006). "Femoral neck cortical geometry measured with magnetic resonance imaging is associated with proximal femur strength." Osteoporosis International **17**(10): 1539-1545.

Marks, R., J. Allegrante, et al. (2003). "Hip fractures among the elderly: causes, consequences and control." Ageing research reviews **2**(1): 57-93.

Martel, D. (2017). Development and Application of a Probabilistic/Mechanistic Model to Investigate the Influence of Safety Flooring on Population-Level Hip Fracture Risk, University of Waterloo.

Masud, T., N. Binkley, et al. (2011). "Official positions for FRAX® clinical regarding falls and frailty: can falls and frailty be used in FRAX®?: from Joint Official Positions Development Conference of the International Society for Clinical Densitometry and International Osteoporosis Foundation on FRAX®." Journal of Clinical Densitometry **14**(3): 194-204.

Matsui, Y., J. Kajzer, et al. (2003). Injury pattern and tolerance of human pelvis under lateral loading simulating car-pedestrian impact, SAE Technical Paper.

Matsui, Y., J. Kajzer, et al. (2003). "Injury pattern and tolerance of human pelvis under lateral loading simulating car-pedestrian impact." SAE International **2003-01-01**(724): 1-12.

Matthews, L. S. and D. Ellis (1968). "Viscoelastic properties of cat tendon: Effects of time after death and preservation by freezing." Journal of biomechanics **1**(2): 65-71.

Mayhew, P. M., C. D. Thomas, et al. (2005). "Relation between age, femoral neck cortical stability, and hip fracture risk." The Lancet **366**(9480): 129-135.

McCloskey, E. V., S. Vasikaran, et al. (2011). "Official Positions for FRAX® Clinical Regarding Biochemical Markers: From Joint Official Positions Development Conference of the International Society for Clinical Densitometry and International Osteoporosis Foundation on FRAX®." Journal of Clinical Densitometry **14**(3): 220-222.

Menegoni, F., M. Galli, et al. (2009). "Gender- specific Effect of Obesity on Balance." Obesity **17**(10): 1951-1956.

Meyer, H., A. Tverdal, et al. (1998). "Weight Variability, Weight Change and the Incidence of Hip Fracture: A Prospective Study of 39000 Middle-aged Norwegians." Osteoporosis International **8**(4): 373-378.

Millard, M., E. Kubica, et al. (2011). "Forward dynamic human gait simulation using a SLIP target model." Procedia IUTAM **2**: 142-157.

Moon, Y. and J. J. Sosnoff (2017). "Safe Landing Strategies During a Fall: Systematic Review and Meta-Analysis." Archives of Physical Medicine and Rehabilitation **98**(4): 783-794.

Moreno, J. and F. Forriol (2002). "Effects of preservation on the mechanical strength and chemical composition of cortical bone: An experimental study in sheep femora." Biomaterials **23**(12): 2615-2619.

Mow, V., S. Kuei, et al. (1980). "Biphasic creep and stress relaxation of articular cartilage in compression: theory and experiments." Journal of biomechanical engineering **102**(1): 73-84.

Muksian, R. and C. D. Nash (1976). "On frequency-dependent damping coefficients in lumped-parameter models of human beings." Journal of biomechanics **9**(5): 339-342.

Nankaku, M., H. Kanzaki, et al. (2005). "Evaluation of hip fracture risk in relation to fall direction." Osteoporosis International **16**(11): 1315-1320.

Nasiri, M. and Y. Luo (2016). "Study of sex differences in the association between hip fracture risk and body parameters by DXA-based biomechanical modeling." Bone **90**: 90-98.

Nazarian, A., B. J. Hermannsson, et al. (2009). "Effects of tissue preservation on murine bone mechanical properties." Journal of biomechanics **42**(1): 82-86.

NCGC (2012). Osteoporosis: Fragility Fracture Risk: Osteoporosis: Assessing the Risk of Fragility Fracture. NICE Clinical Guidelines. R. C. o. P. U. National Clinical Guideline Centre (UK). **146**.

Neuman, M. D., J. H. Silber, et al. (2014). "Survival and Functional Outcomes After Hip Fracture Among Nursing Home Residents." JAMA internal medicine **174**(8): 1273.

Nevitt, M. and S. Cummings (1993). "Type of fall and risk of hip and wrist fractures: the study of osteoporotic fractures. The Study of Osteoporotic Fractures Research Group." Journal of the American Geriatrics Society **41**(11): 1226.

Nguyen, N., S. Frost, et al. (2008). "Development of prognostic nomograms for individualizing 5-year and 10-year fracture risks." Osteoporosis International **19**(10): 1431-1444.

Nielson, C. M., M. L. Bouxsein, et al. (2009). "Trochanteric soft tissue thickness and hip fracture in older men." Journal of Clinical Endocrinology & Metabolism **94**(2): 491.

Nielson, C. M., P. Srikanth, et al. (2012). "Obesity and fracture in men and women: an epidemiologic perspective." Journal of Bone and Mineral Research **27**(1): 1-10.

Ochi, M., Y. Tabara, et al. (2010). "Quadriceps sarcopenia and visceral obesity are risk factors for postural instability in the middle- aged to elderly population." Geriatrics & gerontology international **10**(3): 233-243.

OIDR (2012). Ontario Injury Data Report, Ontario Injury Prevention Resource Center.

Oomens, C. W. J., O. Bressers, et al. (2003). "Can loaded interface characteristics influence strain distributions in muscle adjacent to bony prominences?" Computer methods in biomechanics and biomedical engineering **6**(3): 171-180.

Padture, N. (2001). "Hertzian contacts." Encyclopaedia of materials: science and technology: 3750-3752.

Palevski, A., I. Glaich, et al. (2006). "Stress relaxation of porcine gluteus muscle subjected to sudden transverse deformation as related to pressure sore modeling." Journal of biomechanical engineering **128**(5): 782-787.

Pel, J., C. Spoor, et al. (2008). "Biomechanical analysis of reducing sacroiliac joint shear load by optimization of pelvic muscle and ligament forces." Annals of biomedical engineering **36**(3): 415-424.

Pennal, G. F., M. Tile, et al. (1980). "Pelvic disruption: assessment and classification." Clinical orthopaedics and related research **151**: 12-21.

Peters, A., B. Galna, et al. (2010). "Quantification of soft tissue artifact in lower limb human motion analysis: a systematic review." Gait & posture **31**(1): 1-8.

Pinilla, T., K. Boardman, et al. (1996). "Impact direction from a fall influences the failure load of the proximal femur as much as age-related bone loss." Calcified tissue international **58**(4): 231-235.

Pool-Goudzwaard, A., G. H. van Dijke, et al. (2004). "Contribution of pelvic floor muscles to stiffness of the pelvic ring." Clinical Biomechanics **19**(6): 564-571.

Pretty, S. P., D. R. Martel, et al. (2017). "The influence of body mass index, sex, & muscle activation on pressure distribution during lateral falls on the hip." Annals of biomedical engineering: 1-9.

Pulkkinen, P., F. Eckstein, et al. (2006). "Association of geometric factors and failure load level with the distribution of cervical vs. trochanteric hip fractures." Journal of Bone and Mineral Research **21**: 895-901.
Pulkkinen, P., T. Jämsä, et al. (2008). "Experimental hip fracture load can be predicted from plain radiography by combined analysis of trabecular bone structure and bone geometry." Osteoporosis International **19**(4): 547-558.
Pulkkinen, P., T. Jämsä, et al. (2008). "Experimental hip fracture load can be predicted from plain radiography by combined analysis of trabecular bone structure and bone geometry." Osteoporosis International **19**(4): 547-558.
Pulkkinen, P., S. Saarakkala, et al. (2013). "Standard Radiography: Untapped Potential in the Assessment of Osteoporotic Fracture Risk." European Radiology **23**(5): 1375-1382.
Queen, R. M., P. S. Weinhold, et al. (2003). "Theoretical study of the effect of ball properties on impact force in soccer heading." Medicine & Science in Sports & Exercise **35**(12): 2069-2076.
Reid, I. (2008). "Relationships between fat and bone." Osteoporosis International **19**(5): 595-606.
Reid, I. R. (2002). "Relationships among body mass, its components, and bone." BoneKEy-Osteovision.
Riggs, B. L. and L. J. Melton (1995). "The worldwide problem of osteoporosis: Insights afforded by epidemiology." Bone **17**(5, Supplement 1): S505-S511.
Robinovitch, S., W. Hayes, et al. (1991). "Prediction of femoral impact forces in falls on the hip." Journal of biomechanical engineering **113**: 366.
Robinovitch, S., W. Hayes, et al. (1997). "Distribution of contact force during impact to the hip." Annals of biomedical engineering **25**(3): 499-508.
Robinovitch, S., W. Hayes, et al. (1997). "Predicting the impact response of a nonlinear single-degree-of-freedom shock-absorbing system from the measured step response." Journal of biomechanical engineering **119**: 221.
Robinovitch, S., T. McMahon, et al. (1995). "Force attenuation in trochanteric soft tissues during impact from a fall." Journal of Orthopaedic Research **13**(6): 956-962.
Robinovitch, S. N., R. Brumer, et al. (2004). "Effect of the" squat protective response" on impact velocity during backward falls." Journal of biomechanics **37**(9): 1329.
Robinovitch, S. N., J. Chiu, et al. (2000). "Impact severity in self-initiated sits and falls associates with center-of-gravity excursion during descent." Journal of biomechanics **33**(7): 863-870.
Robinovitch, S. N., S. L. Evans, et al. (2009). "Hip Protectors: Recommendations for Biomechanical Testing – an International Consensus Statement (part I)." Osteop Int **20**(12): 1977-1988.
Robinovitch, S. N., F. Feldman, et al. (2013). "Video capture of the circumstances of falls in elderly people residing in long-term care: an observational study." Lancet **381**(9860): 47-54.
Robinovitch, S. N., W. C. Hayes, et al. (1997). "Predicting the impact response of a nonlinear single-degree-of-freedom shock-absorbing system from the measured step response." Journal of biomechanical engineering **119**: 221-221.
Robinovitch, S. N., L. Inkster, et al. (2003). "Strategies for avoiding hip impact during sideways falls." Journal of Bone and Mineral Research **18**(7): 1267-1273.
Rosatelli, A. L., A. M. Agur, et al. (2006). "Anatomy of the interosseous region of the sacroiliac joint." Journal of Orthopaedic & Sports Physical Therapy **36**(4): 200-208.
Rosen, J. and M. Arcan (2003). "Modeling the human body/seat system in a vibration environment." Journal of biomechanical engineering **125**(2): 223-231.

Rothney, M. P., R. J. Brychta, et al. (2009). "Body Composition Measured by Dual- energy X- ray Absorptiometry Half- body Scans in Obese Adults." Obesity **17**(6): 1281-1286.
Rouleau, L., D. Tremblay, et al. (2012). "Regional variations in canine descending aortic tissue mechanical properties change with formalin fixation." Cardiovascular Pathology **21**(5): 390-397.
Roy, A. and J. A. Carretero (2012). "A damping term based on material properties for the volume-based contact dynamics model." International Journal of Non-Linear Mechanics **47**(3): 103-112.
Sabick, M., J. Hay, et al. (1999). "Active responses decrease impact forces at the hip and shoulder in falls to the side." Journal of biomechanics **32**(9): 993-998.
Sahin, V., E. S. Karakas, et al. (2003). "Traumatic dislocation and fracture-dislocation of the hip: a long-term follow-up study." Journal of Trauma and Acute Care Surgery **54**(3): 520-529.
Salzar, R. S., D. Genovese, et al. (2009). "Load path distribution within the pelvic structure under lateral loading." International Journal of Crashworthiness **14**(1): 99-110.
Sanders, A. P. and R. M. Brannon (2011). "Assessment of the applicability of the Hertzian contact theory to edge-loaded prosthetic hip bearings." Journal of biomechanics **44**(16): 2802-2808.
Sandler, R. and S. Robinovitch (2001). "An analysis of the effect of lower extremity strength on impact severity during a backward fall." Journal of biomechanical engineering **123**(6): 590-598.
Sarvi, M. N. and Y. Luo (2015). A Compound Risk Indicator for Subject-Specific Prediction of Hip Fracture in Sideways Falls. ASME 2015 International Design Engineering Technical Conferences and Computers and Information in Engineering Conference, American Society of Mechanical Engineers.
Sarvi, M. N. and Y. Luo (2015). "Development of an Image-Based Biomechanical Model for Assessment of Hip Fracture Risk." Development **1**: 34060.
Sarvi, M. N. and Y. Luo (2015). "A Two-Level Subject-Specific Biomechanical Model for Improving Prediction of Hip Fracture Risk." Clinical Biomechanics.
Sarvi, M. N., Y. Luo, et al. (2014). "Experimental validation of subject-specific dynamics model for predicting impact force in sideways fall." Journal of Biomedical Science and Engineering **7**(07): 405.
Scheyerer, M. J., G. Osterhoff, et al. (2012). "Detection of posterior pelvic injuries in fractures of the pubic rami." Injury **43**(8): 1326-1329.
Schmitt, K.-U., P. F. N. E. Zürich, et al. (2014). Trauma Biomechanics: An Introduction to Injury Biomechanics, Springer Science & Business Media.
Schneider, P., W. Börner, et al. (1993). "Bone density for prediction of hip fracture." The Lancet **341**(8850): 962-963.
Serina, E. R., C. Mote, et al. (1997). "Force response of the fingertip pulp to repeated compression—effects of loading rate, loading angle and anthropometry." Journal of biomechanics **30**(10): 1035-1040.
Shapses, S. A. and D. Sukumar (2012). "Bone metabolism in obesity and weight loss." Annual review of nutrition **32**: 287.
Shourijeh, M. S. and J. McPhee (2014). "Forward Dynamic Optimization of Human Gait Simulations: A Global Parameterization Approach." Journal of Computational and Nonlinear Dynamics **9**(3): 031018.

Shourijeh, M. S. and J. McPhee (2015). "Foot-ground contact modeling within human gait simulations: from Kelvin-Voigt to hyper-volumetric models." Multibody System Dynamics **35**(4): 393-407.
SMARTRISK (2009). The Economic Burden of Injury in Canada.
Smeathers, J. E. and D. N. Joanes (1988). "Dynamic compressive properties of human lumbar intervertebral joints: A comparison between fresh and thawed specimens." Journal of biomechanics **21**(5): 425-433.
Smeesters, C., W. C. Hayes, et al. (2001). "Disturbance type and gait speed affect fall direction and impact location." Journal of biomechanics **34**(3): 309-317.
Smidt, G. L., S.-H. Wei, et al. (1997). "Sacroiliac motion for extreme hip positions: a fresh cadaver study." Spine **22**(18): 2073-2082.
Smulders, E., V. Weerdesteyn, et al. (2010). "Efficacy of a short multidisciplinary falls prevention program for elderly persons with osteoporosis and a fall history: a randomized controlled trial." Archives of Physical Medicine and Rehabilitation **91**(11): 1705-1711.
Song, E., X. Trosseille, et al. (2006). "Side impact: influence of impact conditions and bone mechanical properties on pelvic response using a fracturable pelvis model." Stapp car crash journal **50**: 75.
Sran, M. M. and S. N. Robinovitch (2008). "Preventing fall-related vertebral fractures: effect of floor stiffness on peak impact forces during backward falls." Spine **33**(17): 1856-1862.
Sran, M. M., P. J. Stotz, et al. (2009). "Age Differences in Energy Absorption in the Upper Extremity During a Descent Movement: Implications for Arresting a Fall." The Journals of Gerontology Series A: Biological Sciences and Medical Sciences **65A**(3): 312-317.
Sran, M. M., P. J. Stotz, et al. (2010). "Age differences in energy absorption in the upper extremity during a descent movement: Implications for arresting a fall." Journals of Gerontology - Series A Biological Sciences and Medical Sciences **65 A**(3): 312-317.
Stinchcombe, A., N. Kuran, et al. (2014). Seniors' falls in Canada: Second report: Key highlights.
Stone, K. L., D. G. Seeley, et al. (2003). "BMD at multiple sites and risk of fracture of multiple types: long- term results from the Study of Osteoporotic Fractures." Journal of Bone and Mineral Research **18**(11): 1947-1954.
Studer, P., N. Suhm, et al. (2013). "Pubic rami fractures in the elderly - A neglected injury?" Swiss Medical Weekly **143**(September): 1-7.
Szarko, M., K. Muldrew, et al. (2010). "Freeze-thaw treatment effects on the dynamic mechanical properties of articular cartilage." BMC musculoskeletal disorders **11**(1): 231-231.
Taddei, F., I. Palmadori, et al. (2014). "European Society of Biomechanics SM Perren Award 2014: Safety factor of the proximal femur during gait: A population-based finite element study." Journal of biomechanics **47**(14): 3433-3440.
Tanaka, S., T. Kuroda, et al. (2013). "Overweight/obesity and underweight are both risk factors for osteoporotic fractures at different sites in Japanese postmenopausal women." Osteoporosis International **24**(1): 69-76.
Tile, M., D. Helfet, et al. (2003). Fractures of the pelvis and acetabulum, Lippincott Williams & Wilkins.
Topp, T., T. Müller, et al. (2012). "Embalmed and fresh frozen human bones in orthopedic cadaveric studies: which bone is authentic and feasible?" Acta Orthopaedica **83**(5): 543-547.
Torimitsu, S., Y. Nishida, et al. (2014). "Effects of the freezing and thawing process on biomechanical properties of the human skull." Leg Med **16**(2): 102-105.

Travison, T. G., A. B. Araujo, et al. (2008). "Lean mass and not fat mass is associated with male proximal femur strength." Journal of Bone and Mineral Research **23**(2): 189-198.
Van den Kroonenberg, A., W. Hayes, et al. (1995). "Dynamic models for sideways falls from standing height." TRANSACTIONS-AMERICAN SOCIETY OF MECHANICAL ENGINEERS JOURNAL OF BIOMECHANICAL ENGINEERING **117**: 309-309.
van den Kroonenberg, A., W. Hayes, et al. (1996). "Hip impact velocities and body configurations for voluntary falls from standing height." Journal of biomechanics **29**(6): 807-811.
Van der Zijden, A., B. Groen, et al. (2012). "Can martial arts techniques reduce fall severity? An< i> in vivo</i> study of femoral loading configurations in sideways falls." Journal of biomechanics **45**(9): 1650-1655.
van der Zijden, A., B. Groen, et al. (2017). "Estimating severity of sideways fall using a generic multi linear regression model based on kinematic input variables." Journal of biomechanics **54**: 19-25.
van Haaren, E. H., B. C. van der Zwaard, et al. (2008). "Effect of long-term preservation on the mechanical properties of cortical bone in goats." Acta Orthopaedica **79**(5): 708-716.
Van Loocke, M., C. Lyons, et al. (2008). "Viscoelastic properties of passive skeletal muscle in compression: stress-relaxation behaviour and constitutive modelling." Journal of biomechanics **41**(7): 1555-1566.
Venkatasubramanian, R. T., W. F. Wolkers, et al. (2010). "Freeze–thaw induced biomechanical changes in arteries: role of collagen matrix and smooth muscle cells." Annals of biomedical engineering **38**(3): 694-706.
Viano, D. C., I. V. Lau, et al. (1989). "Biomechanics of the human chest, abdomen, and pelvis in lateral impact." Accident Analysis & Prevention **21**(6): 553-574.
Wang, T. and Z. Feng (2005). "Dynamic mechanical properties of cortical bone: The effect of mineral content." Materials Letters **59**(18): 2277-2280.
Wang, X., X. Shen, et al. (2002). "Age-related changes in the collagen network and toughness of bone." Bone **31**(1): 1-7.
Weerdesteyn, V., B. Groen, et al. (2008). "Martial arts fall techniques reduce hip impact forces in naive subjects after a brief period of training." Journal of Electromyography and Kinesiology **18**(2): 235-242.
Wettli, A., B. Cook, et al. (2017). Developing a Method of Slowing Brain Tissue Degradation through Temperature, Sodium Bicarbonate and Antibiotics for Traumatic Brain Injury Testing. 13th Annual Injury Biomechanics Symposium. Columbus, OH.
Wilke, H.-J., S. Krischak, et al. (1996). "Formalin fixation strongly influences biomechanical properties of the spine." Journal of biomechanics **29**(12): 1629-1631.
Winter, D. A. (2009). Biomechanics and motor control of human movement, John Wiley & Sons.
WISQARS, C. (2005). Nonfatal Hospitalized Injuries, Both Sexes, All Ages, United States, 2005

Web-based Injury Statistics Query and Reporting System. C. f. D. C. a. Prevention.
Wright, A. D. and A. C. Laing (2012). "The influence of headform orientation and flooring systems on impact dynamics during simulated fall-related head impacts." Medical Engineering & Physics **34**(8): 1071-1078.
Wu, G., S. Siegler, et al. (2002). "ISB recommendation on definitions of joint coordinate system of various joints for the reporting of human joint motion--part I: ankle, hip, and spine. International Society of Biomechanics." J Biomech **35**(11934426): 543-548.

Yang, Y., R. Schonnop, et al. (2013). "Development and validation of a questionnaire for analyzing real-life falls in long-term care captured on video." BMC geriatrics **13**(1): 40.

Zdero, R., Z. S. Bagheri, et al. (2014). "The Biomechanical Effect of Loading Speed on Metal-on-UHMWPE Contact Mechanics." The open biomedical engineering journal **8**: 28.

Appendix 1 Do Obese Long-Term Care Residents Fall Differently than Underweight Residents?

This is a brief summary of an ongoing epidemiological study of the fall circumstances and characteristics of older adults in long-term care. The results included here were presented at the 4th Canadian Obesity Summit, April 28 – May 2, 2015

A1.1 Introduction

While underweight fallers suffer the greatest rate of hip and wrist fractures, obese fallers are also susceptible to lower leg and ankle fragility fractures. Differences in balance control mechanisms, control of body segments during a fall, and impact mechanics may help explain these differences. The goal of this study was to determine whether there were differences in fall cause and circumstances between older adults with high BMI and low BMI who suffered falls.

A1.2 Methods

A validated questionnaire (Yang, Schonnop et al. 2013) was used to analyze real-life fall videos of 25 low-BMI (lowest-available quartile, BMI <20.8) and 25 high-BMI (highest-available quartile, BMI >27.6) older-adult long-term care (LTC) residents to determine the cause and circumstances of each incident. Comparisons were made between BMI groups for the initiation, descent and impact stages of the fall. For the purpose of this appendix, results for all participants, as well as Low- and High-BMI groups separately are presented.

A1.3 Results

Low and high BMI groups did not differ in age (mean (SD) 81.5 (10.1), t=1.036, p=0.306) sex distribution (62% female, X^2=0.764, p=0.382), number of comorbidities (1.5 (0.97), t=0.722, p=0.549), mobility aid use (78% not in use, X^2=1.049, p=0.306), attempts to grasp objects or impacting segments.

For all fall types, there was no effect of BMI on cause of fall (X^2=7.485, p=0.112). The vast majority of fallers were either walking (52) or standing (42%, Figure A.1). For all fallers, incorrect weight transfer was the most frequent cause of falls from standing height (56%, Figure A.2), followed by tripping or stumbling (24%), and contacting another person or object with a hit or bump (22%). However, when compared to all other fall causes, secondary analysis revealed that fallers with high BMI suffered three times more trips (36% vs. 12% of falls within high vs low-BMI group) than low-BMI fallers, respresenting more than a third of all fall causes in that group.

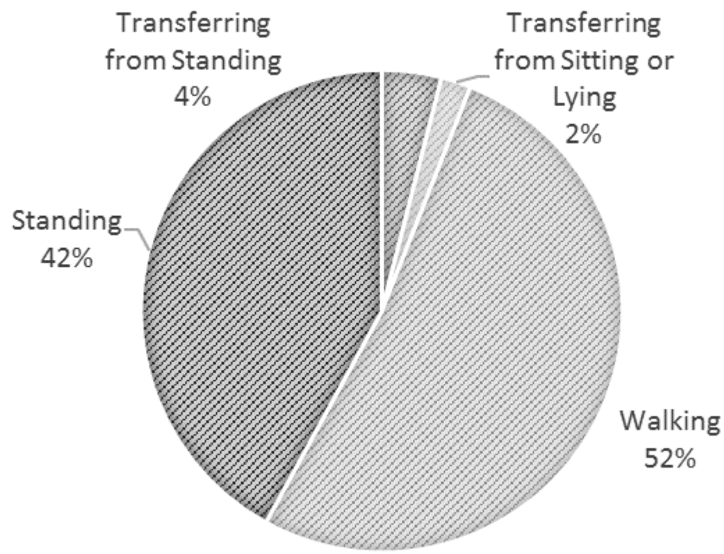

Figure A1.1 Preceding Activity, All Participants

A large majority of fallers were either walking or standing prior to the fall incident. Less than 10% of falls occurred while the resident was transferring from a sitting or standing position.

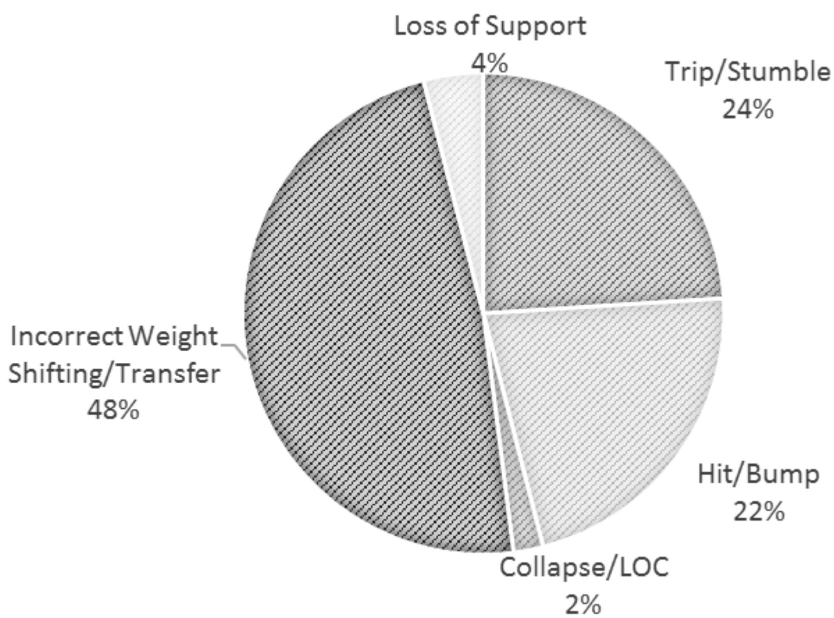

Figure A1.2 Fall Cause, All Participants

There was no effect of BMI on cause of fall. Half of the falls occurred due to internal factors, such as incorrect weight shifting or collapse. The remaining half occurred due to interactions with other residents or environmental causes, such as loss of support, trip or stumble, and hit or bump. However, secondary analysis revealed that tripping or stumbling fall causes were more common in residents with high BMI

There were no BMI-related differences in whether or not the fallers attempted to use a stepping response to prevent a fall (34% no, X^2=0.089, p=0.765), whether fallers used more than one step (75.8% more than one step, X^2=0.010, p=0.922), or the primary direction of stepping (X^2=2.762, p=0.430, Figure A1.3). However, fallers with high BMI are less likely to use large stepping responses (X^2=8.384, p=0.039, Figure A1.4). There was no difference in whether or not an attempt was made to grasp a stabilizing object (62% no attempt, X^2=0.085, p=0.771).

There were no effect of BMI group on primary initial fall direction (X^2=1.529, p=0.675, Figure A1.5) or primary landing direction (X^2=3.635, p=0.162, Figure A1.6). For both groups, there was a significant relationship between initial falling direction and landing direction (low BMI, X^2=16.674, p=0.011; high BMI, X^2=16.424, p=0.012).

BMI group had no effect on whether or not a body segment visibly impacted the ground (Table A1.1), however, 60% of fallers with high BMI impacted a knee during their fall vs. 36% of low-BMI fallers, approaching significance.

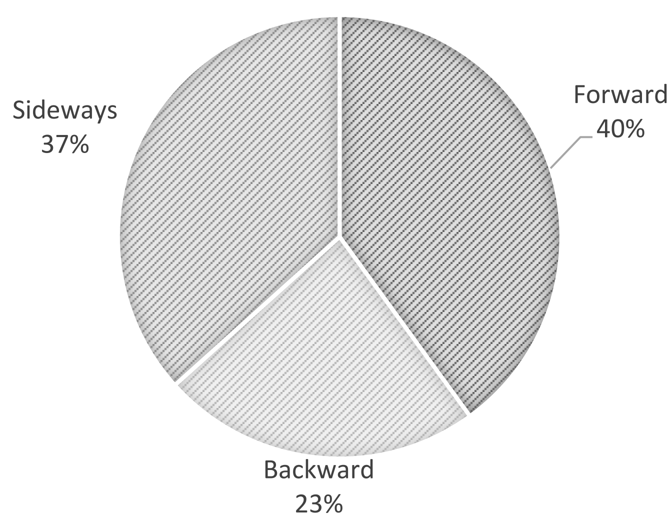

Figure A1.3 Primary Direction of Stepping Response, All Participants

There was no difference in primary stepping direction between high- and low-BMI fallers. Fallers mainly used forward or sideways stepping strategies.

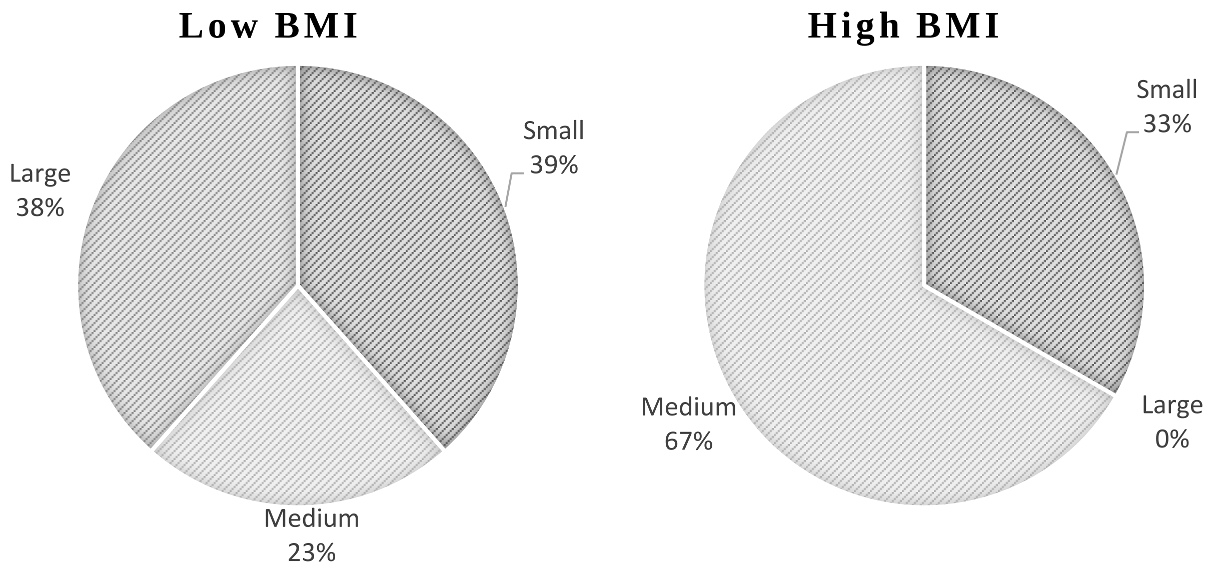

Figure A1.4 Size of Stepping Response, By Group

High-BMI fallers were less likely to use large stepping responses than low-BMI fallers, and relied primarily on medium reactive stepping responses.

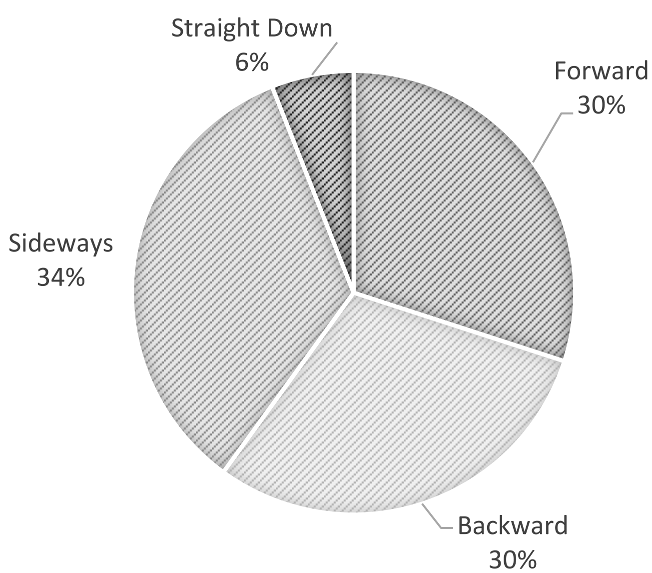

Figure A1.5 Primary Initial Falling Direction, All Participants

There were no BMI-related differences in initial falling direction, with fallers falling forward, sideways and backwards in approximately equal frequency.

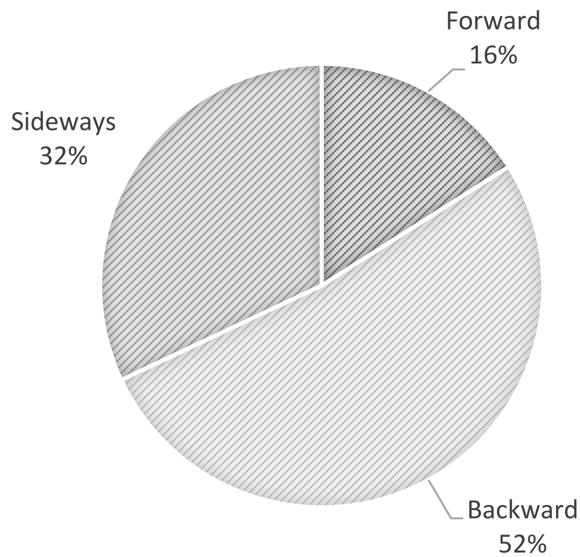

Figure A1.6 Primary Landing Direction, All Participants

There were no BMI-related differences in landing direction, with the majority of fallers landing in a primarily backwards configuration.

Table A1.1 Crosstabulation for Change in Fall Configuration, Low BMI

			Primary Landing Direction			
			Forward	**Backward**	**Sideways**	**Total**
Initial Falling Direction	Forward	Count	4	1	1	6
		Within Initial	66.7%	16.7%	16.7%	100.0%
		Within Landing	100.0%	6.3%	20.0%	24.0%
	Backward	Count	0	7	1	8
		Within Initial	0.0%	87.5%	12.5%	100.0%
		Within Landing	0.0%	43.8%	20.0%	32.0%
	Sideways	Count	0	7	3	10
		Within Initial	0.0%	70.0%	30.0%	100.0%
		Within Landing	0.0%	43.8%	60.0%	40.0%
	Straight Down	Count	0	1	0	1
		Within Initial	0.0%	100.0%	0.0%	100.0%
		Within Landing	0.0%	6.3%	0.0%	4.0%
Total		Count	4	16	5	25
		Within Initial	16.0%	64.0%	20.0%	100%
		Within Landing	100.0%	100.0%	100.0%	10%

Table A.2 Crosstabulation for Change in Fall Configuration, High BMI

			Primary Landing Direction			
			Forward	Backward	Sideways	Total
Initial Falling Direction	Forward	Count	2	1	6	9
		Within Initial	22.2%	11.1%	66.7%	100.0%
		Within Landing	50.0%	10.0%	54.5%	36.0%
	Backward	Count	0	7	0	7
		Within Initial	0.0%	100.0%	0.0%	100.0%
		Within Landing	0.0%	70.0%	0.0%	28.0%
	Sideways	Count	1	2	4	7
		Within Initial	14.3%	28.6%	57.1%	100.0%
		Within Landing	25.0%	20.0%	36.4%	28.0%
	Straight Down	Count	1	0	1	2
		Within Initial	50.0%	0.0%	50.0%	100.0%
		Within Landing	25.0%	0.0%	9.1%	8.0%
Total		Count	4	4	10	11
		Within Initial	16.0%	16.0%	40.0%	44.0%
		Within Landing	100.0%	100.0%	100.0%	100.0%

Table A.3 Impacting Body Segments, All Participants

Segment	Percent of Falls Impacted	X^2	p
Head	34	0.802	0.370
Hip	30	0.857	0.355
Hand	30	0.095	0.758
Knee	52	2.885	0.089

A1.4 Discussion and Implications for this Thesis

The majority of falls (94%) occur during standing-height activities, suggesting that velocities associated with standing height are a realistic initial condition for model simulations. However, more than half of falls resulted in impacts to the knee; a kneeling start position for experimental studies, as well as a lower impact velocity for model simulations may be realistic conditions, and therefore will be incorporated into Studies 1 and 3.

Smaller step responses were observed in overweight fallers than underweight fallers. This may be due to larger limb segment inertia or lower foot-floor clearance, as proposed by Madigan and colleagues (2014), and is less effective for preventing falls (Weerdesteyn, Groen et al. 2008). These results match experimental results (Garman, Scanlon et al. 2014) and injury patterns (Armstrong, Cairns et al. 2012) reported in literature, with a greater rate of tripping by fallers with high BMI than low BMI. Tripping falls and smaller step responses could contribute to the generation of larger moments at the ankle prior to impact which may increase ankle injury risk. This higher rate of falls caused by tripping or stumbling in participants with high BMI indicates that it may be valuable in the future to include initial forward velocity and acceleration components in model simulations. Step responses were primarily in the forward or sideways direction, supporting theories by Nankaku and colleagues (2005) that it is more challenging to employ protective responses during backwards falls.

Excluding the “straight down” falling direction, falls were fairly evenly split between forwards, sideways and backwards initial falling directions, though backwards was the dominant landing configuration (52%) followed by sideways (32%), supporting the theory that rotation during falls may be a critical element in determining injury outcome. Fallers with low BMI typically rotated backwards during the falls, while direction of rotation was more mixed in fallers with high BMI. This may be related to greater anterior-posterior instability in fallers with high BMI (Corbeil, Simoneau et al. 2001; Menegoni, Galli et al. 2009). It may become important to incorporate this rotation in future modeling iterations to discover how it affects shear and rolling components of the impacting pelvis.

Appendix 2 Peak pressure and contact profile during sideways falls on the hip: links with individual characteristics and falling configuration

I.C. Levine and A.C. Laing
Department of Kinesiology, University of Waterloo, Waterloo, ON

Characterization of load distribution in the floor-pelvis contact plane during a fall may improve prediction of hip fracture risk, protective equipment design, and identification of "high-risk" falling configurations. Further, while estimation of the forces applied tothe hip during a fall can be achieved through multi-body modeling, Hertzian and volumetric contact models assume circular contact profiles. No published literature has linked falling configuration or soft tissue thickness (STT) with peak pressure or contact profile. The objective of this study was to test the hypotheses that (1) peak pressure would be greater in males and low-STT participants, as well as during fall simulation protocols (FSP: "Pelvis Release", "Kneeling Release" and "Squat Release") with less hip flexion; (2a) overall contact area and Harmonic 0 (mean radius) would be lower in males and low-STT participants, but similar between FSP; (2b)) the Pelvis Release protocol would produce contact profiles most circular in shape; (3) contact profile elements would negatively correlate with peak pressure. Forty-four young, healthy participants (23 female) consented to undergo an eighteen-trial protocol. STT was measured via ultrasound. Peak pressure, contact area and ellipse descriptors were quantified at time of peak pressure. No pressure or contact profile variable differed significantly between males and females. Peak pressure ranged from 307-9992 kPa, and differed between FSP. Contact Area and Harmonic 0 were lower for low-STT fallers, and lower during Pelvis Release. Contact profiles differed between STT-groups and FSP, and 76.1% of trials had contact profiles with eccentricity greater than 2.0. Peak pressure was negatively correlated with ellipse descriptors only during Pelvis Release. To summarize, peak pressure varied substantially only between falling configurations. However, contact profile characteristics were linked with peak pressure; unexplored individual characteristics or falling kinematics may drive these variables. Finally, contact profiles were substantially "round", but more work should examine the sensitivity of load prediction models to more complex contact profiles.

A2.1 Introduction

The primary theory linking trochanteric soft tissues with hip fracture suggests that fracture risk is reduced through energy absorption by the soft tissues (Cummings and Nevitt 1994; Hayes, Myers et al. 1996; Etheridge, Beason et al. 2005), with magnitude of absorption dependent on soft tissue thickness (STT) (Robinovitch, McMahon et al. 1995). This theory is linked to lower epidemiological risk of fracture in fallers with high BMI (Johansson, Kanis et al. 2014). Mechanistically, however, soft tissue thickness is predictive of fracture risk in women (Bouxsein, Szulc et al. 2007) but not men (Nielson, Bouxsein et al. 2009), though expected force, attenuated by soft tissue, was lower for controls than fracture cases in both studies. Further, despite noted difference in STT between sexes

(Levine, Minty et al. 2014), and positive correlation between body mass index (BMI) and STT (Levine, Minty et al. 2014, Robinovitch, Hayes et al. 1991), energy absorption during a lateral hip impact differs between BMI groups but not sexes (Bhan, Levine et al. 2014)\. Additionally, estimates of pelvic system stiffness differ between sexes but not BMI groups (Levine, Bhan et al. 2013). These inconsistencies highlight the need for further investigation of the mechanisms governing STT reduction of hip fracture risk.

The relationship between STT and reduction of load at the hip may be more complex than absorption of energy through one-dimensional compression. First, quantity of STT is not stagnant: apparent STT increases with degree of hip flexion (Levine, Minty et al. 2014), which would be reflected during falling configurations with differing magnitude of hip flexion. Second, soft tissue distribution of loads, i.e. pressure and contact profile, may be equally important as absorption. This more robust theory supports the design of hip protectors (Robinovitch, McMahon et al. 1995; Robinovitch, Evans et al. 2009) and safety floors Laing, Tootoonchi et al. 2006). Third, the majority of fall simulation protocols used to characterize impact dynamics are constrained to one axis (within the transverse plane of the pelvis); real-life falls comprise substantial non-vertical velocity and loading components. Better understanding of the three-dimensional nature of load distribution may improve prediction of hip fracture risk, protective equipment design, and identification of “high-risk” falling configurations. Therefore, pressure (loading localized at the “danger zone” directly overlying the proximal femur (Choi, Hoffer et al. 2010a; Choi, Hoffer et al. 2010b), or contact area (a measure of the distribution of loads) may improve prediction of hip fracture risk.

While rapid estimation of the forces applied to, and distributed between body segments during a fall can be achieved through multi-body modeling, Hertzian and volumetric contact models (Boos and McPhee, 2013; Gonthier, 2005) assume circular contact. Characterization of model parameters requires experimental data conforming to the force distribution assumptions. However, thigh contact during a simulated fall could increase the geometric eccentricity (deviation from circular) of the contact profile. It is unknown whether contact profiles during sideways falls impacting the hip are suitably ‘circular’ to characterize stiffness and damping parameters for such models.

Radial Fourier Analysis is a morphometric method using semilandmarks (a sequence of equiangular minor landmarks which define a curve) to quantify the shape of a two-dimensional outline such as a contact profile (Lohmann 1983). The method is commonly used in paleontology to discriminate species based on shape . The polar coordinates of the shape are analyzed to determine the primary elements which interfere to produce the curve, with harmonic number (H1…H*n*) indicating the number of lobes (circle=1, ellipse=2, trilobe=3…) and harmonic amplitude indicating the relative contribution of that lobe to the composite shape. Harmonic 0 quantifies the mean radius of the shape, and can be used to normalize the amplitude of H1…H*n*. Therefore, the analysis method can be both sensitive to, and independent of scale. In the context of contact profiles, H0 would be interpreted as a metric related to contact area, H1 would reflect the size of the circular portion of the contact profile, while H2 would indicate the elliptical shape of the contact profile, reflecting distal thigh contact. In contrast, eccentricity simply quantifies the elliptical component. However, these approaches have never been used to characterize contact profiles during lateral impacts with humans. It is also unclear whether Radial Fourier Analysis provides more relevant data regarding pressure distribution than simple eccentricity.

The primary objective of this study was to quantify differences in a) peak pressure, and b) contact profile, between sexes, STT group and fall simulation method, during simulated fall protocols designed to constrain or incorporate realistic falling characteristics. The second objective was to link changes in contact profile with peak pressure. We hypothesized that (1) peak pressure would be greater in males (compared to females) and low-STT participants (compared to mid- or high-STT participants), as well as during fall simulation protocols (FSP) with less hip flexion (i.e impact configurations with reduced available STT). Regarding contact profile, we hypothesized that (2a) indices of contact area would be lower in males (compared to females) and low-STT participants (compared to mid- or high-STT participants), but similar between FSP; (2b) the Pelvis Release protocol would produce contact profiles most circular in shape. Finally, we hypothesized that (3) contact profile elements would negatively correlate with peak pressure.

A2.2 Methods

Forty-four healthy participants (<35 years, 23 female) consented to participate in this study (Table 1). Participant recruitment focused on developing a cohort with a wide variety of body composition. Exclusion criteria included musculoskeletal injury in the past year preventing completion of the protocol, lifetime fracture history, fear of falling, or other health conditions which would make participation unsafe. Transverse-plane STT was assessed via ultrasound (minimum precision 0.17 cm; C60x, 2-5 MHz transducer, M-Turbo Ultrasound, SonoSite, Inc., Bothell, WA) in a side-lying position, similar to that expected during the impact phase of the fall simulations. Participants were grouped into low-, mid- and high-STT groups based the following criteria: males low <3, mid 3.1-4, high >4.1 cm; females low <3.5, mid 3.6-5, high >5 cm. These thresholds represent low- (<18.5 kg/m^2), moderate (18.6-25 kg/m^2) and high- (>25.1 kg/m^2) BMI older adults (unpublished data).

Table A2.1: Mean (SD) participant anthropometric characteristics.

		N	Height (m)	Mass (kg)	BMI (kg/m^2)	STT (cm)
Females						
	Low	7	1.62 (0.04)	54.0 (6.1)	20.4 (1.7)	3.0 (0.4)
STT	Mid	9	1.66 (0.06)	64.6 (10.3)	23.2 (2.8)	4.3 (0.4)
	High	7	1.66 (0.07)	85.8 (20.6)	31.5 (7.9)	6.9 (2.0)
Males						
	Low	8	1.80 (0.07)	72.5 (11.5)	22.4 (2.3)	2.3 (0.5)
STT	Mid	7	1.79 (0.08)	83.4 (10.9)	26.1 (3.2)	3.5 (0.5)
	High	6	1.77 (0.02)	92.1 (9.7)	28.7 (2.9)	8.9 (0.3)

STT represents trochanteric soft tissue thickness. BMI represents body mass index

A2.2.1 Experimental Protocol

An eighteen-trial fall simulation protocol (FSP) consisted of six blocks of trials, each block consisting of one Pelvis Release, one Kneeling Release and one Squat Release protocol (Figure 1), in randomized order. Blocks 1-3 were “training trials”, allowing for participant adaptation to the protocol; Blocks 4-6 were used to determine biomechanical outcomes. All paradigms involved the lateral aspect of the left hip impacting a pressure plate (4096 resistive sensors, each 0.762 by 0.508 cm, 500 Hz; FootScan, RSScan, Olen, Belgium) overlying a force plate (3500 Hz; OR6-7, AMTI, USA). The force and pressure plates were spatially aligned and temporally synchronized using a motion capture system (Optotrak Certus, Northern Digital, Inc., Waterloo, ON).

The primary difference between the protocols is the motion path of the pelvis: a controlled, vertical motion is produced during Pelvis Release, while Kneeling Release produces vertical and lateral motion in an inverted pendulum, and Squat Release typically has more lateral than vertical motion. For the Pelvis Release, the upper body of the participant was supported by a pillow outside the contact area of the force plate. For the Kneeling Release and Squat Release, the participant held a pillow throughout the trial to prevent bracing with their arms during the impact. The Pelvis Release protocol is highly controlled, and represents a scenario where the faller rotates into a horizontal position before impacting the hip directly laterally. The Kneeling Release reflects a scenario where the faller impacts the knee prior to rotating to impact the hip. The Squat release reflects a scenario where the faller flexes the knee, hip and ankle during the descent phase prior to rotating laterally to impact the hip.

In greater detail, for the initial position for Pelvis Release, hips were flexed to 45°, knees were flexed to 90°, and the pelvis was raised in a thin nylon sling using a turnbuckle until the soft tissues overlying the hip were 5 cm above the pressure plate. The participant was instructed to reduce the muscle tension in their body; when the participant reported that they were “relaxed and ready”, the electromagnet supporting the sling was released, allowing the pelvis of the participant to impact the pressure plate. For Kneeling and Squat Release, the participant was supported in the initial position by the researcher, was instructed to lean until their weight was supported by their left side, self-release, and fall “like a pendulum”. For kneeling release, the initial position was hips were flexed to 0°, knees were flexed to 90° and the lower leg was in contact with the starting mat. For Squat Release the initial position was a heel-lifted Squat, with maximal thigh-calf contact and an upright torso. Mean (SD) hip flexion angles for Pelvis, Kneeling and Squat release were 50.9 (28.6)°, 34.7

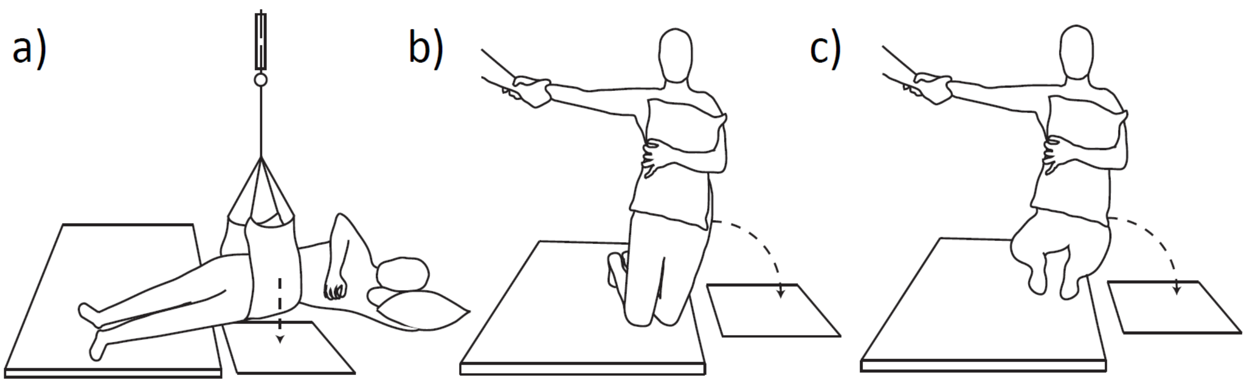

Figure A2.1 Initial position and motion path of the Pelvis (a), Kneeling (b), and Squat Release (c).

(20.0)° and 76.3 (13.2)°, respectively. A minimum of one minute of rest was provided between each trial, during which the participant was asked to stand or kneel without contact between the ground and trochanteric or gluteal soft tissues.

A2.2.2 Signal Processing

Data processing employed customized MATLAB routines (MathWorks, Natick, MA). Peak pressure magnitude (P_{peak}) was determined as the sensel with the greatest magnitude; associated location and time were also extracted. The contact profile (CP) associated with P_{peak_time} was further processed: first the CP was converted to a binary matrix, and an iterative algorithm was used to include active sensels within a three-sensel radius of sensels concurrent with $P_{peak\_location}$ at P_{peak_time}. The final CP was used to mask distal and proximal body segment contacts to determine Contact Area (*CA*). Polar coordinates (relative to $P_{peak\_location}$) were determined for the outermost sensels in the CP (Figure 2). The resulting waveform was resampled to produce a minimum of 100 samples between 0 and 2π. Major axis (*M*) was identified as the wafeform maximum; minor axis (m) was the minimum of the

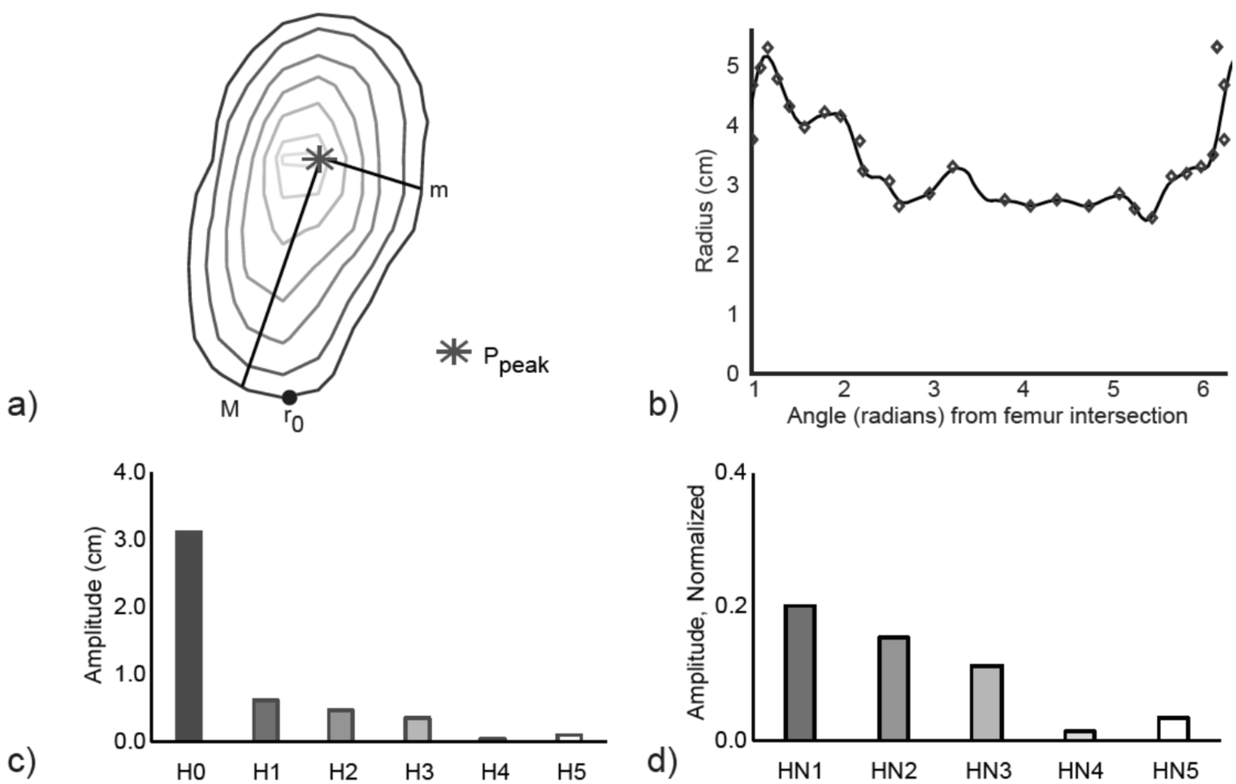

Figure A2.2 Analysis of the floor-pelvis contact profile. The perimeter of the contact area (indigo line, a) is used to develop a waveform (b). Beginning at the femur intersection point (r_0), radii are determined, including major axis (M) and minor axis (m). The waveform is analyzed to produce harmonic amplitudes (c) and normalized harmonic amplitudes (d).

data located $+\pi/2$ and $-\pi/2$ radians from *M*. Eccentricity was calculated as *M/m*. Fourier analysis on the repeated waveform generated mean radius (*H0*) and amplitude of *H1…H5*. Harmonics one through four were also normalized to *H0* (*HN1…HN5*) to determine the relative amplitude of each harmonic.

A2.2.3 Data Analysis

Statistical analysis was performed with a software package (SPSS version 21, Chicago, USA) using an α of 0.05. Mixed-model ANOVA was used to test hypotheses one and two, regarding dependent variables P_{peak} and contact profile components. FSP was treated as a repeated measure, and sex and STT-group as between-subjects factors. When Mauchly's test indicated violations of sphericity for repeated measures, a Greenhouse-Geisser adjustment was employed. A Bonferroni correction was used for STT-group pairwise comparisons to correct for multiple comparisons. Finally, Pearson Product-Moment Correlation (one-tailed) was used to assess the correlation between ellipse descriptors and P_{peak} for hypothesis three.

A2.3 Results

No pressure or contact profile variable differed significantly between males and females (Table A2.2).

Table A2.2: Main effects of sex

Hypothesis	Dependent Variable	F	p
1	P_{peak}	0.293	0.592
2a	*CA*	1.963	0.169
	Eccentricity	3.323	0.076
	H0	2.253	0.142
	H1	0.698	0.410
	H2	1.810	0.187
	H3	3.558	0.067
	H4	0.032	0.858
	H5	0.911	0.346
	HN1	0.028	0.869
	HN2	1.571	0.218
	HN3	3.742	0.061
	HN4	0.000	0.993
	HN5	0.717	0.402

Regarding hypothesis 1, P_{peak} ranged from 307-9992 kPa, and was 29.2% greater during Kneeling Release than Pelvis Release, 71.7% greater during Squat Release than Kneeling Release, and 122.0% greater during Squat Release than Pelvis Release, but not different between STT groups (Table A2.3, Figure A2.3).

Table A2.3: Main effects and significant pairwise comparisons for Hypothesis 1

Dependent Variable	Factor	Pair	F	t	p
	STT		1.179		0.318
	FSP		10.097		0.000**
P_{peak}		Kneeling vs. Pelvis		2.3	0.028*
		Squat vs. Kneeling		2.7	0.010*
		Squat vs. Pelvis		3.8	0.001**

* significant, p<0.05; ** significant, p<0.01

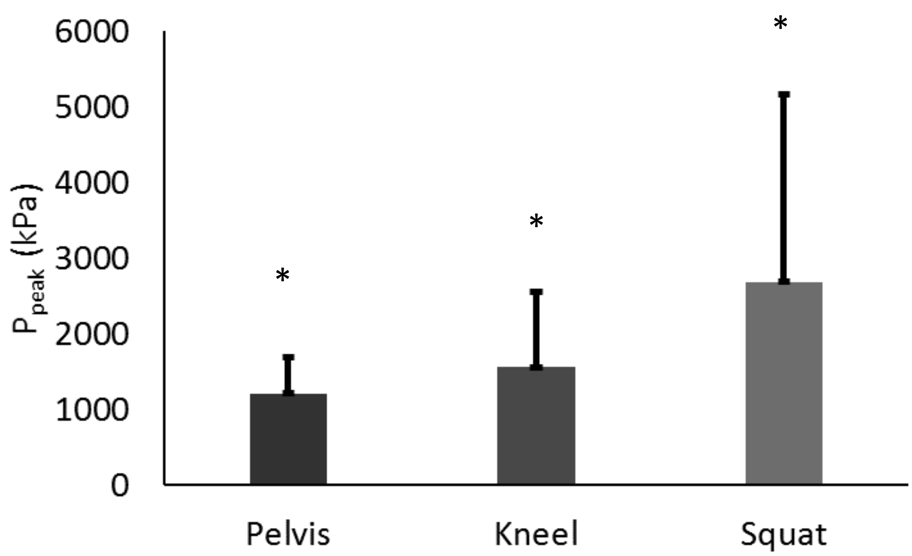

Figure A2.3: P_{peak} for all participants between FSP * all significantly different, p<0.05.

Regarding hypothesis 2a, *CA* and *H0* differed substantially between STT groups (Table 4, Figure 4a,c); in post hoc comparison, *CA* and *H0* were lower only for low-STT fallers. *CA* and *H0* were lower during Pelvis Release compared to Squat or Kneeling Release (Table 4, Figure 4b,d).

Table A2-4: Main effects and significant pairwise comparisons for Hypothesis 2a

Dependent Variable	Factor	Pair	F	t	p
CA	STT		8.892		0.001**
		Low vs. medium		-2.7	0.010*
		Low vs. high		-4.2	<0.001**
	FSP		3.9		0.025*
		Pelvis vs. Kneeling		-2.2	0.033*
		Pelvis vs. Squat		-2.4	0.020*
H0	STT		8.52		0.001**
		Low vs. medium		-3.5	0.001**
		Low vs. high		-4.0	<0.001**
	FSP		9.9		<0.001**
		Pelvis vs. Kneeling		-2.4	0.020*
		Pelvis vs. Squat		-11.1	<0.001**

*significant, p<0.05; ** significant, p<0.01

Regarding hypothesis 2b, eccentricity did not differ between FSP, or STT groups; 76.1% of trials resulted in contact profiles with eccentricity greater than 2.0. Interactions between FSP, STT and harmonics were primarily ordinal, and statistical results did not differ substantially between

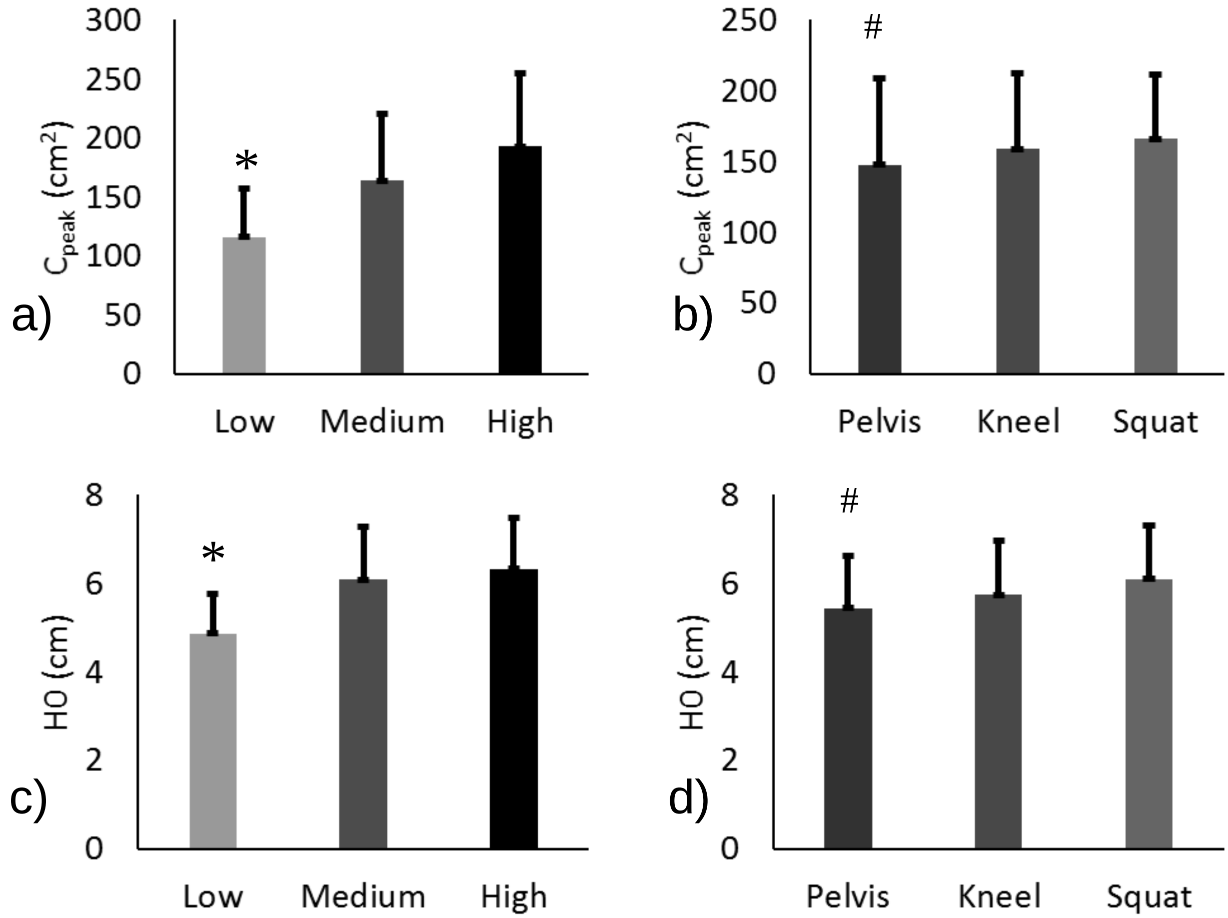

Figure A2.4: *H0* amplitude (solid) and *CA_{peak}* between STT groups (a,c) and FSP (b,d)
Significant differences, $p<0.05$: * Low-STT compared to Medium- and High-STT participants;
Pelvis Release compared to Kneeling or Squat Release.

absolute and normalized harmonics. Additionally, the average amplitude of *H3-H5* did not exceed 1 cm, and did not exceed 0.2 of the normalized signal power, therefore, the results reported will focus on *H1* and *H2*. Amplitudes of *H1* ranged from 0.41-6.31 cm, while amplitudes of H2 ranged from 0.35-3.95 cm. *H1* only differed between FSP for low-STT participants (Table 5, Figure 5). *H1* for Pelvis Release was 41.9% lower than Kneeling Release and 42.6% lower than Squat Release. *H2* differed between FSP (Table 5, Figure 5), but trends differed between STT groups. For medium and high-STT groups, *H2* values averaged 35.0% lower for Squat Release compared to Kneeling Release, and 45.4% lower compared to Pelvis Release. *H2* was 61.6% greater during Kneeling Release than Pelvis Release, and 75.6% greater than Squat Release for low-STT participants.

Table A2.4: Main effects and significant pairwise comparisons for Hypothesis 2b

Dependent Variable	**Factor**	**Pair**	**F**	**t**	**p**
Eccentricity	STT		1.8		0.186
	FSP		1.5		0.239
H1	STT		1.9		0.157
	FSP		8.7		<0.001**
	FSP-STT interaction		3.7		0.008**
	FSP-low STT		12.6		<0.001**
		Pelvis vs. Kneeling		-4.0	0.001**
		Pelvis vs. Squat		-4.1	0.001**
	FSP-medium STT		1.5		0.232
	FSP-high STT		1.8		0.324
H2	STT		0.4		0.657
	FSP		24.5		<0.001**
	FSP-STT interaction		4.9		0.002**
	FSP-low STT		19.6		<0.001**
		Kneeling vs. Pelvis		4.2	0.001**
		Kneeling vs. Squat		5.16	<0.001**
	FSP-medium STT		12.3		<0.001**
		Squat vs. Pelvis		-3.8	0.002**
		Squat vs. Kneeling		-3.7	0.003**
	FSP-high STT		6.6		0.005**
		Squat vs. Pelvis		-3.1	0.015*
		Squat vs. Kneeling		-2.8	0.010*

* significant, p<0.05; ** significant, p<0.01

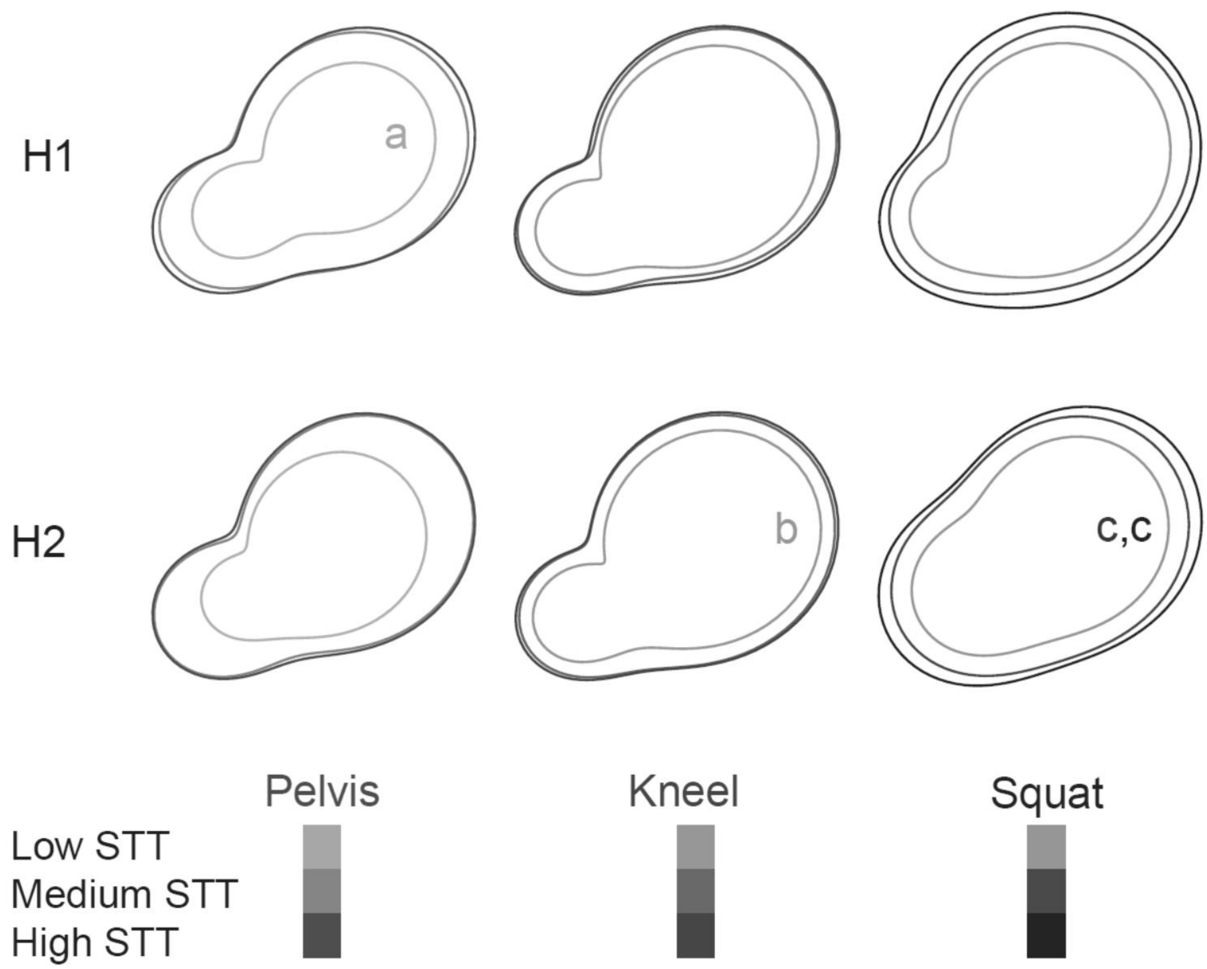

Figure A2.5: Demonstrated manipulation of H1 and H2 between FSP and STT groups. The top row demonstrates mean FSP contact profiles with H1 manipulated to highlight STT-group differences; the second row demonstrates manipulation of H2 between STT groups.

Significant differences p<0.05: a, Pelvis Release lower than Kneeling or Squat Release for low-STT participants; b, Kneeling Release greater than Pelvis or Squat Release for low-STT participants, c, Squat Release lower than Pelvis or Squat Release for medium and high-STT participants.

No contact profile elements were correlated with P_{peak} during Kneeling or Squat Release. P_{peak} was negatively correlated with *CA* and H0…H5 ($p<0.05$), but not eccentricity during Pelvis Release (Figure A2.6).

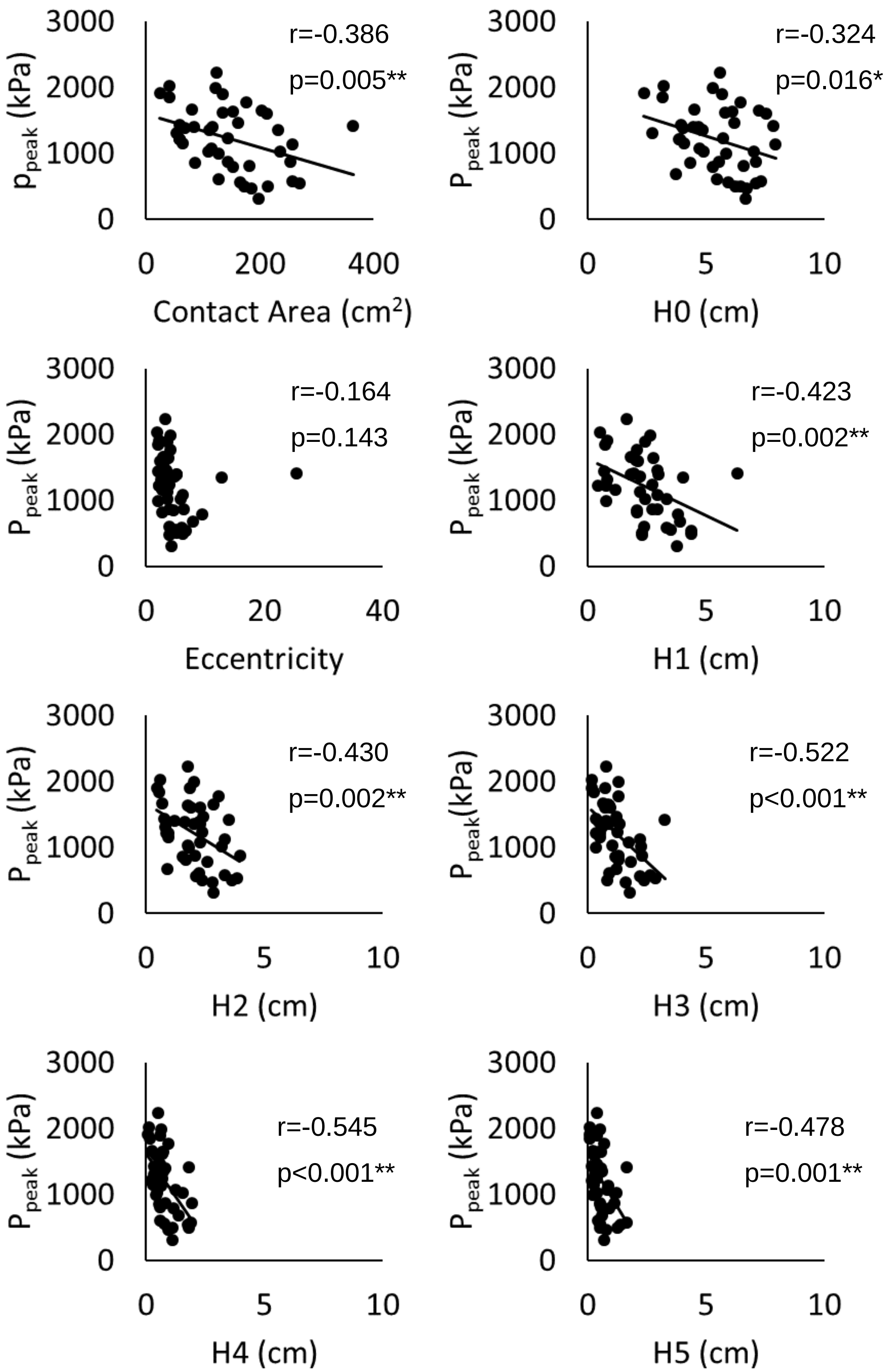

Figure A2.6: Significant correlations between *M*, *H0…H5* and P_{peak} during Pelvis Release.
* significant, p<0.05; ** significant, p<0.01.

A2.4 Discussion

The goal of this study was to determine how load distribution differed between three fall simulation protocols in male and female participants who exhibited a range of trochanteric soft tissue thickness. Regarding hypothesis one, we found that Peak Pressure was greatest during Squat Release, whereas we predicted that greater Peak Pressure would be observed in protocols with less hip flexion. Additionally, we did not find any difference in Peak Pressure between sex or STT groups. Regarding hypothesis two, we found no difference in Contact Area or *H0* between males and females; however, we found that Contact Area was 35.1% lower, and *H0* was 21.4% lower for low-STT fallers compared to medium- or high-STT participants. Furthermore, we found that Contact Area and *H0* during Pelvis Release were 7.1% and 5.25% lower than Kneeling Release, and 11.0% and 10.8% lower than Squat Release. While we found no difference in Eccentricity between fall simulation protocols, sex or STT groups, harmonic analysis was more sensitive to STT and FSP. Harmonic differences were clearest for low-STT participants, however *H2* also differed between fall simulation protocols for all STT groups. Regarding hypothesis three, we found significant negative correlations between Contact area, *H0-H5* and Peak Pressure only in the Pelvis Release trials.

We did not find differences in P_{peak} or *CA* between males and females, despite a 28.7% decrease in STT for males compared to females. Post hoc analysis of the distribution for P_{peak} revealed that, while 90% of mean FSP outcomes had P_{peak} below 4461 kPa, ten Squat Release trial means (five males, five females) and two Kneeling Release trial means (both female) had P_{peak} values exceeding this boundary. P_{peak} was consistent between the trials comprising each mean. These extreme cases may highlight more critical structural skeletal features than sex differences for P_{peak}. Hip axis length, the distance from the lateral surface of the greater trochanter to the medial surface of the pelvic brim, has been identified as a predictor of hip fracture (Broy, Cauley et al. 2015). While we did not measure this component, longer hip axes would, hypothetically, project the greater trochanter further from the pelvis and isolate loading in the “danger zone”; this might explain increased P_{peak} for the extreme cases. The relevance of hip axis length may be counteracted in some cases by STT. We recruited participants with a wide range of STT, and consequently BMI; the effect of these components on the energy of the system has a greater effect than any sex differences. The ratio of hip axis length, or hip projection, to STT may explain outliers in this study, and represents an area of further research.

Further, while P_{peak} during Pelvis Release was similar to that previously reported (Choi, Hoffer et al. 2010a), P_{peak} did not differ between our STT groups, in contrast to a 266% increase in

P_{peak} for low-BMI compared to participants with high BMI reported by Choi et al. The combined effect of mass and STT associated with BMI may have a greater effect on load distribution than STT alone. This is confirmed in our data – when categorized by BMI, we found that P_{peak} was 55.4% higher for low-BMI compared to participants with high BMI (outliers excluded, t=2.2, p=0.038). *H0-H5* correlated negatively with P_{peak}, and differed between STT groups. Accordingly, there is likely a mechanistic relationship between soft tissue distribution of loads and peak pressure that is not captured by STT. Three-dimensional characterization of trochanteric soft tissue may more effectively highlight group differences.

P_{peak} was substantially greater during Squat Release than Kneeling Release or Pelvis Release, despite having flexion and adduction angles associated with greater apparent STT (Levine, Minty et al. 2014), moderate peak forces and contact area. However, visual analysis of videos of each trial revealed that most participants rotated backwards during the Squat Release protocol; the greater trochanter may project further from the pelvis in the posterolateral rather than lateral aspect. Posterolateral impact configurations have previously been linked with greater peak pressure, particularly for low-BMI fallers (Choi, Hoffer et al. 2010a).

Harmonic analysis was more sensitive to FSP-STT interactions than eccentricity, and more strongly correlated with P_{peak}. Amplitudes of *H3-5* were low, and, on average, represented 17.9% of the signal power. However, all six harmonics investigated were negatively correlated with P_{peak} for pelvis release. The link between *H3-5* and P_{peak} is likely due to the interdependence and phase angle of the harmonics. The contact profile is composed of interfering waves, and no harmonic can independently characterize the shape. Interference of the waveforms associated with higher-order harmonics may emphasize aspects of lower-order harmonics (*H0-H2*) rather than influencing independent semilandmarks. Analysis of phase angles would clarify this effect. Higher-order harmonics may have greater utility for contact profiles with higher frequency content, e.g. an impact to an outstretched hand. However, Radial Fourier Analysis is only appropriate for closed curves, and each radius must cross the contact outline only once; other morphometric methods, such as more complex Fourier shape signatures (El-ghazal, Basir et al. 2009) or eigenshape functions (Lohmann 1983) may be more appropriate.

The results of this study have implications for prediction of, and intervention to prevent hip fracture. First, we found that the Squat Release protocol produced substantially greater P_{peak} than the other fall simulation methods, despite moderate peak forces and contact area. This protocol may represent a "high risk" impact configuration; further work should quantify what interactions of anatomy, faller behavior and impact mechanics are responsible for the increase in P_{peak}. Second, we found that all FSP and participants produced substantial *H1* components, which points towards a circular contact profile as suitable for modeling of impacts to the hip. However, further work should assess the sensitivity of models to the influence of higher-order harmonics, and set *a priori* harmonic thresholds. Third, we found limited differences between results of absolute and normalized harmonics, in addition to, and likely due to, ordinal interactions between STT group, FSP and the harmonics. This points towards the scalability of contact profiles based on body composition, a simplification in creating individual-specific injury prediction models, as well as the potential simplicity of incorporation into population-level models. Finally, *H0* was negatively correlated with P_{peak} for Pelvis Release, which suggests that distribution of loads away from the "danger zone" may be of similar importance as energy absorption in reducing peak pressure. Therefore, wearable or environmental interventions to prevent hip fracture, such as hip protectors or safety floors, could be designed to reflect this—a thinner product with better load distribution performance may be more effective than current bulky models. This hypothesis already has support in the case of horseshoe vs. continuous hip protectors (Laing and Robinovitch 2008; Laing, Feldman et al. 2011).

In this study, we quantified P_{peak} and *CA* differences and interactions between fall simulation method, sex and STT groups using morphometric methods. We found that method of falling had the strongest effect on P_{peak}, compared to STT or sex, and substantial effects on several indices of load distribution. Further, we found that STT also had a substantial effect on load distribution. Finally, we found that ellipse descriptors were effective predictors of P_{peak} during some simulated falls.

Appendix 3 Comparison of regressed vs individual parameters

The following table and figures summarize the difference in model performance induced when parameters based on sex or regression relationships were used rather than individual experimentally-determined parameters. All outcomes are based on t-tests with N=31.

Table A3.1 Comparison between individual and regressed model parameters on model error outcomes

	MS		**HZ**		**VG**		**HC**		**VO**	
	t	p	t	p	t	p	t	p	t	p
Err_{max}	-0.6	0.541	-0.8	0.430	-3.3	0.002**	0.0	0.974	-0.3	0.765
Err_{TTP}	0.1	0.939	0.8	0.432	-0.9	0.372	-1.5	0.135	-0.7	0.473
Err_{imp}	-0.9	0.393	-0.2	0.858	-2.5	0.015*	-0.1	0.883	-0.8	0.402
Err_{corr}	-1.6	0.111	0.9	0.372	1.8	0.084	-0.8	0.402	-1.1	0.289

** significant comparison at p<0.05; ** significant comparison at p<0.01*

MS Mass-spring; HZ Hertz; VG Voigt; HC Hunt-Crossley; VO volumetric; Err_{max} *error in prediction of peak force;* Err_{TTP} *error in prediction of time to peak force;* Err_{imp} *error in prediction of the loading impulse between impact initiation and the first minimum of force following peak force;* Err_{corr} *error in prediction of time-varying force within a two-standard-deviation corridor*

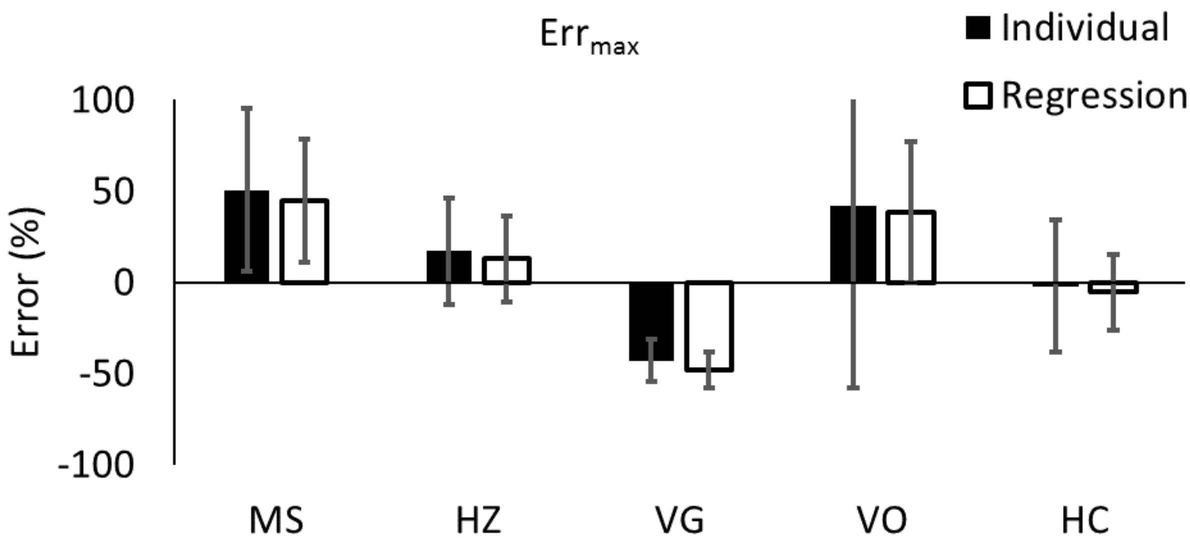

Figure A3.1 Difference in model performance for *Err$_{max}$* between individually-derived parameters and regression-derived parameters

Err$_{corr}$ did not differ between individually-derived and regression-derived parameters for any model except Voigt. Individually-derived parameters were linked with decreased underprediction of peak force compared to regression-derived parameters. This difference is likely related to non-zero damping at initiation of the impact for the Voigt model, i.e. because the damping parameter for this model is sensitive to impact velocity at initial impact and is not corrected by a deflection term when determining damping (as with the Hunt-Crossley and Volumetric models). However, while performance differed statistically, functionally, both individually- and regression-derived parameters resulted in approximately 50% underprediction of peak force.

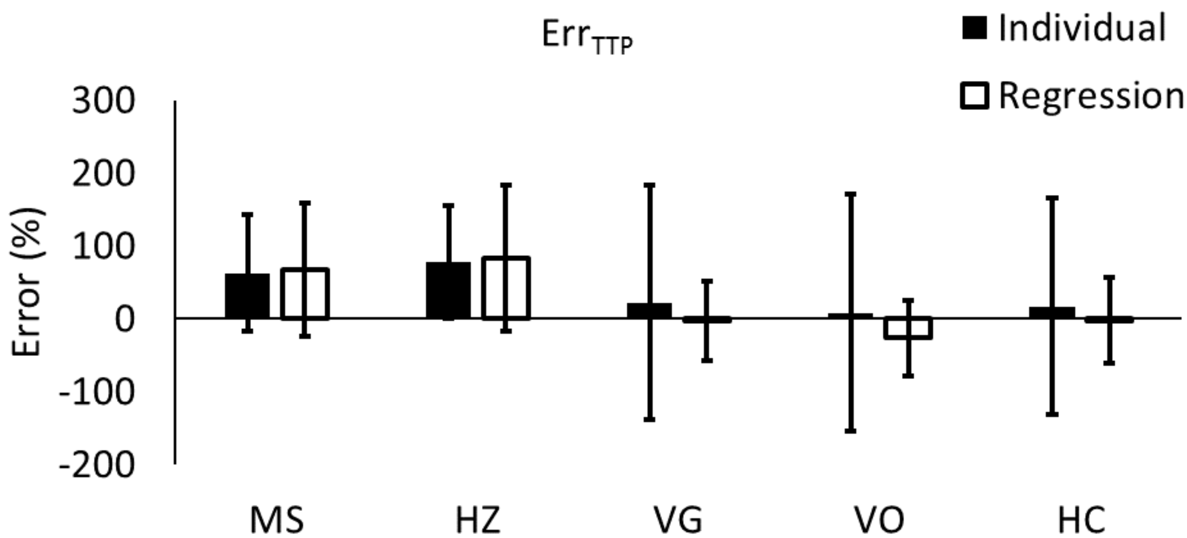

Figure A3.2 Difference in model performance for *Err_{TTP}* between individually-derived parameters and regression-derived parameters

Err_{TTP} did not differ between individually-derived and regression-derived parameters.

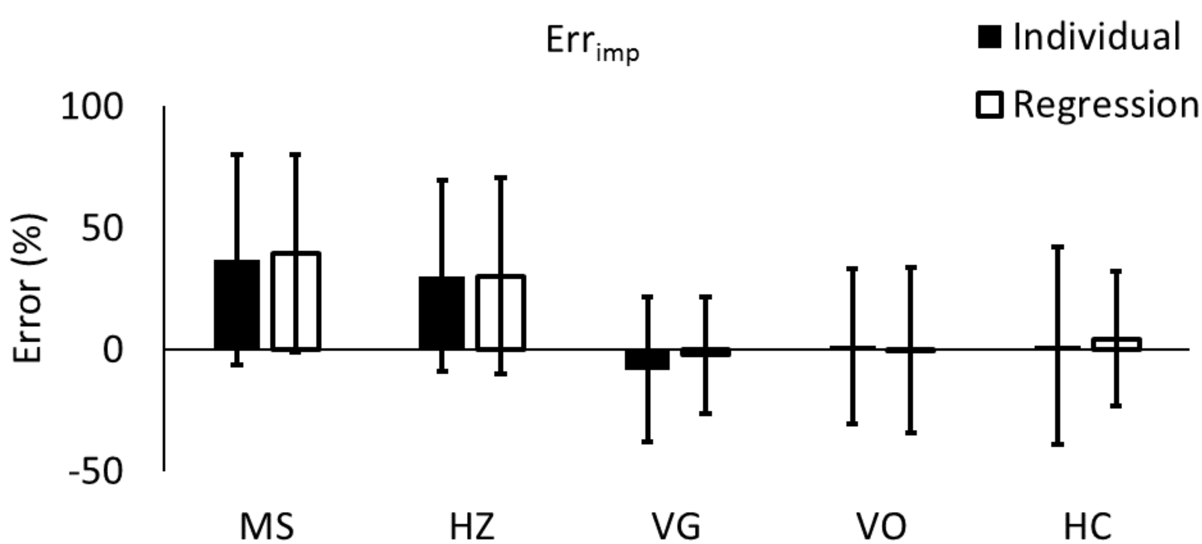

Figure A3.3 Difference in model performance for *Err_{imp}* between individually-derived parameters and regression-derived parameters

Error in prediction of impulse differed only for the Voigt model. Difference between performance of individually-derived parameters and regression-derived parameters is likely linked to difference in prediction of peak force, which also differed for the Voigt model.

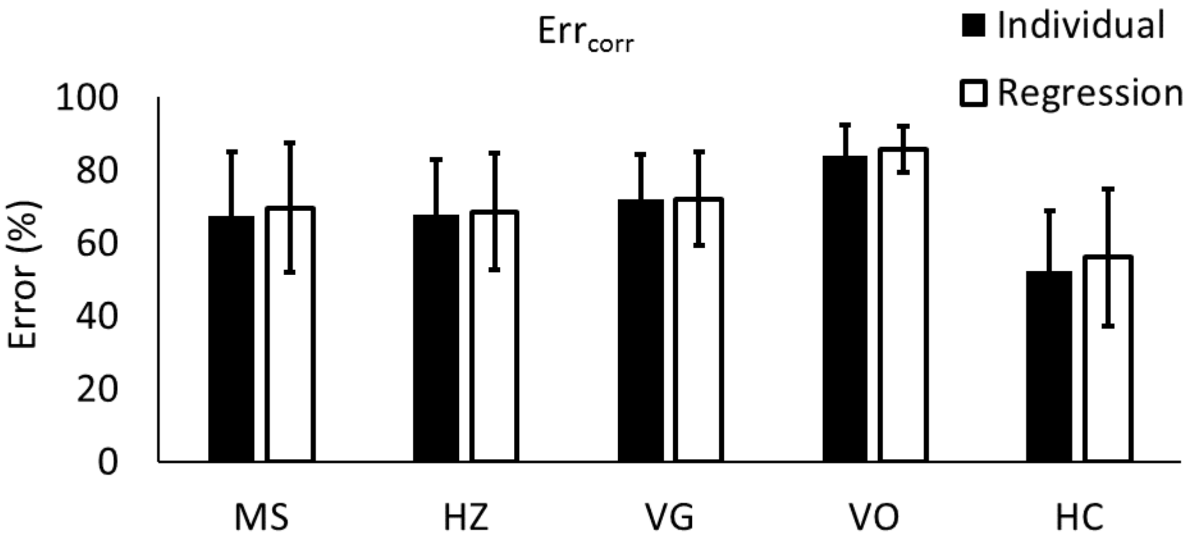

Figure A3.4 Difference in model performance for *Err$_{corr}$* between individually-derived parameters and regression-derived parameters

*Err$_{corr}$*did not differ between individually-derived and regression-derived parameters.

Appendix 4 Extended statistical analysis of model parameters

The following table characterizes the quality of fit between the experimental data and model curve fits over the loading curve (between initial impact and peak force). Across all participants, quality of fit was similar between MS, HZ and HC, slightly lower for VO, and substantially lower for VG. There were no clear trends in quality of fit between males and females or TSTT groups.

Table A4.1: Mean (SD) r^2 values for each model, describing the quality of fit between experimental data and model curve fits

		N	MS	HZ	VG	HC	VO
Females							
	Low	4	0.90 (0.02)	0.93 (0.03)	0.50 (0.03)	0.92 (0.03)	0.88 (0.06)
STT	Mid	5	0.85 (0.08)	0.88 (0.06)	0.57 (0.09)	0.86 (0.10)	0.85 (0.14)
	High	6	0.91 (0.09)	0.94 (0.04)	0.61 (0.12)	0.93 (0.05)	0.91 (0.05)
Males							
	Low	6	0.81 (0.07)	0.73 (0.13)	0.47 (0.16)	0.71 (0.16)	0.63 (0.21)
STT	Mid	6	0.88 (0.06)	0.94 (0.02)	0.46 (0.14)	0.94 (0.02)	0.93 (0.03)
	High	5	0.89 (0.07)	0.83 (0.11)	0.52 (0.09)	0.81 (0.10)	0.74 (0.14)

The following figures summarize relationships between individual characteristics and model parameters. Significant relationships are represented with a trend line and r^2 value.

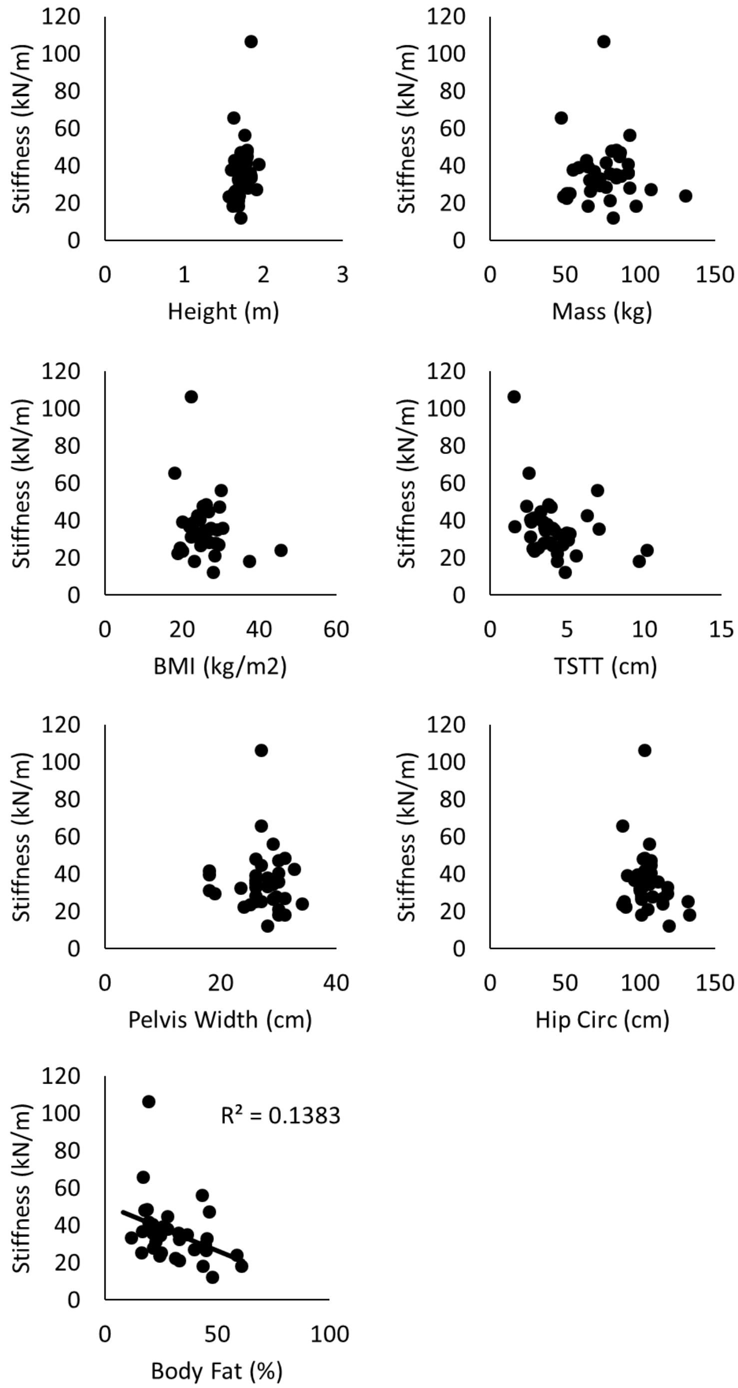

Figure A4.1 Significant relationships between body size, composition and k_{MS}

The stiffness estimate for the mass-spring model was not significantly correlated with height, mass, BMI, TSTT, pelvis width or hip circumference. The stiffness estimate was significantly negatively correlated with percent body fat. Percent body fat was included in the final model to predict k_{MS}.

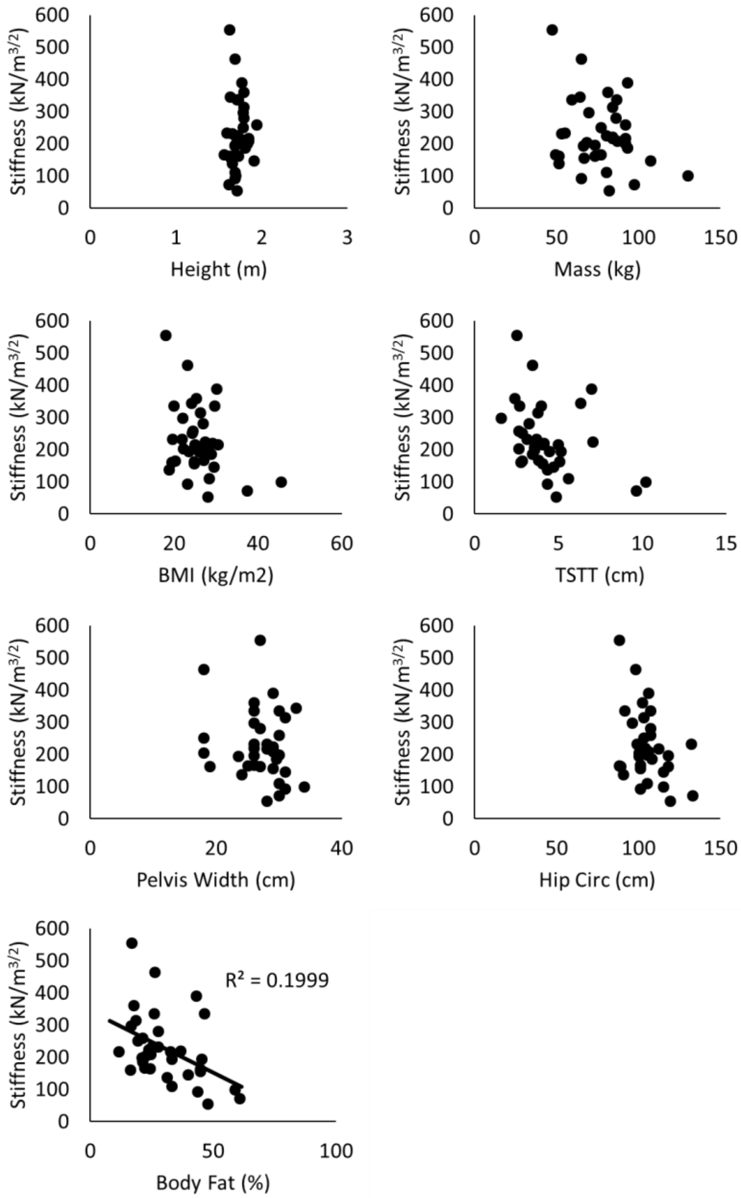

Figure A4.2 Significant relationships between body size, composition and k_{HZ}

Similarly to k_{MS}, the stiffness estimate for the Hertzian model was not significantly correlated with height, mass, BMI, TSTT, pelvis width or hip circumference. The stiffness estimate was significantly negatively correlated with percent body fat. Percent body fat was included in the final model to predict k_{HZ}.

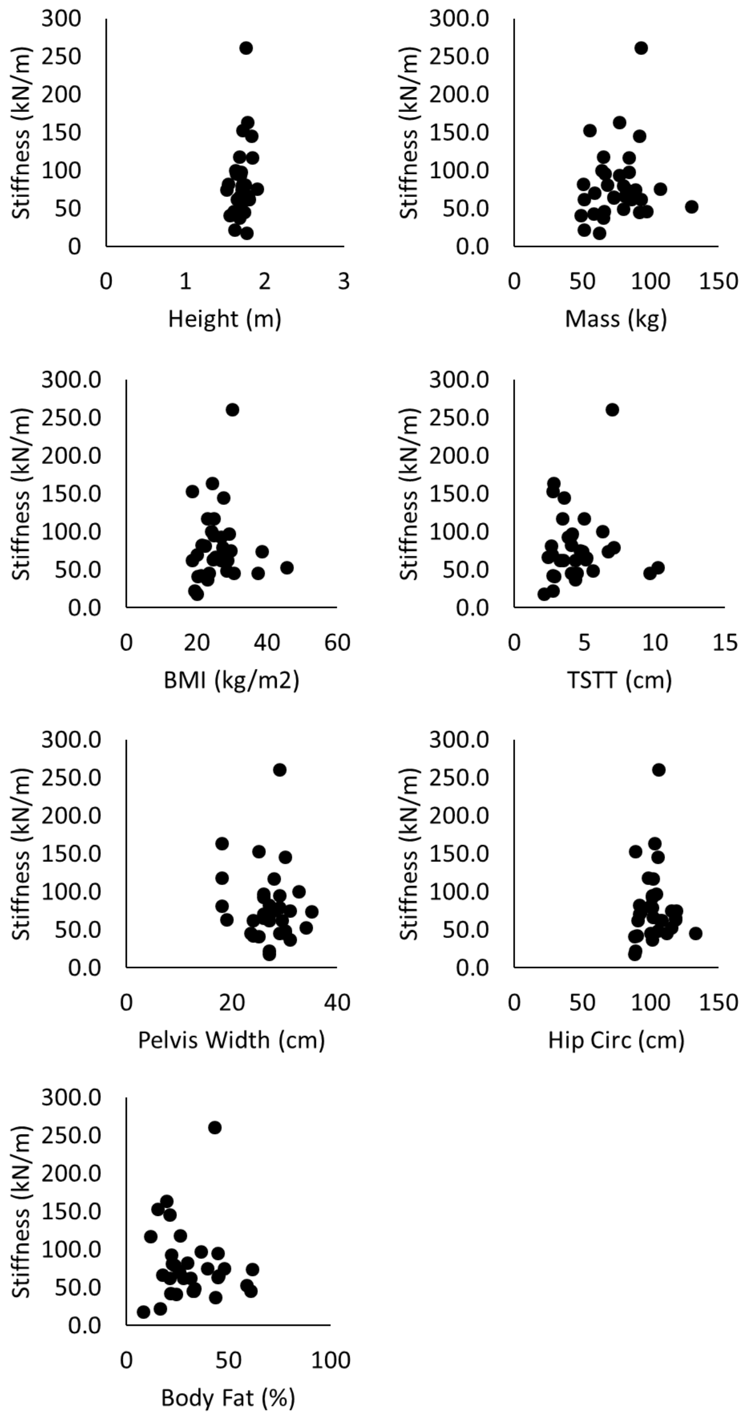

Figure A4.3 Significant relationships between body size, composition and k_{VG}

The stiffness estimate for the Voigt model was not significantly correlated with height, mass, BMI, TSTT, pelvis width, hip circumference or percent body fat. A single stiffness estimate was used for all participants.

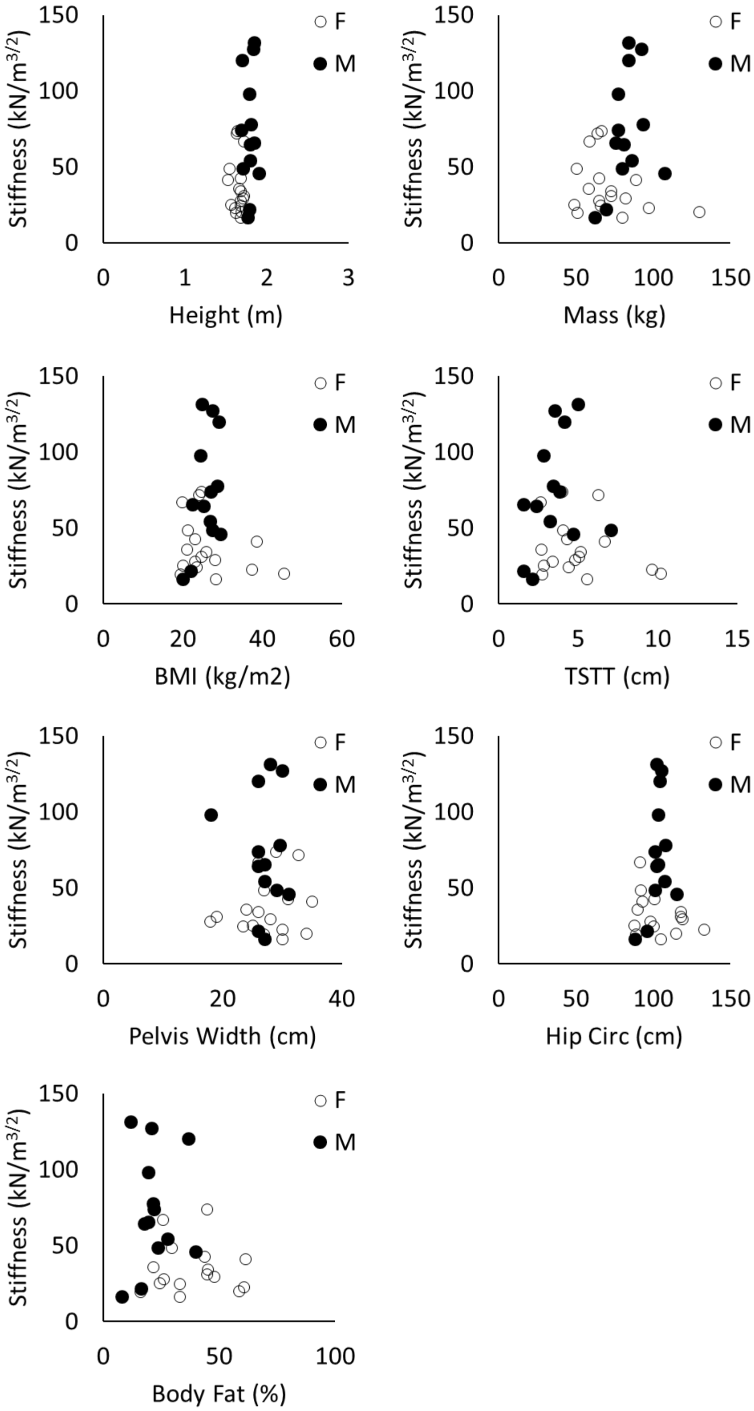

Figure A4.4 Significant relationships between body size, composition and k_{HC}

The stiffness estimate for the Hunt-Crossley model was not significantly correlated with height, mass, BMI, TSTT, pelvis width, hip circumference or percent body fat. However, as noted in Study 2, the stiffness estimate differed between males and females. Therefore, a separate stiffness estimate was developed for males and females.

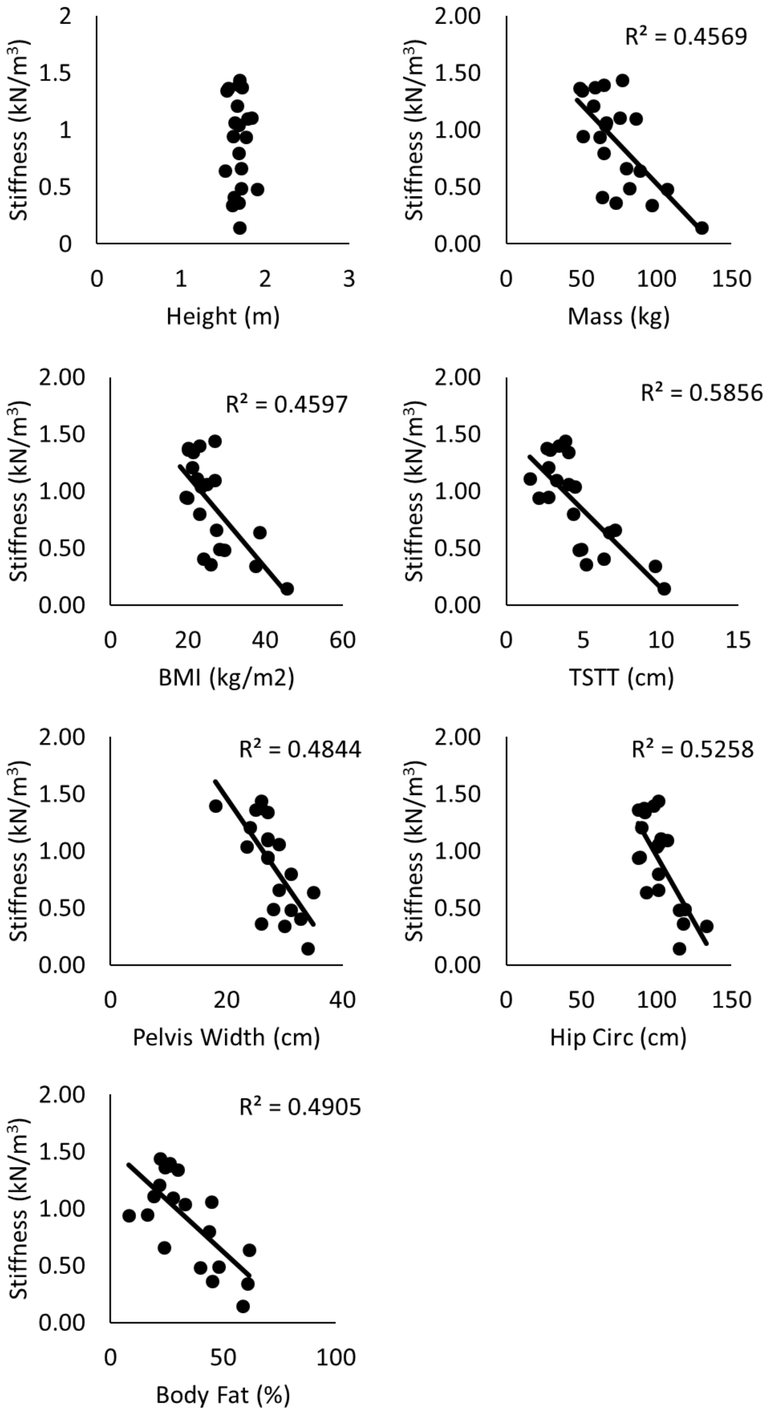

Figure A4.5 Significant relationships between body size, composition and k_{VO}

In contrast to other stiffness estimates, k_{VO} was related to all body size and composition variables except Height. The volumetric stiffness estimate was most strongly related to trochanteric soft tissue thickness. The estimation of k_{VO} was not improved by the addition of other body composition elements, such as pelvis width; therefore, only TSTT was included in the final model.

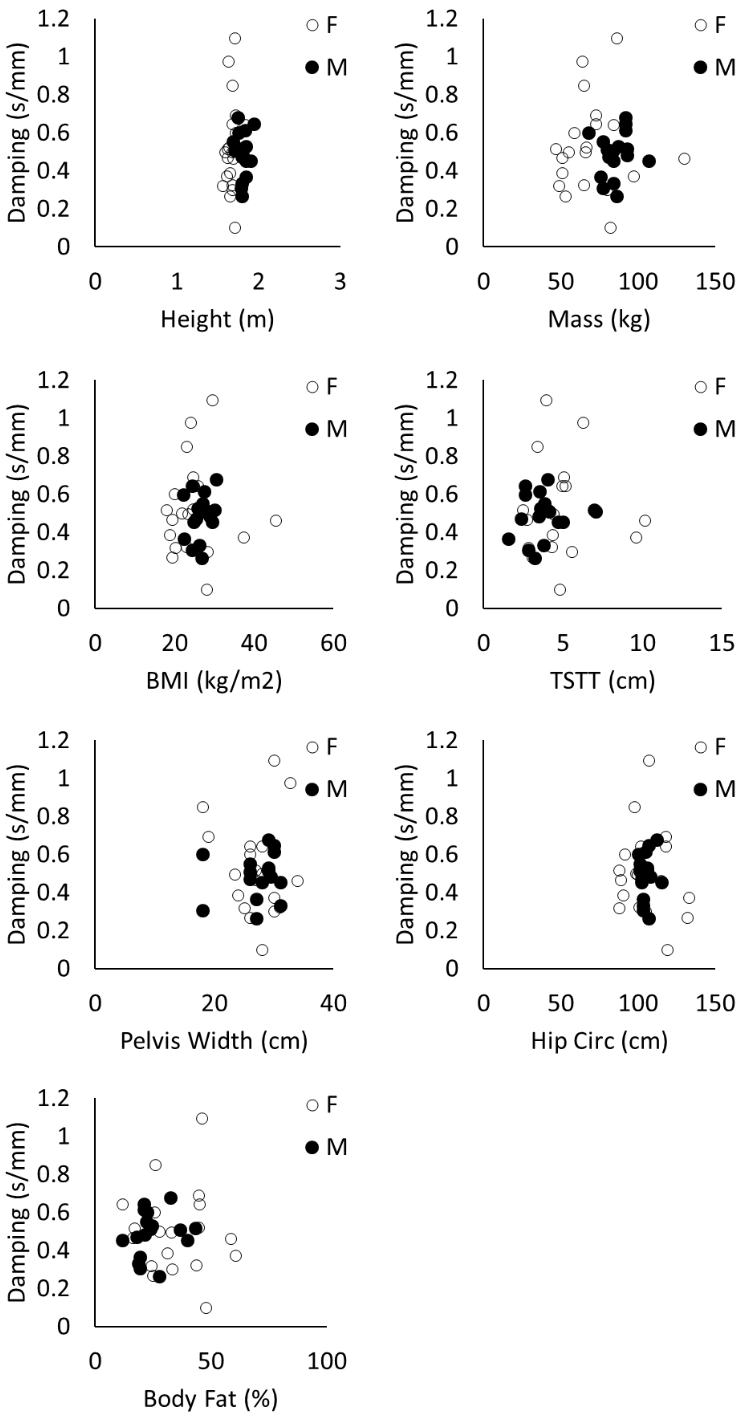

Figure A4.6 Significant relationships between body size, composition and b_{VG}

Similar to k_{HC} The damping estimate for the Voigt model was not significantly correlated with height, mass, BMI, TSTT, pelvis width, hip circumference or percent body fat. However, as noted in Study 2, the damping estimate differed between males and females. Therefore, a separate damping estimate was developed for males and females

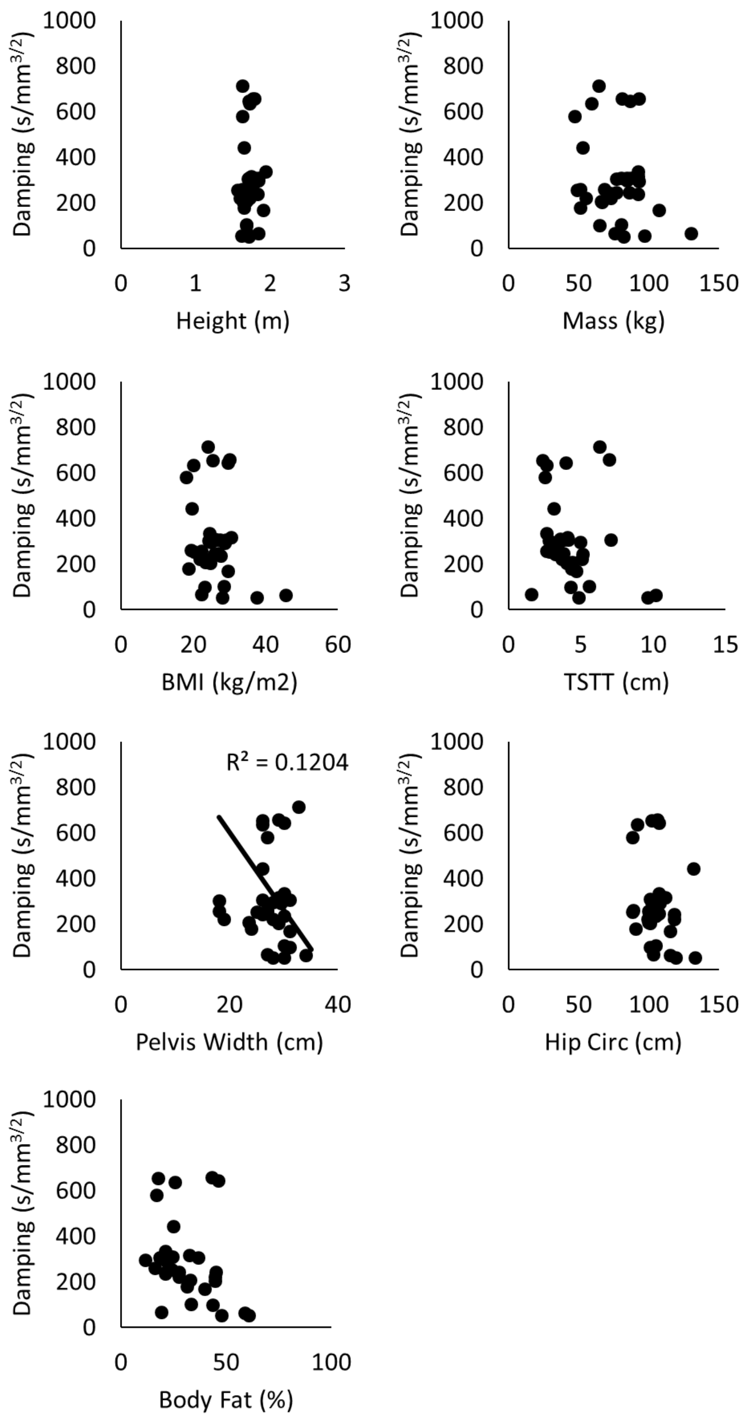

Figure A4.7 Significant relationships between body size, composition and a_{HC}

The damping estimate for the Hunt-Crossley model was not significantly correlated with height, mass, BMI, TSTT, hip circumference or percent body fat. The damping estimate was significantly correlated with pelvis width. Pelvis width was included in the final model to predict a_{HC}

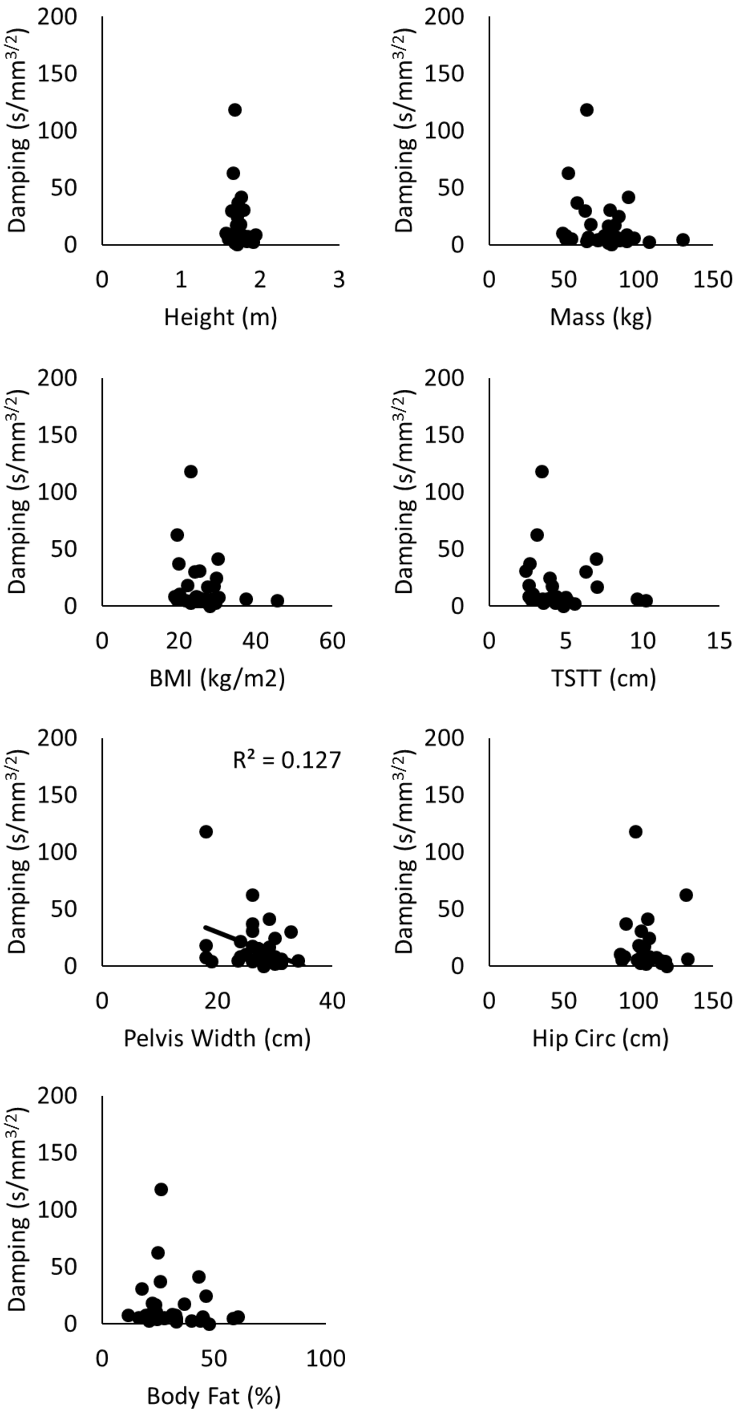

Figure A4.8 Significant relationships between body size, composition and a_{VO}

The damping estimate for the Hunt-Crossley model was not significantly correlated with height, mass, BMI, TSTT, hip circumference or percent body fat. The damping estimate was significantly correlated with pelvis width. Pelvis width was included in the final model to predict a_{VO}.

Appendix 5 Paradigms for simulating falls to the hip: differences in impact configuration, loading and reliability

This study summarizes the differences in peak forces, kinematics and repeatability for three fall simulation methods employed in Chapter 7. The results of this study were presented, in part, at the 19th Biennial Meeting of the Canadian Society for Biomechanics, July 19-22, 2016, and the 40th Annual Meeting of the American Society of Biomechanics, August 2-5, 2016.

A5.1 Introduction

Experimental simulated falls with live participants in impact studies are limited by ethical restrictions in order to prevent injury to participants and require a limited number of either low height, low-energy impacts, or impacts utilizing protective equipment such as crash mats or wearable padding. The first restriction reduces external validity of the impact data, while the second reduces the quality of the kinetic data collected when conclusions regarding unpadded scenarios are desired. For simulating impacts to the hip, paradigms range from as simple and controlled as the pelvis release (Robinovitch, Hayes et al. 1991), to methods involving obstacle avoidance (Smeesters, Hayes et al. 2001), a tether release (Robinovitch, Chiu et al. 2000; Robinovitch, Inkster et al. 2003; Robinovitch, Brumer et al. 2004; Sran and Robinovitch 2008) or moving platform (Feldman and Robinovitch 2007). No current paradigm can be used to simulate a fall from initial loss of balance at standing height through the impact phase with direct measurement of external loading at the hip. Only simulated paradigms from kneeling height or lower have been employed without padding, and the experimental repeatability of these methods is unknown.

It is challenging to balance experimental repeatability, participant comfort, and external validity. The pelvis release paradigm has been noted to be extremely repeatable, but is limited to impact velocity of 1 m/s for participant comfort. Further, the method simulates a falling configuration where the faller has rotated laterally 90° and impacts the ground with a primarily vertical velocity component. Few falls in older adults match these impact conditions, and falling events are highly variable in nature (Robinovitch, Feldman et al. 2013). Observed real-world vertical hip impact velocities range from 0.1 to 4.0 m/s (van den Kroonenberg, Hayes et al. 1996; Nankaku, Kanzaki et al. 2005; Feldman and Robinovitch 2007; Kangas, Vikman et al. 2012; Choi, Wakeling et al. 2015), while horizontal impact velocity averages 1.16 m/s (Choi, Wakeling et al. 2015) in older adults; both are dependent on falling configuration and faller control strategies (van den Kroonenberg, Hayes et al. 1996; Robinovitch, Brumer et al. 2004; Nankaku, Kanzaki et al. 2005; Groen, Weerdesteyn et al. 2007). While a directly lateral impact has been hypothesized to be the riskiest falling configuration for hip fractures, fallers typically fall in more complex configurations (Robinovitch, Feldman et al. 2013; Choi, Wakeling et al. 2015), and commonly impact other body parts during descent (both intentionally and not, such as the hand and knee) (Choi, Wakeling et al. 2015). Finally, active control of descent using eccentric muscle contractions has been identified as a strategy to reduce energy during a fall (Robinovitch, Chiu et al. 2000; Sandler and Robinovitch 2001). Realistic impact configurations and control strategies may be more accurately simulated using a fall simulation paradigm initiated from a kneeling or squatting position rather than a passive sideways fall.

Therefore, the primary goal of this study was to characterize and describe differences between falling configuration, pelvis velocity at impact, and peak force, during three fall simulation paradigms (FSP): Pelvis Release, Kneeling Release and Squat Release. The second goal was to determine differences in repeatability between FSP. We hypothesized that (1) Peak vertical ($F_{vertical}$), and shear (F_{shear}) forces and impact velocity ($V_{vertical}$,V_{shear}) will be lower for Pelvis Release than Squat Release or Kneeling Release; (2) impact configuration would be similar between paradigms; (3) repeatability of outcome variables will be similar across FSP.

A5.2 Methods

Forty-four healthy participants (<35 years, 23 female) consented to participate in this study. Exclusion criteria included musculoskeletal injury in the past year preventing completion of the paradigm, lifetime fracture history, fear of falling, or other health conditions which would make participation unsafe.

A5.2.1 Experimental Protocol

An eighteen-trial fall simulation paradigm (FSP) consisted of six blocks of trials, each block consisting of one Pelvis Release, one Kneeling Release and one Squat Release paradigm (Figure A5.1), in randomized order. Blocks 1-3 were “training trials”, allowing for participant adaptation to the paradigm; Blocks 4-6 were used to determine average biomechanical outcomes. All paradigms involved the lateral aspect of the left hip impacting a force plate (3500 Hz; OR6-7, AMTI, USA). Motion of the pelvis and left thigh were tracked using three-dimensional motion capture (Optotrak Certus, Northern Digital, Inc., Waterloo, ON) at the maximum sampling rate (300 Hz) for the number of markers used. We used one cluster on the sacrum, and one on the left thigh, each with four

Optotrak Smart Markers Digitized markers were used to estimate motion of the right and left anterior superior iliac spine and posterior superior iliac spine, along with the left lateral and medial femoral condyle to allow estimation of relative motion of the pelvis and femurs during the paradigm. These marker positions are consistent with the Bell (1989) pelvis and ISB standards for the pelvis, femur and hip (Wu, Siegler et al. 2002). Additionally the position of the left (impacting) greater trochanter was digitized to estimate impact velocity at the hip.

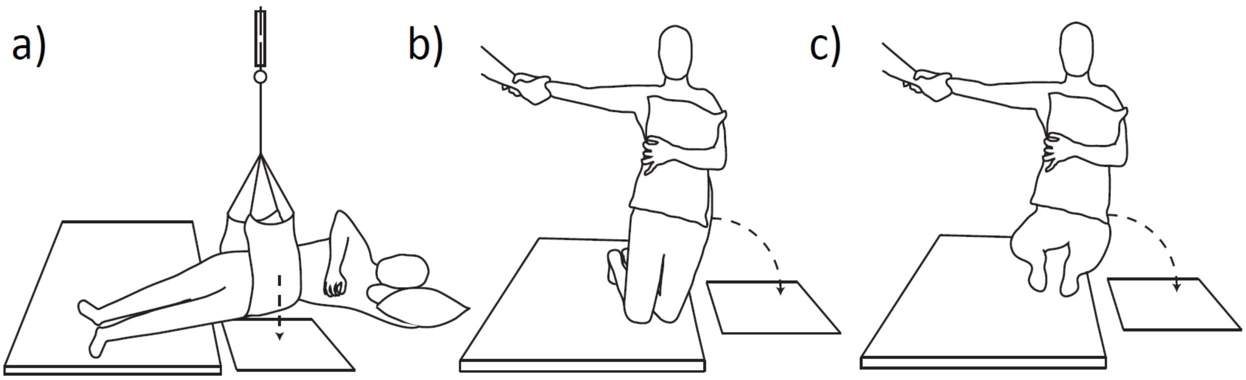

Figure A5.1 Initial position and motion path of the Pelvis Release (a), Kneeling Release (b), and Squat Release (c).

The primary difference between the paradigms is the motion path of the pelvis: a controlled, vertical motion is produced during Pelvis Release, while Kneeling Release produces vertical and lateral motion in an inverted pendulum, and Squat Release typically has more lateral than vertical motion. For the Pelvis Release, the upper body of the participant was supported by a pillow outside the contact area of the force plate. For the Kneeling Release and Squat Release, the participant held a pillow throughout the trial to prevent bracing with their arms during the impact. The Pelvis Release paradigm is highly controlled, and represents a scenario where the faller rotates into a horizontal position before impacting the hip directly laterally. The Kneeling Release reflects a scenario where the faller impacts the knee prior to rotating to impact the hip. The Squat release reflects a scenario where the faller flexes the knee, hip and ankle during the descent phase prior to rotating laterally to impact the hip.

In greater detail, for the initial position for Pelvis Release, hips were flexed to 45°, knees were flexed to 90°, and the pelvis was raised in a thin nylon sling using a turnbuckle until the soft tissues overlying the hip were 5 cm above the pressure plate, consistent with a 1 m/s impact velocity (for blocks 1-3, the height was reduced to <0.1 cm to reduce participant discomfort). The participant was instructed to reduce the muscle tension in their body; when the participant reported that they were “relaxed and ready”, the electromagnet supporting the sling was released, allowing the pelvis of the participant to impact the pressure plate. For Kneeling and Squat Release, the participant was supported in the initial position by the researcher, was instructed to lean until their weight was supported by their left side, self-release, and fall “like a pendulum”. For kneeling release, the initial position was hips were flexed to 0°, knees were flexed to 90° and the lower leg was in contact with the starting mat. For Squat Release the initial position was a heel-lifted Squat, with maximal thigh-calf contact and an upright torso. A minimum of one minute of rest was provided between each trial, during which the participant was asked to stand or kneel without contact between the ground and trochanteric or gluteal soft tissues.

A5.2.2 Signal Processing

We used a customized MATLAB routine (MathWorks, Natick, MA) to process the time-varying signals. Briefly, the filtering of impact data and methods of selection of cut-off frequencies have been the subject of debate. Impact events occur rapidly--in the case of this data set, a time-to-peak-force of 0.02-0.09 s would be expected. Implementation of a low-pass filter would, therefore, potentially over-smooth the impact event, reducing the impact peaks. To conserve peak force values, we therefore did not filter force prior to determining the peak force value. We downsampled the force data (to 300 Hz, matching the kinematic data) and filtered all time-varying signals with a fourth-order dual pass 100 Hz Butterworth filter, which has previously been used for pelvis release experiments (Levine, Bhan et al. 2013), and was selected based on observed mean power frequency during lateral impacts to the hip.

An automated point-selection routine was developed to determine key data coordinates for further analysis. Each trial was segregated by defining an initial quiet (unloaded) region ($F_{initial}$), the beginning of impact (when force exceeds two standard deviations of the mean in the quiet region preceding impact, T_{imp}, F_{imp}) and peak force (T_{max}, $F_{vertical}$, F_{shear}). Bias ($F_{initial}$) was subtracted from $F_{vertical}$ and F_{shear}. Impact velocity ($V_{vertical}$, V_{shear}) was determined for the left hip over the two data points directly preceding T_{imp}. F_{shear} and V_{shear} were calculated as the resultant of the two shear vectors in the plane of the impact surface. Hip joint angles (femur relative to pelvis, resolved in a $Hip_{flexion}$, $Hip_{adduction}$, Hip_{axial} sequence), and pelvis and femur inclination angles ($Pelvis_{inclination}$, $Pelvis_{axial}$, $Femur_{inclination}$, $Femur_{axial}$) were determined at T_{max}.

A5.2.3 Statistical Analysis

All statistical analysis was performed using a software package (SPSS version 21, Chicago, USA) using an α of 0.05. Regarding the hypotheses one and two, we used a one-way ANOVA to test the effect of FSP (repeated measure) on impact characteristics. Pairwise comparisons using a Bonferroni correction were employed when significant main effects were observed. Regarding the third hypothesis, we used intraclass correlations (ICC (3,1, absolute agreement)) to determine the consistency of impact characteristics for the averaged trials (4-6). Ranges of ICC values >0.9 were deemed to have excellent repeatability, 0.75-0.9 good repeatability, 0.5-0.75 moderate repeatability, and <0.5 poor repeatability (Koo and Li 2016). Additionally, we used a paired t-test to determine whether the first (training) trial differed from the averaged trials (4-6).

A5.3 Results

Paradigm means (x), medians (-), quartiles 1-3 (box) and range (whiskers) for all impact characteristics are plot in Figure A5.2 and Figure A5.3.

All impact characteristics for Kneeling Release and Squat Release were significantly for all metrics except repeatable except Femur inclination for Squat release. Impact characteristics were found to have lower ICC scores for Pelvis Release (Table A5.2). Adaptation effects were significant for all paradigms, most evident during Squat Release (Table A5.1).

Both V_{shear} and $V_{vertical}$ differed between paradigms ($V_{vertical}$, F(2,86)=3.4, p=0.036, V_{shear}, $F_{(2,86)}$=106.1, p<0.001). V_{shear} was 73.5% lower for Pelvis Release compared to Kneeling Release (t(43)=12.8, p<0.001) and 67.2% lower compared to Squat Release (t(43)=11.1, p<0.001) while $V_{vertical}$ was 8.2% greater for Pelvis Release compared to Kneeling Release (t(43)=2.7, p=0.010). Peak forces differed in both directions across paradigms ($F_{vertical}$, $F_{(2,86)}$=36.4, p<0.001; F_{shear}, $F_{(2,86)}$=39.7, p<0.001). $F_{vertical}$ was 32.3% lower during Pelvis Release compared to Kneeling Release (t(43)=-7.2, p<0.001), and 28.5% lower compared to Squat Release (t(43)=-6.6, p<0.001). F_{shear} was 84.1% greater during Squat Release than Pelvis Release (t(43)=7.8, p<0.001) and 95.5% greater than during Kneeling Release (t(43)=7.0, p<0.001).

Regarding impact configuration, no significant differences were found between paradigms for $Pelvis_{inclination}$, $Femur_{axial}$, or $Hip_{flexion}$. Significant main effects were found for $Pelvis_{axial}$ ($F_{(2,86)}$=3.1, p=0.049) and $Femur_{inclination}$ ($F_{(2,86)}$=5.0, p=0.008). The pelvis rotated 17.1° more posteriorly (t(43)=2.5, p=0.043), and the femur was aligned 13.3° closer to parallel with the floor (t(43)=-3.25, p=0.006) during Squat Release than Kneeling Release. Significant main effects were found for Hip_{axial} ($F_{(2,86)}$=15.2, p<0.001) and $Hip_{adduction}$ ($F_{(2,86)}$=3.5, p=0.032). In pairwise comparisons, Hip_{axial} differed significantly between all three paradigms, and was greatest for Squat Release (vs. Pelvis Release, 4.9°, t(43)=2.5, p=0.042; vs. Kneeling Release, 10.8°, t(43)=5.5, p<0.001). The hip was 8.3° more abducted during Squat Release compared to Kneeling Release (t(43)=-2.7, p=0.027).

Table A5.1 Protocol Repeatability

Characteristic	FSP	Average trial repeatability: ICC	CI	p	Training trial differences: t	p
$F_{vertical}$	PR	0.332[d]	0.128-0.543	0.001	---	---
	KR	0.807[b]	0.686-0.893	<0.001	3.40	0.002**
	SR	0.822[b]	0.699-0.906	<0.001	3.25	0.002**
F_{shear}	PR	0.601[c]	0.420-0.754	<0.001	---	---
	KR	0.469[d]	0.256-0.666	<0.001	2.20	0.033*
	SR	0.546[c]	0.330-0.733	<0.001	6.10	<0.001**
$V_{vertical}$	PR	0.348[d]	0.112-0.587	0.002	---	---
	KR	0.637[c]	0.449-0.788	<0.001	-4.55	<0.001**
	SR	0.585[c]	0.369-0.766	<0.001	-0.007	0.995
V_{shear}	PR	0.092[a]	-0.127-0.366	0.213	---	---
	KR	0.596[c]	0.397-0.762	<0.001	-1.069	0.292
	SR	0.624[c]	0.408-0.796	<0.001	9.834	<0.001**
Hip_{flex}	PR	0.145	-0.073-0.414	0.105	1.35	0.185
	KR	0.700[c]	0.528-0.831	<0.001	-1.10	0.280
	SR	0.711[c]	0.520-0.849	<0.001	13.976	<0.001**
$Hip_{adduction}$	PR	0.284[d]	0.040-0.547	0.011	-4.64	<0.001**
	KR	0.562[c]	0.361-0.736	<0.001	-0.86	0.394
	SR	0.699[c]	0.406-0.795	<0.001	-7.94	<0.001**
Hip_{axial}	PR	0.243[d]	0.017-0.501	0.018	8.51	<0.001**
	KR	0.687[c]	0.515-0.821	<0.001	0.77	0.447
	SR	0.624[c]	0.508-0.841	<0.001	-8.54	<0.001**
$Pelvis_{inclination}$	PR	0.216[d]	-0.009-0.475	0.031	0.82	0.418
	KR	0.711[c]	0.547-0.835	<0.001	-0.24	0.815
	SR	0.799[b]	0.653-0.897	<0.001	2.04	0.050
$Pelvis_{axial}$	PR	0.242[c]	0.005-0.504	0.023	3.45	0.002**
	KR	0.763[b]	0.620-0.868	<0.001	0.50	0.620
	SR	0.799[b]	0.653-0.898	<0.001	0.659	0.514
$Femur_{inclination}$	PR	0.432[d]	0.193-0.657	<0.001	2.75	0.010*
	KR	0.502[c]	0.287-0.695	<0.001	-0.58	0.568
	SR	0.201	-0.40-0.479	0.053	5.726	<0.001**
$Femur_{axial}$	PR	0.473[d]	0.239-0.687	<0.001	-1.20	0.239
	KR	0.634[c]	0.445-0.786	<0.001	1.36	0.182
	SR	0.488[d]	0.246-0.706	<0.001	-4.675	<0.001**

a. Excellent repeatability; b. good repeatability; c. moderate repeatability; d. poor, but significant repeatability; * significant differences between first trial and average trials, p<0.05; ** significant differences between first trial and average trials, p<0.01.

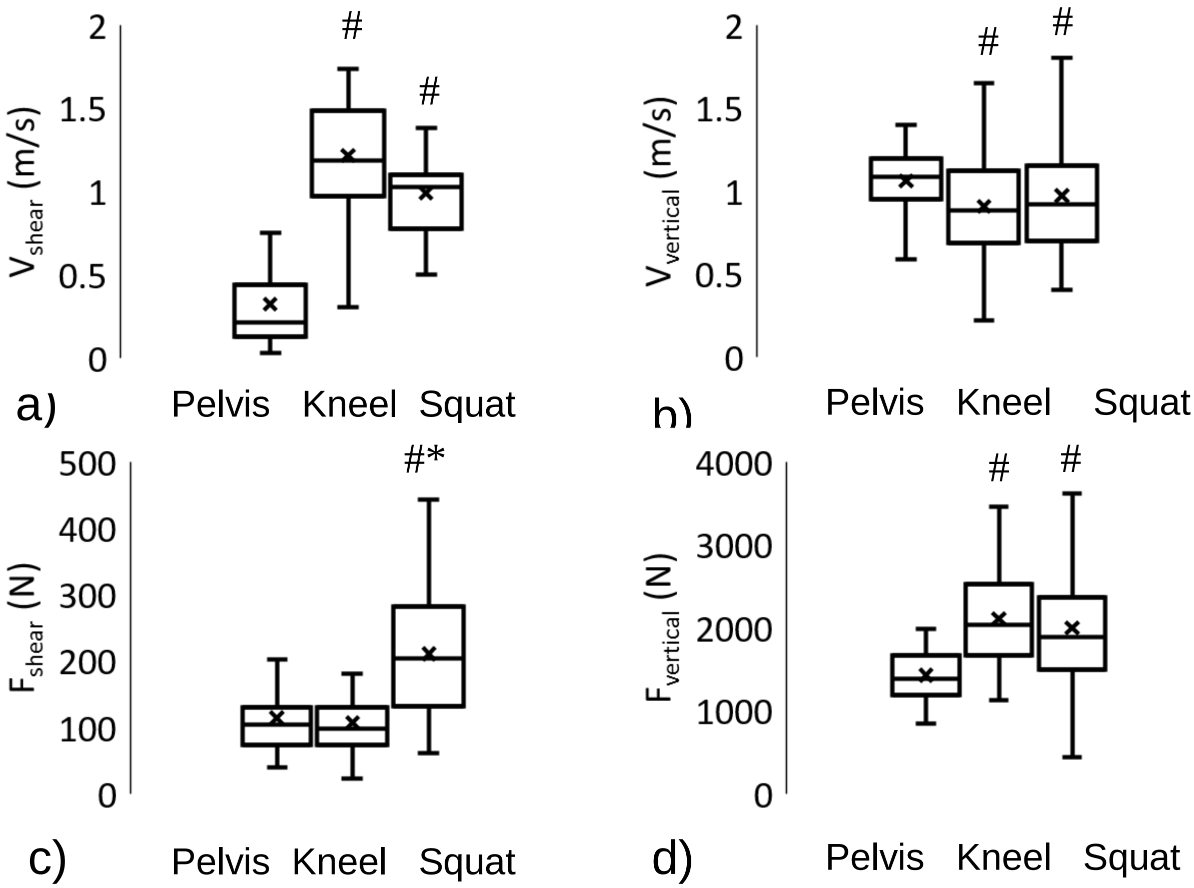

Figure A5.2 Paradigm comparisons for impact velocity and peak force

Significant differences at $p<0.05$ from (#) Pelvis Release and (*) Kneeling Release are indicated for (a) V_{shear}, (b) $V_{vertical}$, (c) F_{shear}, and (d) $F_{vertical}$.

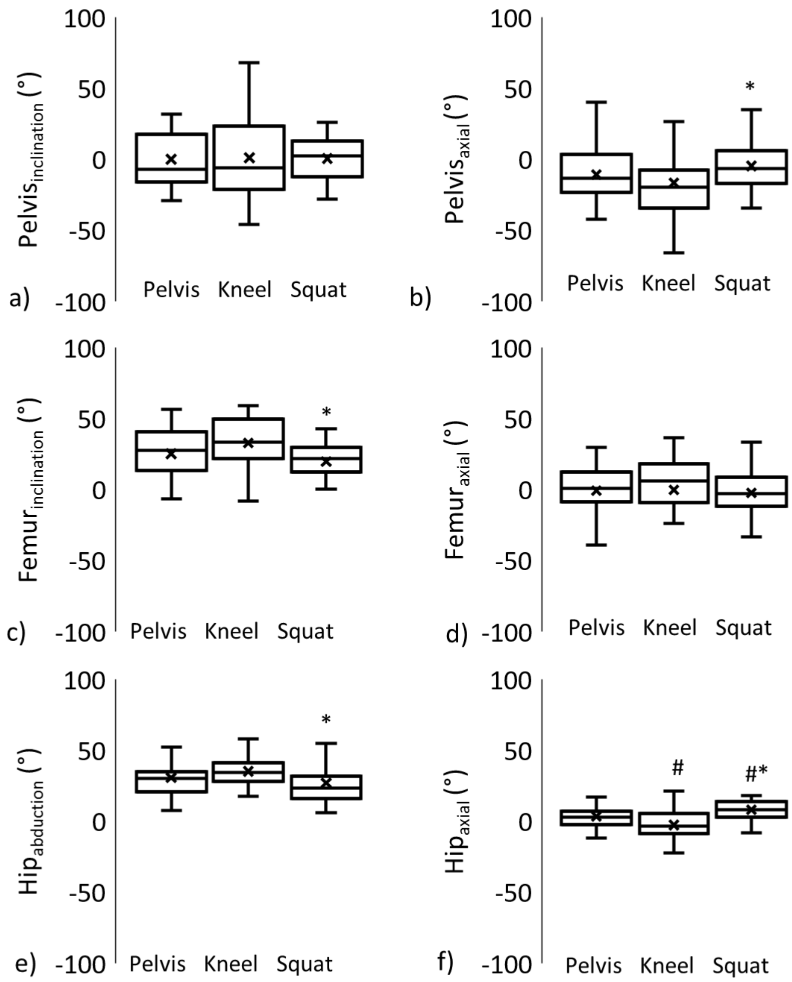

Figure A5.3 Paradigm comparisons for impact configuration

Significant differences at $p<0.05$ from (#) Pelvis Release and (*) Kneeling Release are indicated for (a) $Pelvis_{inclination}$, (b) $Pelvis_{axial}$, (c) $Femur_{inclination}$, (d) $Femur_{axial}$, (e)$Hip_{abduction}$, (f)Hip_{axial}, and (g)$Hip_{flexion}$. For inclination angles, positive values indicate the proximal aspect is closer to the impact surface, and the distal aspect is above the impact surface. For axial angles, positive values indicate backwards rotation. For abduction angles, adduction is positive. For flexion angles, flexion is positive.

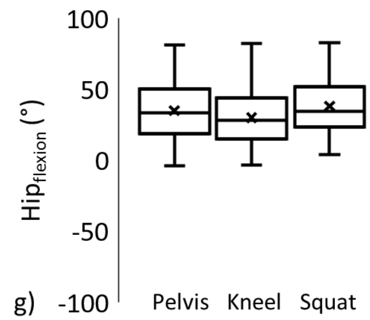

A5.4 Discussion

In this study we aimed to characterize and describe differences between three fall simulation paradigms. We found that shear velocity differed substantially between paradigms, while vertical velocity differed between paradigms by less than 10%. In contrast, both vertical and shear force differed between paradigms. Impact configuration differed between paradigms substantially. Differences were greatest for Squat Release, a configuration associated with posterior rotation of the pelvis and greater inclination angle of the femur. Repeatability varied across paradigms, and was consistently lower for Pelvis Release compared to Kneeling or Squat Release. Adaptation effects were present for all three paradigms.

The magnitudes of force and velocity, and repeatability of Pelvis Release were more similar to Kneeling and Squat release than expected. While we found that $F_{vertical}$ was lower for Pelvis Release compared to the other protocols, $V_{vertical}$ was greater. Additionally, V_{shear} was lower only compared to Kneeling Release, and F_{shear} was lower only compared to Squat Release. We observed no differences in pelvis inclination angle between paradigms, but we were unable to track torso motion during this study. However, qualitative analysis of the secondary video clarified that the torso was oriented more laterally during Pelvis release, and more vertically above the pelvis during Squat and Kneeling release. Load sharing between the pelvis and distal structures during the Pelvis Release protocol is minimal (Robinovitch, Hayes et al. 1997), however, when the Pelvis Release is performed with an upright torso position, forces at the hip increase by (on average) 36% due to the contribution of the head, arms and torso to the effective mass of the pelvis. Additionally, though ICC scores were lower than expected for Pelvis Release impact configurations, within-subjects variability was also low—across paradigms, variability was 10.2 (12.0)° for $Hip_{flexion}$, 7.3 (8.3)° for Hip_{axial} and 6.9 (8.8)° for $Hip_{adduction}$, and did not differ substantially between paradigms. Therefore, the inconsistency may have little functional relevance for simulating falls, though meticulous positioning, cueing of the participant, and multiple trials are recommended.

Control strategies appeared to have a strong effect on repeatability for Kneeling and Squat release. Average Squat Release trials were 268.8 (278.0) N lower than first Squat Release trials while velocity remained constant, and average Kneeling Release trials were 355.3 (364.1) N lower than first Kneeling Release trials, with a 21.9% decrease in $V_{vertical}$. This can be explained by different control strategies. During Kneeling Release, participants employed a velocity-reduction strategy, which was likely achieved through eccentric contraction of the lateral hip musculature. During Squat Release, participants employed a configuration-change strategy--differences were observed for five out of seven configuration variables during Squat Release (reducing $Hip_{flexion}$, and increasing $Hip_{adduction}$ and internal Hip_{axial} from the initial trial), but no configuration variables differed between first and average trials for Kneeling Release. These configuration changes were likely employed with the goal of distributing loading to distal regions (knee, abdomen), and initiating a backwards-rolling pattern. These results may be compared to those by Groen and colleagues (2007), who found that a rolling strategy was used by judo practitioners to maintain kinetic energy during a fall rather than directing the energy directly into the proximal femur. Similarly, Robinovitch et al. (2004) found that active control during a squat response was effective at reducing impact velocity (and presumably, impact force) during a backwards fall. Finally, Hsiao and colleagues (1997) found that protective responses during unexpected falls converged on similar patterns with repeated trials. Therefore, impact mechanics are sensitive to active control and adaptation of impact velocity and configuration during a simulated fall.

The direction of the adaptations we observed over consecutive trials were not consistent across participants. For example, 31.8% of participants during Squat Release, and 29.6% during Kneeling release increased average trial forces compared to the first trial block. These participants may have approached the initial trial blocks with hesitation and increased forces as they became more comfortable with the protocol, were unable to determine an appropriate strategy to reduce peak forces, or became fatigued and were ineffective at reducing peak forces during later trial blocks. These differences were not captured by our statistical comparison—i.e. different directional strategies may have reduced mean differences between first and average trials.

Our results have implications for implementing fall simulation paradigms in experimental and modeling protocols. We found that although consistency of impact characteristics vary between average trials of each protocol, the variance may not be substantial enough to warrant selection of one protocol over another. All three protocols are likely consistent enough during average trials to allow for comparison between interventions (e.g. wearable hip protectors or safety floors). However, adaptation effects were more substantial—first trials differed substantially in impact configuration, velocity and force from average trials. Further investigations into falling configuration and control strategies would clarify whether average trials or first trials are more similar in configuration and behavior to falls from standing height. Additionally, we found substantial increase in F_{shear} for Squat Release compared to Pelvis Release or Kneeling Release, and $F_{vertical}$ for Squat and Kneeling Release compared to Pelvis Release. Further work should clarify how participant control strategy (muscle activation, control of trunk position), and other biomechanical aspects, such as load distribution within the pelvis and between body segments, differ between protocols, and what effects those differences might have on experimental outcomes. Finally, we found substantial differences in falling configuration between protocols, particularly with regards to posterior rotation of the pelvis and inclination of the femur. Changes in loading direction of the magnitudes we observed have previously been found to have a substantial effect on fracture tolerance (Keyak, Skinner et al. 2001). These differences should be accounted for when modeling internal loads at the hip and within the pelvis as these slight changes likely have a substantial effect on locations of peak stresses in the proximal femur.

To summarize, we described and found differences between impact characteristics for three fall simulation protocols. Differences in impact characteristics were linked to paradigm constraints and participant control strategies. While repeatability ranged widely between protocols, we found that all three were consistent for most variables at a level of “moderate” or better, but caution experimenters to use consistent initial conditions to maintain repeatability. Finally, adaptation effects were substantial, differed in direction, and remain a significant consideration for implementation of a fall simulation protocol.